Politecnico di Torino

Dipartimento di Ingegneria Meccanica,
Aerospaziale, dell'Autoveicolo e della Produzione

MSc Degree in
Mechanical Engineering
LM-33

Thesis

FEM Multi-Physics Analysis of Li-Ion Batteries

Author: FERRACIN Davide

Relator: SOMA' Aurelio
Co-Relator: MOCERA Francesco

A.Y. 2020 – 2021
April 2021

Abstract

In the last years, driven by the growing concern for the environmental conditions, new emerging technologies have been directed towards a “greener” concept, in optic of a future complete sustainability in the way humans conduct their lives within the world. In the well-known automotive field, the role of the so far used internal combustion engine is becoming outdated because of the new applications which involve a full rather than partial electric propulsion powertrain. At the basis of the functioning of these new generation of systems, in both electric and hybrid electric vehicles, one ends up finding the energetic storage to take place in the electrochemical cells, i.e. the batteries. Many recent studies have focused on batteries and first of all on their chemistry: among the various available setups, Li-Ion batteries have received particular attention since they are able to store and deliver great amounts of powers with respect to other competitive solutions, are cleaner in their production chain, and present a long lifespan. From an engineering point of view, however, the attention is totally dedicated to find out the optimal way to of simulating the behaviour of the cells, so that their status could eventually be totally predictable in online applications. In the development of this work, starting from a broad introduction aimed at defining the Li-Ion batteries as the best energy storage systems in their field, particular attention will be carried on an innovative simulating process which is totally able to mimic the functioning of these elements, validated from the experimental testing campaign conducted in parallel. Thanks then to effective simulating solutions, safer, newer, and more efficient designs of battery packs could be achieved, and the time-to-market from the research and development phase would get eventually reduced.

Summary

List of figures

List of tables

Chapter 1

Introduction

Scenario

The aim of the following work is to provide the necessary knowledge to understand the phenomena taking place within a Li-Ion battery, as well as to contextualize its functioning and use in an electric vehicle. Subsequently, when the technicisms are acquired and the devices are properly known, according to the current state of the art, an experimental analysis conducted using a finite-element-based software will be carried on highlighting the critical issues in the field of study, with its results that are going to be validated by the by the traditional tests conducted in laboratory.

The research group under whose supervision this work has taken form studies the application of the electrification in the powertrain of the so-called “working vehicles”. Each motorized machine intended to move cargos rather than passengers is generally referred to as a working vehicle, and the diffusion of these machines has taken an accelerated pace in the last century, leading to cover an outstanding amount of fields of application: extra-urban transports, construction, agriculture, are only few of the involved sectors, but nevertheless are the ones that together give the largest share in this so-big market. Based on the technology inherited from the last generations, however, the functioning of these machines still relies over the use of fossil fuels, but with the recent advent of the hybrid and full-electric propulsions in the automotive field, extensive researches have already begun to apply such changes also in this sector. Indeed, since these vehicles have to be blame for the generation of a large amount of pollutant emissions, a technological revolution has become necessary, but the difficulties meet in the design of these new products, though, are numerous. Think that, for instance, whenever an electric working machine is designed, major performances are expected than those required in the well-known automotive field: the supplied traction forces and peak powers must be high enough to sustain the efforts at which the machine undergoes, and all this should not interfere with the autonomies reached by the new electric powertrains. To meet these requirements, increases in the weights and dimensions of the energy storage systems—i.e. the “heart” of the electric vehicles—are necessary.

It could be said that the market of the working vehicles has already passed in the last years throughout an important evolution, destined to lead to the final worldwide adoption of hybrid and full-electric concepts. Several manufacturers, today, manage in developing new technical solutions to improve the efficiencies of the first hybrid machines: among the companies involved in the generational change, for instance, Komatsu, Caterpillar, Hitachi, Hyundai, John Deere, Claas and Merlo [1] can be found to be the most promising ones, with the recent disruption of Nikola, for what concerns the long-range road transportations. The final target for the future is to apply the widely known pure electrical propulsion deriving from the automotive field, effectively integrating it with the requirements of these so-different machines, obtaining at the end a class of zero-emissions and high-performances vehicles.

The severe and extreme working conditions that have to be withstood during the functioning of these latters signs a difficulty in both their design and manufacturing: the need of very large energy storage systems (ESSs), the necessity of reliable envelopes that structurally protect the integrity of the accumulators, and the optimization for the distribution of masses inside the bodies, only account for few of the difficult challenges that the engineering has to face up in the following years. Nevertheless, leaving apart different issues that may be met, it has been found that the most important aspect designing hybrid or full-electric vehicles is the creation of a performant ESS. The results obtained with the battery packs belonging to the automotive field are not yet sufficient for an application in other sectors, where together with the higher performances also a more predictable and a safer behaviour of the devices is sought. Hence, the starting point, nowadays, is the improvement of the already existent ESSs where better outcomes are going to be reached settling the basis for a deeper future development and integration.

As a consequence of what has been introduced up to now, to properly characterize and understand the nature of the ESSs, references will be made in this work with a particular focus in the automotive field, since both the hybrid and pure-electrical concepts have already been present on the market for many years. At the end, indeed, being the technology shared between different categories and products, once that the characteristics at the basis of an electric powertrain gets totally understood, it will be easy to apply this to several fields of research: from the small electronic devices—i.e. smartphones, laptops, etc.—to the biggest working machines.

Electrification of land vehicles

The electrification of the vehicles' powertrain has been an engineering success of the last years, but which presents a very long history of almost two centuries. The first full-electric vehicle was invented in the far 1834, but due to the associated limitations and the contemporaneous development of the internal combustion engine (ICE), these rapidly vanished from the scene. In the same way, the later discovery of hybrid concepts did not obtain more success: despite the first hybrid had already been patented at the beginning of the 20th century, the technology has been put apart in favour of the more affordable and reliable conventional cars, mainly due to the new efficient assembly chains techniques involved in the creation of ICE-based vehicles, together with the presence of the two world wars which pushed the requirements of these latters. However, because of the environmental problems the humanity is facing up nowadays, interests in hybrid and full-electric powertrains have grown again thanks to their limited polluting emissions. Moreover, several factors concurred in the exponential development of these technologies: above all, the first oil crisis of the early 70s has highlighted the necessity of having alternative sources of propulsion [2]. As a consequence, with the natural improvements of the already existent discoveries, at the beginning of the millennium the Honda Insight and the Toyota Prius were the first hybrids available in a world niche market—mainly focused into the eastern countries, most of all in Japan and China. In the years that followed, several carmakers introduced hybrid models, for example, among the firsts, the Ford presenting the hybrid version of the Escape and the Lexus with the RX400h. The production of full-electric vehicles, differently from the hybrid ones, already started in the last decades of the 19th century, principally in America, Britain, and France, but still presenting poor products in terms of performances and reliability. Following the history, the first, most iconic example regards the electrical taxi use by the London Electric Cab Company [3]. Later on, the California Institute of Technology (CalTech) and the Massachusetts Institute of Technology (MIT) have been the pioneers in the research which, throughout the 70s and 80s, aimed at providing efficient full-electric powertrains able to withstand long travels: the 1998 marks an important date in the electrification of land vehicles, when a prototype have been driven from Los Angeles to Detroit, exhibiting a great success with no component failures. The rest is recent history, with the focus into the electric field of Chinese and Japanese carmakers that have led to important technological improvements and, consequently, to the first sales—also thanks to an already developed knowledge in the field, got by the hybrid vehicles, which given to those countries an important advantage in the first years. In the meanwhile, in the famous Silicon Valley, in California, the two entrepreneurs Tarpenning and Eberhard together with the young energetic engineer Straubel and the tycoon Musk, founded together a company named Tesla Motors. The creation of the first prototype—i.e. the Tesla Roadster—signed a non-return point in the launch of the full-electric vehicles: the Roadster is still today the fastest commercial car in the world, and its first rides have shown the outstanding efficiency of a new powertrain, reliable, performant, and lasting. Passed the years, the largest share of the electrical vehicles' market, nowadays, is controlled by the Tesla, thanks to the production of a fleet of first-class products, whose most sold one is the Tesla Model S, shown in *figure 1*.

FIGURE 1 - Tesla Model S

The role of the Tesla in the worldwide diffusion of the electric vehicles has been and still is of fundamental importance: the company had indeed as its unique goal the adoption of the new electrical-based technology in the automotive field, and during the last twenty years has continuously been pushing the research of new concepts, leading also to become one of the leaders in the manufacturing of Li-Ion batteries—and the first carmaker that manages to produce them by its own [4]. If the trend is not going to change in the following years, by the 2050 the human global population will at least reach 10 billion of individuals, and the request of vehicles will as well rise exponentially up to 2.5 billion, according to the forecasts of C. C. Chan, represented in the *figure 2*. In a world in which all the vehicles are propelled with fossil fuels, several issues will come out due to the emptying of the oil reserves and the resulting pollutant emissions in the atmosphere. Furthermore, even the approach in the market and the development of the hybrid concepts is only partially the solution to these problems. Indeed, they reduce both the emissions and the requirements of oil, but are still dependent on it, and considering that the environmental protection and the energy conservation are growing concerns that regard everyone, the development, validation, and spreading of new full-electric vehicles has taken an accelerated pace to fulfil these needs. However, because of the long times that such an innovation would require, also "only" the reduction in the emissions results to be a good compromise. Putting things together, the future passage between hybrids and full-electric powertrains is necessary: it could be provided an emission-free ride, both for urban and out-of-urban transportation, thanks to an improved autonomy given by newer and larger ESSs than those found in the first hybrids. Moreover, apart from the creation of vehicles, these discoveries carry the potential to disrupt the "green" market: new energy use, environmental care, high-tech promotion, creation of new industries, economic development of the investing countries, etc., are only few of the advantages in pushing the research in the electric field. In other words, the knowledge, improvement, and consequent adoption at large scale of this new technology is really able to change the future world, and this is what Tesla, most of all, has always tried to make people aware of.

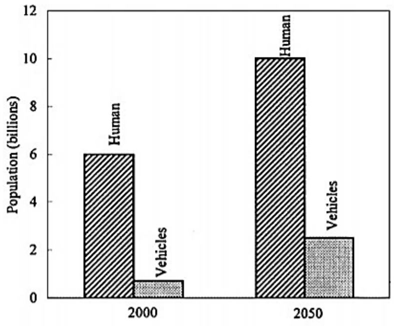

FIGURE 2 - Population vs vehicles forecast

The modern-class of vehicles, both hybrids and full-electrics, are definitely new machines with respect to their ancestors produced in the 19th and 20th centuries: they can be defined as road vehicles based on a modern electric propulsion, coming from the symbiotic functioning of electric motors, power converters, and energetic accumulators, all connected and controlled by integrated softwares able to monitor the vehicles' performances. At the basis of the expected outcomes, however, the most determinant device is the ESS, or simply "battery pack". Its characteristics have been largely studied in the last years to get the performances of the cars at the zenith, and being it part of the electric powertrain, obviously, a deeper knowledge of its working parameters will surely result in a clearer expectation and definition of the vehicle's entire behaviour. Nevertheless, before to go deeply into explaining the ESSs, an overview over both the hybrid and full-electric powertrains is needed, so that the role of the batteries will successively be clarified by knowing the components whose functioning relies over them.

Electrification of land vehicles - **Hybrid**

Hybrid electric vehicles (shortly called, since now on, "HEVs" or "HVs") are equipped with a single powertrain that is able to combine an ICE together with an electric motor, which in turn is properly fed by the current generated into the battery pack. This technology allows to consume less fuel and to emit less harmful products than done with the traditional ICEs: so, HEVs are able to provide strong benefits from an environmental point of view, something that nowadays is somehow as valuable as the performances of the whole car. Indeed, to support their diffusion, beginning in the 00s, states and local governments implemented a broad set of incentives to stimulate a higher adoption of the hybrid technology, many of which are generous, worth several thousand dollars, and helps in reducing costs associated with the purchase of an electrified vehicle [3].

The main difference between an ICE-based vehicle, a conventional one, and a so-called “hybrid”, is the presence of an ESS within the powertrain: thanks to this latter, the basic propulsion obtained with the ICE gets improved, both by rinsing its efficiency and lowering the consumption as well as the emissions. However, the issues that still limit the diffusion of these types of environmental-friendly cars most concern with the energy storage itself. For instance, problematics such as the limited vehicle autonomy—which is responsible for the so-called "range anxiety"—, the system’s life expectations, the correct definition of some functioning parameters (such as voltages, currents, and temperatures), all together present today a hard engineering challenge. On the other hand, the advantages provided by the adoption of the HE technology are remarkable for the automotive field: both a reduction in the emission and an improved fuel economy can be accomplished. Concerning this latter aspect, for example, the ICE present in the HEVs can be stopped when the car is at rest, such as when a stop is reached—taking the feature’s famous name “Start&Stop”—and consequently switched on again only when the starting phase has already been performed by the electric motor alone. Another interesting feature derives from the regenerative braking: the kinetic energy in excess that results from a forced deceleration (when brakes act over the wheels) is stored in the ESS, charging it again of a small useful amount for the subsequent starting phase. Then, furthermore, apart from these small savings in the fuel consumption, a certain range of silent operations with zero emissions is possible, whenever the hybrid is driven in the pure electric mode. The problem with this last ability, nevertheless, is the limited travel autonomy that results due to the small ESSs: the necessity of the ICE is so that it is possible to overcome the limitation and assure a supplementary range of travelling. Obviously, finally, the latest solutions allow the pure electric driving range to be extended, whenever indeed the battery pack is found to be rechargeable. The task is simply accomplished by connecting a plug to an electric grid, giving to this latter type of vehicle the name of “plug-in” hybrid (PHEVs).

Summarizing, depending on the features that are presented in a hybrid car, an initial classification can be made being based on the so-called “degree” of electrification [1, 6].

- **Micro hybrids**

  Micro HVs are a simple evolution of the conventional ICE-based cars, rather than complex vehicles that rely on the partial electrification of the powertrain. They allow indeed the driver to take advantage from basic features, such as the “Start&Stop” and the regenerative braking, resulting in small savings in the consumption of fuel around $5 \div 10\%$, and consequently reducing of a small extent the emissions. At the end, they are almost never taken into account when speaking about hybrids, since these do not present a proper electric motor within the powertrain.

- **Mild & medium hybrids**

  Mild HEVs rely on a major degree of electrification than seen for the micro hybrid ones, presenting a battery pack together with an integrated electric motor within the hybrid powertrain. In general, it can be said that this class of vehicles provides the implementation of several basic functions already present in the micro hybrids: in addition to the Start&Stop and the regenerative braking, for instance, in the mild hybrids an additional torque is supplied to the ICE's shaft by the electrical motor, improving like this both the acceleration and the braking of the car, with the consequent fuel saving ranging between $10 \div 20\%$ during the normal city-driving. An even higher support provided by the electric motor ends up resulting in another class of HEVs, the so-called medium hybrids.

- **Full & plug-in hybrids**

Full HVs are once again equipped with an electric motor fed by a proper battery pack, but which is now able alone to completely sustain the motion of the car, resulting in a temporary emission-free propulsion. Depending on the state of the ESS or on the choice of the driver, the propulsion can be totally or only partially sustained by the ICE, although this obviously results in a certain level of pollutant emissions. However, in the normal city-driving, these latters are generally found to be reduced of an extent varying between $20 \div 50\%$, which is actually the best result achieved in the hybrid category. The plug-in HVs also belong to the class of the full-hybrids: whenever the batteries can be recharged, with the vehicle at rest and connected to a grid, the amount of energy in the electric accumulator is restored, so that the motion could be totally sustained only thanks to the electric motor.

The aforementioned classification is resumed in the following *table 1*.

TABLE 1 - Classes and features of the hybrids

Vehicles	Start&Stop	Regenerative braking	Motor assist	Full-E drive
Conventional ICE	Possible	Minimal	No	No
Micro HEVs	Yes	Minimal	Minimal	No
Mild HEVs	Yes	Modest	Modest	No
Medium HEVs	Yes	Yes	Yes	Modest
Full HEVs	Yes	Yes	Yes	Yes

A totally different classification, on the other hand, can be made regarding the relative position of the ICE and of the electrical motor in the vehicle's powertrain [3], obviously whenever both are present (i.e. not in case of micro hybrids). In particular, the following four different setups for the powertrain's connections may be found: "in series", "in parallel", "in series-parallel" (also called "combined"), and complex.

- **"In series" connection**

With this type of connection, the traction forces are provided by the electric motor. However, whenever the battery pack is found to be empty, the ICE is activated and the mechanical power coming from it gets converted into electricity, thanks to the presence of a generator, and so, accordingly, stored in the ESS for a future use. So, when the level of charge is considered to be satisfactory, the ICE is switched off and the electric motor starts again to provide the traction with the ESS's electric power supply.

- **"In parallel" connection**

Here, the two motors are coupled together with a single shaft via two separate clutches, so that the traction may be provided by one motor rather than from the other, and, as extreme condition, even contemporary by both of them. An advantage of this setup is that whenever the ICE is working, the electric motor could be enabled to function as a generator, so that the battery pack gets recharged as it has already been seen with the "in series" connection.

- **Combined connection**

With this configuration, which is also called "power-split", both the features seen in the two previous classes of hybrids are provided: only at the cost of an additional mechanical connection between the generator and the electric motor, it is possible to combine the advantages of the "in series" and "in parallel" setups. Obviously, the major building complexity gets translated into a rise of costs, resulting then to be a solution principally adapted in high-class HVs.

- **Complex connection**

Similarly to the combined configuration, the additional feature presented by this type of connection is found in the fact that there is a bidirectional power flow allowed to pass within the electric motor. Hence, the peculiarity of this operating hybrid architecture results to be the versatility. Even if major costs and difficulties in the design have to be faced up, the solution results to be the best choice for the 4WD (four-wheel-drive) vehicles—i.e. vehicles where the traction is provided at both the axles, rear and front one.

A clear schematic view of the four different setups of the powertrain in HVs is represented in the following *figure 3*.

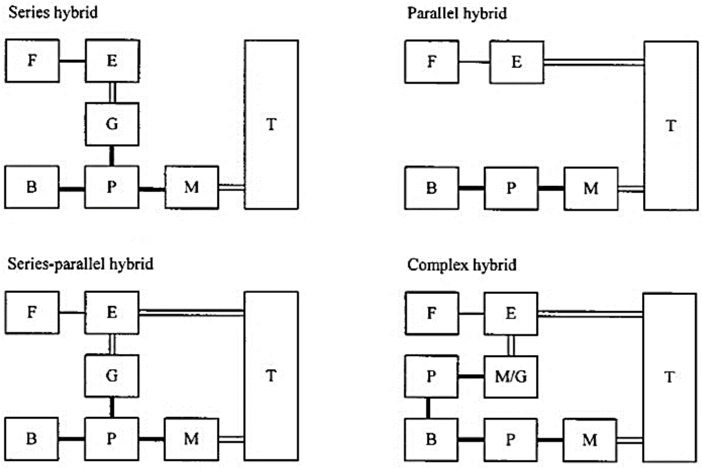

FIGURE 3 - Setups of the hybrid powertrains

As it can be noted, the transmission (T) is always found to be mechanically connected to the electric motor (M) and the ICE (E), apart for the "in series" setup, where the electric motor is the only one aimed at suppling torque to the driving axle, and the presence of the ICE is exclusively required to recharge the ESS. Furthermore, a fundamental component allowing the interaction between the ICE and the electric motor is the generator (G): connecting indeed the ICE with the battery pack (B), it allows to translate any mechanical input into an electrical output, so that the rotative motion of the ICE's cranking shaft is directly coupled with the phenomena taking place within the ESS. Summarizing, in other words, the recharge of the battery pack by part of the ICE can only be accomplished in case a generator is placed between the two components, and consequently, the functioning of the electric motor also relies over the presence of this component. Finally, other elements that are shown in the *figure 3*, always found to be part of the hybrid powertrains, are the fuel tank (F) and the power converter (P). This latter, in particular, makes possible the AC/DC electricity conversion in order to allow the electric motor to work being fed by the battery pack.

Concluding, the HVs are key products placed in between two extremes: the ICE-based vehicles and the pure electric ones. Their role has been and still is of fundamental importance in the reduction of pollutant emissions, tanks to both a certain range of emission-free run and an improved fuel economy. However, in a world where the development towards an even more sustainable way to travel is sought, their presence would eventually be totally replaced by the future total-emission-free solutions. A graphical resume about the hybrid technology, with respect to the ICE-based and the full-electric ones, is provided in the *figure 4*.

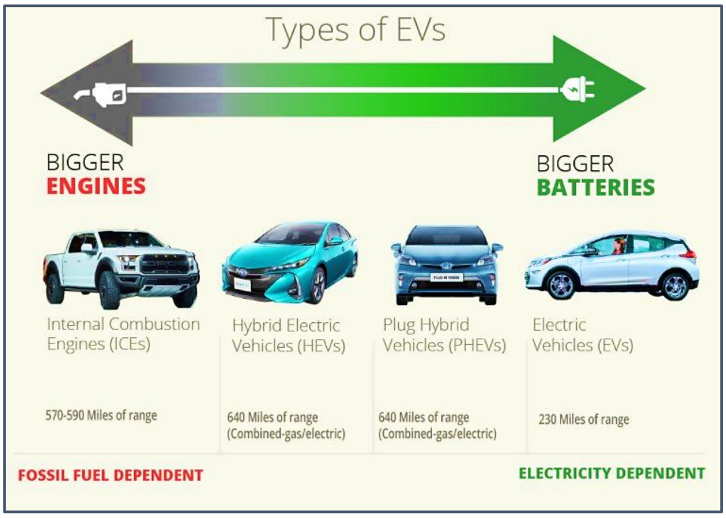

FIGURE 4 - ICE-based, hybrid, and full-electric vehicles

Electrification of land vehicles – **Electric**

All the powertrains providing propulsion to an EV relies on the electric current which is supplied by the battery pack. To better understand the role of this component, a parallelism can be done. The ESS is actually seen as tank full of water, as represented in the *figure 5*: a certain initial level of energy is represented by the amount of water stored within the case, and the more the flow gets delivered to feed the external load (i.e. the electric motor and power electronics) the more the energetic content of the ESS is lowered. The electrical parameters dealing with the battery pack's functioning are principally three: the voltage and the current, proper parameters of the ESS, and the electrical resistances, found to be part of the electrical circuit with respect to which the battery pack operates with.

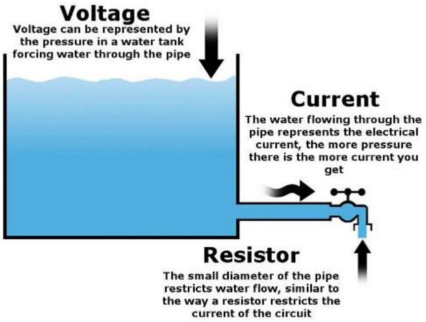

FIGURE 5 - Water tank parallelism of an ESS

When the battery pack, on the other hand, is found to be empty, it can be recharged simply by plugging the vehicle with a charging point: the ESS, at rest, is refilled taking the necessary electric energy from the public grid, for instance at home or in the so-called "charging stations", which nowadays are being built all over the world to sustain and promote the electric diffusion. Speaking then of the current generated by the battery pack, it feeds the electric motor which is actually the element that provides the traction force. The range that with a full ESS can be travelled broadly changes depending on the carmakers, although the most recent products can cover up to $300\,miles$. The differences in the autonomy are given by the pack's size and by the efficiency of the components belonging to the powertrain, but obviously also depend on the type of vehicle, for instance being related to its aerodynamic. Apart from that, one of the most important advantages that is found in the EVs is their mechanical design, presenting less than the $80 \div 90\%$ moving parts with respect to an ICE-based car: the vehicle wastes less energy—which is then, consequently, available for the traction—, energy that could have been originally lost in order to win the inertia of these components or to cope with the local inefficiencies. Moreover, the almost-no-moving-parts solution influences the safety degree of the vehicles, which are less prone to suffer from mechanical failures and hence generally provide a longer life service than those meet in hybrids or conventional cars.

Although this work is going to focus principally on the phenomena taking place within the ESS, rather than on the whole powertrain's functioning, it is also interesting and useful to see the role of the principal components concurring the creation of the vehicle motion [7].

- **Electric engine**

  The electric motor is the necessary component which is able to supply the mechanical power to the wheels, where the transmission of the motion towards them takes place thanks to the drivetrain. It can be both a direct current (DC) or an alternate current (AC) motor, but in the next years the AC ones have been preferred, becoming commonplace.

- **Inverter**

  Whenever an AC-type of motor is used, the inverter (or power converter) is a necessary component which allows to change the current from being DC, provided by the ESS, to become AC, fitting like this the "form" of the electric energy with the motor requirements.

- **Drivetrain**

The drivetrain is defined as the set of components that together concour in matching the motor with the wheels. Note that it does not consider the presence of the electric motor, whose inclusion is only taken into account in the powertrain [8]. Dealing with the drivetrain, however, is useful to highlight the fact that in the EVs a single-speed transmission is normally used.

- **Batteries**

The batteries are the ESSs, and hence, as suggested by the name, are the components which are used to store the energy then required to run the electric motor, resulting at the end to be the "heart" of the EVs. Each single battery concurs in supplying electrical energy which got previously stored within the electrochemical cells: the more is the energy the whole pack—intended as the component which is formed by several batteries—is able to supply to the downstream circuit, the longer will be the range that the vehicle can travel.

- **Other auxiliary components**

Another fundamental component needed to complete an EV's powertrain is the charger input: without this "port" and the electrical connections inside the vehicle chassis, indeed, the ESS would not be able to be re-filled of energy, and consequently once that it is discharged its life would be ended. At last, finally, the so-called "thermal system" (or simply "cooling system") accounts for a set of elements aimed at maintaining a proper operating temperature range for the previously seen components, in particular for the battery pack and the electrical motor. The battery pack, however, generally presents a dedicated thermal management system, whose functioning and peculiarities are going to be treated mor in detail in the *Chapter 3*.

As a medium of comparison, *figure 6* and *figure 7* provide a good representation of the powertrains respectively belonging to a full-electric vehicle and to a hybrid one [9,10].

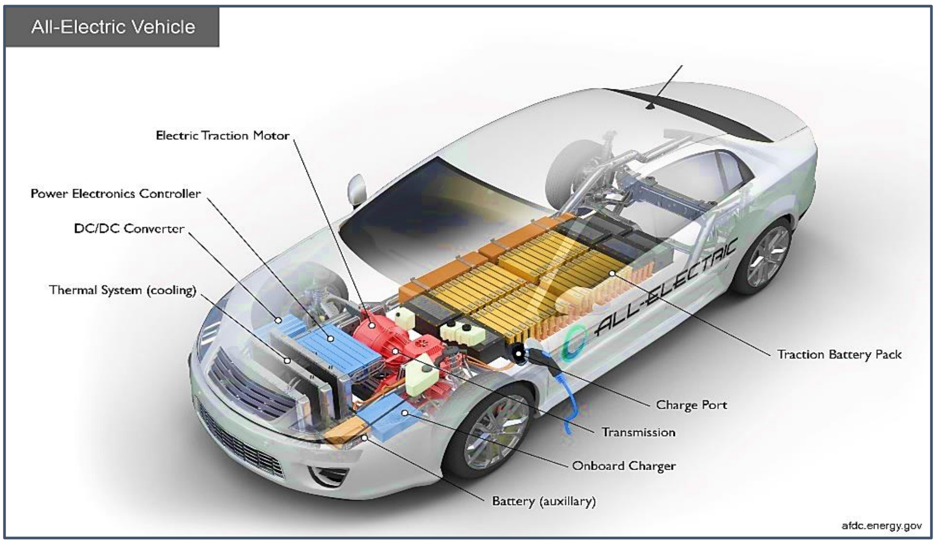

FIGURE 6 - Full-EV's powertrain

Note that from the *figure* 6 it can be highlighted that, according to what has been said up to now, there is not the necessity to have an exhaust system in the EVs, differently from the hybrid ones, where a certain amount of emissions could be present.

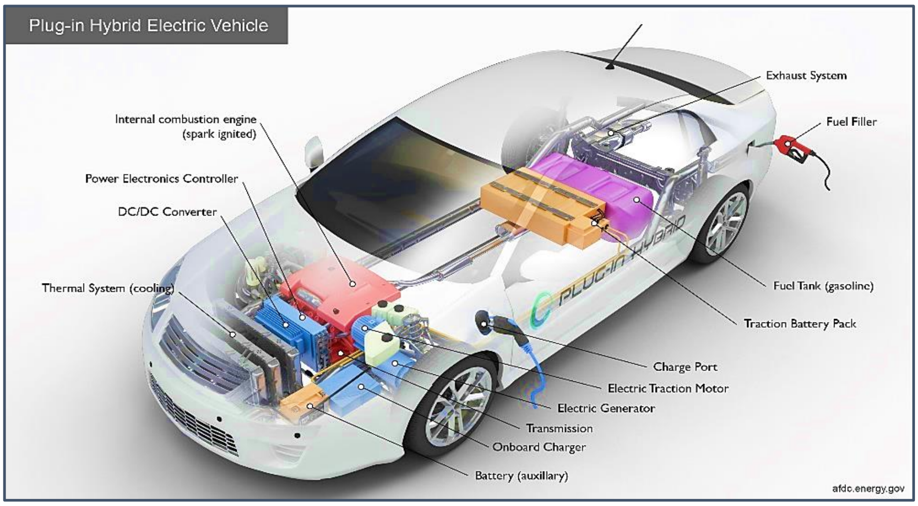

FIGURE 7 - PHEV's powertrain

Generalities about the full-electric field

As it is now already clear, the full-EV's functioning relies on the electrical energy supplied by the battery pack to the external circuit, and being this work aimed at technically characterizing these devices during both charge and discharge cycles, it is interesting to provide some basic background on how this phenomena take place. Let start by recalling which are the magnitudes in play. The kiloWatt ($kW = 10^3\ W$) could be used to denote the power that the pack is able to provide during the discharge or, on the contrary, to receive during the recharge. The kiloWatt-hour ($kWh = 10^3\ Wh$), on the other hand, is aimed at taking into account an energy, resulting from a certain power multiplied by a unit of time. In the same way as seen from the pack's point of view, then, with this magnitudes it is possible to consider the energies exchanged between the different systems in the powertrain.

To initially have an idea of the energies in play while an EV is used is very important, since, according to them, the design of the battery pack could vary in terms of both, dimensions, and weights. For instance, as a medium of comparison, it could be thought that on average an US family composed by four people annually consumes around $3100\ kWh$ at home, while the quota of energy generally required by an electric car is around $2000\ kWh$, in the same period of time. These numbers give an indication of how much the ESSs are critical components in the vehicle, mainly because of they are asked to work at the maximum of their abilities.

Apart from the previous considerations, the amount of energy required for an electric vehicle to move in considerable. Then, as a consequence, being indeed not possible to store all at once a great amount of energy within a battery pack—otherwise its dimensions will be senseless for the vehicle's purposes, thinking that the ESSs must be built in such a manner to fit with the mobile transportations demands—, this would later need to be recharged when part of the energy that was initially able to supply has been delivered. Speaking more technically, the discharge of a battery pack characterizes the range that a vehicle is still able to travel. Some effective ways to extend this autonomy have been inherited from the hybrid concepts, such as the Start&Stop and the regenerative braking. However, both the improvements do not allow the vehicle to circulate without the real need of a long stop for a recharge: the only effective way to completely refill and reset the ESS's capacity of providing energy can be accomplished by plugging the vehicle connecting it to an electric grid.

There are three types of chargers in the market, since these are dependent on the type of battery pack, on the materials that compose it, and on its dimensions, resulting at the end in three different recharging speeds that are allowed to take place.

- **Slow**

  The so-called "slow charging speed" typically supplies powers up to $3\,kW$, and is usually found wherever the charge takes place overnight or at the workplace, requiring about $8 \div 10\ hours$ for a complete refill of the ESS.

- **Fast**

  The "fast charging speed" involves powers between 7 and $22\,kW$, and is normally found in the charging stations in car parks, supermarkets, leisure centres and houses with off-street parking, generally taking around $3 \div 4\ hours$ for a complete recharge.

- **Rapid**

  Typically involving powers up to $43\,kW$, the "rapid charging speed" is compatible only with EVs that have a rapid charging capability, since other "standard" batteries could be found to be deteriorated if not able to bear the high charging rates, given by high batteries' voltages that may damages the materials of the electrochemical cells. In this case, the charging time, usually, is of $30 \div 60\ minutes$. One of the best examples of application for this kinds of recharges could be found in the so-called "Tesla Super charging stations", shown in the *figure 8*.

FIGURE 8 - Tesla Super Charging Station

The advantage in recharging a battery pack obviously, is that this action re-establishes the initial amount of milage which the vehicle is allowed to run. Once again, depending on the carmaker's ability in creating the overall product, minimizing the energetic wastes and improving the batteries' performaces, different vehicles result in different capabilities in terms of travelling autonomy, which actually signs the disctance that could be run by a car without the need to be stopped and charged again. To have an idea, the autonomies presented by some full-EVs are here provided in the following *table 2* [7].

TABLE 2 - Some autonomies

Vehicle	Autonomy $[miles]$
Volkswahen E-Golf	125
Hyundai Kona Electric	250
Jaguar I-Pace	220

Nowadays, however, many carmakers directly sell their produts already together with a charging plant to be settled at home, so that the values mentioned above are only quite representative, and change from supplier to supplier. Apart from this, it could be said that the worldwide diffusion of EVs is also related to the availability of charging stations "on-the-road". In Europe, for instance, the creation and diffusion of these stations is still proceeding, even if in the last years different incentives have promoted the research and the construction of many sites in the major cities, principally by part private companies. The US, on the other hand, are found to be few years ahead with respect to the European Community, mainly because of the huge distribution of these products have already been started by the Tesla itself, also thanks to the collaboration with the company Solar System, the biggest American retailer of solar panels.

The autonomy alone, intended as an outcome of the EVs, is not the only parameter which should be considered in order to characterize the performances of the full-electric technology. For instance, we've seen that the electrical ESS has to be designed so that it will store a sufficient amount of energy (kWh)—also taken into account by the so-called capacity (Ah) of the batteries—, but at the same time it needs also to be able to supply the adequate peak power (kW), in order to meet the everyday-drive requirements. Indeed, having the ESSs to undergo to several cycles of charge and discarge, these have to be built with materials able to withstand the different working conditions after repeated operations, without showing issues such as internal overheating or excessive material degradation. To be sure to meet these requirements, the difficult and precise design of the battery pack is usually left to specialized company: like this, the carmakers can shift all the R&D forces over the design of the vehicles, with the production of batteries that is left to secondary retailers—in the case of Tesla, for instance, for long time, the production of the ESSs has being left to Panasonic. At the end, autonomy, peak powers, energy containt within the pack, all these parameters are "easily" determined when building a battery pack thanks to the physic phenomena that describe them. It is much more difficult, on the other hand, to establish the requirements for the construction of a battery pack in terms of weight, volume, and cost. In other words, there is not a specific rule governed by a phisic law that says how to build the pack, as long as this accompishes its targets. Obviously, there are some limits not to be overcome that both carmakers and retailers take into account, thresholds that would otherwise preclude the successful design as well as the sales of the products. Indeed, obviously, to increase the dimensions of a battery pack gives the consequent rise of weight, up to when it is reached a value for which the advantages provided by a larger stacking of batteries are anihlitaed by the effects given by a bigger mass of the vehicle to be moved—which means that more traction is requided to be supplied by the powertrain. Hence, it is possible to say that the practical limits to be set in order to achieve workable designs are rather arbitrary, althought they should be considered. As example, to take counciousness of a battery pack's dimensions and positioning within a vehicle body, a clear view is provided in the *figure 9*.

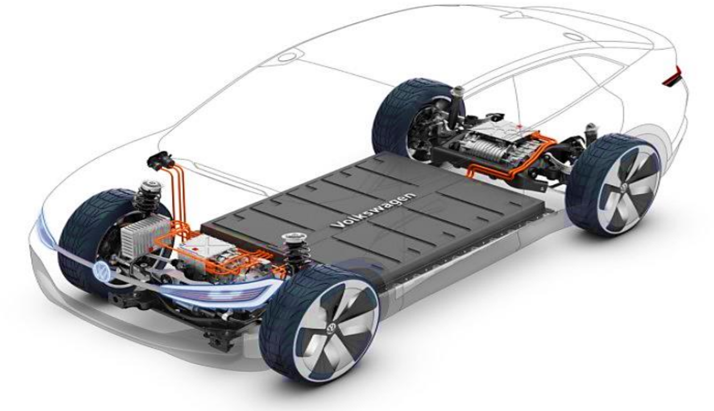

FIGURE 9 – Volkswagen's battery pack [11]

Summarizing what has been said up to now, the most importat performances expected to be accomplished by an ESS to have it properly working are collected in the *table 3* [12], together with the parameters belonging to both, the vehicle and the pack itslef, that take part in their efficient achievement.

TABLE 3 - Expectations for a battery pack

Requirement	Deals with…
Optimal size and weight	• Cell's materials (for their provided electrical outputs) • Available space in the body of the vehicle • Required performances of the vehicles
Long driving range	• Battery's capacity • Powetrain's efficiency
High peak power	• Battery's materials • Number of batteries forming the pack
Driving cycles capability	• Battery's materials (ability to withstand a certain load-cycle history)
Reduced overheating and degradation	• Battery's materials (thermal stabality, chemical reactivity) • TMS (i.e. the cooling system)
Low cost of manufacturing	• Materials involved • Degree of safety • Dimensions • Required performances of the vehicles (low- or high-class cars)

In the two following parts of the work, *Chapter 2* and *Chapter 3*, the aim is to explain more and more in detail how a battery pack is composed and how it works, from the smallest basic units that form it to the whole complete functioning of the system. Up to now, indeed, it has been seen what its role is within an electric vehicle and what are the outcomes that may be expected from it, in order to have a well-performant powertrain. However, the dependency of these latter expected results to such many internal parameters, denoting that the entire vehicle's functioning relies over several important aspects to be carefully checked, as shown in the *table 3*, highlights the necessity of the further larger analysis.

Tesla supremacy

At the end of this introduction, it could be interesting to see how far the research into the electric mobility has arrived, and how far in the next years still would go. The Tesla's vehicles are today, by far, the most developed ones in the market, even if in the meanwhile other carmakers are bringing their products close these outstanding levels. As a matter of fact, the technical data coming out from the performances of the ESSs, and in general from the powertrains found in the different Tesla's concepts, are already astonishing. The specs of some commercial vehicles, for instance, are here in the following summarized in the *table 4*.

TABLE 4 - Some specs of Tesla's vehicles (from the Tesla website)

Tesla…	Weight in lbs	Acceleration (… peak powers)	Autonomy in $miles$	Life span in $years$ or $miles$
Model S	4921	$0 \rightarrow 60\ mph$ in $2.3\ s$	348	8 or 150000
Model 3	4036	$0 \rightarrow 60\ mph$ in $3.2\ s$	299	8 or 120000
Model X	5531	$0 \rightarrow 60\ mph$ in $2.6\ s$	305	8 or 150000
Model Y	4416 [13]	$0 \rightarrow 60\ mph$ in $3.5\ s$	291	8 or 120000

Despites the results are good from the electric mobility point of view, when compared to those of the other well-known ICE-based vehicles, these still have to get largely improved in order to be comparable. Not only the autonomy of the electric cars has to be raised in order to get closer and overcome the one provided by the "ancient" combustion technology, relying over a fuel tank, but also the reliability in the electrical powertrains should get better. However, following the trends of the last decades the investors of the "green" market are becoming more and more confident in the fact that this revolution is not far in time. To provide some data, for instance, and to show how fast the research in the field is going on, it could be presented the comparison between the first Tesla's vehicle, i.e. the so-called Roadster, and the second release of the company, the Model S. When submitted to the 2-cycle EPA test procedure in the far 2006, the Roadster "only" presented 244 miles of autonomy: the results were already impressive for that time, and still today they overcome the autonomies provided by several high-brand vehicles. However, the improvement reached in only few years of development of the technology with the creation of the new

Model S has been impressive as well, as it is shown in graph represented in the *figure 10*, with something close to 50 miles of additional range being added to the initial developed vehicle.

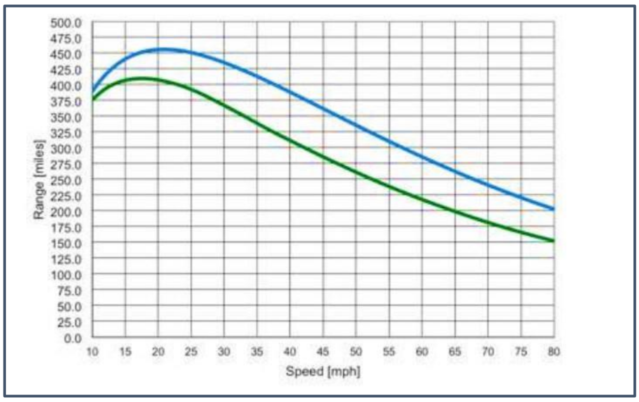

FIGURE 10 - Autonomy vs speed characteristic (Tesla Roadster, [green] and Tesla Model S [blue])

Chapter 2

Li-Ion technology

Electrochemical cells

The so-called “electrochemical cell” is the basic unit composing a battery, and it is defined as a system which is able to provide electrical energy taking advantage from the chemical reactions occurring between its internal elements [15]. On the other hand, also the opposite behaviour could be used to provide the definition of these systems: by using an external sources of electrical energy, this gets stored inside the electrochemical cells once that the chemical reactions are triggered and sustained in the opposite direction. Both the two definitions are important, since the first one describes the discharge of a cell, while the latter accounts for the principle at the basis of its rechage. The bidirectional behaviour presented above is only found in the so-called “secondary” cells, while the “primary” ones, differently, are only intended for a single-life application, and being not suitable for the recharge they are not applied in the field of the EVs—thus not studied in this work. Several different kinds of ESSs exist in engineering, and their classification is principaly made according to the type of cell over which they rely on. Indeed, from the most generic definition of these devices, it comes out that the energy conversion between an input and its stored form can be accomplished in many ways: mechanically, thanks to the deformation of an elastic element, or thermally, by working over a system’s thermodynamics. However, whenever the electrochemical cells are considered, the electrochemistry is the governing subject that has to be studied since it regulates the phenomena over which the batteries—which actually are the electrochemical ESSs—are based on.

Even within the category of the electrochemical cells, neverthelss, it is found a large diversity among the “types” of cells that could be used. Dozens of different concepts which presented a different chemistry governing their functioning have been built in the history, but the researches conducted the last century have highlighted that the most performant ones, and hence the mostly used, are the electrochemical cells based on the chemical reactions occourring respectively with and between the following compounds.

- Li (Li-Ion);
- Lead and acid;
- Ni and metal hydrade (NiMH);
- Ni and Cd.

The types of cells written above have shown the best results when applied to the field of the electric mobility. In fact, whenever an electrochemical cell is evaluated, the following parameters usually define its performances as well as it capability to sustain the requests of an electric powertrain:

- High energy density;
- High specific energy and specific power;
- High efficiency in the energetic conversion;

- Low self-discharge rate;
- Long calendar and cycle lives;
- Fast charge and slow discharge times;
- Low or even null self-heating;
- Large safe-operative temperature range.

Thus, let start by performing a rough comparison between the previously presented chemisties, where each one of the resulting electrochemical-based ESSs has its own advantages and drawbacks that necessarily need to be balanced, providing as output the best choice for the specific application. The four aforementioned cells with a resume of their own relative pros and cons, are presented in the following *table 5* [16].

TABLE 5 - Electrochemical cells

Cell's name	Relative pros	Relative cons
Li-Ion	• Outstanding specific energy and power • Long calendar and cycle lives • High efficiency • Good operating temperature ranges • High reliability • Eco-friendly materials • Low self-discharge rate • Fast recharge	• High cost • Safety concerns related to thermal runaway • Lithium and cobalt bottlnecks in the manufacturing chain • Weak recovery and recycling schemes
Lead-acid	• Low cost • Mature technology • Reliance on abundant and cheap materials • Good efficiency • No memory effect • Low self-discharge rate	• Modest specific energy and power • Short cycle life • Performance highly sensitive to temperature • Limited reliability • Long charging time • Safety concerns related to gas release
NiMH	• Low cost • Good specific energy and power • Good efficiency • High reliability • Eco-friendly materials • Good safety • Good operating temperature ranges • Fast recharge	• High self-discharge rate • Memory effect • Short cycle life • Weak recovery and recycling schemes
Ni-Cd	• Low initial cost • Outstanding calendar and cycle lives • High reliability • Good self-discharge rate • Good safety • Extensive operating temperature ranges • Fast recharge	• Modest specific energy and power • Memory effect • Low efficiency

As it can be seen, a set of good features is always present for each of the resulting batteries. However, as a starting point, one has to consider that their application is here intended for the though field of the electrical mobility, fact that led to the definition of the Li-Ion cells as the best and most performant ones in meeting the requirements of H and EVs, becoming the common choice among the other ESSs. Let consider, for instance, what has been put in evidence and proved to be not optimal in case of lead acid, NiMH, and Ni-Cd cells. In particular:

- **Lead-acid cells…**

  Despites largely reliable, they still present a short life-span. Moreover, the nominal voltage they're able to provide is low, being only around $2\ V$. Deep discharges of the battery, futhermore, produce lead sulfates that generally signs the "death" of the device, and are hardly preventible.

- **NiMH cells…**

  They have been largely used in the first HEVs, but due to the reduced provided autonomies have been put apart in the EVs' development, where longer full-electric travelling ranges are sought.

- **Ni-Cd cells…**

  Althought extensively used in many applications, they are no longer developed nowadays at all in the automotive field. In particular, this happened because of the discovery of a very short life-span whenever submitted to frequent charge/discharge cycles and a fast degradation of the cells is the principal drowback of this chemistry.

Beating the rivals with respect to most of the disadvantages listed above, the Li-Ion electrochemical cells result in giving batteries that are highly reliable, present a very long life and energy storage capacity, and are also able to operate at over twice the potential of the lead-acid or NiMH ones. Hence, among all the metals that are available for the cells' chemistry, the lithium is considered to be the most promising one. Furthermore, it is widely available in nature and nontoxic, light and electropositive, and all the resulting ESSs and battery packs are characterized by an outstanding potential for the energy conversion and storage. Nevertheless, the lithium "alone" is a very reactive chemical compound, and so it has been challenging in the last years to find a good compromise for its safe integration in the automotive field. To face up this latter aspect, Li-Ion batteries are no longer built using pure metallic lithium in their cells, but rather using Li-metal compounds that are still able to supply the necessary ions, elements over which the entire funtioning of the devices is based.

Concluding, it has to be said that apart from the different types of ESSs, other solutions are already present in the market but only account for a small shear of it, while for what concerns the future prospectives, the fuel cells are expected to outcome the remaining limitations still given by the Li-Ion batteries.

Batteries

The so-called "Li-Ion" battery (LIB) is today the mostly used rechargeable ESS in the world, also thanks to its extensive application in the automotive field. As it has already been shortly explained, its functioning is based over the electrochemical effects taking place within the basic elements that composes it, namely the cells. However, up to now it has only been shown why the Li-Ion cells are commonly preferred at the expenses of the other ones, i.e. those presenting different chemistries, but to properly understand the functioning of the electrical accumulators, a deeper analysis is required. Hence, in order to provide a more complete knowledge over the subject, in the following sections of this chapter and after a brief introduction to the technology, the working principles and the common materials involved in the construction of the Li-Ion batteries are going to be presented, concluding then with the common architectures found in the market.

Eventually, before to start focusing over the devices themselves, the appropriate terminology must be introduced. With the word “cell” only the basic electrochemical unit forming the battery is considered—i.e. the electrochemical cell—, even if nowadays the term “battery” itself is sometimes commonly used when referring to a cell, and vice versa. A most correct use of this latter, however, is found to be applied to the device that includes many cells together. With “battery pack”, finally, is univocally considered the collection of batteries together with the case, the electrical connections, and the electronics dealings with the control and the protection of the components. In between these two extreme units there is the so-called “module”, resulting by an assembly of batteries electrically connected between them in series rather than in parallel.

FIGURE 11 - Cells, modules, and battery pack

Batteries – **Discovery and application**

Despite the fact that only nowadays the electrical powertrains are getting equipped with Li-Ion-based battery packs, the very first battery has been developed and presented by Yoshino in the 1985, based on the earlier studies of Goodenough, Whittingham, Yazami and Mizushima. To highlight the importance in the technological discovery, later on in the 2019, the Nobel Prize in Chemistry was given “*for the discovery and the development of the Li-Ion battery*” to Yoshino, Goodenough, and Whittingham [17]. The commercialization of the device suddenly takes places in the 90s thanks to the tech giant Sony, showing an outstanding volume of sales. Today, the LIBs are well known power components of portable electronic devices such as smartphones, tablets, and laptops, but nevertheless these batteries have also become key elements in the development of the society towards the energy sustainability, finding their most important applications in both the H and EVs’ powertrains, being indeed the most promising ones in terms of performances, simplicity of construction, safety, and environmental impact of the whole manufacturing cycle [18]. At the end, recently, the largest shear of the market is found to be in the portable electronic devices, but in the last decades it is being overtaken by the increasing demand of the road transportation. Furthermore, the Li-Ion technology has also found uses in the aerospace sector, such as in satellites and in aviation, and even if it is still a topic under research, it has the potential to be utilized in power supply systems, both off- and in-grid connected. Great improvements have also been achieved in the medical field, for instance with long-life hearing aids, while for what concerns the sensors, many self-powered devices are nowadays largely used. The list of applications in which the Li-Ion batteries' discovery is found to play an important role can go on and on, highlighting once more the importance of these ESSs in the everyday-life. In this work, however, the focus will be on the automotive applications only, although a good knowledge about the subject finds countless perspectives both from an industrial and research point of view.

Batteries – **Components and functioning**

The functioning of each battery is possible thanks the effective integration of the four components that gives its internal structure, forming at the end the basic set of elements of a Li-Ion electrochemical cell:

- Cathode;
- Anode;
- Electrolyte;
- Separator.

Furthermore, some other additional elements have to be considered in addition to those giving the cells: the metallic collectors are the "terminal" part of the electrodes, where the electric potential gets built up, while the case provides the necessary leak-proof encapsulation of the internal structure, retaining the liquid electrolyte. At last, the electrical tabs, whenever are present, define the joining between the two collectors and the external circuit. Introducing then the functioning of a battery, let start defining in a general manner the anode and the cathode as two elements made of compounds containing lithium atoms.

It is possible to find a battery working in two opposite ways: discharge and recharge. However, since the recharge of an ESS is an externally sustained process, from now on the discharge will be considered as the common working condition of a battery, resulting from the natural occurrence of the chemical reactions taking place within the cells. It could be observed that, whenever the device is supplying energy to an external load, the anode is the reducing element which releases electrons in the circuit because of its oxidation, and hence, consequently, it is where positively charged lithium ions (Li^+) are produced. On the other side, the cathode is the oxidant element: it receives the electrons coming from the conductive circuit, and thanks to the chemical reduction which takes place at its surface recombines them with the Li^+ previously delivered by the anode. The principal features and roles played by the electrodes during the discharge of a battery are summarized in the following *table 6*.

TABLE 6 - Features and roles of the two electrodes (discharge)

Electrode	Pole	Type of agent	Chemical reaction taking place	Produces…	Receives…
Anode	Negative	Reducing	Oxidation	Li^+ and e^-	-
Cathode	Positive	Oxidant	Reduction	-	Li^+ and e^-

Obviously, the opposite behaviours in terms of produced and received elements is observed with the recharge of the ESS, as well as for the chemical reactions that are found to take place over the components, while both the poles and the type of agent describing the electrodes keep being the same. A clear schematic view of the functioning of an electrochemical Li-Ion cell, here for both the working conditions, is shown in the *figure 12*.

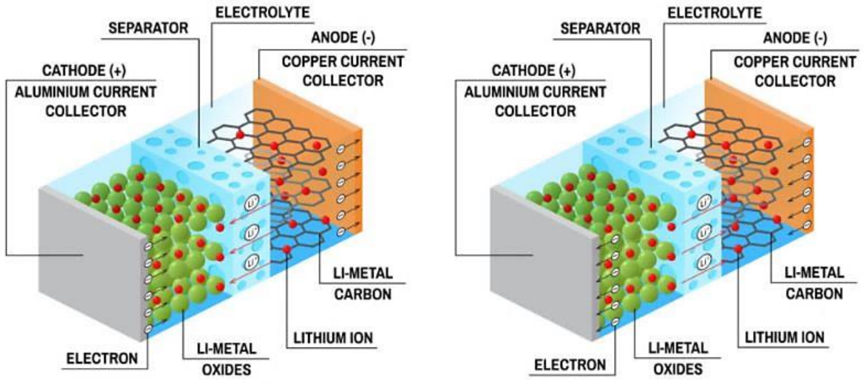

FIGURE 12 - Charge (left) and discharge (right) of a Li-Ion electrochemical cell

The motions of the ions and of the electrons within the devices are allowed thanks to the conductive media of which the cell is provided: indeed, the ions travel through the electrolyte and across a porous membrane—also called "separator" in the image above—while the electrons flow in the conductors forming the electrical circuit. Obviously, to have the correct functioning of the whole battery, both the electrolyte and the separator as well as the conductive circuit have not to take part to any internal chemical reaction. Furthermore, as it is well known, the electric current's toward is for convention set to be opposite with respect to the electrons' direction of motion: during the discharge, the electrons move from the anode to the cathode, and the current flows from the cathode to the anode, while on the other hand, the opposite happens during the charging phase. In the following *figure 13*, for instance, the discharge phase is reported.

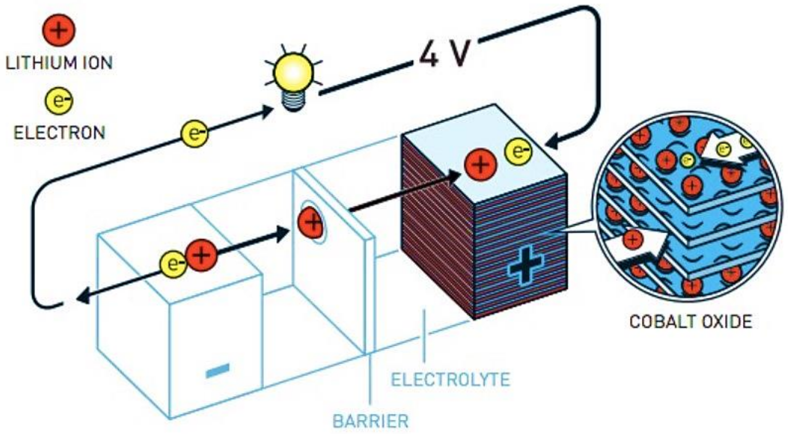

FIGURE 13 - Motion of electrons and ions during the discharge

At last, it is also important to report that the process of discharge lowers the electrical potential built in correspondence of the battery's terminals due to a reduction for the whole cell's electrochemical potential, while, on the contrary, during the charging phase, the electrochemical potential gets re-established.

Batteries – **Materials**

Several types of Li-Ion batteries can be found in the market, and despite the fact that their technical functioning is exactly the same, their properties largely change depending on the so-called "Li^+ donator", which is actually the type of cathode. Indeed, since the Li-based material of which the cathode is composed results to be one of the main determinant characters for the entire functioning of the cells—differently from the compound forming the anodes, which only slightly changes the property of the batteries—this has been chosen as the reference electrode. After extensive years of research and experimental campaigns, six compounds are found to be nowadays the mostly used ones in the creation of LIBs [19]:

- Lithium cobalt oxide (LCO);
- Lithium manganese oxide (LMO);
- Lithium iron phosphate (LFP);
- Lithium iron fluorosulfate (LFSF);
- Lithium nickel cobalt aluminium oxide (LNCA or simply NCA);
- Lithium nickel manganese cobalt oxide (LNMC or simply NMC).

Depending then on the compound, different types of phenomena are triggered by the molecular lattice of the electrodes, principally in terms of ionic exchanges and chemical reactions. The lattice structures presented by the four mostly used cathodic materials are presented in the *figure 14*.

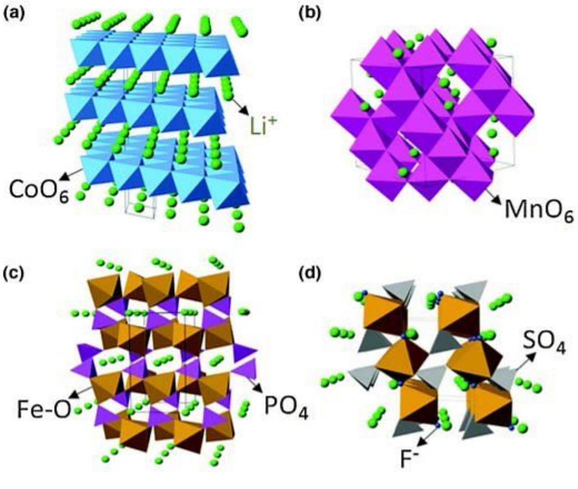

FIGURE 14 - Cathodic lattice structures (layered LCO [a], spinel LMO [b], olivine LFP [c], and tavorite LFSF [d])

It has to be highlighted the fact that all the different solutions show a higher impedance than that of the pure metallic lithium, outcome of a lower electrical conductivity and diffusion capacity. However, on the other hand, the advantage is found in the fact that by using them all the issues related to the reactivity of the pure metal are overcome. Addressed the choice of the compound, then, the manufacturing of the cathode is another challenging task: after extensive researches, it has been found that by powdering the Li-based material and successively blending it with highly conductive carbon provides the best results, with solvents and binders that are used to properly shape the thin foils in which the electrode gets manufactured. Obviously, it has to be reminded the fact that due to the variety in the chemistries of the compounds as well as because of the manufacturing processes, the different batteries results in showing various characteristics.

Speaking then of the anodic materials composing the Li-Ion batteries, the choice is quite restricted. In particular, these ranges between:

- Graphite;
- Lithium titanate (LTO)

The graphite provides the best results in terms of cell's performances, even if some battery manufacturers have recently started to use the lithium titanate ($Li_4Ti_5O_{12}$) as a non-graphitic compound. Apart from that, once again and despite the differences in their nature, the manufacturing processes used for the creation of anodes are the same found for the cathodes. In the *figure 15*, as it has been already done for the cathodic materials, are shown the lattice structures of the graphite and of the Li titanate.

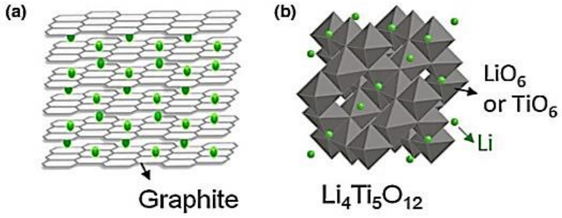

FIGURE 15 - Anodic lattice structures (graphite [a] and Li titanate [b])

Furthermore, a representation of how the Li^+ exchange takes place between cathode and anode, and where these particles are placed in the respective electrode's lattices, is provided by the *figure 16*.

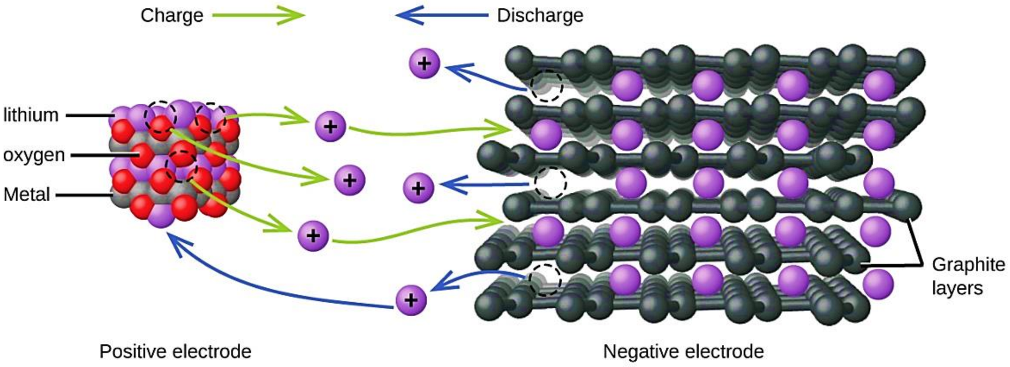

FIGURE 16 - Exchange and "deposition" of lithium ions

At the end, it is also important to recall that subsequent to the manufacturing process of the electrodes' materials, both the anode and the cathode are "pasted" respectively over a copper and an aluminium foil, which are so-called "charge collectors". Part of these collectors protrudes from the battery's case and are generally known as "poles": the poles, in turn, are connected to metallic sheets named "tabs", whose function is to provide a site for the successive joining of the metallic conductors creating the electrical circuit.

Summarizing, the performances of the Li-Ion batteries are largely dependent on the cell's materials: in particular the cathodic compounds play the most important role, mainly because of their chemical reactivity, which is in turn function of the lattice structures—where this latter aspect deals with the internal resistance of the material against the ions' flux, hence involving both the phases of extraction and deposition of the Li^+ from and on the electrode. In the following *table 7*, thus, the most important pros and cons [19, 20] for the four mostly used cathodic compounds are going to be summarized—considering the aforementioned LCO, LMO, LFP, and LFSF.

TABLE 7 - Properties of batteries (depending on the cathodic material)

Cathode name	Pros	Cons
LCO	• High theoretical specific capacity of $274\ mAh\ g^{-1}$ • Outstanding theoretical volumetric capacity of $1363\ mAh\ cm^{-3}$ • High average voltage of $3.8\ V$ • Low self-discharge • Good cycling performance	• High cost • Very low thermal stability and frequent thermal runaways • Capacity fade at high current rates or during deep cycling
LMO	• High energy density provided to the cell • Low cost • Outstanding average voltage of $4.1\ V$ • Eco-friendly materials	• Mn^{3+} ions tend to block Li^+ diffusion • Poor cycle stability • Low theoretical volumetric capacity of $596\ mAh\ cm^{-3}$
LFP	• Acceptable average voltage of $3.4\ V$ • Outstanding thermal stability • High power capability • Low self-discharge • Good cycling performance	• Low theoretical volumetric capacity of $589\ mAh\ cm^{-3}$ • Low electrical and ionic conductivity
LFSF	• Low cost • High average voltage $3.7\ V$ • Low activation energy and high recharge rate	• Very low theoretical volumetric capacity of $487\ mAh\ cm^{-3}$ • Low theoretical specific capacity of $151\ mAh\ g^{-1}$

The most recently developed cathodic material, only discovered in the 1995 and commercially lunched in the 1997, as well as the most promising one for the large batteries used in the automotive field, is the LFP. The chemical compound $LiFePO_4$, indeed, is now a certainty in the mass market of cathodes for both the hybrid and full-electric vehicles, even if the production of high-quality powders is still expensive and difficult. These cathodes result to be non-toxic and provide almost a null thermal runaway, in addition to the chemical stability shown over the long run [19]. However, cobalt-based cathodes still cover the largest shear in the worldwide production of Li-Ion batteries: against it, recently, many governments and privates have shifted their interests on the LFP due to its lower environmental impact, mainly for what concerns the whole manufacturing process of the raw materials, resulting this to be the most eco-friendly solution. The last generation ESSs show an outstanding high cycle life together with a long calendar life, which generally exceeds the 5 years, together with a reasonably large energy density. The self-discharge rates of LFP Li-Ion batteries are extremely low, and furthermore, the electrical potentials result to be almost independent from the “amount” of discharge—aspect, this latter, which is going to be seen more in detail with the definition of the “SoC”. Moreover, another advantage is that the charging phase for these ESSs does not cause issues if the voltage is kept below the threshold value of $4.5\ V$: fast recharges are admitted with this kind of technology, and no internal degradation is observed.

Another fundamental component for the functioning of the electrochemical cells is the electrolyte, and it is generally found in form of a liquid mixture of lithium salts and organic solvents. The electrolytic bath provides the medium for the movement of the Li^+ between the two electrodes, and hence the correct choice is rather important: it has to fit both chemically and physically with the two electrodes, giving the possibility to the ions to flow between the two terminals.

Commonly used lithium salts are:

- Lithium-hexafluorophosphate (LiPF6);
- Lithium-perchlorate (LiClO4);
- Lithium-hexafluoroarsenate (LiAsF6).

On the other hand, the organic solvents used to create the mixture allow to increase the Li^+ mobility within the bath, resulting to be fundamental for all the cell’s performances. The mostly used organic solvents for the purpose are:

- Ethyl-methyl-carbonate;
- Dimethyl-carbonate;
- Diethyl-carbonate;
- Dropylene-carbonate;
- Ethylene-carbonate.

Apart from these liquid-based electrolytes, solid ones have been recently developed: they manage to conduct the Li^+ replacing the conventional organic electrolytes, which are flammable and toxic. In addition to drastically improve the safety of the battery, solid state electrolytes works well in conjunction with Li-metals at the anode (Li-titanate) and increase the cell voltage and the energy density of the battery. Among the others, sulphide-based solid electrolytes (and principally the “Lithium Tin Phosphorus Sulphide”, $Li_{10}SnP_2S_{12}$) are the most highly sought and promising ones adopted for all-solid-state Li-Ion batteries, mainly thanks to the high conductivity the provide.

Finally, the last component having a role in the Li-Ion batteries that still needs to be seen is the porous separator. The component is found to be settled inside the electrolyte bath, between the cathode and the anode, acting as a safety element for the whole battery. Its aim indeed is to prevent the direct contact between the two electrodes—which otherwise generates the so-called “short-circuits”—while still being permeable to the Li^+. The porous membranes are generally found with thickness around $15 \div 25\ \mu m$, made of polymeric compounds based on polyethylene and polypropylene. The major issue shown by these elements is that in case of early signs of thermal runaways they could start to melt, losing the permeability to the ions’ flow by which are characterized: whenever the problem appears, the cell is found to be irreparably damaged, but still being able to avoids major negative consequences such as an uncontrolled overheating, and hence, consequently, even the explosion of the battery pack. Today, different kinds of ceramic separators are commonly used, while, as a cheaper solution, polymeric separators which are only superficially coated with ceramic layers are intensively adopted. These latter solutions concur in providing superior thermal and chemical stability, lower internal resistances to the ions' flow, and a faster Li^+ pick up, all thanks to a more wicking element.

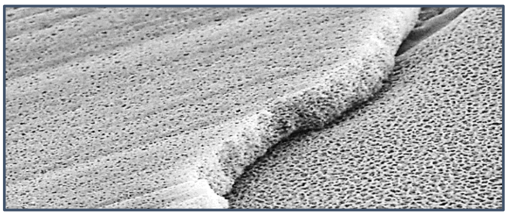

FIGURE 17 - Ceramic-coated separator (view at the microscope) [21]

Batteries – **Architectures**

Now that the physical and electrochemical phenomena regulating the functioning of an ESS have been explained, it is interesting to see how all this gets technically applied in the Li-Ion batteries, which, despite the differences for what concerns the used internal material, can be found in three different shapes [22]: prismatic, cylindrical, and "pouch".

- **Prismatic**

  Introduced in the early 90s, no universal format exists for the prismatic batteries, since each manufacturer design its own. This shape is principally adopted whenever the machine carrying the devices undergoes to some sort of mechanical efforts, since the rigid external case is made of aluminum—a light but rather stiff metal—and designed so that the whole body can withstand shocks, providing an optimal mechanical resistance. Furthermore, the regular shape of the cell assures to optimally expolit the spaces within the battery pack. For what concerns their use in the electric powertrains, in both H and EVs, these batteries are normally provided with capacities ranging between $20 \div 50\ Ah$.

FIGURE 18 - Prismatic Li-Ion battery (Panasonic)

- **Cylindrical**

  Cylindrical LIBs are adopted for both the automotive field and "big" transportable electronic devices. In order to provide a view on their spreading in the market, only in the 2013, 2.55 billions of these components were globally produced. As a matter of fact, Tesla's battery packs specifically rely on the units represented in the *figure*

19. However, the two main drawbacks that are found with this architecture is the high weights together with the low packaging densities. Nowadays, they are manufactured to supply capacities of $2.2 \div 3.9\ Ah$, and even if these latter values are largely minor than those seen for the prismatic cells, the so-called cylindrical "18650" ones—$18\ mm$ of diameter and $65\ mm$ of height, shown in the image below—are characterized by the highest energy density in the market, and thus are largely exploited in the electrical mobility.

FIGURE 19 - Cylindrica Li-Ion battery (Panasonic)

- **Pouch**

The pouch batteries are a new concept of architecture for the Li-Ion cells, only introduced in the late 90s. They are the smallest ones among the others and are not equipped with any sort of external case able to bear deformations and shocks in a comparable way with the previously seen architectures: only a thin polymeric ply covers the cells' internal elements, preventing leakages and exposition to the environmental factors. However, due to the fact that the battery pack is properly protected from an own rigid external case, also these elements suit for severe working environments. The pouch batteries show the most efficient use of space within the battery pack, achieving the $90 \div 95\%$ of "package density", and are characterized by capacities up to $40\ Ah$. The issues with this architecture, on the other hand, are mainly related with the excessive swelling: the internal overpressure could indeed crack the thin cover compromising the whole functioning of the cells.

FIGURE 20 - Pouch Li-Ion battery (Targray)

Finally, it should be highlighted the fact that the choice of a battery's architecture for a particular application is mainly governed by its cost, the desired life-span, and by the required densities of energy and of power of the battery pack. Furthermore, concluding and putting together all what has been seen in this chapter, a clear view at the different architectures internal elements' disposition is provided in the following *figure 21*.

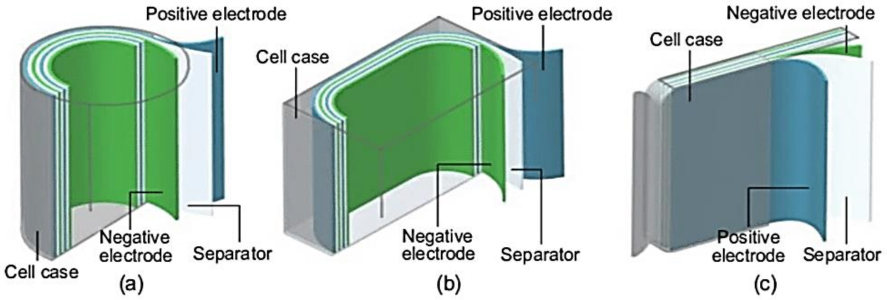

FIGURE 21 - Internal structure of Li-Ion batteries (cylindrical [a], prismatic [b], pouch [c])

Batteries – **Performances**

In the last sections of the work, the general knowledge over the most important aspects characterizing the Li-Ion batteries has been addressed: both the hardware of the ESSs and their internal functioning principles have been shown, as well as some general peculiarities coming out from the different technologies that could possibly be adopted. However, it would be now interesting to focus over a more practical presentation of data in order to highlight, once more, the advantages that the adoption of the Li-Ion electrochemical cells is able to provide with respect to the other solutions in terms performances. Thus, in the following *table 8*, the average specs expected to be found for the principal ESSs are summarized [1, 19, 20]. Note that by simply comparing the data it results to be clear why the adoption of the Li-Ion batteries has now taken an accelerated pace, leaving behind the development of other previously used chemistries.

TABLE 8 - Expectations for the mostly used ESSs

ESS	Spec. energy $[Wh\,kg^{-1}]$	Spec. power $[W\,kg^{-1}]$	Energy density $[Wh\,l^{-1}]$	Power density $[W\,l^{-1}]$	Max. potential $[V]$	Cycle life $[-]$	Operative temp. $[°C]$	Spec. cost $[\$\,kWh^{-1}]$
Li-Ion	70 ÷ 200	250 ÷ 2000	140 ÷ 400	400 ÷ 500	3,7	500 ÷ 6000	−20 ÷ 50	670 ÷ 2000
Lead-acid	20 ÷ 50	25 ÷ 350	60 ÷ 180	400	2,0	200 ÷ 2000	−30 ÷ 50	60 ÷ 270
NiMH	30 ÷ 80	140 ÷ 500	50 ÷ 150	210 ÷ 360	1,2	500 ÷ 2000	−40 ÷ 60	250 ÷ 300
Ni-Cd	60 ÷ 120	150 ÷ 1500	130 ÷ 400	400 ÷ 480	1,2	500 ÷ 1500	−20 ÷ 60	200 ÷ 1000

Putting together all the information acquired by the table above, it is clear why the LIBs result to be the best for what concern an application in the field of the EVs.

On the other hand, focusing then more in detail on the different types of Li-based cells, these have been seen to be largely influenced by the different chemical compounds used in the two electrodes. Today, in fact, the battery manufacturers still produce cathodes with many materials, but yet outstanding results are obtained with the three mostly diffused compounds: LCO, LMO and LFP. Once again, some expected specs for the usually found combinations of materials between cathodes and anodes are summarized, here in the following *table 9*.

TABLE 9 - Expectations for the mostly used types of LIBs

Cathode	Chemical formula	Reference anode	Cell's potential $[V]$	Cell's s. energy $[Wh\ kg^{-1}]$
LCO	$LiCoO_2$	Graphite	$3.7 \div 3.9$	140
LMO	$LiMnO_4$	Graphite	4	120
LFP	$LiFePO_4$	Li titanate	$2.3 \div 2.5$	100

Apart from the great results that have been achieved in the last years, many efforts in the technological development have been concentrated at increasing the specific energy the cells are able to supply, and by working on innovative compounds the target of $250\ Wh\ kg^{-1}$ is expected to be eventually achieved in the near future. Moreover, by increasing the knowledge and the experience of the manufacturers, also the aspects related to both the device's degradation and cycle life are surely going to be improved too. Nevertheless, the working safety is a crucial condition for the battery commercialization, and this may require sacrifices for what concerns the achievable performances in the characteristics mentioned above. Concerning the costs of the lithium cells, finally, they are expected to get significantly reduced in the short term, with the possibility to achieve levels of $350 \div 500\ \$\ kWh^{-1}$ in the 2025, up to even $200 \div 300\ \$\ kWh^{-1}$ in the 2030 [23]. Obviously, the decrease in the market's prices will be pushed down only as a consequence of the worldwide requests of such devices, since no new material is expected to hit the product lowering its cost.

Operative challenges

When compared with the other ESSs the LIBs certainly provide several advantages: among the others there are the very high energy and power densities, long lives and cyclability, environmental friendliness, etc. However, when the application regards the automotive field, several concerns arise with respect to the safe and optimal use of these devices which generate real challenges affecting both their design and final operative conditions. As a result, some restrictive working conditions must be defined because of some limitations the cells have, both of technical and practical nature, as described in the following *table 10*. From a technical point on view, for instance, the likelihood of fires and short circuits in the battery pack must be prevented, meaning that there is the necessity to create an adapt environment. On the other hand, the limited physical characteristics of the batteries create in some way the need to face up problems raising by the overall weights and dimensions.

TABLE 10 - Resume of the LIBs' main problems

Cells' limits	Dealing with their design…	Dealing with their materials…
Issues	• Weight • Dimension	• Capacity • Overheating • Short circuit

The list of the principal challenges that one has to face up for the effective integration of the electrochemical ESSs when building a battery pack is provided in the following pages, together with some technical solutions that are nowadays commonly used.

- **Weight**

One of the most important differences that is found between the use of ESSs and fossil fuels is the amount of energy density they are able to provide. This property is defined as the quota of energy supplied per unit of weight by the media itself that releases the energy, hence the whole battery pack when the batteries are considered or, for instance, the liquid gasoline for the fossil fuels used ICEs. The modern Li-Ion batteries present an average specific energy of “only” $150\,Wh\,kg^{-1}$, while the gasoline is able to provide specific energies between $12 \div 13\ kWh\ kg^{-1}$ [24]: for this aspect, fossil fuels are better than LIBs of a factor of eighty(!). Moreover, it has also to be considered that the gasoline, being liquid, is also more practical to be transported within a moving vehicle. As an outcome, when the battery packs are designed for pure EVs, these ends up being necessarily big and heavy in order to be able to store the necessary amount of energy when working. Thus, a lot of efforts in the last years have been put in decreasing the vehicles’ weights, since the higher is the load to be moved, the higher the consumption of energy will be, and as a consequence the ESS gets discharged “faster”.

One way in which it is possible to globally reduce the weight of a vehicle is by working over the chassis of the car: the adoption of lightweight and composite materials is the common choice, both for their low burdens and high mechanical properties. On the other hand, it is more interesting for both HE and EVs to design a more efficient battery pack, since it accounts for a very big share in the whole weight of the body. For example, it has been seen in the *table 4* that the total weight of a Tesla Model 3 is of $4036\ lbs$, and considering that the vehicle’s whole battery pack weights $1054\ lbs$ [25], it results that this latter accounts for more than the 25% of the total load to be “fed” by the ESS. Li-Ion batteries are already the best solution among the ESSs in term of provided specific energy, but further technological and design improvements in the cells and in the packs may lead to rise the performances: very light aerosol-like electrolytes, module and pack’s housings, as well as new solutions for the modules’ cooling and power electronics, all together will concur in the future to maximize the outcomes reducing the weights.

- **Dimension**

Similarly to previous problem, another relevant aspect that limits the use of the ESSs regards the overall size the battery pack takes. To limit the dimensions of the pack it is once again useful to have batteries presenting their specific energy as high as possible, even if in this case the best indicator is the energy density (or energy capacity) of the device. Also under this point of view the Li-Ion batteries are the best solution among the other ESSs, being able to present levels of $140 \div 400\ Wh\ l^{-1}$. Moreover, apart from the general size of the cells, their shape is of fundamental importance for the energy density of a pack. The following *figure 22* provide a good view of the different setups of the modules derived by the different batteries’ architectures.

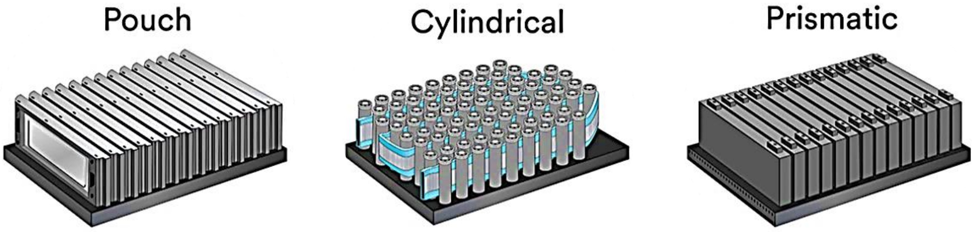

FIGURE 22 - Types of cells and resulting modules

Dealing with the dimensions of the pack, furthermore it has also to be considered that whenever the cells result to be more prone to overheating it is mandatory to try spacing them out, and obviously the opposite should happen in case of a good thermal stability. At the end, the resulting parameter to be considered dealing with the physical disposition of the cells within a battery pack or a module is the package density, which gives in percentage the amount of space occupied by the cells within the entire disposable one provided by the upper-level system.

- **Capacity**

Directly dealing with the autonomy of an EV, the so-called "capacity" of the single cell is the parameter interest: while the first measure is expressed in miles or km, the latter considers more the electrochemistry of the battery, specifying the amount of energy that the ESS is able to contain by indicating the constant current that could possibly be delivered within an hour of operation, taking like this the physical dimensions of Ah. One of the main problems of the batteries in general is that their capacities are function of some "external" parameters, and hence vary, sometimes significantly. Most of all, the temperature is one of the most important factors influencing the performances of the ESS: under standard conditions, the autonomy of the vehicle is maximized, but the problem is that this decreases for higher temperatures and fall of even a greater extent for lower ones—generally below the $0\ °C$. The control of the heat fluxes normally involved in the functioning of the battery pack takes place with an appropriate thermal management system, which is going to be explained more in detail in the following chapter of the work.

- **Overheating**

Being the major character in the capacity's fade, the problem of overheating for cells also affects their physical internal health, and hence have to be properly characterized apart. Neglecting the changes in temperatures given by the environmental conditions, the rising and lowering of the temperature always take place within the battery pack. For instance, during the functioning of one battery, in case of both charge and discharge, the ESS has to deal with variant temperatures: it is known that when the devices are providing the peak powers, the Joule dissipations within the electrical circuits are remarkable, and if the structure of the pack is not designed to withstand the working conditions by ejecting a certain amount of heat, very high temperatures may be reached inside the case. Apart from the lowering of the performances, the extreme risk is to end up with thermal runaways, i.e. the uncontrolled increases in temperature self-sustained by the electrochemical reactions taking place within the cells. This phenomena may even lead to explosions and emissions of toxic gases, with catastrophic consequences for the vehicle's passengers. Depending on the involved chemistry, it has been found that the ESSs present different ranges of temperature in which are able to work effectively and safely, without consequently presenting decaying performances or risks of thermal runaways. The Li-Ion batteries show one of the highest thermal stability among all the other ESSs, together with a reasonably large safe operative range, normally comprised between the two extremes of -20 and $50\,°C$. However, despite these positive features presented by the LIBs, the presence of a thermal management system is commonly required in order to control and tune the properties found at the level of the cells: this increases the costs, the design complexity of the pack, and decreases the overall energy density of the electrical source in an EV.

- **Short circuit**

Short circuits can be found to take place inside the electrochemical cells and are another issue to be considered in the pack's design, since the phenomenon can trigger itself even spontaneously, causing thermal runaways. When a LIB is under charge, as it is now already well known, Li^+ travel from the cathode to the anode, while flow on the opposite way during discharge. At the end of a recharge-discharge cycle, in correspondence of the anode, the net amount of ions reaching it (during the charge) and then leaving it (during the discharge) is major than zero—i.e. a certain amount of ions, after two subsequent "specular" operations of charge and discharge, remains over the anode. Piling up several of these operations during the life of a battery, the phenomenon results in spiny projections, also called "dendrites", as shown in the *figure 23*. The dendrites grow starting from the anode's surface up to reaching the separator, where, if this latter gets overcome, a short circuit may arise whenever they touch the cathode.

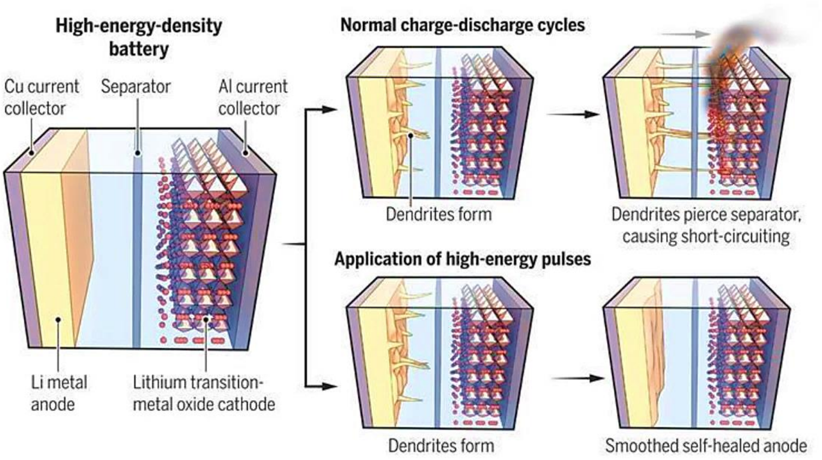

FIGURE 23 - Formation, development, and prevention of dendrites

One interesting way in which the phenomenon may be avoided is to recoat the anode with materials that either block, deviate, or are able to contain the dendrites during their formation. However, the presence of the dendrites can be also allowed for a certain time, as long as no damages take place within the cell, being then eliminated. For instance, it has been seen [26] that whenever high energies are involved, the inner temperatures of the batteries may increase up to reach $60\ °C$, which is a limit value low enough to assure the components' safety, but also high so that the diffusion of the retained ions forming the dendrites is stimulated. Hence, as a result, the short circuits could get prevented while the previously "wasted" ions are let to complete their run.

To conclude this last chapter, it is important to recall the fact that all the limitations listed up to now are proper of the electrical drivetrains for EV, brought by the ESSs themselves. However, several technical solutions in the last years have helped the integration of these cells within the moving vehicles, thanks to all the engineering breakthroughs that have concurred together in the creation of a rather complex but almost-perfectly functioning type of energetic system: the battery pack.

Chapter 3

EV’s battery pack

Purpose and functioning

The functioning principles of a Li-Ion battery, together with the materials that compose it, the advantages provided as well as the concerns met when it is used, are now all well-defined elements. From an engineering point of view, then, to see how these small cells could be effectively integrated in the electrical powertrain of an EV, is important to go up of one conceptual level in the system, studying the battery pack. The battery pack (shortly called, since now on, “BP”) is considered to be the heart of the EV. Starting from the fact that the battery alone is not enough “capable” to support the requirements of an electric motor in terms of energies and powers, hundreds or thousands of these cells must be connected together: the devices are piled up together and arranged in standard units, the modules, which ends up forming the final BP with a precise set of characteristics and properties. The final purpose in the creation of this quite big system is to create a reliable unit able to be the power source for the whole vehicle [27], meeting the high requirements of the electric motor. An idea of the complexity of a BP, containing in it several modules together with the power electronic and the management subsystems, is provided in the following *figure 24*, where the BP of the Audi hybrid Q7 e-tron is shown. Note that, since the vehicle is a PH one, the dimensions of the BP are very limited if compared to those of a pure EV.

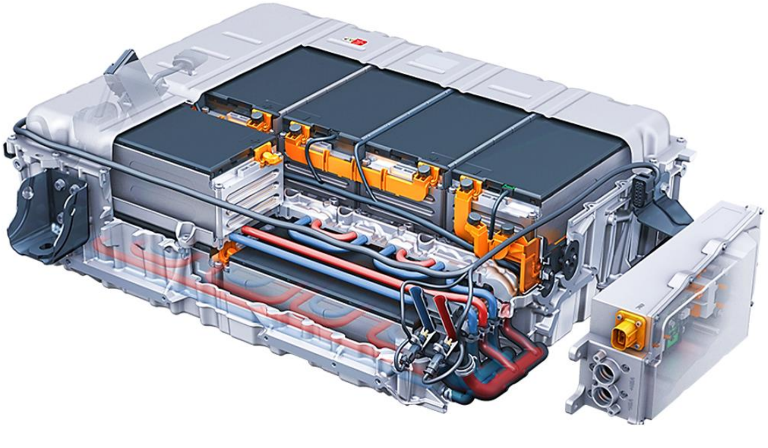

FIGURE 24 - Audi hybrid Q7 e-tron BP [28]

Being the BP basically formed by a high number of batteries, the pack itself can be considered as a large ESS on its own: from now on, indeed, in order to provide a clear terminology, the pack will be said to be a “global” ESS from the vehicle point of view, formed by many “local” ESS—i.e. the Li-Ion batteries. Thus, resuming, the BP’s presence is a necessity in both H and EVs, since it gives access to several advantages in what concerns many aspects, differently than simply obtained by having batteries connected together. In particular, the global ESS results to present high and stable voltages and energies and assures the necessary protection and integration of the subcomponents and systems used for the correct functioning of the whole electric powertrain.

Here in the following, a set of important topics to be discussed is provided, highlighting the benefits of using a battery pack in place of simply connected cells.

- **Voltage**

The BP presents at its terminals a high voltage, major than the one found in the small local ESSs. This comes from the fact that connecting together the cells, the voltages at their tabs can be summed up or not, respectively when the “in series” or “in parallel” connections are used. More in particular, the “in series” connection is performed joining two terminals presenting the opposite polarity, while the “in parallel” one, on the contrary, is found whenever two tabs with the same polarity are connected together. A schematic example regarding the “in series” connection between batteries is provided in the *figure 25*, from which also results easy to think about the “in parallel” one.

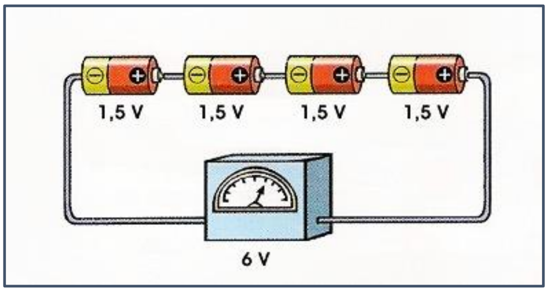

FIGURE 25 - "In series" connection of cells

In this field, the presence of a battery pack mainly allows a safe and stable allocation for the small batteries, as well a protection for the electrical wiring nd power electronics which is involved in the local ESSs’ functioning.

- **Energy**

The global ESS presents a very high energy content since it simply sums up the ones of the cells. Differently from the previous point, here the global energy is tried to be maximized, and considering the amount of batteries that a pack contains, the outcomes in terms of kWh are remarkable. However, the importance I building up a BP are mostly the same already depicted above.

- **Protection**

The battery pack is also intended to structurally protect the batteries and the electrical connections from the external environment, enclosing them inside a protective light case. In this way, the previously seen issues related to shocks, for instance, are no longer a problem for the local ESSs, whatever they architecture is, as long as the box is found to be properly designed to bear these efforts. In general, it could be said that the design of the housing depends to a great extent on the components it has to accommodate, and to the physical protection it has to provide for them: in the automotive field, where high powers and high energies are involved, a very stiff but light case is necessary. For this purposes, hence, the aluminium is the best choice, both for its high specific properties that come with a reasonably high heat dissipation capacity, adding a contribution to the heat removal which is performed by the cooling system.

- **Integration**

  In addition to the previously mentioned abilities, the battery pack also accommodates the necessary monitoring systems, heaters, coolers, and the devices for the electric protections, all together within a single and safe environment. One great example of integration is the one of the sensors: dealing with the battery monitoring system, the on-board computer relies on a software examining the data coming from several sensors, which are found to be directly integrated inside the housing walls, hence really isolated from the external environment.

Design features

Since the BP is not simply considered as an array of small batteries, but rather it also includes the power electronics and the necessary systems to assure its functioning, it results to be a very complex system to be designed and placed accordingly on board in a vehicle. Despite the improvements in the field of safety that have been made in the last decades, for what concerns the large BPs used in the EVs, concerns related to the devices' functioning during the normal drive are still present. The issues are generally thought to derive from two different sources: it has been studied that many factors affecting the reliability of the Li-Ion technologies arise during the manufacturing process, but also a long and continue exposition in time to extreme environmental conditions may affect the outcomes of the EVs. Belonging to the first class of problems, they derive from the chemical nature of the materials composing the cells: when impurities are present, as well as when irregular concentrations and non-coherent joining procedures are found, the batteries may act in unexpected ways. On the other hand, the environmental temperatures at which the vehicle gets exposed, pressures, mechanical and thermal shocks, vibrations, etc., all belongs to the second class of problematics. As a consequence, during the years, several strict regulations have been introduced in order to improve and to guarantee the safety of use of the local ESSs, providing a precise "state of the art" to be followed in both the manufacturing and testing of batteries: the most followed in this field are the SAE ones, related to the mechanical design of the pack and to the evaluation of its performances. Furthermore, among all the advantages that result when a standard is coherently followed, it could be found that after many years the technology at the basis of an electric vehicle have been normalized becoming reliable, understandable, and easily reproducible [28].

A safe and reliable operating BP needs to carry with its design several necessary features able to contrast the most important and dangerous problems taking place when the vehicle is travelling. These issues, as it has already been introduced in the last chapters, mainly are:

- Thermal runaways of the cells;
- Internal occurrence of vibrations;
- Structural internal damages due to crashes.

Furthermore, in addiction to each one of these issues, also the sliding motion of the cells within the modules must be restricted, so that electrical failures in the pack are preventively avoided. Considering as a starting point static and constrained cells within the case, the following list presents the design features that are suggested to be used by the standards.

- **Against thermal runaways…**

Let start defining the so-called “thermal runaway” as the beginning of an exothermic chain reaction where the batteries start to self-heat at a rate of more than $0.2\ °C\ min^{-1}$, according to Hallaj et all [30]. Passed that threshold, a further heat generation leads to an even higher self-heating rate and eventually ends up with the spontaneous combustion of the chemical components forming the cells.

Thermal runaways can arise due to different problems within a battery pack:

- Short circuits in the electrochemical cells;
- Physical abuse of the batteries—i.e. deep discharges;
- Manufacturing defects;
- Extreme environmental temperatures.

One of the solutions that is normally adopted in the BPs in order to prevent the thermal runaways of the batteries is to provide design in which this is found to be divided into a number of isolated compartments divided by means of thermal barriers—i.e. the modules. Furthermore, an air gap is required to be found between the modules as well as at the top and at the bottom surfaces, since these spaces denies any form of conductive heat exchange. Moreover, at the cell level, several rigid spacers are used, settled between adjacent batteries, as it is shown in the *figure 26*. Furthermore, it is useful to note that in order to maintain a low mass of the whole pack, and hence maintaining also a high specific energy, the spacers within the modules are only locally placed in correspondence of the upper and lower part of the batteries, and not running along all their heights.

FIGURE 26 - Cylindrical Li-Ion cells with spacers

- **Against vibrations…**

The most advanced BPs are also designed to isolate the modules from the undesired vibrations that originate at the level of motors, transmissions, and wheels in contact with the irregular ground. Apart from the problems that can be met if the batteries are not properly constrained, dynamic loads develop, acting then over the subsystems and so damaging the electrical connections. Furthermore, for resonance frequencies around the $100\ Hz$, the issue is that delamination could take place between the plies forming the electrochemical cells (i.e. electrodes and separators) within a battery. It is mandatory to prevent this latter phenomena, since it was one of the main causes of the low life span presented by batteries in the first EVs. To stabilize the entire BP it is usually applied a compressive force over the panels creating the case whenever these are fastened to the frame–-which could be seen as the “skeleton” of the BP. On the other hand, speaking of the electrical connections between the tabs and the conductive wires, a solution where the tabs themselves “wrap” the conductors gets usually adopted, so that, for instance, problems related to the forming of ageing cracks in welded seams due to small vibrations are avoided.

- **Against crashes…**

Because of its dimensions, the BP is usually placed in the underbody of the vehicle where a more horizontal development rather than a vertical one is allowed, exploiting like this the free spaces resulting from the elimination of the exhaust system previously present in the ICE-based vehicles. Also, being a heavy component, the pack should be positioned in such way that the overall cars’ centre of gravity remains low, and, from the thermal point of view, it needs to be placed in such a way so that the appropriate air recirculation is received and consequently the heat dissipation is allowed and maximised. Given the risky disposition of the BP that at the end results to be mounted beneath the seating area, as it is shown in the example provided in the *figure 27*, the integrity of the BP must be preserved in case of impacts coming from the rear, front or side directions. This latter aspect is generally reached initially by spacing it apart from the front and the rear ends of the chassis, while, for the lateral impacts, a set of shocks absorbers together with sandwich panels form the protection media.

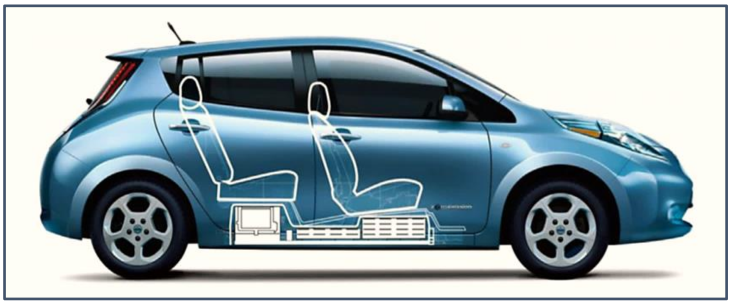

FIGURE 27 - Nissan LEAF positioning of BP

Apart from the low energies that can be exchanged in small hits and ends up being simply “discharged”, heavy damages of the BPs with catastrophic consequences may result from tremendous impacts at high velocities. The saving of the battery pack is accomplished thanks to a series of motion converter: the systems are nothing more than kinematics able to instantaneously move and rotate the box, settling this into a different position, at an higher elevation and no longer parallel to the underbody of the vehicle. These solutions are commonly adopted to preserve the integrity of the battery pack, but although the “central solution” of the battery pack with respect to the vehicle chassis is usually chosen, some carmakers still place it in the rear side of the vehicle, adopting consequently different safety strategies. However, perhaps because of the discretion of the companies, Arora et all [29] do not provide an objective explanation of the variants, but these may be finally imputed to both the dimensions and weights of the packs and the impact they have over the dynamic of motion. Indeed, as it is now well known, the BP could largely change depending on the required performances, and another important aspect is given by the several needs of different types of vehicles: for instance, the optimal positioning of a BP for a sedan would not be the same one of a SUV.

Functioning status monitoring: BMS and TMS

The last part of the work has provided a good background over the common challenges that are found and have to be faced up whenever Li-Ion batteries are used in the field of the EVs, and hence integrated in the design of an electrical powertrain. In particular, two classes of issues have arisen, where each one has to be treated in a proper manner.

- **During the design of BPs…**

  The first class is mainly related to the design of the BP: it accounts for concerns related to the body such as the weight, dimensions, and optimal positioning within the chassis of the vehicle. However, each carmaker tends by its own to adopt the optimal solution that suits with the needs of vehicle, and hence these issues can be considered as overcome once that a precise battery pack for a certain product is built. In other words, it could be expected that each company already choses the best design for the specific purposes.

- **During the functioning of BPs…**

  The second class of problematics, on the other hand, deals with the values presented by some working physical parameters, and so with the pack's functioning: it does no longer account for some issues easily preventable during the design and the manufacturing of the job, but rather considers the phenomena taking place whenever the device is working, both at the level of the BP and of the electrochemical cells. High and low temperatures, high voltages and deep discharges as well as short circuits, all together concour in reducing the operative window in which the batteries are allowed to optimally work, and hence have to be effectively monitored.

Wanting to analyse more in the detail the latter point, it is necessary to better understand how the characterization of the working parameters is performed by introducing the so-called "battery management system" (shortly called, since now on, "BMS") and "thermal management system" (shortly called, since now on, "TMS").

- **BMS**

  A BMS is defined as an electronic system that studies the status of a rechargeable BP in real-time, controlling its subcomponents' behaviour during the working phase. It is mainly aimed at restricting the batteries from operating outside the safe functioning area by calculating data, reporting them to the on-board softwares, integrating these with the environmental parameters, and studying the outcomes. At the end of the control loop, the BMS provides feedbacks to the BP for adjusting some working parameters of the cells, such as temperatures and the voltages at the terminals, but also acts balancing the capacities of the ESSs. Obviously, whenever the functioning of the cells is studied, this task deals with the observation of the two different charging and discharging phases. It could be generally said that low voltages and deep discharges usually lead to the reduction of the electrolyte's properties, while extremely high voltages and overcharges bring the positive electrode to develop a great amount of heat within the battery. Hence, ideally, thanks to the BMS every single battery composing the modules would be working under proper operating conditions, and faults get preventively avoided thanks to fault diagnoses. Nevertheless, the BMS is able to provide different important functions, but the greatest one deals with the thermal control and correction feedback [31]. Every time that a vehicle is travelling, indeed, one of the most important parameters to be checked within the battery pack is temperature: it defines the working status of the entire device and assures to have a safely working BP, performing appropriate charging and discharging performances. For the management of the aforementioned quantity, however, it is necessary to implement the BMS with a TMS.

- **TMS**

The operations performed by part of the cooling system relies on the instruction coming from the BMS: depending to the temperature distribution inside the BP, indeed, the BMS enables the TMS to start heating or cooling the modules, so that their functioning keeps being in the best-performances temperature range. High-precision thermocouples are found to be placed all around and inside the BP and the modules, detecting the temperatures in play, and whenever a risk of fault is predicted by the on-board software of the BMS, this latter selectively enables the TMS to work over that specific portion of the device, tuning its temperature.

The "hardware" at the basis of the TMS takes usually advantage from the action exerted by one of the following cooling media [32]:

- Fresh ambient air;
- Liquid water with glycol;
- Phase change material (PCM).

Air cooling systems generally present a very light structure, with a simple design, that obviously is translated in low costs of application. However, both the low conductivity and low specific heat capacity of the air, when used as heat removal medium, make the cooling performances not as good as the ones obtained with the other agents. Nevertheless, passing from a "passive" setup to an "active" one, thanks to the insertion of small fans and to the inclusion of small cooling channels running on the pack and modules' cases, the latter solution provides acceptable results in terms of heat removal. The use of phase changing materials, then, is one of the latest solutions adopted in the TMSs: thanks to the latent heat of PCMs, the heat generated by the small batteries can be effectively absorbed and "stored". The best results, however, are found whenever a liquid cooling system is used: both the high thermal conductivity and the high specific heat capacity of the liquid assure optimal outcomes. Furthermore, with this latter kind of cooling media, the resulting structure is compact, and hence less volume gets occupied by the whole battery pack resulting in high specific energies and powers. Tesla and General Motors, citing some carmakers, were the first companies to adopt this kind of TMSs at the expenses of the air-based ones. Physically speaking, it could be said that the ability of heat transfer between the coolant medium and the batteries basically depends on several fluids' properties, in particular on its thermal conductivity, viscosity and density, and on the flow rate whenever the system is of the “active” type.

Different setups of the TMS for effectively cooling the pack can be found: for instance the modules can be directly inserted into the cooling media, or differently, small channels are placed inside the panels created in the case of the pack, and so the coolants are allowed to flow throughout them. These channels, furthermore, even today are under crucial development: both the cross-sectional area and the path followed by the fluid are studied, resulting in different effectiveness. A practical example of a liquid-based TMS applied to a battery module can be seen in *figure 28*.

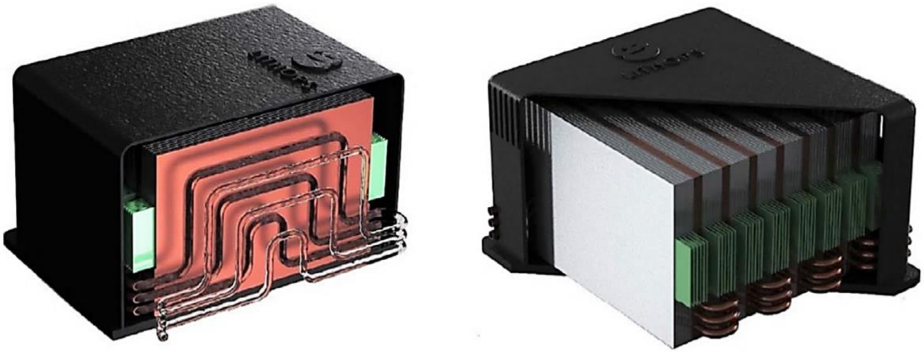

FIGURE 28 - TMS at the level of the module

To conclude the section, it is important to specify that the TMS is a necessity in most of the EVs: the electrochemical cells have to be maintained in a certain proper temperature range of operation, and since the inner self-heating always takes place, the need to control the consequences has become common. The temperature increase within a battery is a phenomenon triggered by the combination of different causes all concurring contemporary, and it is dangerous: this latter can induce undesired physical and chemical reactions within the cells, and the materials involved in their construction may lose efficiency, or even undergo to more dangerous behaviours. However, apart from the performances’ decay due to the normal heating of batteries, the most critical working conditions are found to be reached above $50\ °C$. Also, the TMS takes care of the temperature decrements below the $0\ °C$ since even if the safety operational limit is settled at $-20 \div -30\ °C$ for the LIBs, the performances of the ESSs lower of a great extent whenever these works in a very tough environment.

Engineering working parameters

To monitor and tune the actual estate of a BP, the BMS works with a dedicated software: each control loop performed by the digital core needs several input to be communicated, so that certain outputs allow the controlled physical quantities to vary accordingly depending on them. For instance, the TMS receives as input, coming from the BMS. the temperature adjustment that must be provided by the cooling media, and hence sets its flow rate within the cooling channels. On the other hand, other parts of the BMS are intended for the control and monitoring of the electrical quantities. Here, the “form” in which the energy gets supplied to the external loads has to be properly computed and tuned, since quantities such as voltages, currents, and capacities of the batteries, all together define the performances of the entire powertrain. However, when dealing with the working status of the cells, apart from the standard physical signals measured by the appropriate sensors, the BMS has to control different abstract indicators. Hence, summarizing, the signals processed by a BMS can be of two different natures: from one hand, some of them are direct measurements of physical quantities, for instance voltages and currents, while on the other hand, others result to be non-physical parameters by which it is possible to estimate the ESSs' status. In the following pages, taking advantage from the work of Lu et all [33], the most important operative parameters are presented together with the methods used by the BMS to estimate or directly compute them.

Engineering working parameters – **SoC**

The state of charge of a battery (shortly called, since now on, "SoC") denotes the quota of the remaining electrical energy still able to be delivered with respect to the total "initial" one, present once that the battery was fully charged. As a consequence, the SoC ends up being a percentage: when it is equal to 100%, then it denotes that the ESS is fully charged, while, on the contrary, when is signs 0%, it means that the device is found to be empty, since no available energy is left to be used. To compute the SoC, as it has been said, the amount of energy present within the battery is used: for this purpose, is computed the capacity of the cell, measured in Ah. The dimension denotes the amount of current that can be constantly delivered by the battery in an hour to be filled out. Obviously, knowing the SoC and the initial capacity of the battery (C_{in}, where in is for "initial") it is simple to know the remaining energy present within a cell (C_r, where r is for "remaining") after a certain period of functioning. It is also important to note, moreover, that the SoC depends on the time, since the actual capacity of the battery changes with it: the parameter, indeed, decreases during the discharge and increases during the recharge of the device.

$$SoC = \frac{C_r}{C_{in}}$$

Apart from the SoC of a single battery, it also possible to compute the parameter of an entire module, even if is not as trivial as it could be thought. Indeed, the module's SoC depends on the ones of the cells, but many considerations have to be done. One module can be simply built as an array of several batteries connected in parallel, and thanks to the self-balancing characteristic of the parallel connection, this ends up being treated like a single "big" battery, where its state of charge (SoC_m, where m is for "module") is estimated by considering the one of the single ESSs (SoC_i, where i is for the $i-th$ battery within the module). Thus, for a battery module presenting parallel connections between its basic elements, the state of charge is the following:

$$SoC_m = SoC_i$$

When, on the other hand, the batteries within the same module are thought to be connected in a serial way, the self-balancing property of the connection is no longer present: considering the un-uniformity presented by the system, it would be better to see different and more reliable estimation methods than the last one. For small unbalances, and assuming that the initial capacity and the SoC for each single cell in the battery module are known, the global working parameter is calculated from the level of energy still present inside the whole module with respect to the total initial one, found when fully charged.

$$SoC_m = \frac{C_{m,r}}{C_{m,in}} = \frac{SoC_i\ C_{i,in}}{C_{i,in}}$$

However, whenever large unbalances are present between the batteries and no balancing device is applied to the module, another more specific formula have to be used. The initial total level of capacity which is generally available to be delivered by the module is now equal to the amount of capacity stored in the "less performant" battery, and thus it does no longer represent a generic data among all: indeed, once that this amount has been totally supplied to the load, even if the other cells still retain an additional amount of energy, these are not able to deliver it without damaging the circuit.

$$C_{m,in} = \min(C_{i,in})$$

So, it is simple to obtain the SoC of the whole module, according to this latter general law:

$$SoC_m = \frac{C_{m,r}}{C_{m,in}} = \frac{C_{m,r}}{\min\left(C_{i,in}\right)}$$

Now it is necessary to go deeper in the analysis, characterizing both the two quantities, $C_{m,r}$ and $C_{m,in}$, taking the parameters at the level of the local ESSs. Whenever the module gets discharged, the SoC of each of its batteries gets contemporary lowered, knowing that a certain quota of capacity has been delivered from all of them ($C_{i,del}$, where del is for "delivered").

$$C_{i,del} = (1 - SoC_i)\ C_{i,r}$$

On the other hand, the remaining amount of capacity in a general $i - th$ cell is found to be:

$$C_{i,r} = SoC_i\ C_{i,in}$$

Thus, recalling that $C_{m,in}$ is the initial capacity available to be supplied by the whole module, composed by the "future" delivered and remaining ones, one gets that:

$$C_{m,in} = \min\left(C_{i,in}\right) = C_{m,r} + C_{m,del} = \min(C_{i,r}) + \min(C_{i,del})$$

Hence, substituting the values of $C_{i,r}$ and $C_{i,del}$ in both $C_{m,in}$ and $C_{m,r}$, the expression for the module's SoC is finally obtained as follows.

$$SoC_m = \frac{C_{m,r}}{C_{m,in}} = \frac{\min(SoC_i\ C_{i,in})}{\min(SoC_i\ C_{i,in}) + \min\left((1 - SoC_i)\ C_{i,in}\right)}$$

At the end, it could be said that whenever a precise estimation of the cells' state of charge is allowed, the corresponding parameter to the entire battery module could be calculated, whatever is the nature of the connections between the cells inside it. Indeed, up to now it has been simply considered in the analysis that the cells within a module are connected either "in parallel" or "in series", but it is well known that in the reality a combination of the two modes is present. However, as simple as it may seem, it is still challenging to estimate the on-board and on-line state of charge of the Li-Ion batteries without considering respectively a destructive analysis or the interruption of the pack's power supply to the load.

At this point, the parameter to be detected is known—i.e. the SoC—, as well as its role within the battery pack and its meaning in the whole context, but what has still to be presented is the method by which the BMS estimates these "abstract" quantities. The most reliable way used to determine a cell's SoC is the so-called "discharge method", performed under controlled discharge rate and environmental temperature. This test is able to effectively find out the remaining charge of the battery in terms of capacity (previously denoted with C_r), so that simply by knowing the initial maximum one, then the SoC can be computed. However, considering that the computational time required is quite long, and that when the test is completed the battery is found to have no remaining power, this particular method is only applied for laboratory research, being not useful and suitable for the BMS to be performed on-line in vehicle. Then, one effective method used by the software of the BMS to evaluate the SoC of the batteries, and consequently of the modules, is the so-called "Ampere-hour integral", commonly named "Coulomb counting". Here, initially, two different instant of time are considered: t_0 denotes the initial time of the computation, and t' a general instant of time, subsequent to t_0. The state of charge at the zero-instant is known, namely SoC_0, coming from a previous analysis or being characterized by the maximum capacity of the battery, when this is found to be fully charged. By knowing then the actual capacity of the ESS, the current I supplied by the device, and imposing the so-called "Coulomb efficiency" η—which is major than 1 during the discharge and smaller for the recharge—, the formula used for the SoC estimation results to be the following one:

$$SoC = SoC_0 - \frac{1}{C_r}\int_{t_0}^{t'} \eta\, I\, dt$$

The obtained results with the Ampere-hour prediction method are characterized by a satisfactory precision. However, it has to be highlighted that the outcomes depend on the precision of the SoC_0 value, and furthermore, the Coulomb efficiency is highly variable during the battery's functioning, since it is influenced by the SoC itself, by the temperature, and by the delivered current, hence difficult to be predicted on-board during the device's functioning. Thus, it is important to remember that a small malfunctioning in the apparatus could lead to cumulative errors, and hence to fail the detection of the SoC. At last, another effective method in the evaluation of the SoC is the direct measurement of the so-called "open circuit voltage", usually found to work in conjunction with the latter explained one. Indeed, since the SoC is related to the retained amount of Li^+ in the electrodes, it can be estimated by knowing the open circuit voltage of the cells. This is a very precise evaluation method, but it can only be correctly carried on after a long rest of the batteries, and consequently, it is usually adopted when the vehicle is at rest, so that when this gets switched on the value of SoC_0 is precisely known, and the Coulomb counting procedure is no longer affected by cumulative errors. Finally, it has to be recalled the fact that the methods presented in this chapter are only some among the most important ones. For instance, new precise methods of estimation involving approaches using neural networks and fuzzy logics are nowadays under development.

Nevertheless, apart from this large analysis on the evaluation on the SoC, it is important to remember that at the basis of everything there is the fact that a reliable estimation for this parameter allows to evaluate the residual autonomy for the entire vehicle, and furthermore, many other battery's working parameters, as it is going to be see, depend upon it.

Engineering working parameters – **SoH**

Another important parameter that is required to be evaluated by the BMS is the so-called "state of health" of the battery (shortly called, since now on, SoH). The SoH comes out from an estimation and is necessary to reflect the ageing status of a cell. It provides as a result a reading of the remained ability of the ESS to supply energy, when found to be fully recharged, with respect to the initial performances assured by a "fresh" battery [34], which is nothing more than a battery which has still to undergo to its first cycle of discharge/recharge.

All the batteries age with time, and the challenges introduced in the previous chapters become more and more difficult to be faced up. However, one of the most critical aspects deriving from the use of these devices, is their "loss of capacity". After each cycle of discharge and subsequent recharge, indeed, the battery if found to have a lower level of initial capacity (and so, for what we've seen, a lower SoC_0). Hence, the SoH results to be a reliable indicator of how much of the available lifetime energy throughput of the battery has been consumed, and how much is left. Using a formula, the state of health of a battery is defined by the ratio between the capacity after a complete recharge (C_{in}) and the fresh initial one ($C_{in,new}$).

$$SoH = \frac{C_{in}}{C_{in,new}}$$

Once again, the parameter ends up being a percentage value, ranging from 100% whenever the battery is new, up to 0%. Obviously, the 0% is only a theoretical outcome since it is never reached in the automotive field. Indeed, whenever the SoH lowers, this means that the vehicle is losing part of its initial maximum autonomy: consequently, thresholds ranging between $80 \div 75\%$ of SoH are normally applied for the LIBs used in EVs, which are then signed as "no longer compliant".

The carmakers have equipped the BMS with different evaluation methods of the parameter, since, at the end, any quantity that changes significantly with the ageing of the device (for instance the cell's impedance or conductance) can be used as a basis for providing a reliable indicator of the operative health of the system. Nevertheless, the several ways are usually combined with the more direct measurement which is assured by the computation of the capacity levels, and consequently with the state of charges. Finally, it is also worth to recall that there are also some irreversible phenomena, not strictly caused to the ageing of the technology, which induce sudden falls of the SoH: among the others, collisions of the vehicle and short circuits.

Engineering working parameters – **SoF**

Up to now, two different but connected working parameters have been depicted: the state of charge describes how much energy is still available to be delivered with respect to a fully-recharged ESS, while the state of health provides an estimation of how much the batteries are far, in term of global performances, to their former fresh counterparts. Putting things together, the state of function (shortly called, since now on, "SoF") reflects the device's readiness in terms of usable energy, by observing the SoC in relation to the still available capacity, taking at the end the mathematical form of a ratio between the remaining available energy in the battery (C_r) and the maximum possible energy which could be stored inside it ($C_M = C_{in,new}$, where M is for "max") whenever this is found to be fresh and fully charged.

$$SoF = \frac{C_r}{C_M}$$

Hence, for what concerns the whole status of the batteries, this indicator is the most complete one. The problem which has led to the introduction of the SoF, faced up during years of development of the electric technology, was the following: when a battery gets recharged it signs a SoC of the 100%, but still its value would mean the presence of a small amount of energy stored within the device, since, for instance due to the ageing effects, the SoH of the battery is found to be very low. Thus, whenever a certain amount of energy has to be properly contextualized, it needs to be related with the maximum possible one found in fresh batteries.

Finally, it is worth to recall that apart from this latter definition of SoF, sometimes the state of function is used for another purpose: the parameter could be defined as a Boolean variable, where if its value is equal to 1 then the battery under study is able to meet the energetic demand of the powertrain, while the opposite is found whenever its value equals 0.

Engineering working parameters – **Voltage**

Although, for what has been seen up to now, the BMS works on estimating different "abstract" parameters, the voltage provided by each single battery is another fundamental working indicator, since by this the ability of the entire BP in meeting the requirements of the electric motor largely depends. As it is now well known, the electrochemical cells are the basic elements composing the batteries, whose output is a conjunction of electrical potential built at their tabs and delivered current in the conductors. To support the whole system's functioning, furthermore, a certain level of potential has to be maintained and assured through the ESSs, and hence critical threshold values must be carefully detected—it is important to not pass the so-called "cut-off" potential. To properly estimate the voltage in a battery, differently as it may be thought, a useful indicator is found to be the degree of discharge (DoD). The DoD is nothing more than the mirrored counterpart of the SoC: in particular, their sum always equals one. It has been found, indeed, that the more the battery gets discharged, the more the potential is lowered. A positive aspect may be found in this latter behaviour for what concerns the estimation of the potential. Indeed, the major difficulties found in the voltage measurement are mainly related to its nature: the battery packs are based on the contemporary functioning of hundreds or even thousands of small batteries, and the necessity of a very precise measurement is a challenging task since also the so-called "accumulated potential" is detected when whatever battery's one is directly measured thought physical tools, and an unified compensation for the error or elimination method does not yet exist. Hence, taking advantage from the relation that connects together the voltage and the SoC (or the DoD), the rapid and correct estimation of the batteries' potentials it is possible, once that the sensitivity of the SoC (in terms of mV^{-1}) is known. An example of this latter relation can be provided by the work of Lu et all [33]. Apart from this indication, then, reliable methods are coupled with this latter in order to provide to the monitoring system a real measurement of the voltage, rather than only its estimation. Among the others, the resistance voltage divider, the optical coupling isolation amplifier method, and the discrete transistor method are the most important ones.

Balancing

Depending on the parameters that are constantly estimated and directly calculated, both at the level of the batteries and of the whole battery pack, then sent to the BMS and studied by it, to perform the so-called "balancing" of the batteries is a common operation that has to be necessarily done. Many forms of unbalances could exist, since according to the thermodynamic definition each difference that is found for a certain property within a system gives an unbalance. Nevertheless, when speaking of ESSs, the energetic unbalance have to be considered. To start, in order to assure a battery pack's future well-functioning, a basic condition that has to be provided during its design is the physical uniformity between all the ESS that compose it, but due to the inefficiencies and difficulties that are already met in the manufacturing phase of the devices, no one of the battery results to be completely as perfectly the same as the other. However, these differences are initially minimal, and hence negligible. After a certain period of use, on the other hand, these physical inequalities both grow and build up, concluding by giving a certain amount of batteries whose outcomes are no longer closed between them. As it has been previously seen, voltage, SoC, capacity, and internal equivalent resistance (related to the SoH), all together concur in defining the operating conditions of a battery, characterizing it in a proper manner. Thus, the unbalance of properties results in presenting different working parameters and functioning statuses among the interconnected ESSs, which is not an optimal condition.

To better describe how the unbalances are created during time, one important phenomenon has to be studied: the self-discharge of the battery, taken into account by the self-discharge rate (shortly called, since now one, "SDR") parameter. The SDR denotes the "velocity" with which an ESS gets self-discharged, depends on the temperature at which the battery is found as well as on its state of charge, and accounts for the capacity loss of the device when this is in an idle mood. To give an idea for the magnitude of the self-discharge, the one found in LIBs is usually very low if compared to the other technologies, ranging between the $3 \div 5\%$ loss of initial capacity per month when the battery is switched off, but still has to be taken into account being not negligible. However, the presence of a non-constant temperature profile in a battery module/pack during its functioning, will result in non-uniform self-discharge rates among the cells. In other words, some batteries get discharged faster than others, and so, obviously, the remaining energy to be delivered is lower in the most discharged ones than in the latters. This is, shortly, mainly how the energetic unbalances are formed during time in a battery pack. Thus, resuming: the non-uniformity among the capacities of the ESSs is mainly caused by the non-uniformity of the self-discharges.

Obviously, this phenomenon does not give an efficiently working BP, and hence has to be prevented as well as compensated. Indeed, despite the small values in play that have been previously presented for the LIBs, problems related to overcharges or deep discharges of the ESSs may arise, and this is why an equalization between the capacity level of the different cells has to be performed. The equalization can be chemical or physical, but the chemical method is not found to be applied in Li-Ion batteries. The physical equalization method, on the other hand, takes advantage from the application of external supplementary electrical circuits, and can be either dissipative or non-dissipative.

- **Dissipative physical equalization**

  The capacity in excess found in some cells with respect to others gets totally dissipated, resulting at the end to be a waste of energy thinking to the loss of autonomy from the vehicle point of view.

- **Non-dissipative physical equalization**

  The non-dissipative method acts by transferring the surplus of energy where it is actually necessary.

Despite the different methods of equalization between cells, three different targets may be imposed to be reached within a battery pack:

- A uniform voltage;
- A uniform SoC;
- A uniform capacity.

The method whose purpose is to bring all the capacities at the same level is the most important one, since the BMS is constantly trying to completely make use of all the energy present in the cells. Although the parallel connection is said to be "self-balancing", and hence does not require any adjustment by part of the BMS, for a serial connected module of batteries, this property is no longer present. In this latter case it is straightforward that the whole resulting capacity of the system is always equal to the one of the battery presenting the worst status, hence the one with less initial capacity (limit which is settled in order to avoid deep discharges or overcharged of the other connected batteries).

A clear schematic representation dealing with the cells' balancing is provided in the following *figure 29*.

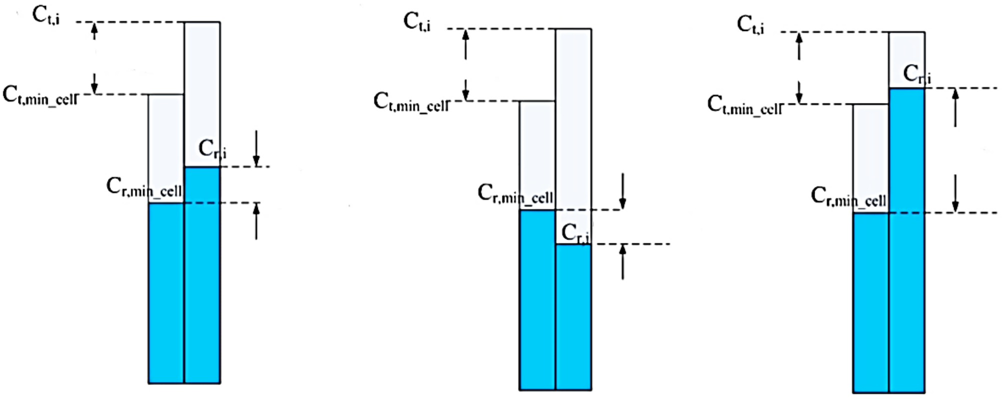

FIGURE 29 - Different cases of necessary (or not) physical equalization between connected cells

The less performant battery (represented by the shorter slot) is found to be in different coupling conditions, in terms of energetic contents, with respect to another $i-th$ cell. In the first case (left hand side), which is the most common one, no equalization is needed, since neither deep discharges nor overcharges of the $i-th$ general battery are going to take place. Also note that, differently as it may be thought, the less charged battery remains like this since it is better to have a less performant system than a damaged one, whenever this is possible. However, an energetic transfer between cell is required in case the less performant cell is found to be more charged than the other (middle picture) or in case a large amount of energy difference is found (right hand side) with the less performant battery which is also the one presenting minor capacity. Respectively, in these latter two cases, deep discharges of the $i-th$ ESS takes place whenever the less performant one gets totally discharged, and overcharges, on the contrary, when this gets fully recharged. Putting things together, and knowing that physical equalities are almost impossible to be reached, the best solution is to bring the system in the first condition, so that either deep discharges and overcharges should be avoided.

Chapter 4
Analysing Li-Ion cells

Functioning characterization

The general characteristics of a Li-Ion battery have been largely addressed in the previous chapters of the work, as well as its functioning and integration within the powertrain of a car. Up to now, however, the focus on the subject was more from a theoretical point of view, but the knowledge regarding the state of the art of the LIBs is now clear enough to introduce practical approaches used for the analysis of their performances.

As it has already been previously introduced, the SoC is one of the most critical parameters to be identified by the BMS when dealing with EVs, since inaccurate estimates of the value can cause abuse events, carrying with themselves significant implications for the safety of the overall car [35]. It is therefore crucial to understand the models which are able to improve the accuracy of the computation by considering directly the electrochemical phenomena taking place within a cell.

To date, many approaches have been developed for calculating this parameter, including the aforementioned Coulomb counting, where although the technique results to be simple and easy to be implemented, errors can be accumulated by the integration function and thereby reduce the accuracy of the computation. Another commonly used method for estimating the SoC is based on defining the connection between this and the cell's voltage, but the latter does not appear to be effective for Li-Ion solutions due to the plateau presented in the charging/discharging characteristics. Recently, however, physics-based methods have been applied showing inherent advantages over the traditional ones: these techniques turn out to provide estimates that are resistant to sensor errors and less dependent on the nature of the inputs, but the main problem for real-time applications results in the computational complexity of the coupled partial differential equations that are used to describe the physical processes taking place inside the battery. It could be said, at the end, that to theoretically build a conceptual bridge connecting the theory with the reality is not a trivial task, since the need is to translate the complex physical phenomena at the cells' level into readable and manageable quantities for the on-board computer dealing with the BMS. To accomplish the task, therefor, various types of models are today generally used to simulate and analyse the behaviour the LIBs, as shown in the following *figure 30*.

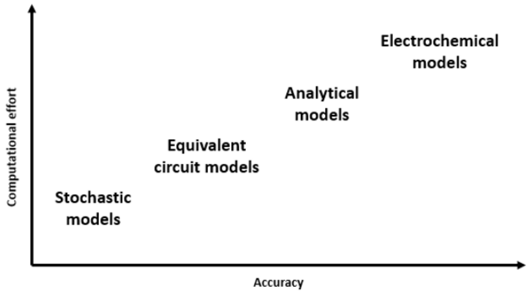

FIGURE 30 - Computational cost vs accuracy for different types of models

The different typologies of models take their name depending on the solving technique by which these take advantage from, as briefly introduced in the following points.

- **Electrochemical models**

  The electrochemical models are by far the most accurate ones, being able to effectively describe the reactions taking place inside the cell, and hence turns out to be principally used in order to optimize the materials involved in the physical construction of the batteries. These consider different mechanisms of power generation and connect the outputs with the macroscopic quantities which are actually presented to the user, such as cell's voltages and delivered currents. However, these types of models result to be quite complex and time-consuming in their resolution, since involve coupled system of space-time partial differential equations.

- **Analytical models**

  The analytical analysis of Li-Ion batteries is performed by means of empiric equations describing the behaviour of the ESS. This last modelling technique is a very powerful tool, since only with few equations a good approximation of the reality could be reached, but, on the other hand, it does not fit with the on-board BMSs.

- **Stochastic models**

  In a similar way to the latter, stochastic procedures describe the cells in an abstract way, considering small uncertainties in the nature of the input parameters, and hence providing as outputs results in form of distributions of probabilities. It could be said, in general, that these models are used in conjunction with the analytical ones, mainly for research activities and not for online applications.

- **Equivalent circuit models**

  The equivalent circuit models are by far the mostly used ones since they provide a direct and precise connection between the modelized cell and the reality: very simple electrical circuits mimic the behaviour of the Li-Ion batteries with the use of circuital elements, such as resistors and capacitors, resulting at the end in an intuitive concentrated parameters approach.

Hence, apart from the analytical and stochastic models, which are yet used but not so interesting from an engineering point of view, both the electrochemical and equivalent circuit ones deserve a broader investigation in order to highlight the principles at their basis, since usually turn out to be implemented in the on-board BMS for accurate estimations of the SoC parameter.

Functioning characterization – **Electrochemical models**

The particularity among the electrochemical models is that they are able to describe the internal reactions taking place at the level of the cells, including the intercalation and the deintercalation of the Li^+ in the electrodes. This is possible since the models consider all together three transport phenomena: migration, diffusion, and convection [36].

However, apart from the generalities that many electrochemical models shear, relevant differences exist in the way they process the inputs providing the final output. As a starting point, it is important to understand that the physical phenomena are modelled by a set of coupled partial differential equations (PDEs) whose resolution require a certain spatial discretization of the inner part of the batteries, accomplished by using the finite elements, finite differences, or finite volumes techniques. When applying one of such discretization methods, the electrochemical model finally results in thousands of states (equations). Then, in order to simplify the resolution, the different approaches are aimed at finding a way to reduce the number of those states. The two mostly studied and applied solving techniques proving reliable electrochemical models involves the so-called “pseudo-two-dimensional” (P2D) and “single particle modelling” (SPM) approaches.

- **P2D approach**

The P2D-based electrochemical model assumes that for each point of the electrodes there is a spherical particle which is representative of the active material, and so considers one spatial dimension for the electrode’s thickness (x) and another spatial dimension for the radius of each particle (r). However, although this modelization provides very complete and reliable models, these turn out to strongly depend on the accuracy of material’s parameters which are specific to each cell design, both in terms of the geometry and the chemistry, and so, as a consequence, not all are transferable from one design to another. In this optic, finding a suitable set of values necessary to simulate a specific battery is one of the main challenges in cell’s modelling. Apart from the parameters’ detection, several highly nonlinear PDEs are used to solve problems related to porous electrode and concentrated solution theories, in addition to the kinetics equations [37]. At last, it has to be said also that, mainly due to its complexity, several simplified versions of the P2D approach have been implemented in the last decades, such as the SPM technique presented in the following point. A clear view showing the theory under the P2D solving technique as thought is represented in the *figure 31*.

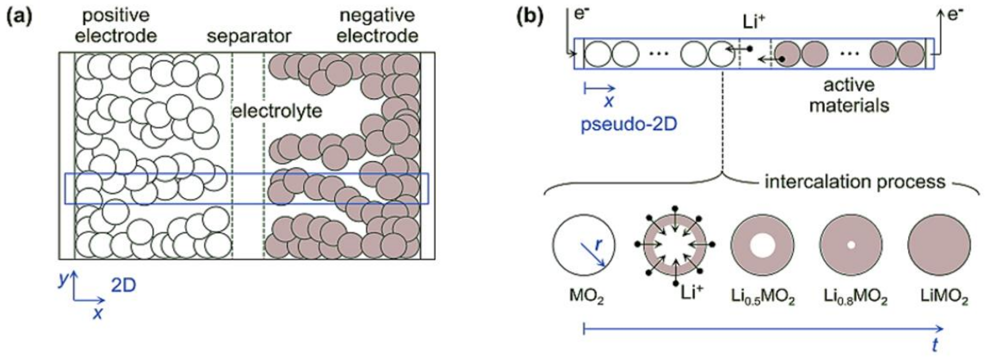

FIGURE 31 - The traditional 2D model (a) approximated to the pseudo-2D one (b)

- **SPM approach**

Implementing a real-time BMS using the spatial discretization method is computationally prohibitive and on-board memory demanding, and therefore, in order to develop an electrochemical model for real-time battery management, deriving a simplified and computationally efficient mathematical model, is crucial. The SPM is a typical example of a simplified electrochemical model which uses less than 10 states, in which each electrode is modelled by a single "big" spherical particle, but whose spatial variations of potentials within the electrodes cannot be determined by using the SPM. Hence, as a consequent, in the electrochemical models is thought that the electrolyte concentration is constant in both, time and space, fact that does not hold for high-current applications and thus needs a further development. The representation of the SPM approach is shown in the following *figure 32*.

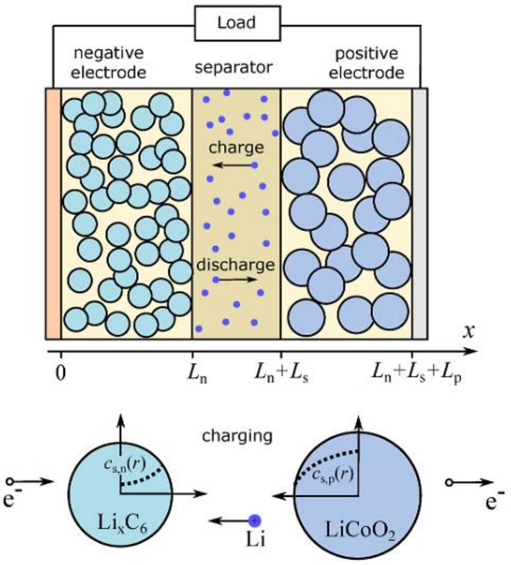

FIGURE 32 - The traditional 2D model (up) approximated to the SPM one (low)

Summarizing, with the P2D electrochemical model all the cell's dependent quantities—i.e. electric potential, concentration of Li^+, flux of these at the boundaries of the spherical active material particles, etc.—end up being partially differentiated with respect to the independent ones, which in turn are the spatial macroscale and microscale coordinates and the temporal one, respectively x, r, and t. The model resulting from the SPM technique, on the other hand, approximates both the anode and the cathode as two single spherical particles neglecting like this the different local concentrations of the lithium ions within the active material: this latter variant improves the calculation speed by lowering the computational costs of the analysis, keeping on offering a good accuracy also for low current rates, feature that usually returns problems when applied to the P2D electrochemical model. Unfortunately, the drawback still remains the reliable description of what locally happens whenever high currents are in play, with both the implemented approaches, i.e. the P2D and SPM ones.

The link between the electrochemical models and the SoC estimation performed by the EVs' on-board BMS is given by the so-called "empirical formulations", whose aim is to fit the output describing the cells' behaviour into simple and manageable formulas. When dealing with electrochemical models, in both the forms based on the P2D or SPM approaches, the Shepherd's empirical formulars are the mostly used. In general, the empirical modelling want to describe the terminal voltage of the cell representing it as a mathematical function of the SoC and the of the current, resulting in an essentially nonlinear characteristics describing the ESS [38]. Shepherd, in particular, developed an equation to describe the behaviour of a cell in terms of voltage at the terminals (V_{batt}) by taking into account the open circuit potential (V_{OC}), the equivalent internal resistance of the device to the current flow (R_{eq}), and the current itself (I_{batt}) [1]. This approach is effectively used to study discharges at constant rates—namely whenever the current delivered or used to recharge the ESS is constant.

$$V_{batt} = V_{OC} - \left(K\frac{C_{in}}{C_{in} - I_{batt}t}\right) + Ae^{-B\,I_{batt}t} - R_{eq}I_{batt}$$

Apart from the previously introduced parameters, C_{in} is found to be the maximum capacity of the cell (i.e. the initial one) and K the resistant coefficient of polarization, while A and B are constant parameters deduced from the behaviour of the battery during characterizing tests. Furthermore, the exponential part of equation is necessary since it helps in better describing the phenomena taking place at high levels of SoC. It is important to highlight the fact that all the quantities previously mentioned, with a deeper investigation that is not going to be presented in this work, are obtained thanks to the discussed electrochemical models. Going on from the initial empirical formula, it could be shown that the dependency of the cell's potential to the SoC is implicitly given by the term $I_{batt}t$.

$$SoC = \frac{C_r}{C_{in}} = 1 - \frac{C_{del}}{C_{in}} = 1 - \frac{I_{batt}t}{C_{in}} \rightarrow \frac{C_{in}}{C_{in} - I_{batt}t} = \frac{1}{SoC}$$

Thus, the final adjusted writing could be obtained by putting in evidence the dependency on the SoC of the parameter V_{batt}.

$$V_{batt} = V_{OC} - \frac{K}{SoC} + Ae^{-BC_{in}(1-SoC)} - R_{eq}I_{batt}$$

Other empirical formulations aimed at completing the electrochemical models exist apart from the one proposed by Shepherd. They differ from the last one by adding parameters in the equation, so that specifical phases and behaviours are considered and described in a more appropriate way. Among the others, the most important ones were proposed by Nerst and Unnewehr.

Functioning characterization – **Equivalent circuit models**

The equivalent circuit models (shortly called, since now on, "ECM") are very intuitive and easy to use, and hence very interestingly applied in analysing Li-Ion batteries. When compared to the electrochemical ones, indeed, the ECMs enable to understand better the electrical characteristics of the battery, and furthermore, depending on the way the circuits are thought, the model also provides freedom in designing reliable structures depending on the results that are wanted to be highlighted. With this approach, an electrical circuit is intuitively built up: it consists of a voltage source, a serial resistance, and one or many resistance-capacitance networks. The number of RC-branch present within the model characterize the entire analysis: they have a proper time constant which takes into account the diffusion processes of the Li^+ inside the electrolyte and inside the porous electrodes, as well as the charge transfers and double-layer effect inside the electrodes—in other words, from a circuital point of view, the RC-branch are intended to describe the dynamic phenomena taking place within the battery. Once again, then, empirical formulas enable to translate the circuital quantities—i.e. current, potentials, etc.—and hence the battery's behaviour, into external parameters such as the voltage present at the cell's terminals. In the literature [38] it is usually found that the four mostly used equivalent circuit models are the "Rint", the "Thevenin", the so-called "partnership for a new generation of vehicles" (PNGV), and the "general non-linear" (GNL) ones. The resulting circuits mainly differ in terms of structures, presenting additional connections and electrical components, but can nevertheless be considered as the completion and evolution of one with respect to the other, as it is briefly shown in the following part of this chapter.

The Rint ECM is generally known as the simplest equivalent circuit model, since it only involves a potential source (V_{OC}) and a serial resistance (R_0, also sometimes denoted with R_S), as shown in the *figure 33*.

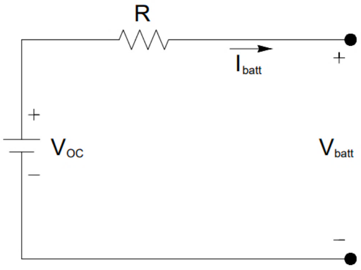

FIGURE 33 - Rint ECM

In the image above, V_{OC} denotes the open circuit voltage, i.e. the voltage across the terminals in the presence of a null current. It is known, then, that whenever a current flows within an ESS, the open circuit potential experiences a drop due to the presence of an internal resistance: V_{batt}, hence, is the voltage across the battery when this is working under a current I_{batt}, supplied to the connected electrical load (considering a discharging). R, finally, is the internal equivalent resistance of the cell: according to the model all the "resistive" phenomena taking place within the ESS are summarized and accounted in this parameter, which results at the end to be equal to sum of the Ohmic resistance R_{Ω} and the polarization resistance R_p. The governing equation of the model, concluding, is very simple:

$$V_{batt} = V_{OC} - RI_{batt}$$

The advantage in using a Rint model is that it has a very small number of parameters that need to be determined, and hence it also shows low computing efforts. Unfortunately, on the other hand, it is not able to describe the dynamic characteristics of the cells, for which at least one RC-branch has to be used. For this purpose, the Thevenin model is here represented in the *figure 34*.

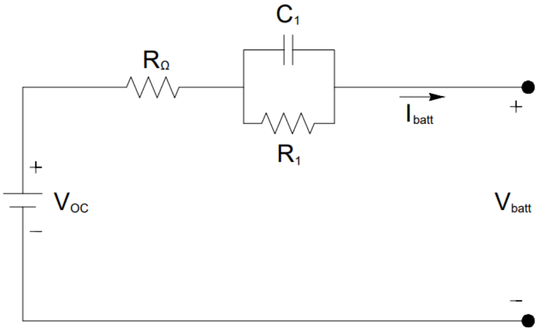

FIGURE 34 - Thevenin ECM (1RC)

Note that, differently from the Rint ECM, using the Thevenin approach the series resistance R only takes into account the Ohmic phenomenon, since the polarization turns out to be englobed within the RC network, where R_1 and C_1 both considers the overtensions. The product R_1C_1 provides the time constant τ_1, proper magnitude of the transitory phase, but, however, it has been seen that the model including only one RC-branch suits in describing small dynamic transitory, while for longer ones it is necessary to add other networks. As a result, the good compromising in terms of computational costs and accuracy is normally reached with a 2RC-branch model, even if 3RC-branch ones are also commonly found to be applied, as shown in the following *figure 35*.

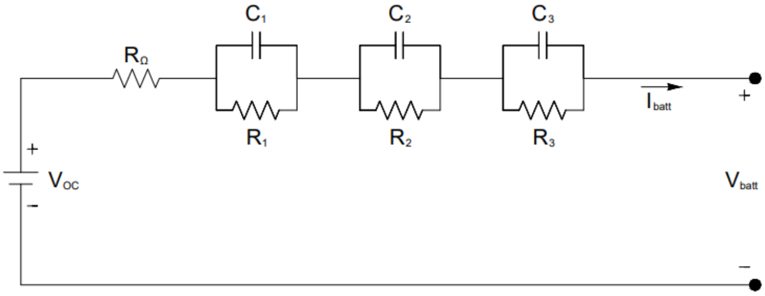

FIGURE 35 - Three-RC-branch Thevenin ECM

Finally, to conclude the analysis, the PNGV ECM is obtained by simply adding to the basic Thevenin circuit a capacitor in series to the open circuit voltage source, describing like this the variation of the potential in time because of the accumulation of energy within the electrical load. Then, the GNL model uses the same approach of the PNGV one on a 2RC-branch circuit, describing what is called the “concentrated polarization effect”. However, these last examples won’t be treated in detail in the work since too much complex and expensive in terms of computational costs for the TMS’s applications, but obviously result to be the most accurate ones and turns out to be extensively used in research activities.

Functioning characterization – **Comparison**

At this point it could be useful to summarize what have been seen up to now in this chapter, also in order to justify the future choices that hare going to be made in the next part of the work, where the carried out experimental practices and simulations—these latters making use of an equivalent circuit model—are going to be presented.

The differences between the approaches are now clear: considering the electrochemical models as the most complete and accurate ones, some simplifications could be added, so that using mathematical equations the empirical models are developed, while studying the electrochemical reactions with a parallelism, thinking to real physical electrical components, ends up giving the ECMs. Obviously, other methods have been also developed in these last years, but for the purposes of this work the most important ones to be known are those previously presented.

Accordingly, in the following *table 12*, the pros and cons given by the different approaches are summarized, as well as the models’s methods used to estimate the output parameter, namely the potential at the terminals of the cells during their functioning (V_{batt}).

TABLE 11 - Features of the most important modelling techniques

Modelling approaches	Electrochemical models	Empirical models	Equivalent circuit models
Solving technique	V_{batt} from PDEs	$V_{batt} = f(V_{OC}, I, SoC)$	$V_{batt} = f(V_{OC}, I, SoC, R_i, C_i)$
Pros	• High accuracy for the calculation of V_{batt}	• Simple mathematical expressions • Computational efficiency	• User-friendly • Optimal also for the SoC estimation
Cons	• Time consuming • Extensive knowledge of the cell's materials is needed	• Limited capability in describe the entire profiles of charge/discharge • Relies on the parameters detected in the electrochemical models	• Complex parameters' identification process

Thermal characterization

The role played by the temperature in a LIB should be integrated within the different types of models previously seen, rather than being neglected. Indeed, the definition of the thermal behaviour of a cell turns out to be useful both from a theoretical and a practical point of view: respectively, the electrochemical models are implemented with additional inputs, with the optimizations of the cell's materials as well as of the cooling systems which could be achieved in the designing phase [39], while concerning the ECMs, the circuital parameters get updated, depending directly on the temperature at which they are found.

The internal temperature of a battery influences the amount of energy available to be supplied, and also the temperature of the external environment can determine a variation of the parameters over which both the electrochemical and ECMs are based on. For these and many other reasons, it is important create a thermal model and to introduce a certain dependence on the temperature in the various approaches already seen. Mainly two advantages come together from this latter operations:

1. First of all, having an efficient model means that the BMS is able to estimate and predict the evolution of the internal temperature of the cells inside the BP, and therefore, consequently, allows the TMS to act accordingly.
2. Furthermore, the thermal information from the model can improve the accuracy of the estimations running in the BMS, used, as we have seen, to calculate both SoC and SoH. Likewise, the parameters found with these latter approaches will be even closer to the reality.

The thermal modelling of Li-Ion batteries can in general be accomplished using equivalent circuits, creating a parallelism between the phenomena of interest and the electrical components. "Translating" the circuital elements, the capacitors now represent thermal capacities, the resistors correspond to the inverse of the heat exchange coefficients, and the current generators will reproduce thermal sources (a more detailed resume related to connection between electrical and "thermal" circuits is shown in the *table 12*, at the end of the section). Obviously, as it has been seen for the electrochemical analysis, also in case it is possible to choose models of a different degree of complexity.

The simplest model that can be realized is shown in the *figure 36*, where the battery is considered as an adiabatic body. However, because of the fact that in the reality the cells continuously exchange heat with the surrounding environment, the results in terms of temperature obtained from this model are neither reliable nor realistic, but it is interesting in order to start studying the losses present in the electrical devices.

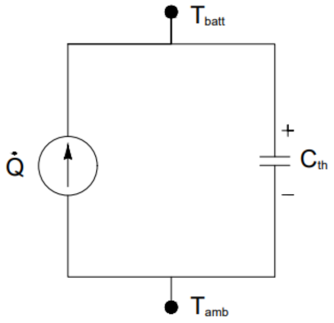

FIGURE 36 - Simple thermal model described by an equivalent circuit

One equation that can initially be obtained from the elemental equivalent circuit is the one that highlights the increase in the temperature within the battery during its functioning, and hence the internal one of the ESS (T_{batt}). Considering with $\dot{Q}$ a generical heat flux, indeed, it is possible to obtain the relationship by simply applying the electrical governing equations to the thermal model.

$$\dot{Q} = C_{th} \frac{dT}{dt} \rightarrow \cdots \rightarrow T_{batt} = T_{amb} + \frac{1}{C_{th}} \int \dot{Q}\, dt$$

Note that the heat flux is not thought to come from the outside of the case, but rather it is generated inside the electrical accumulator, acting as an heat source.

To improve the reliability of the model in estimating the T_{batt} parameter, then, two heat exchanges have to be considered: respectively, the conductive and the convective phenomena referred to the rigid case of the cell with respect to the environment are accounted by two thermal resistances (R_{cond} and R_{conv}), both in series with respect to the heat source. A clear representation of the improved thermal model is shown in the following *figure 37*.

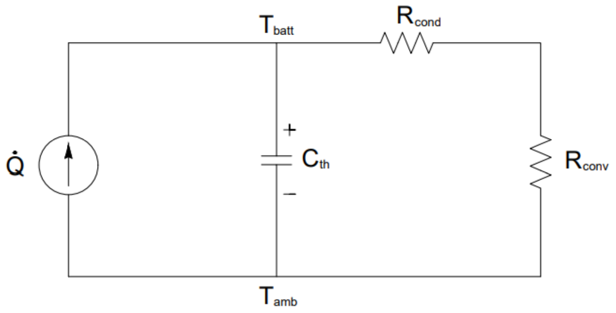

FIGURE 37 - Advanced thermal model described by an equivalent circuit

Differently from before, in this more complex case, the equation that estimates T_{batt} takes into account also both the conductive and convective phenomena, improving the accuracy of the model.

$$T_{batt} = T_{amb} + \frac{1}{C_{th}} \int \left(\dot{Q} - \frac{T_{batt} - T_{amb}}{R_{cond} + R_{conv}} \right) dt$$

However, apart from the thermal models and the equivalent electrical circuits, studying the thermal behaviour of a battery also deals with the definition of the internal heat source within a cell, namely studying the parameter $\dot{Q}$, as done in the following section.

TABLE 12 - Electrical circuits for thermal simulations

Electrical reference element	Electrical quantity	Electrical dimensions	Equivalent thermal quantity	Equivalent thermal dimensions
Voltage source	Potential, V	Volt $[V]$	Temperature, T	Kelvin $[K]$ or degree Celsius $[°C]$
Current source	Current, I	Ampere $[A]$	Heat flux, $\dot{Q}$	Watt $[W]$
Resistor	Resistance, R	Ohm $[\Omega]$	Thermal resistance, R_{th}	$\left[\frac{K}{W}\right]$
Capacitor	Capacity, C	Farad $[F]$	Thermal capacity, C_{th}	$\left[\frac{J}{K}\right]$

Thermal characterization – **Internal heat generation**

The heat generated inside a LIB during its functioning is a highly variable quantity as it depends on working parameters such as current, SoC, inner temperature and ageing of the cells (hence on the SoH). In the literature it is normally found that up to four phenomena have to be considered acting together in the heat generation: electrical losses, changes in entropic level, side reactions, and liquid mixing. However, even if the accuracy in the final prediction of T_{batt} gets slightly lowered, some assumptions could simplify the calculation of $\dot{Q}$: according to Thomas et all [40], side reactions are given by ageing phenomena that turn out to be slow enough to be neglected during simple analysis of charging and discharging of LIBs, while the heat generated by mixing results to annihilate during the normal functioning a cell, being negative during the creation of concentration gradients and positive when those gradients disappear. As a consequence, only the heat coming from changes of entropy (also called “entropic heat”, $\dot{Q}_{\Delta S}$) and the one coming from electrical losses ($\dot{Q}_{el}$) are considered to contribute in the internal heat generation of a Li-Ion battery.

$$\dot{Q} = \dot{Q}_{\Delta S} + \dot{Q}_{el}$$

The two types of contribution to the internal heat generation could be then seen more in detail, also in order to find out reliable mathematical equations to be used in the $\dot{Q}$ definition.

- **Entropic (or reversible) heat**

Whenever a cell gets charged or discharged there are some structural changes that continuously take place within the electrodes’ lattices, mainly because of the intercalation or deintercalation of Li^+. These phenomena necessarily release or absorb energy from the surrounding environment—surrounding the electrode—resulting in generation or consumption of heat, namely giving $\dot{Q}_{\Delta S}$, respectively positive or negative. The physical quantity that turns out to be used in this analysis is the entropy S, or better the entropic variation ΔS, which is fixed for a given cell at a defined level of SoC. It has been derived, then, that the entropic heat is inversely proportional to the variation of entropy of the cell: for instance, if ΔS is positive and increases (i.e. there is an increment of entropy within the system) $\dot{Q}_{\Delta S}$ decreases because a certain amount of energy is required in order "to sustain" this change, and vice versa. Let start by presenting the following formula:

$$\dot{Q}_{\Delta S} = -I_{batt} T_{batt} \frac{\Delta S}{nF}$$

Apart from the already known quantities involved in the proportionality, n is the number of electrons taking place in the electrochemical reaction and F is Faraday's constant. Obviously, because of the difficulty in ending up with reliable values of n, the entire fraction $\Delta S/nF$ is usually replaced by the partial derivative of the open circuit voltage with respect to temperature, more convenient to use.

$$\frac{\Delta S}{nF} \cong \frac{\partial V_{OC}}{\partial T} \rightarrow \dot{Q}_{\Delta S} \cong -I_{batt} T_{batt} \frac{\partial V_{OC}}{\partial T}$$

Hence, by simply computing the term $\partial V_{OC}/\partial T$ from the experimental tests, knowing that both the quantities are function of the SoC and depend on the electrode types, it results to be easy to derive the entire entropic heat $\dot{Q}_{\Delta S}$.

- **Electrical losses**

As it has already been seen, the open circuit voltage represents the potential that is found at the cell's terminals when this is disengaged from the electrical load, or simply when no current is passing through the current collectors. Whenever a connection with the downstream components is created, and so the electrical current gets enabled to flow in the conductors, this voltage suffers a drop in its value and the effective potential that is going to be found is the one previously named with V_{batt}, slightly minor than V_{OC}. This voltage drop, coming out during the discharge—or, in the same way, the voltage increases during the charging phase—, corresponds to an irreversible transformation of electrical energy into heat. The difference between V_{OC} and V_{batt} is called "overvoltage" (ΔV), and the electrical losses turn out to be the product between this latter value and the flowing current I_{batt}.

$$\dot{Q}_{el} = I_{batt} \Delta V = I_{batt}(V_{OC} - V_{batt})$$

Hence, it could be said that the electrical losses turn out being calculated by knowing the estimation of V_{OC}, function on the SoC and of the current sign, and by directly measuring V_{batt} and I_{batt}.

Focusing more on the phenomena causing the overvoltage, then, it is now known that it borns because of the current that flows through the cell's internal resistances and due to the phenomena related to the battery's polarization. In particular, the resistant elements are principally found to be the current collectors and the additives placed around the active material, while the polarization happens because of the diffusive behaviour of the Li^{+}, with the creation or release of concentration gradients evolving in time and space within the electrodes and the electrolyte. Hence, putting these latter things together, the electrical losses can all be accounted by considering an equivalent resistant parameter (R_{eq}), taking the following form:

$$\dot{Q}_{el} = I_{batt}(V_{OC} - V_{batt}) \rightarrow \dot{Q}_{el} = I_{batt}^{2} R_{eq}$$

Note that, from this latter formula, the electrical losses result to be always present in a Li-Ion battery, and, above all, always positive.

Concluding the analysis related to the heat generation within an electrochemical cell, it is quite common to neglect the contribution given by the entropic heat, since for the currents in play that are normally required to a BP this latter term results to be several order of magnitude minor than the one accounting for the electrical losses. Hence, at the end, the quantity $\dot{Q}$, namely the terms that describe the internal heat generation of a Li-Ion battery, is normally found according to the following simple formula:

$$\dot{Q} = \dot{Q}_{\Delta S} + \dot{Q}_{el} \cong \dot{Q}_{el} = I_{batt}(V_{OC} - V_{batt}) = I_{batt}^{2} R_{eq}$$

Computed the value of $\dot{Q}$, this could be finally entered in the thermal model.

Typical characterizing tests

After having introduced in the previous section the electrochemical and thermal methods used for the characterization of a functioning Li-Ion battery, it is now necessary to understand when these are applied, and therefore the types of cycles that are normally performed in the research and development phase of the cell. In fact, a certain number of standards have been introduced to manage the different tests to which a battery is submitted, so that a certain degree of comparability is also found between tests carried out in different environments and times. As explained by Scrosati et all [41], the tests that turns out to be applied to the LIBs are generally classified depending on their aim: done in order to determine the performances of the product or to determine its functioning safety.

- **Performance tests**

The methods used to determine the performances consist in testing the electrical behaviour of a battery under the normal operating conditions characteristic of the EVs. The so-called "input" tests are for fresh batteries, while the "life" ones are aimed at measuring, periodically, the main specific parameters of the cells during weeks, months, or even years, to understand how the performances of the ESS got reduced in time—for instance, in this latter case, it could be computed the capacity of the battery and the correspondent loss of this during ageing.

- **Safety tests**

The safety tests, differently from the previous ones, are usually destructive tests able to provide reliable information on the different failure modes which caused the failing of the cell. Obviously, in this case, once that the test is completed the battery is no longer able to work and hence to provide further data.

For what are the objectives of this work, with different characterizing tests applied to a cell aimed at defining its specs and functioning features, as it will be fully explained in the next chapter, it is more important at this point to focus on the first class of testing procedures, namely the “performance” ones.

Typical characterizing tests – **Performance tests**

To practically quantify the performances of a LIB, several testing methods could eventually be carried on, where different “modalities” of charge and discharge follow predefined regimes, specified by either a certain current level or power magnitude. The obtained results, then, are assessed against established goals or compared to their nominal counterpart, and they mostly refer to values of:

- Capacity in Ah;
- Energy in Wh;
- Maximum current in A;
- Power in W.

In general, it turns out that the most common performance tests are aimed at characterizing and describing an entire set of batteries, namely the BP subsequently used in an EV. Here, the voltages and power levels in play may reach values far above $300\ V$ and $25\ kW$, and hence the system need an appropriate control of its behaviour under such a high electrical “stress”. Hence, by measuring and studying the resulting values from a working BP, also an appropriate check could be performed dealing with the electronics and failsafe devices. However, it is interesting the ability of the tests to be eventually scaled down in order to be applied to modules and even to the single cells, whenever the parties involved in the testing campaign have interest in the information obtained at these “deeper” levels. To successfully perform this scaling, the tests usually do not indicate fixed magnitudes as output, but rather they use reference quantities, such as for instance values of maximum voltage and the minimum “cut-off” one, the maximum charging current and the “1C” one, etc., so that that the resulting BPs can be adjusted depending on the specifics of the tested cells.

Going more into detail, the most important tests that are nowadays commonly performed in the field of research and development for LIBs are here in the following presented.

- **Constant current discharge**

  With this constant current tests (CC), once that the battery has been led to a fully charged state ($SoC = 1$), it subsequently gets discharged with a constant current level until the cut-off potential, specified by the manufacturer, is hit. The discharge current that is used depends on the actual application for which the cell is intended for, and it is considered in the form of “C-Rate” (C) rather than with the standard form of current measured in A. The definition of the C-Rate is directly related to the nominal capacity of the ESS, since the level of Ah denotes the amount of current that could eventually be delivered by the cell to completely discharge it in (theoretically) exactly $1\ h$: hence, a battery with a nominal capacity of $xx\ Ah$ presents a C-Rate of $1\ C$ whenever this is discharged with current of $xx\ A$. For this kind of tests, if high powers could be required to the ESS, the current usually correspond to values of C-Rate between $1 \div 10\ C$, while whenever low power applications are involved, the discharge current may take values of C-Rates below $1\ C$. In this cases, the final objective of the experiment is usually to find whether both the measured capacity and the corresponding energy content of the battery agree with the values given by the manufacturer, and, as a consequence, these kind of characterizations are normally done previously to other more sophisticated tests. Finally, according to the suggestions of the standards, these tests are intended to be performed at a stable ambient temperature of $25 \div 30\ °C$, but are nevertheless also applied at stable temperatures within the range of $-20 \div 40\ °C$ in order to estimate the fade of performances of the EVs in different climatic conditions.

- **Pulse power characterization**

LIBs also need to be tested and characterized with pulses of power, since to the cells are normally required rapid and accurate responses to disruptive demands of powers. Therefore, with this kind of tests there is the intention to emulate part of a generic current profile at which a battery of an EV undergoes during its life: it considers, indeed, the simulations of the effects coming from accelerations (discharge of a cell) and braking (recharging a cell, if one considers the presence of regenerative braking), since rapid voltage drops and surges during, respectively, discharges and charges are common phenomena and must therefore be characterized.

These particular tests have become known in the last years with the name of “Hybrid Pulse Power Characterization” (or, shortly, HPPC). According to the relative standard, the pulse of discharge normally uses the totality of a normalized current value, while the charging pulse turns out to be close to the $75\ \%$ of the latter: it could be said that, after a cycle of discharge and recharge, the energy is not completely restored in the simulated braking portion. The pulses generally last $0.1 \div 20\ s$ for high-power applications and up to $120\ s$ for high-energy and low-power ones, with the pulse for the recharge of the cell that results to be generally shorter than the discharging phase one. Obviously, also depending on the actual cells under study, as well as on their future applications, different timing schedules and C-Rates are used to create the pulses. As an example, in the following *figure 38* a simple and typical one-cycle current pulse test is respreseted, with the current that has been normalized at a value of 1.

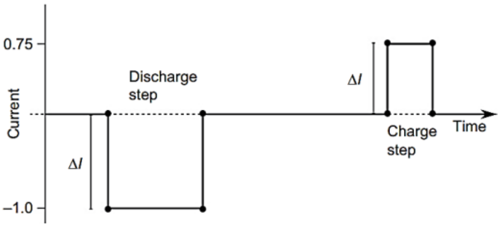

FIGURE 38 - Example of a single current pulse test profile

As a result of the application of a cycle such as the one represented in the previous image, also being in accordance with the theory, the voltage profile takes approximately the shape shown in the following *figure 39*.

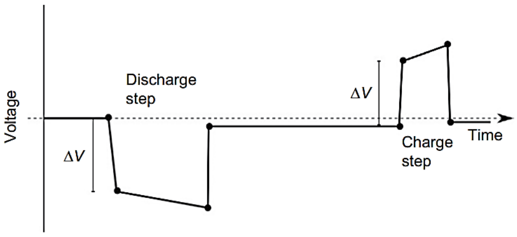

FIGURE 39 - Voltage profile deriving by the application of pulses

- **Variable power discharge**

In this other more specific testing procedure, the battery is led to sustain a variable power profile which is based on a certain standardized driving cycle. This is useful from an electrical point of view, since a driving cycle normally provides information regarding the speed of a vehicle, but it is not able to indicate the power demand at the BP's level. Several driving cycles are used for this purpose, and among the most important ones are usually found those deriving from the following standards:

- Federal Test Procedure (FTP-75), from the USA;
- New European Driving Cycle (NEDC), from the Europe;
- "JC08", from the Japanese Ministry of Environment.

It is also interesting to highlight the fact that the standards mentioned above were originally intended to measure the emissions and the fuel economy of ICE-based vehicles but are nowadays applied in the same way to estimate the electrical energy consumption and driving range of EVs. However, some particular regimes have been specifically developed to be representative of the power consumption of an EV. For instance, these include the Federal Urban Driving Schedule (FUDS) and the Dynamic Stress Test (DST): the FUDS is nothing more that the FTP-75 standard drive cycle applied to a specific EV, while the DST turns out to be a simplified version of the FUDS, presenting the same average value of power discharged. An example of DST is shown in the following *figure 40*.

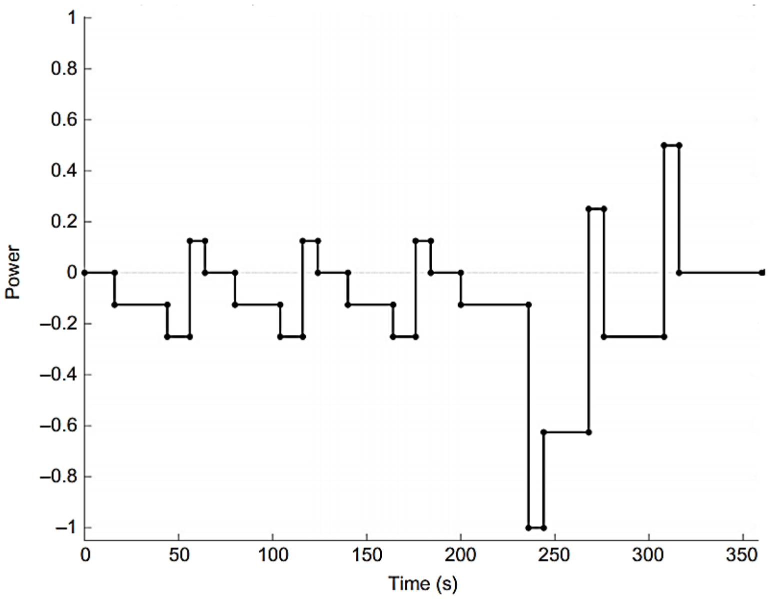

FIGURE 40 - Example of DST dynamic discharge regime

- **Storage**

When the storage test is applied to a LIB, also called “no-load” test, the device gets previously charged up to a certain level of SoC and then left at rest at a defined temperature, without being used, for an extended period of time. The cell’s capacity is measured at the beginning of test by applying a constant C-Rate discharge, and then computed again at the end of the storage period in the same way, so that it is possible to observe the retained charge and the corresponding loss of capacity, if any, whenever the Li-Ion cells are not connected to any external load. The initial level of SoC is normally found to be in the range of $50 \div 100\ \%$, and the storage period may last from 1 up to even 90 days.

- **Cranking power**

At last, with this other kind of procedure, the battery’s ability to start or crank another energy system is tested. To do so, the cells to be characterized are normally found at a low SoC, usually around the $20\ \%$: at this point, the battery is discharged with a short duration, high-current pulse for a few times, whit pulses of $2 \div 5\ s$ and a $10\ s$ pause in between each other. Normally, the procedure is mostly intended to be applied below the $0\ °C$ in order to characterize the charging and discharging capability of the electrochemical cells in tough environmental conditions.

At the end of the analysis, it could also be interesting to summarize what have been seen up to now, as done in the *table 13*. However, it has to be reminded the fact that several other more specific tests exist, aimed at characterizing the behaviour of Li-Ion batteries in particular operative and environmental condition. Nevertheless, with the inputs that have been shown with the procedures presented in this latter section, it would be easy to also understand all the others.

TABLE 13 - Most common testing procedures applied to LIBs

Test	Utilizes…	Scope	Initial SoC	Duration
CC discharge	Currents at a defined and constant C-Rate	To characterize the static capacity	Normally 1	From few minutes to few hours (function of the C-Rate)
Pulse power characterization (HPPC)	Positive and negative pulses of current	To characterize the serial resistance	Normally 1 (but not necessarily)	Hours
Variable power discharge	Positive and negative pulses of power	To mimic a driving cycle	Normally 1	Hours
Storage (no-load)	Cell at rest	To characterize the self-discharge	Between $50 \div 100$	Days
Cranking power	Positive and negative pulses of current	To characterize the ability of working in tough environments	Around 20	Minutes

Considerations

As it has been seen in this last chapter, the complex system that is a Li-Ion battery needs an appropriate and structured methodology of analysis. The various discoveries that have been made in recent decades have helped in defining what are the main modelling techniques used for these systems, and how to extract the quantities and values of interest from them. Each model brings with it different advantages and disadvantages and can be defined in some way to be unique, appropriate for the application it carries out. Testing methods, on the other hand, precisely help these models to be taken to a higher level of practice, where the results obtained implement the quantities of information that describe the technology and, in this way, allow its constant development through careful research activities.

In the following two chapter, a practical experience aimed at characterizing a Li-Ion cell is going to be addressed, and in order to study the system, a 2RC-branch ECM will be studied. As it has been explained, indeed, these user-friendly models allow to end up with a precise and fast characterization of the principal behaviours of the electrochemical battery, they are sufficiently accurate and require no particular long time in being solved. From the testing point of view, on the other hand, three different kinds of discharges will be used to broadly study the cell, explained later on in detail: HPPC, CC, and pulsed discharges (this latter, shortly called “PD”, is nothing more than a variant of the previously studied HPPC test).

Chapter 5

Simulated discharges of a large-format prismatic Li-Ion battery

Introduction to the CFD

To understand and to predict how all the elements that compose an electric vehicle work, both individually and together, and to optimize their design as well, the use of the so-called "computational fluid dynamics" (CFD) is able to return a robust and reliable final product. In fact, considering all the conceptual levels of an EV, ranging from energy sources, batteries and BPs, up to the electric motors and to external vehicle's aerodynamics, the ability to simulate behaviours is often the key step performed to achieve optimized results in various fields. Consequently, the role of the simulation in daily research and development is constantly becoming important: it can help engineering teams in investigating problems to better understand complex chemical reactions, fluid flows, heat transfers, electrical performances, and many more features that determine the performance of a system itself.

Going more in the detail, however, the goal of this entire work can be summed up in wanting to perform a CFD analysis to characterize the thermal behaviour of a Li-Ion battery through the finite element modelling (FEM) technique, applied herein by using the "ANSYS" software. As it has been seen, indeed, the general performance of all the EVs is based on their rechargeable ESSs, where engineers usually face the challenges of optimizing their energy density, thermal stability, charging speeds, lifecycle, and costs. Multiple field of the physics—including fluid dynamics, thermal, electrical, electrochemical, and structural—interact in determining the abilities of these systems in accomplishing theirs tasks, and hence the designers must consider not only the impact of each type of physics but also their interactions within a cell and at the BP's level. ANSYS provides a complete Li-Ion battery simulation solution that simultaneously considers all the multiple physics domains and incorporates detailed multiscale design to provide accurate predictions [42].

Wanting to perform a simulation at the cell's level, the analysis needs to start with a hybrid pulse power characterization (HPPC) of the system: the information coming from the HPPC test will then provide the measurement of the open circuit potential (V_{OC}) versus the SoC of the ESS, and of the transient potential under pulse discharges. These data, subsequently, are going to be used to identify the parameters for an equivalent circuit model (ECM), representative for the entire electrical behaviour of the cell. Eventually, many individual cells can be connected together in order to create a model for the module/pack which is useful to obtain prediction of the overall vehicle's performances. Nevertheless, before to go on it is important, once again, to highlight the fact that the cells' electrical performances are coupled in a two-way manner with their thermal behaviour, where this latter can be determined with a good accuracy by performing a CFD simulation. For this purpose, Fluent, an integrated software of ANSYS, will be used in order to connect together the ECM of the cell with the CFD thermal results. However, for simple that it may actually seem to get results through a simulation, it is going to be discovered in this chapter how complex the path that leads to these is, and how much transversal knowledge is necessary in order to obtain reliable results that can then actually highlight the role of CFD simulations and FEM analyses in the research field.

Testing campaign

Previously to the simulations carried on in the ANSYS environment, a certain number of characterizing tests have been performed on the reference cell. Although these experiments have been done in another moment with respect to the development of this work, it is necessary to introduce them in order to have a complete background and knowledge on the subject, also since the performed simulations are strictly based on the results previously obtained within the testing campaign. Hence, to explain the laboratory experiences, reference will be made to the Thesis project of R. Capuano [43].

The LIB that has been tested, characterized, and subsequently simulated in this experience, presented a large prismatic architecture with a LiFePO4 cathode (LFP-type) and a graphitic anode. The nominal capacity assured by the manufacturer is of $25\ Ah$, while the nominal functioning voltage turns out to be of $3.2\ V$, although it is reminded that the two quantities are slightly dependent upon the temperature of the environment in which the system is found to operate. Just to have a view of the ESS, externally, it looked like the ones shown in the following *figure 41*.

FIGURE 41 - Tested Li-Ion batteries

Three different typologies of tests have been performed on the battery in quest: HPPC, CC and pulsed discharges, all with the consequent CC recharge done in order to carry on again the cell to the level of $SoC = 1$. Apart from the different discharging techniques given by the types of tests, whose aim and results are going to be explained more in detail later on, it is also important to give a sight to the instrumental apparatus used to perform such experimental campaign, herein the following presented.

- **EA-EL 9080-400 instrument**

Produced by the company “Elektro-Automatik”, the unit had the task of requiring from the battery, in a regulated manner, a constant current: the cell, like this, got discharged until it reached a pre-defined cut-off potential. Obviously, this instrument was used for all the tests that are going to be presented, since despite the “pulsing” nature of the HPPC, CC, and PD procedures, the power gets taken and given from and to the ESS by applying a constant current. Furthermore, other functionalities of the tool that differ however from our scope, allow the battery to work with a constant voltage rather than constant inner equivalent resistance, both at the expenses of a variable current in time. At the end, resuming in other words, it could be said that the unit was used to mimic the presence of an electric load.

FIGURE 42 - EA-EL 9080-400 instrument

- **QPX-600DP instrument**

Produced by “Aim TTi”, to this tool has been given the function of power supply element. Like the basic version “-600D”, the -600DP one is a dual output DC power supply with a maximum overall power of $1200\ W$, suitable to both bench and systemic applications. The version that was used for this experiment incorporated a fully digital remote control as well as an analog one.

FIGURE 43 - QPX-600DP instrument

- **NI PXIe 6363**

The national instrument (NI) is a state-of-the-art multifunction input-output module used for reliable data acquisitions, structured with an advanced timing and synchronization technology. It is provided with an absolute accuracy for the $\pm\ 0.5\ V$ range of $100\ \mu V$ at full scale. Differently from the other instruments seen so far, the principal part of the component, which is actually its circuit board, is the heart of the whole testing rig.

FIGURE 44 - National Instrument PXIe 6363

- **NI LabVIEW**

LabVIEW is an integrated development environment for the NI visual programming language, the so-called “G”. The software was used for the data acquisition and storage, together with the overall process control.

- **PT-100 resistance thermometer**

Aimed at calculating the temperature of the tested Li-Ion cells, a “PT-100” resistance thermometer (RT) was used.

The so-called “RTD” (resistance temperature detector) is a measuring instrument which put in relation the voltage at the terminals of a simple electric circuit with the actual temperature at the level of the sensing element and is hence able to detect this latter quantity by computing the electrical potential variation. More in detail, a platinum wire, which is actually the sensing element, is found to provide a certain temperature dependent resistivity to the inner flow of a standardized current of $1\ mA$, described by the following law:

$$\rho(T) = \rho_0\big(1 + \alpha(T - T_0)\big)$$

Where ρ is the resistivity of the material, T the detected temperature, α the sensitivity of the platinum wire, and the “0” subscript denotes the relative quantities at the reference temperature, for industrial applications, of $0\ °C$. Obviously, the passage from the resistivity of the material to the resistance of the wire, important for the computation of the electric potential in the reference circuit, is practically given by the geometrical characteristics of this latter. Taking advantage from the law presented above, the sensing element is led in contact with the surface whose temperature is wanted to be detected, and by the changes in its resistance, then translated in changes of potential at the instrument’s level, the measurement is accomplished with a good accuracy.

A clear view of the RTD is provided in the following *figure 45*, even if the platinum wire cannot be seen since it is found to be directly inglobed into the contact needle.

FIGURE 45 - Example of a PT-100 RT

At last, always referring to the actual temperature measurement method applied to the experiments of interest, it is necessary to highlight that only one measuring point was selected for the thermal characterization of the cell: the centre of the largest face of the external case. According to the theory, in fact, the point taken in consideration is the most crucial one where one can detect the increase in temperature at the "interface" level of the ESS. Obviously, it is important to remind the fact that in the future analysis only the external chassis is considered as a comparative measuring point, despite the fact that both the internal active material and the tabs are actually warmer and more indicative. However, it will be interesting to see how the heating of these latter regions is then translated to the battery's case, where this latter could be found to be in contact with other elements of the module/pack and can therefore influence their performances.

Summarizing, the entire instrumental setup used for the testing campaign is represented in the following *figure 46*. As it can be seen, the Li-Ion cell was connected with the element simulating the presence of the electric load and the one acting as a power supply, and the entire experimental activity turned out to be regulated in conjunction by the input-output module and the LabVIEW software (which is the PC Control Unit). Regarding the latter, the practical interface was useful to allow the user defining the discharging and recharging cycles which the ESS was submitted to.

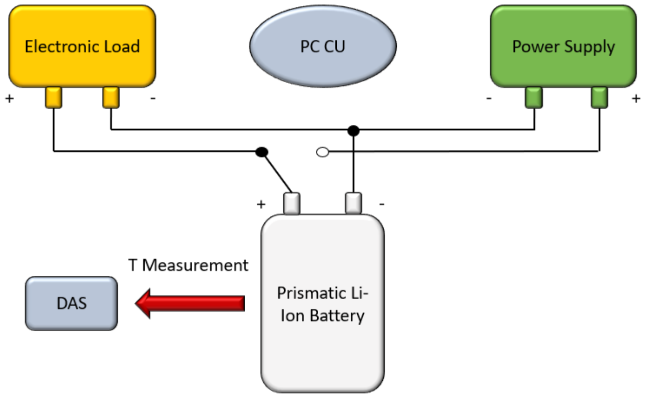

FIGURE 46 - Overall instrumental setup

Knowing now the composition of the whole experimental bench as well as its functioning principles, the discharging cycles that were performed during the testing campaign are going to be presented, together with their characteristics and results. It also worths to highlight the fact that, in this section, whenever a graph is going to be presented, it actually shows the real experimental data: these were initially acquired by the LabVIEW data acquisition system (DAS), then reorganized and plotted thanks to the functionalities of MATLAB in reading *.lvm* (i.e. "LabView measurements") files.

- **Discharge “HPPC”**

A standardized test needs initially to be carried on in order to allow the full characterization of the ESS, previous to the CC and PD tests, the ones that are then actually going to be compared with the performed simulations. With this aim, the so-called “hybrid pulse power characterization” discharge test is what fits at best for the purposes of the analysis. Ten short and subsequent discharge/charge power pulses at constant current were applied, and after them a certain time of CC discharge was then imposed in order to lower the level of the SoC of the $10\ \%$, ending up to fully discharge the LIB. The aim of the test is simple: the presence of both, the pulses and the CC discharges, allow to obtain the parameters describing the 2RC-branch ECM, as it is going to be explained more in detail in the next section of the chapter.

The entire HPPC test was thought to be composed by the following phases:

1. CC discharge: $2C$ for $10\ s$;
2. Rest: $50\ s$;
3. CC charge: $2C$ for $10\ s$;
4. Rest: $50\ s$;
5. CC discharge: $1C$ for $6\ min$;
6. Rest: $60\ min$;

At the end, the overall duration of the experiment is of $37200\ s$ (around $10\ h$ and $20\ min$), taking care to the fact that the resting phase is not required at the last cycle due to the fact that the battery already arrives presenting a $SoC = 0\ \%$ after the last $1C$ CC discharge. A single cycle of the current profile resulting from the experiment, from the battery’s point of view, is partially shown in the following *figure 47*: the discharges correspond to positive currents, and viceversa for the recharges.

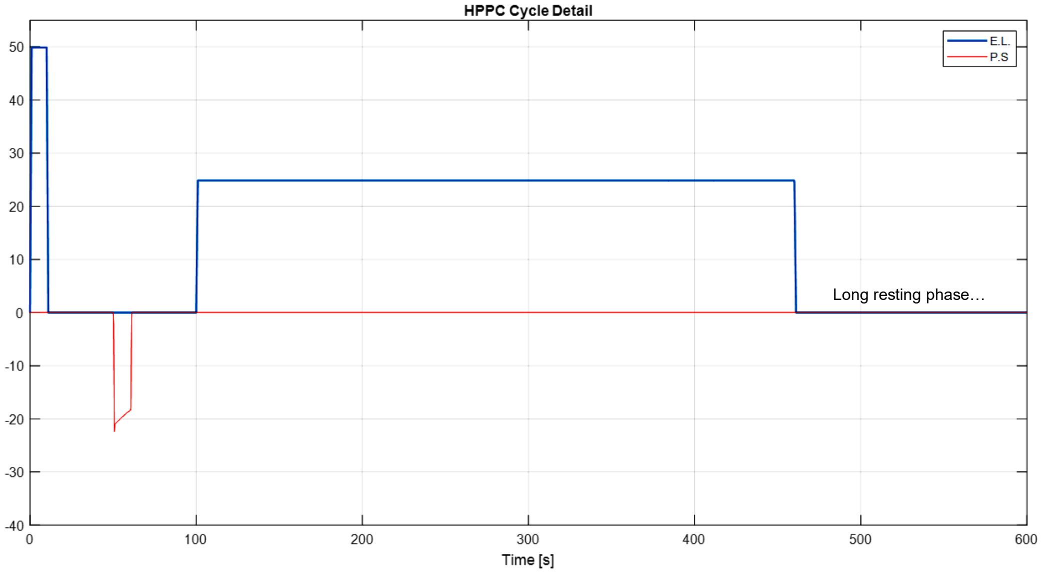

FIGURE 47 - HPPC current profile

Subsequently, the data regarding the voltage profile of the cell have been recorded, here reported, completely, in the *figure 48*.

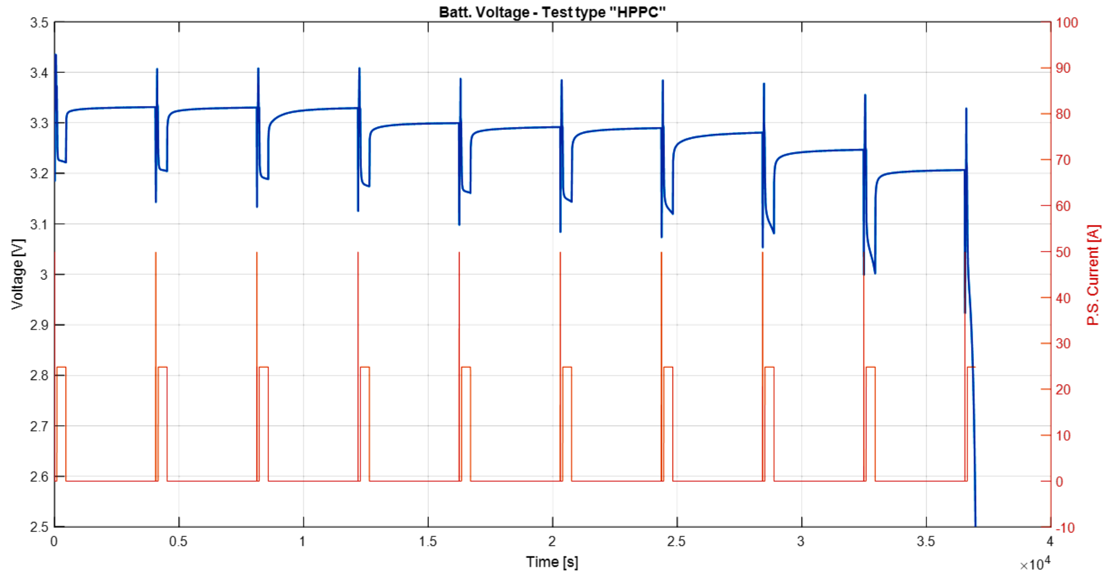

FIGURE 48 - HPPC voltage profile

Then, because of the pulsating nature of the discharge, the temperature detected by the PT-100 resistance thermometer shows, accordigly, a particular pattern: as it is represented in the *figure 49*, as far as the cell gets discharged the temperature increases and subsequently lowers during the long resting phases.

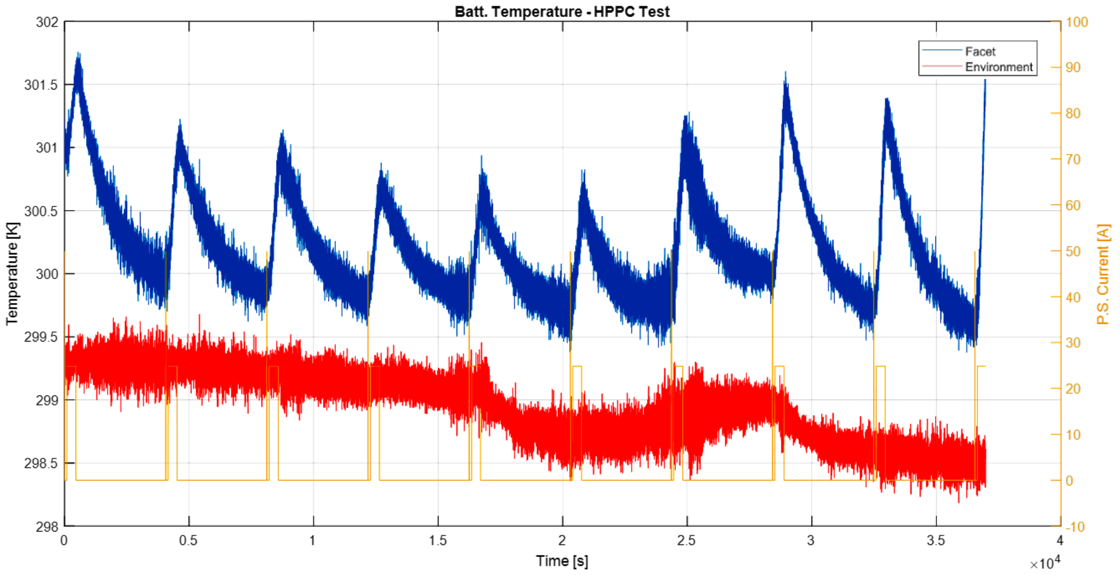

FIGURE 49 - HPPC temperature development

Note that, for what concerns the small power pulses, they turn out to be so short to almost not affect the temperature development, while, on the other hand, a small influence of the environmental temperature could be detected in the general trend, expecially in the last part of the experiment.

- **Discharge “CC”**

Four different CC discharge tests were performed respectively imposing to the experiment values of C-Rate of $0.5C$, $1C$, $2C$, and $3C$, whose magnitude was known by starting from the capacity of the cell as provided by the manufacturer—and also confirmed thanks to the precedent HPPC test. As it has been done in the previous case, the three types of discharges were aimed at completely exhausting the battery, and hence presented different durations: according to the definition of C-Rate, the tests lasted respectively $2\,h$, $1\,h$, $30\,min$, and $20\,min$, as it is clearly visible in the *figure 50*, representing the resulting voltage profiles.

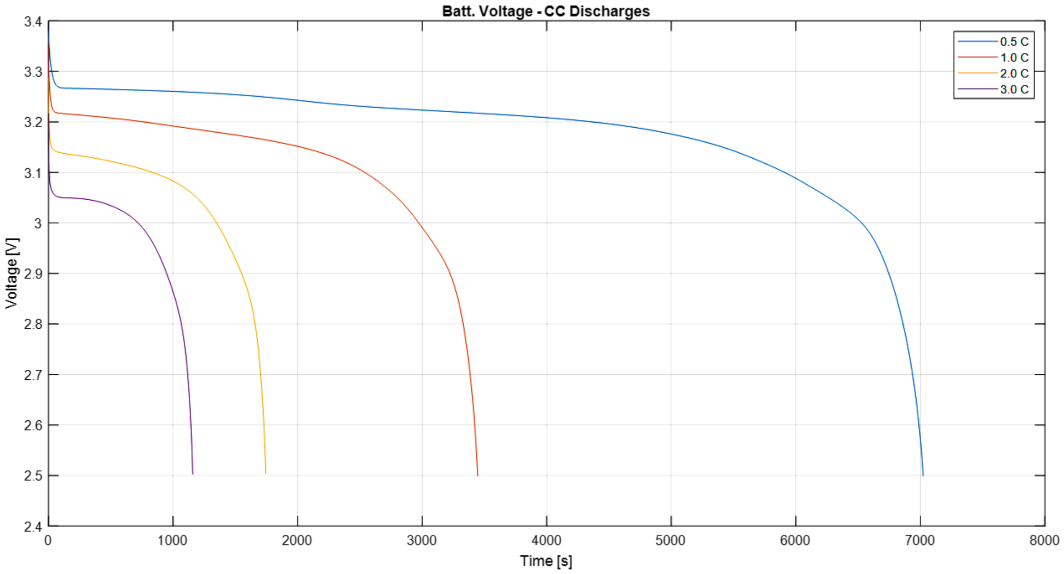

FIGURE 50 - CC voltage profiles

Furthermore, as also previously done, the resulting temperature development detected by the measuring instruments are reported, here in the *figure 51*.

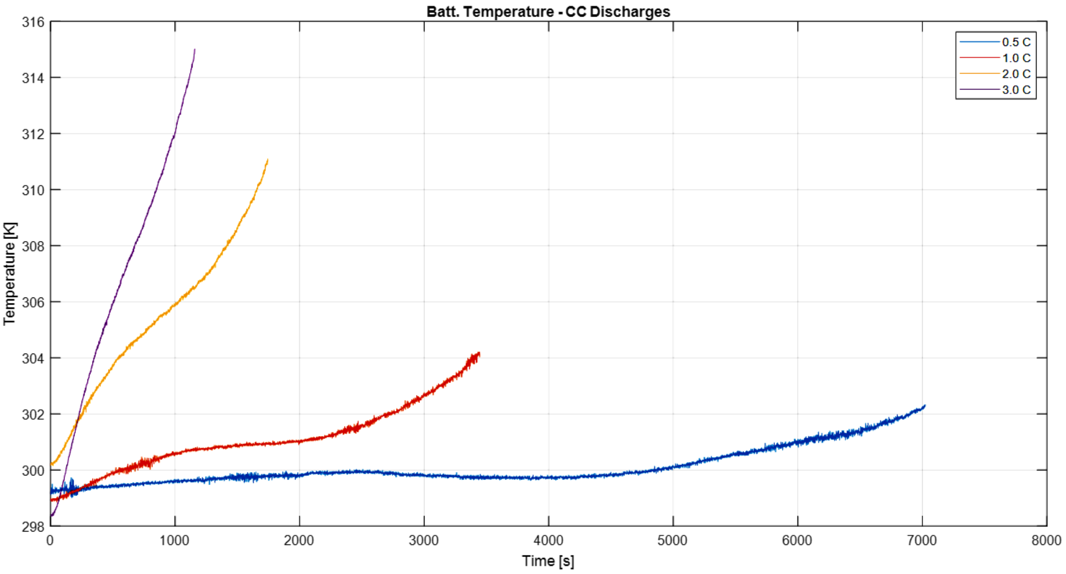

FIGURE 51 - CC temperature developments

Differently than before, in the CC discharges, the role played by the environmental temperature is only secondary: the development of temperature along the tests is only slightly influenced by the latter since higher magnitudes are present with respect to the previously analysed HPPC test. However, the effect of the ambient temperature could be mainly seen in the values detected for the first instants of the discharges, defining the environment indeed a sort of boundary condition to the different experiments. Furthermore, obviously, the effects of a change in the ambient temperature are mainly visible whenever small C-Rates are applied: there, the general temperature development keeps low values, and is hence more sensitive to thermal changes in the external enviroment. In general, therefore, it could be said that since the enviromental temperature is quite regular along the duration of the experiment, its role within the different temperature developments is going to be neglected in this work.

- **Discharge “pulsed”**

At last, four different pulsed discharges have been carried out in the experimental campaign. The involved C-Rates for the CC discharging phases are the same previously introduced: from $0.5C$ up to $3C$. However, even if the discharges took the same time that has been seen for CC tests, the resting phases among each pulse differ, and hence the overall duration of the experiments are found to be different too.

Knowing now from the previous plots the correlation that is present between the resulting potential profiles and the applied currents, in order to obtain a direct graphical comparison among the different experiments, in the following *figure 52* all the four potential profiles are simply displayed.

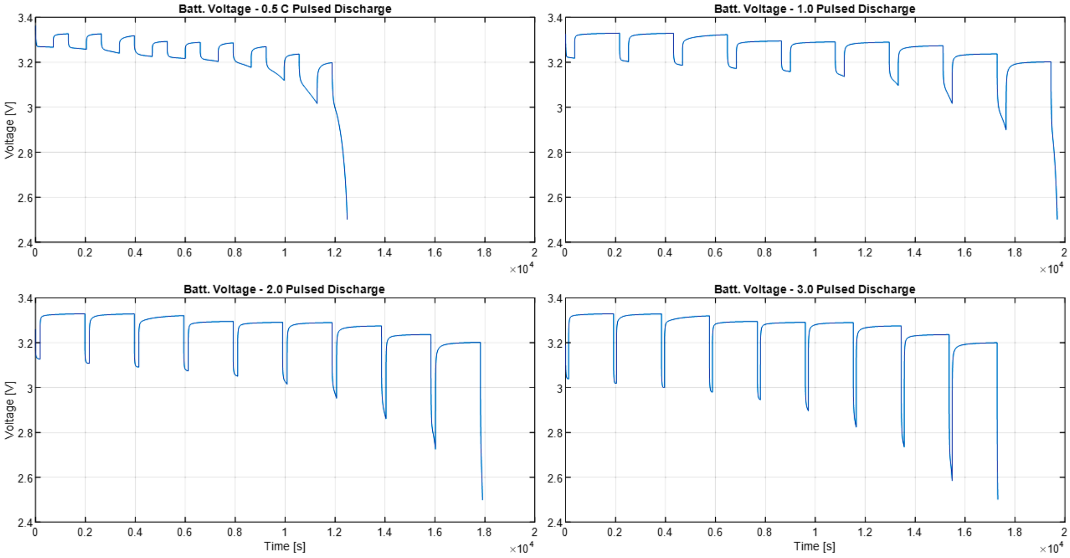

FIGURE 52 - PD voltage profiles

In the same way as done above, the temperature development is presented in the next page with the *figure 53*. Note that, in this case, according to what has been previously said for both the HPPC and CC discharges, the ambient temperature should be reported as well in the plots because of its higher influence on the temperature developments. Indeed, whenever the general trend of the temperature along a specific experiment turns out to be close to the its environmental counterpart, a small variation of the latter could slightly change the pattern of the former. Furthermore, another thing to be considered for such experiments is their duration: lasting in general more than $10^4\ s$, if the environement is not well conditioned, fluctuations in the boundary counditions are allowed to take place, and consequently needs to be integrated in an analysis to produce accurate results.

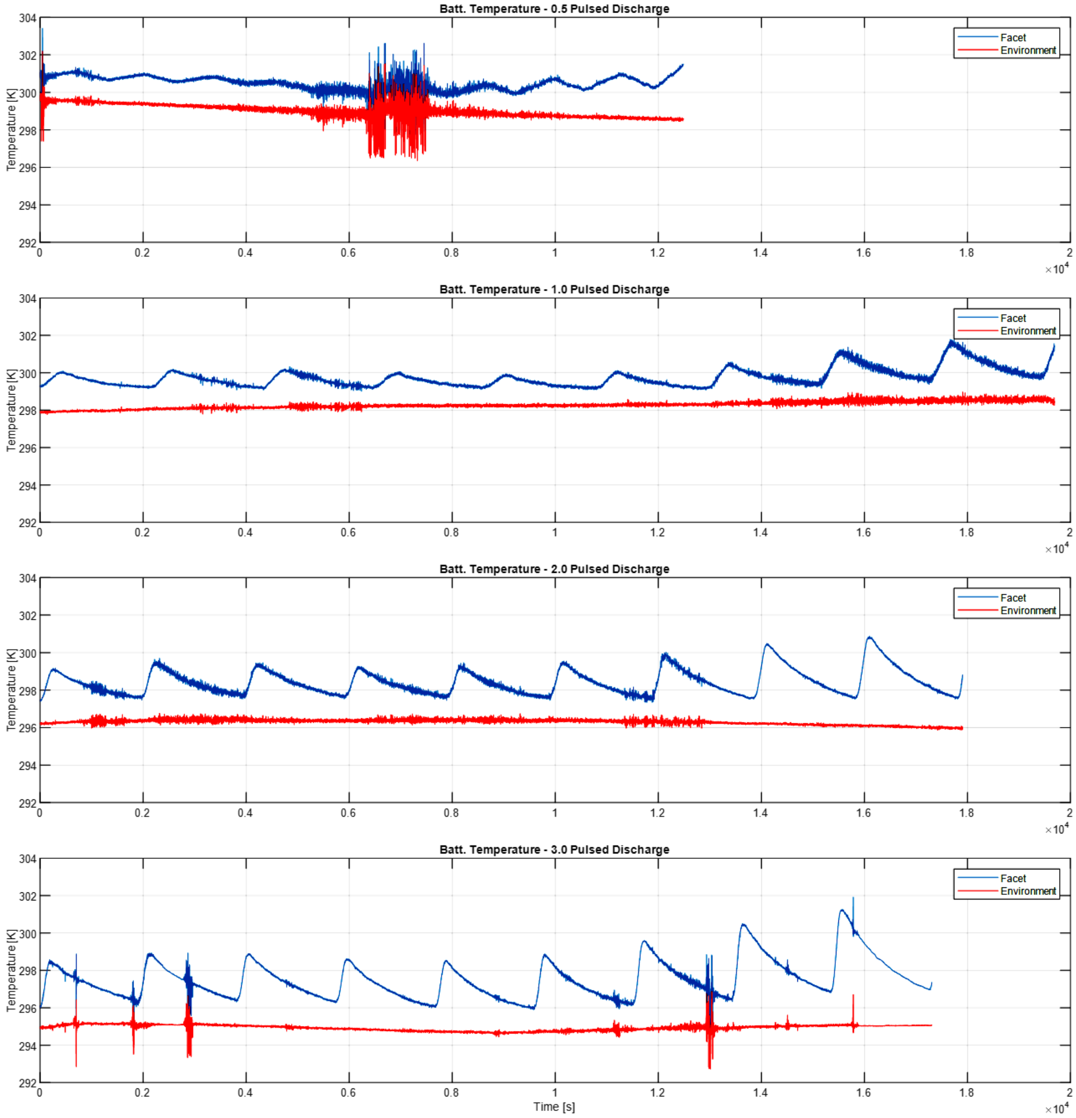

FIGURE 53 - PD temperature developments

Apart from the already expected fluctuating behaviours of the temperature developments, given by the pulsating nature of the imposed current profile, from the last set of images is also interesting to highlight the accuracy and sensibility of the measuring devices: even small changes in the thermal status of the environment are immediately detected, and consequently found their counterpart on the battery's surface, resulting in "strange" and unpredictable thermal profiles, such as the one represented in the PD test performed at $0.5C$.

At this point of the work, previous to the whole ECM definition and the subsequent simulating campaign, it could be interesting to summarize what are the outputs obtained so far. Starting indeed by knowing the entire instrumental apparatus which is involved in the experimental tests, togheter with the types of tests themselves under analysis, different magnitudes result to be of interest depending on the type of performed discharge. For instance, the HPPC procedure will be necessary in order to allow the complete caracterization of the battery with the ECM approach, while, the CC and pulsed discharges are important in order to effectively study the goodness of the simulations conducted in the ANSYS environment. Respectively, then, the data obtained by the former will serve as a case study for the behaviour of a continuosuly working Li-Ion battery, in a certain kind of working "steady state", while the latter suits for a dynamic-type analysis, thanks to the current's pulsating characteristics. However, keeping the numerical data for the direct comparisons that are going to be made in the following sections of the chapter, one important conclusion that can be obtained so far is that the higher the C-Rates involved in any type of discharge are, the higher is the temperature increment within the cell, as simply graphically suggested by the *figure 51* and the *figure 53*.

Definition of the ECM

The imaginary connection bridge that lies between the practical experimental world and that of the simulations is composed of a reliable model capable of describing the cell under analysis. In the particular case addressed in this work, the creation and the study of a 2RC-branch ECM has been chosen, being one of the best modelling techniques which is able to mimic the ESS. For its complete definition, the Simscape environment in "Simulink" was used.

Simulink is a software used for modelling, simulating, and analysing complex dynamic systems, developed by the US company MathWorks within the well-known software MATLAB. Simscape, more in detail, is an extension of the former which allows the user to easily create models of physical systems within the Simulink environment, presenting built link-based components that directly refers to block diagrams and other more complex modelling paradigms. Apart from the generalities of the program, it turns out that one of biggest field of application of Simscape is related with the electrical mobility, being it in fact able to reproduce components such as electric motors, TMSs, and ESSs.

The physical-based and semi-empirical modelling techniques producing ECMs, able to effectively mimic the functioning of Li-Ion batteries in a user-friendly way, have been largely addressed in the previous chapter. It is possible, so, to directly face in the description of the phases composing the design of a Li-Ion cell within the described environment. The simple model, which is shown in the following *figure 54*, is based on the integration of different standardized blocks which have been implemented by MathWorks, suitable for the reproduction of an ESS. Different elements can be recognized in the 2RC-branch scheme presented in the next page, each one aimed at representing, specifically, a part of the ECM:

- A voltage generator is used to create the open circuit potential of the battery whose magnitudes, from now on, are called either OCV or V_{OC}, and are measured in V.
- The three resistances, respectively, are the serial one, called either R_0 or R_S, and the two belonging to the RC branches, R_1 and R_2. All the quantities referred to these elements have the dimensions of Ω, even if turn out to have the order of magnitude of $m\Omega$.
- Finally, two capacitors, C_1 and C_2, once again belonging to RC branches, are both measured in F.

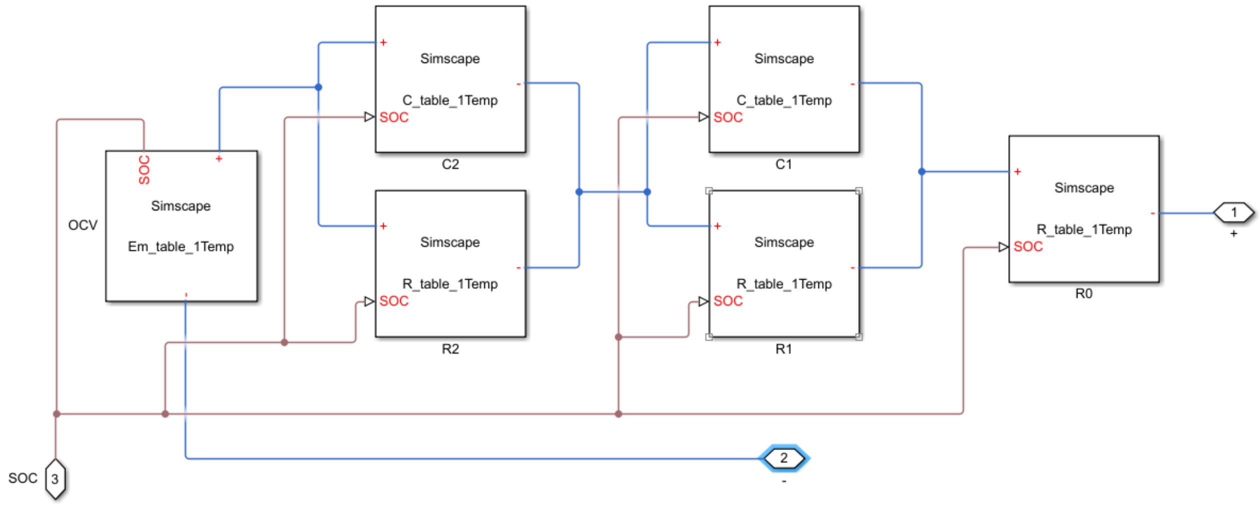

FIGURE 54 - Simulink Simscape Li-Ion battery two-RC-branch ECM

Regarding all the elements introduced above, however, it is necessary to highlight the fact that despite the common representations found in Simscape, where the electrical circuit components are actually designed following the standard rules, in this case, higher-level types of blocks were necessary since each of them also needs to be able to read and process the physical signal of the SoC. Hence, eventually, all the blocks needed a more detailed own design, here hidden under the so-called "mask". Moving up of a level, then, it is possible to see a more complete representation of the system under analysis mimicking all at once the complex experimental setup, seen at the beginning of the chapter.

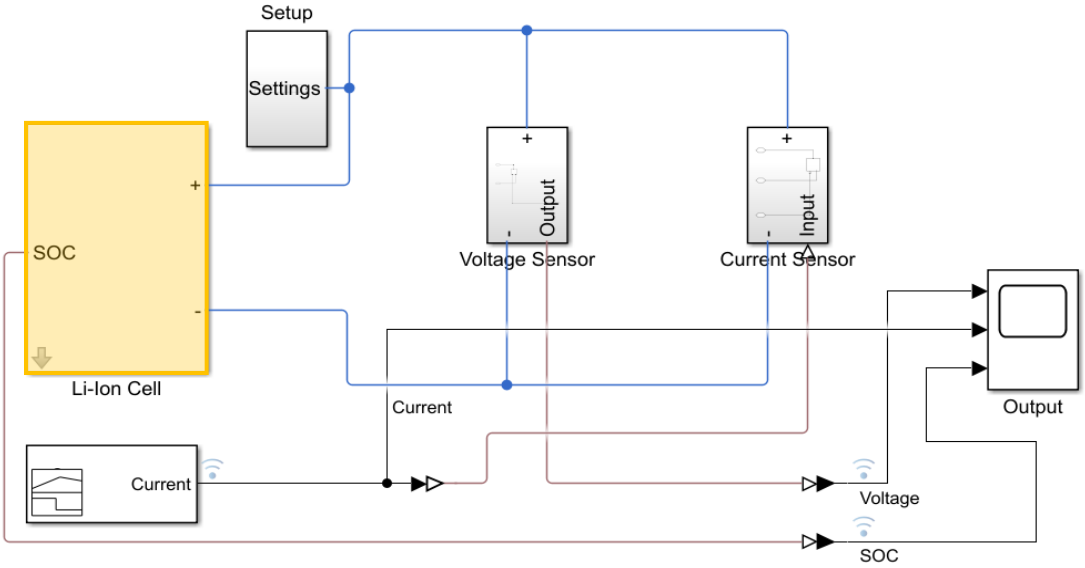

FIGURE 55 - Simulink Simscape experimental bench

To better explain the composition of the "bench" in the Simulink environment, proceeding from the left to the right in the *figure 55*, the following blocks are recognized in the composition of the system:

- An input block allows the program to get data from a *.xlsx* file and translate them at the software's level. In this work, in particular, the table contains the current profile which is actually applied during the HPPC test: from the records of the LabVIEW instruments, the data have been initially transferred in MATLAB and then passed to an *.xlsx* format in order to be effectively read by the Simulink model.

- The "Li-Ion Cell" block includes the 2RC-branch ECM previously introduced and represented in the *figure 54*.
- The "Setup" block, then, simply defines a reference for the electrical circuit of the Li-Ion battery thanks to the so-called "grounding".
- The two blocks with the function of sensors provide the output of the cells in terms of voltages and current (V_{batt} and I_{batt}). However, due to the nature of the analysis, the current sensor actually turns out to impose the current profile coming from the input block, and hence it accomplishes the function of a variable current generator.
- The final "Output" block is the so-called Simulink's Scope, where the incoming physical signals are plotted in order to allow the user to see the results of the simulation in a simple and effective way.

Also note that, in the Simulink environment, all the signals of the model move within defined paths: in the example above, the blue lines represent the conductors of the electrical circuit, the red/brown ones describe the movement of the physical signals belonging to the system, and the black lines, finally, accounts for the movement of the same physical signals at the Simulink's computing level—from the generating signal block to the scope, etc.

Now that the model has been introduced, what has been done in the Simulink environment is in the following described. The aim of the next part of the work is to fully characterize the battery in the Simulink environment for the future simulations that are going to be conducted in ANSYS, so that the values of the parameters that are going to be used in the ECM—such as R_S, R_1, C_1, etc.—will reflect exactly the real ones belonging to the Li-Ion cell under study. To obtain such results, two steps must necessarily be performed:

1. First of all, a "fake" simulation is going to be applied within the Simulink Simscape project described up to now.
2. Subsequently, a parametrical analysis will be carried out: the fitting of the outputs coming from the Simulink's Scope with the real curves, found from experimental dataset, will provide the correct ECM's parameters which are going to be the degree of freedom of the computation.

The aforementioned passages are necessary because of the fact that, since the values of the ECM's parameters are not directly accessible to the user, and also because of their implicit relationship with the energetic content of the cell—i.e., the SoC—, "fictitious" ones will initially be selected for all the quantities of interest. Then, as it is going to be explained more in detail later on, the initially imposed ones will be subsequently fitted thanks to the data coming from the real experiments, so that this parametrical definition of the problem, eventually, will end up with the correct definition of the ECM. Thus, in the following part of the section it is going to be provided an accurate description of both the two phases of the analysis aimed at finding out the ECM's parameters: the initial "fake" simulation and the subsequential data fitting.

- **Fake simulation**

To perform any simulation with the model that has been prepared, it is initially required to setup a certain amount of data within it. The battery's capacity, for instance, whose nominal value provided by the manufacturer is of $25\ Ah$, here has been settled to $25.5\ Ah$ after being properly calculated with a script in MATLAB, based on the real behaviour of the cell coming from the HPPC test. Indeed, by simply taking advantage from the already known "Coulomb counting" method, the integration of the net amount of current delivered with respect to the time gave the latter value, thought to be as reliable as the former. Furthermore, also the level of the initial energetic losses ($Q_{in,l}$) with respect to the calculated capacity needs to be addressed: for sake of simplicity, a value of $Q_{in,l}$ of the $0\ \%$ was chosen, where the percentage is calculated with respect to the energy level defined by the capacity. Settled these latter values, it is now time to speak of the parameters of the ECM, actually the values that make the following simulation "fake". Here, the method consisting in the compilation of so-called "look up tables" (LUTs) has been addressed. The LUTs could be defined as matrices, in this case composed of 10 rows and 1 columns—hence resulting at the end to be simple strings—that respectively account for 10 different SoC levels and 1 temperature range for the characterization of the parameters. For each one of the ECM's parameters a LUT has been considered so that these (R_S, R_1, C_1, etc.) could be expressed in dependence to the SoC level of the battery (1, 0.9, 0.8, etc.). Note that, by considering unidimensional LUTs, the parameters end up initially thought to be independent from the temperature. The primitive LUTs used for the "fake" simulation are shown in the following *table 14*, and subsequently explained.

TABLE 14 - LUTs for the initial simulation

ECM circuital parameters	$V_{OC}\ [V]$	$R_S\ [\Omega]$	$R_1\ [\Omega]$	$C_1\ [F]$	$R_2\ [\Omega]$	$C_2\ [F]$
At $SoC = 1.0$	3.4033	0.0030	10^{-4}	10^{4}	10^{-3}	10^{6}
At $SoC = 0.9$	3.3313	0.0029	10^{-4}	10^{4}	10^{-3}	10^{6}
At $SoC = 0.8$	3.3303	0.0030	10^{-4}	10^{4}	10^{-3}	10^{6}
At $SoC = 0.7$	3.3292	0.0030	10^{-4}	10^{4}	10^{-3}	10^{6}
At $SoC = 0.6$	3.2995	0.0031	10^{-4}	10^{4}	10^{-3}	10^{6}
At $SoC = 0.5$	3.2916	0.0032	10^{-4}	10^{4}	10^{-3}	10^{6}
At $SoC = 0.4$	3.2897	0.0033	10^{-4}	10^{4}	10^{-3}	10^{6}
At $SoC = 0.3$	3.2807	0.0033	10^{-4}	10^{4}	10^{-3}	10^{6}
At $SoC = 0.2$	3.2467	0.0034	10^{-4}	10^{4}	10^{-3}	10^{6}
At $SoC = 0.1$	3.2067	0.0035	10^{-4}	10^{4}	10^{-3}	10^{6}

The 2RC-branch ECM is described in total by six parameters, here entered within the look up tables above in two different forms: computed (real) and fictitious (fake). Starting from the former typology, only two set of quantities turn out to be the real ones for this analysis, since these could actually be obtained by working on the HPPC test's data: the parameters describing open circuit voltage (V_{OC}) and the ones for the serial resistance (R_S).

- Generally speaking, the open circuit voltage V_{OC} is the value of the potential that is found in the HPPC test characteristic curve whenever the cell is at rest and disengaged from the electrical load.
- The serial resistance of the battery, R_S, on the other hand, could be obtained by simply dividing the voltage drop that results from the application of a certain current by this latter value. In other words, whenever the cell is found to be connected to an electrical load, a certain fall of potential at its terminal is induced with respect to the open circuit one found in the previous case. The following formula describes how the serial resistance could be obtained:

$$R_S = \frac{V_{OC} - V_{batt}}{I}$$

Apart from V_{OC} and R_S, all the remaining parameters (R_1, C_1, R_2, and C_2) were fictitiously inserted, since not yet known. Also take into account that because of the very complex and time-consuming nature of the parameter fitting which is going to be performed it turned out to be better to already provide the "fake" values at least with a proper order of magnitude, easily found in the literature. Doing in this way, the subsequently fitting between the results is going to last few minutes, compared with several hours in case no adjustments to the results are initially accounted. Using the LUTs presented so far, by launching the simulation in the Simulink environment, the obtained results could be seen from the "Scope", here shown in the *figure 56*.

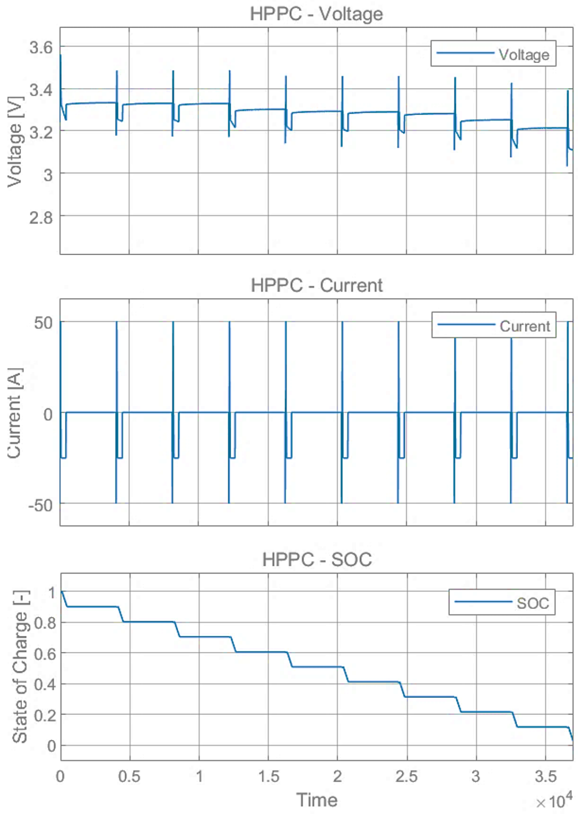

Figure 56

As it can be seen, starting from the lower graph, the SoC (rightly) progressively lowers of 0.1 at each pulse in the HPPC test, perfectly mimicking the reality, as well as it happens for the imposed current profile, which is actually the input to the analysis. However, always take in mind that due to the parameters that have been imposed in the LUTs, the voltage profile of the discharge does not match exactly the real one represented in the *figure 48*, even if the behaviours given by the correct values of both V_{OC} and R_S could be already recognized in the pattern. What is still remaining to do with the subsequent data fitting, therefore, is to find out the correct parameters for the description of the dynamic behaviours of the cell, i.e. those of the RC branches: R_1, C_1, R_2 and C_2.

- **Data fitting**

Once that the results previously shown are obtained, one can pass to perform the following step: the data and the curve fitting necessary to obtain the real values of the ECM's parameters. To do so, in the experience it has been taken advantage from one extension available in the Simulink environment, named "Parameter Estimator". Within the tool, it is initially necessary to provide two set of data:

1. The real voltage profile recorded during the HPPC test, labelled by the program as "measured" curve.
2. The voltage profile initially simulated by Simulink as described in the previous step, labelled by the program as "simulated" curve, which is actually the "fake" one shown in the *figure 56*.

The two curves appear in the plot window, and obviously, due to the fact that the performed simulation relies on a certain amount of fictitious parameters, they are not perfectly superimposed, as visible in the *figure 57.*

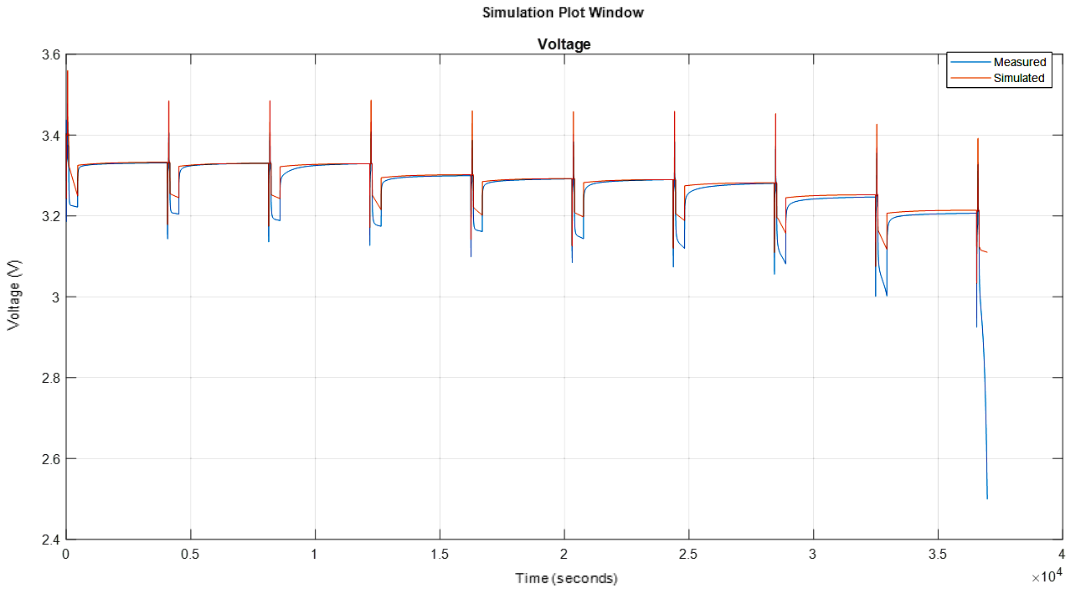

FIGURE 57 - Comparison of measured and simulated curves (before fitting)

At this point, it is required to define the quantities of the analysis that are going to change (i.e. the degrees of freedom) and consequently let the program perform the fitting between the two curves. As it has been already said, the set of values describing the behaviour of the cell in terms of V_{OC} and R_S with respect to the SoC have already been obtained, and hence need to be excluded from the analysis. It turns out that the remaining parameters R_1, C_1, R_2, and C_2, are actually the ones which are actually going to be involved in the future changes. Translating then what is going to happen at a graphical level, making reference to the image above, the red curve (showing the results of the "fake" simulation) is going to be more superimposed to the blue one (showing the real experimental results), in a smoother manner too, since the values describing the dynamic behaviours of the LIB—the ones belonging to the two RC branches of the ECM—will be led to be closer to the real ones. So, launching the fitting, the parameters get gradually adjusted up to convergence, and the plot window finally displays the two curves as visible in the *figure 56*.

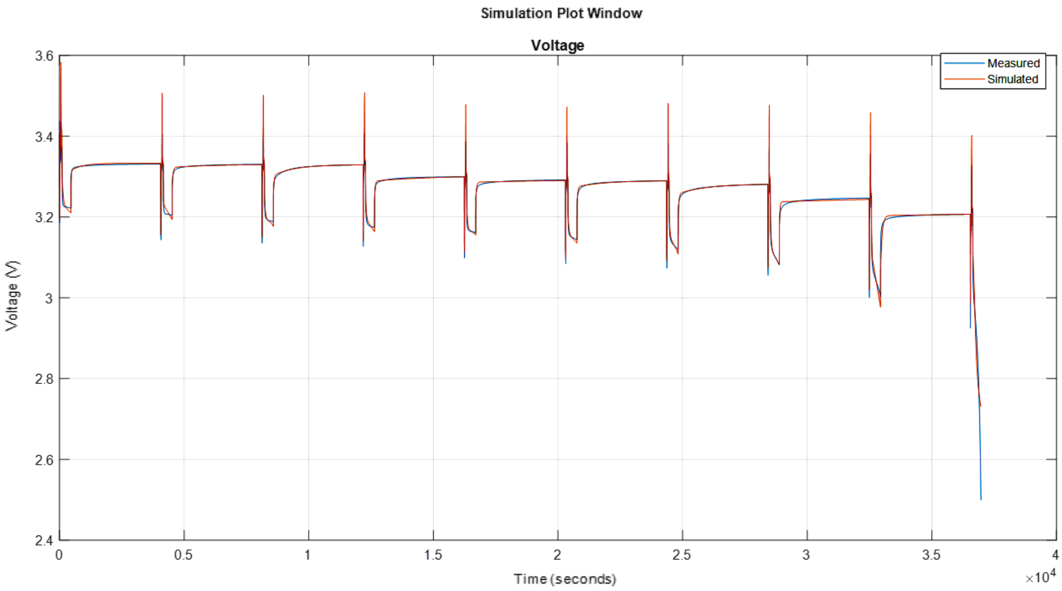

FIGURE 58 - Comparison of measured and simulated curves (after fitting)

Then, by moving back to the MATLAB's Workspace, the LUTs' new parameters, now the real ones instead of "fake", take the values presented in the following *table 15*.

TABLE 15 - Definitive LUTs

ECM circuital parameters	V_{OC} $[V]$	R_S $[\Omega]$	R_1 $[\Omega]$	C_1 $[F]$	R_2 $[\Omega]$	C_2 $[F]$
At $SoC = 1.0$	3.4033	0.0030	0.0028	$1.2389 * 10^4$	0.0013	$1.0598 * 10^3$
At $SoC = 0.9$	3.3313	0.0029	0.0011	$1.2478 * 10^4$	$2.44 * 10^{-4}$	$1.7383 * 10^6$
At $SoC = 0.8$	3.3303	0.0030	0.0023	$1.4407 * 10^4$	0.0029	$5.9148 * 10^5$
At $SoC = 0.7$	3.3292	0.0030	0.0020	$1.2692 * 10^4$	0.0068	$9.8306 * 10^4$
At $SoC = 0.6$	3.2995	0.0031	0.0019	$1.3124 * 10^4$	$1.09 * 10^4$	$3.6618 * 10^6$
At $SoC = 0.5$	3.2916	0.0032	0.0020	$1.5080 * 10^4$	0.0042	$6.3913 * 10^5$

At $SoC = 0.4$	3.2897	0.0033	0.0024	$1.1562 * 10^4$	0.0018	$5.2433 * 10^5$
At $SoC = 0.3$	3.2807	0.0033	0.0027	$1.0993 * 10^4$	0.0075	$1.1617 * 10^5$
At $SoC = 0.2$	3.2467	0.0034	0.0028	$7.0413 * 10^3$	$4.97 * 10^{-5}$	$6.6729 * 10^6$
At $SoC = 0.1$	3.2067	0.0035	0.0070	$1.0618 * 10^4$	0.0100	$1.3386 * 10^4$

Now that all the LUTs are effectively representing the behaviour of each parameter as function of the SoC, one last step has to be performed before to move in the ANSYS environment. The ECM, indeed, in order to be used, requires the data obtained up to now to be expressed in the form of polynomial curves of the $5th$ order with respect to the SoC. For instance, considering the generical parameter P, the following polynomial equation needs to be obtained from the relative LUT:

$$P = p_0 + p_1 * SoC + p_2 * SoC^2 + \cdots + p_5 * SoC^5$$

Where the set of values $p_0, p_1, p_2, \ldots, p_5$ composes the so-called "coefficients" of the $5th$ order polynomial curve. Also from a theoretical point of view, this operation results to be obvious and necessary: it is now clear that a certain parameter takes a value at one level of SoC, but it will be more correct to consider continuous smooth curves, so that all the values belonging to a certain interval of SoC are properly defined, continuously and not only discretely. To perform such an operation, the "Curve Fitting" tool of MATLAB has been used: by simply passing to the program the set of values composing the x and the y coordinates of the plot (i.e. the SoC and the LUT's parameters, respectively), the fitting that brings to the definition of a curve from the set of points in the parameter vs SoC plane is automatically performed after having imposed the grade of the polynomial (i.e. $5th$). The outcomes of this latter procedure are fundament for the development of the work: for each one of the six ECM's parameters are now available its own six coefficients describing the $5th$ order polynomial curve in the parameter vs SoC plane (i.e. p_0, p_1, etc.).

However, before proceeding in the next phase of the analysis, two important things have to be previously discussed.

- First of all, as it is well known, all the parameters apart from R_S are cell's dependent, meaning that they are a characteristic of the system under study, and are not function on the type of test. Hence, all the quantities related with the RC branches as well as the V_{OC} will be kept as valid for both CC and pulsed simulated discharges.
- On the other hand, the serial resistance is a magnitude which is a characteristic of the test performed, and no longer of the battery under study. Up to now, thanks to the look up table presented above, the R_S parameter which has been obtained thanks to the "curve fitting" tool is related with the HPPC test only, while the specific ones that are going to suit for the CC and pulsed discharges procedures still need to be found.

Thus, simply by already knowing the values of $V_{OC}(SoC)$ from the HPPC procedure and the voltage $V_{batt}(SoC)$ for each of the other different tests (CCDs and PDs at different C-

Rates) together with the currents in play, the R_S parameters function of the SoC could be found by applying the following formulas:

$$R_{S,CC}|_{SoC} = \frac{V_{OC,HPPC} - V_{batt,CC_i}}{I_{batt,CC_i}}|_{SoC}, \qquad R_{S,PD}|_{SoC} = \frac{V_{OC,HPPC} - V_{batt,PD_i}}{I_{batt,PD_i}}|_{SoC}$$

Where "$|_{SoC}$" reminds that each discrete value of R_S has to be computed for a specific level of state of charge. In other words, for each time that the SoC decreases of 0.1 starting from its initial value of 1, one has to take the value of voltage from the $HPPC$ test and the corresponding potential of the test under analysis. Also takes into account that, being the open circuit voltage a quantity that does not depend on the type of test, this latter could be also computed by the PDs' voltage profiles: it yields indeed that $V_{OC,HPPC} \equiv V_{OC,PD}$.

All the resulting coefficients of the $5th$ order polynomial curves that have been found are presented herein the *table 16*, recalling that apart from the serial resistances' ones all the others are common among the different typologies of tests.

TABLE 16 - ECM 5th order polynomials' parameters

ECM polynomials' parameters	p_0	p_1	p_2	p_3	p_4	p_5
R_S HPPC test	0.003503	0.000928	-0.0094	0.02316	-0.02622	0.01108
R_S CC $0.5C$ test	0.01931	-0.08461	0.2409	-0.4069	0.3916	-0.1582
R_S CC $1.0C$ test	0.01393	-0.05135	0.1348	-0.2192	0.2106	-0.08578
R_S CC $2.0C$ test	0.007439	-0.01193	0.006043	0.008104	0.002094	-0.008511
R_S CC $3.0C$ test	0.005639	-0.006514	0.002769	0.0005234	0.001165	-0.001074
R_S PD $0.5C$ test	0.0007118	0.06797	-0.3726	0.8302	$-\ 0.823$	0.3007
R_S PD $1.0C$ test	$//$	$//$	$//$	$//$	$//$	$//$
R_S PD $2.0C$ test	$//$	$//$	$//$	$//$	$//$	$//$
R_S PD $3.0C$ test	$//$	$//$	$//$	$//$	$//$	$//$
R_1	0.01396	-0.1126	0.3693	-0.5555	0.3784	-0.09182
R_2	0.02458	-0.2275	0.8698	-1.516	1.231	-0.382
C_1	$2.69E+04$	$-2.72E+05$	$1.32E+06$	$-2.63E+06$	$2.36E+06$	$-7.87E+05$
C_2	$-1.94E+07$	$-3.30E+08$	$-1.60E+09$	$3.32E+09$	$-3.10E+09$	$1.06E+09$
V_{OC}	2.862	5.51	-25.6	55.35	-55.39	20.75

Nevertheless, it could be interesting to spend some time analysing the coefficients of the R_S curves, which, as it is now clear, are actually obtained by knowing the LUTs of the different (function of the test) serial resistances. Let's hence start by graphically represent the discrete values obtained calculating the R_S as explained so far, herein the following *figure 59*, values which indeed "generates" the polynomial curves.

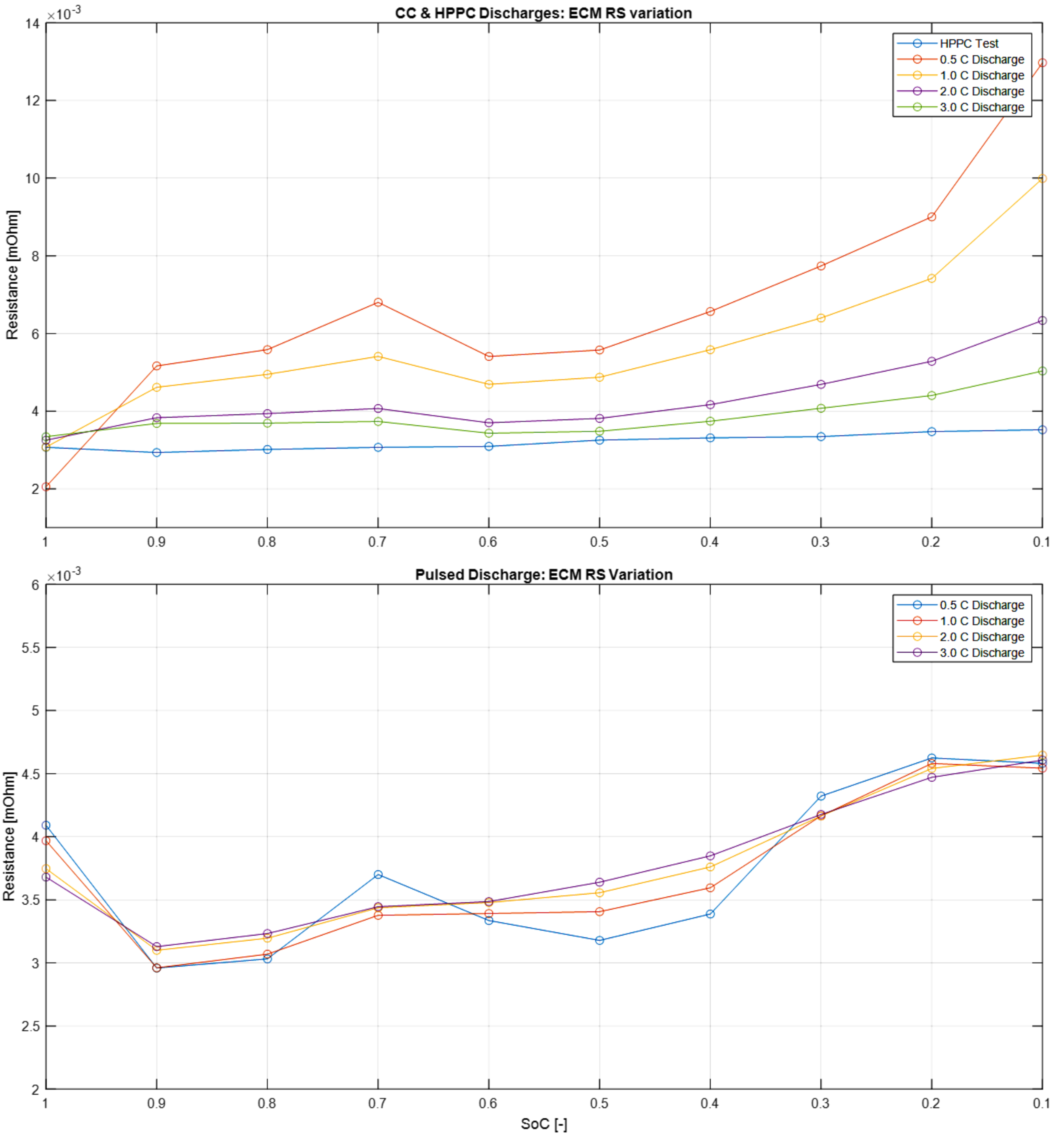

FIGURE 59 - R_S $5th$ order polynomial curves

The two types of tests that are going to be considered in the development of the simulations in this chapter, the CC discharges and the pulsed ones, necessarily need to be treated differently from the beginning, as suggested by the R_S behaviours along the discharges. Resuming indeed the most interesting aspects deriving from both the dataset and from the images, the following conclusions could be made:

- **For the constant current discharges…**

From the upper graph shown above, it can be highlighted that among the different CC discharges there is a certain degree of dependence of the serial resistance to the C-Rate: R_S turns out being major for small values of C-Rates while smaller for the higher ones, behaviour which is particularly pronounced as far as the discharge proceeds. This latter fact could be eventually explained by the values reached by the temperatures within the Li-Ion battery: a major temperature indeed, which is the result of a higher applied current, turns out in improving the Li^+ diffusion across the porous membrane as well as their intercalation/deintercalation with respect to the electrodes. Putting things together, the general pattern of the tests shows a certain resistance's increase along the discharge, which is however attenuated in case high temperature arise from the application of high currents, and hence, concluding, quite big differences are found between a test performed at $0.5C$ and another one at $3C$. In other words, the easiness with which a current flows within a Li-Ion battery is basically function of the applied current itself.

- **For the pulsed discharges…**

On the other hand, concerning the pulsed tests, the dependency on the C-Rate of the R_S parameter is not as strong as in the previous type of discharges. Also in this case, however, a simple theoretical explanation is able to confirm the graphical results: after the long resting periods subsequent to the discharges, the internal chemistry of the battery has had enough time to reorganize its structure, phases that are also accompanied by the decrease of the temperature that characterizes an idle battery (i.e. at rest). This latter phenomena take place for all the different types of pulsed tests, so that whenever a current gets applied to the device (i.e. the pulse begins) the R_S parameter is no longer influenced by the temperature but rather only by the amount of energy which is still present within the ESS. In other words, differently from the CC discharges previously analysed, the discrete values of R_S, in this case, are no longer influenced by the temperatures since the battery is always found to be fully at rest when the power pulses are applied. As a consequence of this latter phenomena, the local (function of the SoC) values of the serial resistance present only small differences among themselves which happens because of the different C-Rates, but the $5th$ order polynomial curves turn out being (almost) superimposed, thanks to the common general trends of the parameters. Hence, concluding, the six polynomials' coefficients are going to be maintained from analysing one test rather than the others, as written within the *table 16*.

To finally conclude the section, a brief summary playlist is shown with the aim of collecting all the steps that have been performed in this last part of the work.

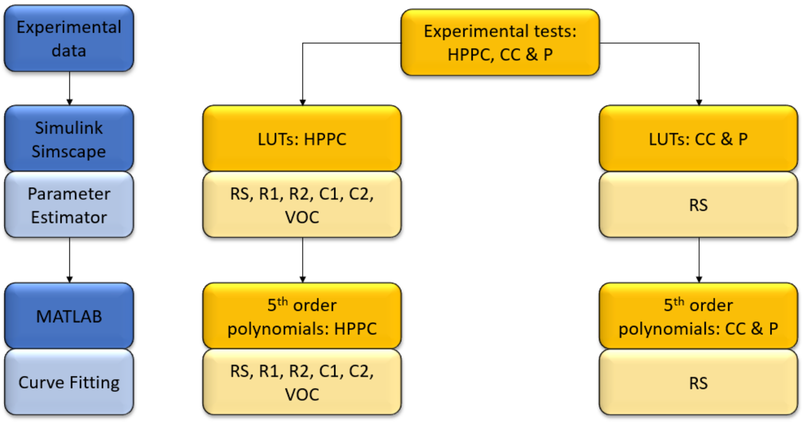

FIGURE 60 - Summary playlist to define the ECM

Now that the ECM has been completely defined, with the behaviours of its parameters during the discharge which is fully known thanks to the $5th$ order polynomials, all the information must be passed in the ANSYS environment to conduct the simulating campaign.

Multi-physics simulation

In the previous section of the chapter all the background which was necessary in order to understand and perform the simulations in the ANSYS environment, both theoretical and practical, has been addressed. Hence, moving on, it could be once again useful to present a summary playlist in the following *figure 61* introducing like this all the steps that are going to be performed in the following part of the work: the multi-physic simulation of a Li-Ion cell.

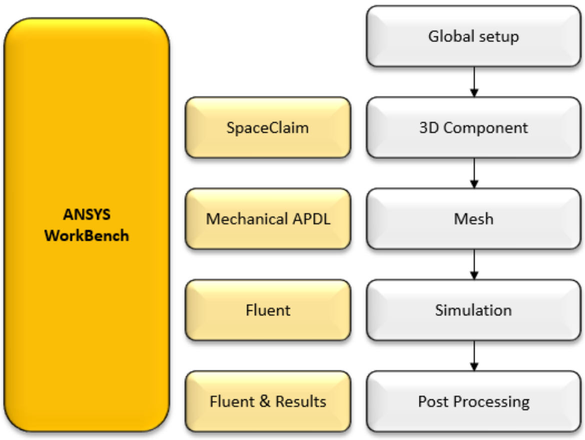

FIGURE 61 - Summary playlist for the simulation in ANSYS WorkBench

Explaining better the image above, initially, the system under analysis needs the creation of its CAD counterpart, which is then going to be meshed taking advantage from the FEM technique. In this way the simulation could eventually be performed, and the results processed in a user-friendly environment like that of ANSYS. However, as it will also be seen, for simple that it may seem, a certain level of transversal knowledge is necessary in order to move across the different softwares that enable to perform such operations.

The starting point to perform any simulation within the ANSYS environment is the setup of the problem in the so-called “ANSYS WorkBench” platform, the backbone which is able to provide a comprehensive and integrated simulation system. Using WorkBench will result in higher productivity, thanks to the pre-settled working flow which defines the integrated applications within the software to perform the analysis, allowing like this the access to multi-physics system’s level capabilities. The platform, as it can be seen from the *figure 62*, is indeed based around an innovative project schematic view which ties together the entire simulating process: wanting to perform a transient thermal simulation for a Li-Ion battery, it has been chosen to take advantage from the setup provided by the “Fluid Flow” pattern, which apart from the preparation of the analysis, carries out the simulation within the so-called “ANSYS Fluent” solver.

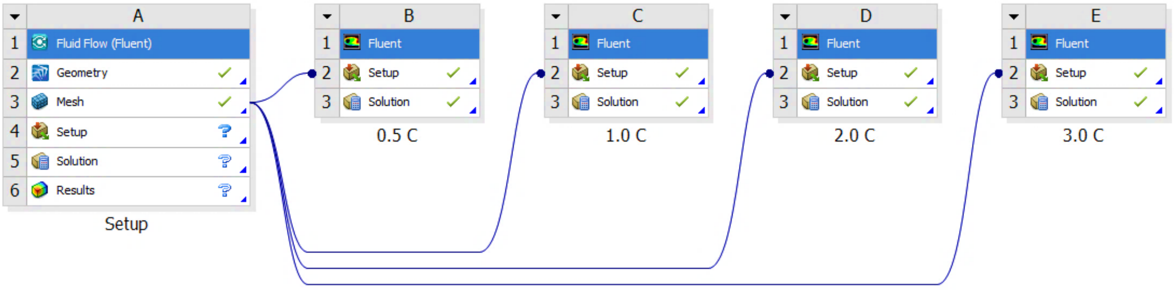

FIGURE 62 - ANSYS WorkBench analysis setup

By simply double-clicking on the different steps of the simulation (Geometry, Mesh, etc.) the platform redirects the user to the relative working tool within the ANSYS WorkBench package, herein addressed in the next sections of the chapter.

Multi-physics simulation – **Geometry**

The first step to be performed in the multi-physics analysis is the creation of the battery's three-dimensional CAD counterpart, which is then going to be used as a virtual reference for the subsequent simulations. The 3D CAD (Computer Aided Design) reproduction of the body, in the case of this work, has been accomplished thanks to the SpaceClaim tool, the software serving as the built-in 3D modeler for ANSYS WorkBench. Similarly to all the common CAD softwares, the components belonging to the overall system were created by initially sketching their profile in 2D mode, in the so-called "Sketch Plane", operation then followed by the already known extrusion, performed wanting to pass to a 3D geometry.

Nevertheless, many challenges were faced during the modelization of the cell. As it has been already seen, the studied system is a large prismatic Li-Ion battery of the LiFePO4 type. Obviously, the modelization of the device involves the whole set of elements that compose it, but, however, of particular importance is the volume that is made up of anodic and cathodic plies wound on themselves, which is actually the part of the cell where the Li^+ exchange takes place. The entire portion of space occupied by this so-called "active material", together with the electrolyte and the separators, which are both present between the pairs of electrodes, was considered as a single, geometrically continuum, unit. Apart from the geometric features of the component, its thermal and electrical properties will be adequately addressed and defined in the following sections of the work. Herein below, designed in the SpaceClaim environment, all the elements that were thought to take in the modelization a Li-Ion cell are introduced.

- **Rigid external case**

The rigid aluminium external case of the prismatic battery, mainly aimed at isolating and protecting the inner active material, has been reproduced by considering it as composed by three different elements: a lateral case, an upper cover, and a lower one. By initially settling a cartesian reference frame, the lateral case, which is a rectangular-based parallelepiped $1\,mm$ thick, is found to be $167\,mm$ high with a footprint $74\,mm$ wide and $31\,mm$ deep, considering respectively the body's main three dimensions. Accordingly, the sizes of the two covers could be deduced from the latter set of data: the lower one is a simple parallelepiped $1\,mm$ high with the rectangular footprint defined above, as well as the upper one. In the latter case, however, two openings must be taken into account since are necessary in order to host the tabs and part of the upper paper separator. These openings turn out to measure $24\,mm$ and $10\,mm$ respectively for the rectangles' major and minor dimensions.

The graphical counterpart of what has been explained up to now, is shown in the complete view of the battery presented in the following *figure 63*.

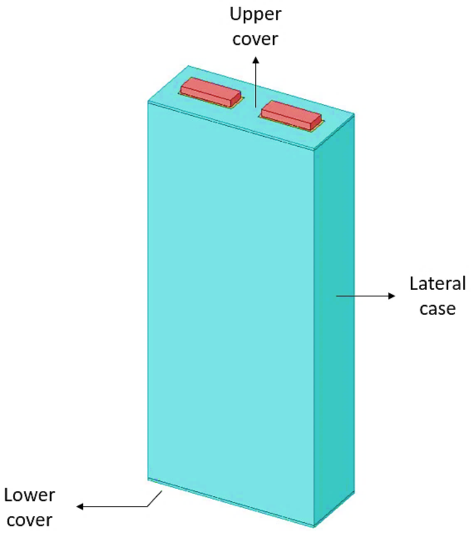

FIGURE 63 - Battery's complete isometric view

- **Paper separators**

Between both the two cover plates and the inner active material has been taken into account the presence of thin paper separator, $1\,mm$ thick with a footprint $72\,mm$ wide and $29\,mm$ deep (i.e. just fitting with the lateral case). The lower one takes the simple form of a rectangular-based element, while for the upper one, once again, the presence of the tabs has to be considered and hence the separator turn out being integrated with the relative cover plate, as shown in the following *figure 64*.

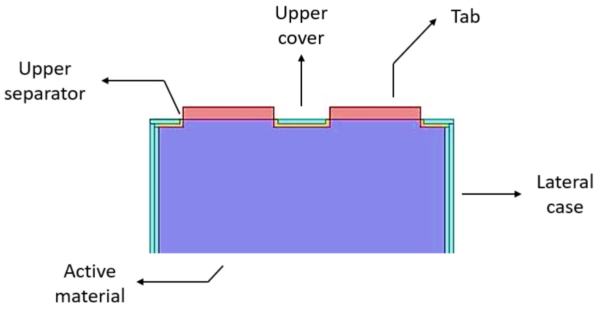

FIGURE 64 - Battery's upper cross section

- **Air gap**

In order to consider the clearances that are present between the lateral case and the inner active material, also the relative air gap has been modelized. Here, a 3D component $1\,mm$ thick has been placed in correspondence of the internal walls of the lateral case, ending up being $165\,mm$ high with a footprint $72\,mm$ wide and $29\,mm$ deep, considering in its height the integration with the separators. The small layer could be seen from the *figure 64* reported in the last page, as the adjacent component of the lateral case. Note that at this point of the design one has the complete external envelope of the cell (i.e. lateral case and cover plates), in total $196\,mm$ high, together with the elements signing the interface between these latters and the active material (i.e. paper separators and air gap).

- **Active material**

As it has already been introduced, the so-called “active material” takes into account the portion of space where a Li-Ion battery develops all the phenomena of heat generation as well as the electrochemical ones—i.e. the movement and the exchange of the Li^+ between the electrodes and across the electrolyte bath. In the case of this work, the active material is thought to present uniform properties, and hence has been modelized as a continuum body: relying on what has previously defined, the component fills the entire inner space of the cell, as well as the holes present in the upper separator in and upper cover, up to the interface with the external environment, as it is visible from the *figure 64* (reference to the purple element).

- **Tabs**

Finally, the last elements that need to be created are the tabs, components whose function is to connect the active material with the electrical circuit, extarnal to the cell. The small parallelepipeds, $3\,mm$ high, $24\,mm$ wide, and $8\,mm$ deep, are found to be exactly settled on the active material in corrispondence of the openings of the upper cover plate, once again shown in the *figure 64*, fitting with the design of both the upper cover plate and the paper separator.

Hence, now that the entire 3D reference component has been created, is necessary to discretize it in space by “meshing” its body, operation that requires the passage to another software in the ANSYS WorkBench environment. Note only that, finally, all the materials related to the different elements of the geometry have not yet been settled, hence the CAD file will automatically recognize them as solid components: the proper assignement will be only completed in the last part of the job in the Fluent environment.

Multi-physics simulation – **Mesh**

The so-called “finite element modelling” (FEM) is a numerical technique aimed at seeking approximate solutions for problems described by partial differential equations (PDEs) thanks to a reduction of these latters to systems of algebraic equations [44], easily solvable. The FEM maintains a dominant position in the scenario of numerical approximation techniques, being the kernel of most of the automatic analysis codes available on the market, such as the one of the simulating tool ANSYS Fluent. The main feature of the method is the discretization of the physical domain thanks to the creation of a grid, the so-called “mesh”, composed by primitives, or finite elements, of an encoded form: triangles and quadrilaterals for 2D domains and tetrahedra and hexahedron for 3D domains. On each element, characterized by this elementary form, the solution of the problem is assumed to be expressed by the linear combination of functions called “basic functions” or “shape functions”. It is important however to highlight the fact that sometimes the basic functions are approximated, and consequently the solutions will not necessarily be the real ones, but on the other hand are able to provide the least error on the whole solution. Wanting therefore to proceed in the analysis by discretizing the CAD component previously created, Mechanical APDL (where APDL is for “ANSYS Parametric Design Language”) is the software provided in ANSYS WorkBench that is going to be used, being the ANSYS finite element solver. However, it has to be highlighted that despite the fact that numerous simulations could be run on the tool, for the purposes of this work, this latter is only used with the aim of “meshing” for the system under analysis, while the CFD computation will take place on a different program.

Opening Mechanical APLD and loading the 3D component, the goal is to discretize the entire body with a reasonable fineness, proportional to the degree of precision to be obtained. The analysed Li-Ion battery model shows a geometric simplicity that will eventually favour the creation of a very regular and simple mesh, without great distortions in the grid. To create it, it is simply required to change some mesh-related parameters in the relative dialogue box. The dimension, for instance, passes from the default value of $9 * 10^{-3}\ m$ up to the dimension of $4 * 10^{-3}\ m$. Furthermore, another option to be set refers to the type of finite elements involved in the meshing: it has indeed been decided to act with quadratic tetrahedral primitives, and the program must be instructed accordingly. Finally, the last adjustment that needs to be done is the definition of the “types” of 3D elements coming from SpaceClaim: the mode “defined by geometry” could be left for all the parts of the cell since the option is already saying to the program that these parts are solid bodies, while it needs to be changed in “fluid” for the air gap. Doing in this way, only the solid components are going to be submitted to the creation of the mesh, while the air gap will be treated in the appropriate manner, considering hence the convective phenomena of heat transport while neglecting the electrical ones. Launching the creation of the mesh, the graphical outcome is shown in the following *figure 65*.

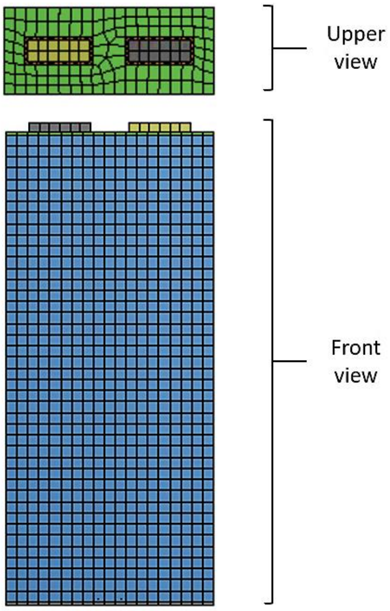

FIGURE 65 - Meshed battery

As it can be seen from the image above, by chosing the appropriate size of the elements it is possible to have a very ordered grid, where the only distortions turns out to be generated by the presence of the tabs, hence in the upper cover plate. Furthermore, apart from this latter representation, it is also interesting to see the cross section of the discretized component, where one can highlight the of 3D nature of the finite elements that compose the inner part of the body. Note that in the following image it has been chosen to present the entire cutted primitive in order to let understand its dimensions in the general context.

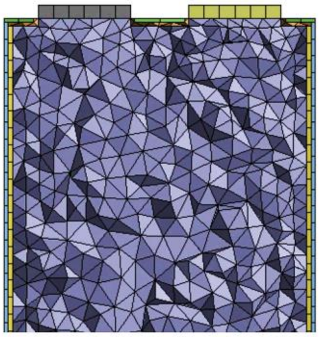

FIGURE 66 - Meshed battery's upper cross section

One last thing that necessarily needs to be done in the Mechanical APDL environment is to set the so-called "named selections" for the future simulations in Fluent. One named selection collects directly all the nodes and edges of the finite elements belonging to the components previously defined, treating this latters as a single entity. In other words, when the material of a component is going to be created, thanks to the named selection of the relative part, this is going to be assigned to all the primitives composing it. Overall, six named selections are going to be defined, here in the following introduced with the assigned names:

- "$Case\_Zone$", including the lateral case and both the upper cover and the lower one;
- "$Separator\_Zone$", including both the upper and the lower separators;
- "$NTab\_Zone$" and "$PTab\_Zone$", for the positive and the negative tabs, whose polarity is initially arbitrarily defined;
- "$EMat\_Zone$", including the active material;
- "$AirGap\_Zone$", including the air gap.

Another advantage arising from the creation of the named selections is the automatic definition of the interfaces of the components with the external environment, and consequently the definition of the superficial named selections generally called "$\ldots\_Wall\_Zone$", whose boundary conditions are going to be settled in Fluent. However, due to the fact the $EMat\_Zone$ is internal to the cell and in contact with another 3D element, i.e. the air gap, it is necessary to manually create another superficial named selection, called then "$EMat\_Wall\_Zone$". Doing like this, it will be possible in the setup of the simulation to also define a certain kind of "internal boundary condition", from the battery's point of view, for the active material surrounded by air, which is going to be initially thought as at environmental conditions.

Hence, having also completed the preparation of the 3D CAD model, thanks to the inclusion of a mesh and the creation of the appropriate named selections, it is now time to pass to the Fluent environment within ANSYS WorkBench.

Multi-physics simulation – **Setup**

It is now known that during the life of a battery its "health", or in general its performances, tends to slowly deteriorate due to many irreversible physical and chemical changes that take place inside it. Conventional engineering methods for analysing these behaviours require numerous and costly attempts, mostly in the form of long and complex testing campaigns. Innovation in this field, therefore, has required R&D process that involve different disciplines and scales, moving from the single electrode to the complete battery pack: as a consequence, it is born the need for a complete battery development process that will require a multi-physics simulation, including structural, electronic and system analysis. With the aim of performing this type of analysis, ANSYS Fluent is able to simulate the performances of Li-Ion batteries, both reducing development costs and accelerating the so-called "time-to-market". More specifically, concerning the arguments treated in this work, the thermal management of the battery remains essential to ensure maximum performances and avoid early failures and costly replacements. The temperature involved in the Li-Ion cells, in fact, affects many characteristics: from the autonomy of the EV to its safety of use and life cycle. Thus, with the precise aim of characterizing in detail the thermal behavior of a battery and taking into account all the physical phenomena during its operation, Fluent offers the best thermal simulations which could then turn out in the design and subsequent production of an economic and effective cooling plant, for instance.

As a starting point for this section, it has to be reminded the fact the apart from the simulations carried out on the Li-Ion cells, many different CFD-based analyses could be performed in the Fluent environment, ranging from heat exchangers up to the modern fuel cells. Consequently, hence, the program must be initially instructed about the type of object one wants to study. Opening ANSYS Fluent, within the so-called "text user interface" (TUI), a set of commands has to be written in order to call the complete pre-imposed setup of the problem:

$$define/models/addon-modules/8$$

Here, in particular, the number 8 calls the module of the "Dual-Potential Multi-Scale Multi-Dimensional" (MSMD) Li-Ion battery. Now that both the CAD model and its mesh have been uploaded in Fluent (operation automatically performed thanks to the WorkBench features) and the program is enabled to work on it since it is recognised as an ESS, the entire set of features available for the setup of the simulation have been initialized correctly, so that it subsequently remains to properly define them. All the operations that are going to be made from this point on are herein the following listed and detailly explained.

- **Preparation of the analysis**

  First of all it is important to let Fluent check the model which has been uploaded, in order to see if something went wrong in the FEM design performed in Mechanical APDL, and consequently if there are some discontinuities within the mesh. The overall control is automatically carried on by simply clicking on the "Check Mesh" and "Check Body" features of the programs.

  Since nothing should have affected the discretization of the battery, one should move on enabling the energetic analysis and settling the simulation type to "transient", operations for which it is simply required to click on the appropriate boxes.

- **MSMD battery settings**

The window for setting the parameters of the Li-Ion battery is automatically displayed by clicking on the “Model” tab and opening the relative model, namely the so-called “MSMD Battery Model”. Nevertheless, before proceeding it could be interesting to briefly explain the theory at the basis of the MSMD battery model.

As it has been seen, indeed, the difficulty in modelling a battery is mainly given due to its multi-domain and multi-physics nature. When performing a thermal analysis, such as in the case of this work, the goal is principally to determine the temperature distribution at the battery’s length scale: here, the physics governing the Li^+ transport phenomena occur in the anode-separator-cathode sandwich layers. With the aim of linking the simulation as much as possible within the theory and consequently to the reality, in Fluent, both the battery thermal and electrical fields are solved in the CFD domain using the following set differential equations:

$$\frac{\partial\, \rho C_P T}{\partial t} - \nabla(k\, \nabla T) = \dot{q}$$

$$\nabla(\sigma_+\, \nabla\varphi_+) = -j$$

$$\nabla(\sigma_-\, \nabla\varphi_-) = j$$

Where, respectively, σ_+ and σ_- are the electric conductivities for the positive and negative electrodes, φ_+ and φ_- are the phase potentials for the positive and negative electrodes, j is the volumetric transfer current density, and $\dot{q}$ is the heat generation rate happening during the function of the cell—which, as it has been seen in the *Chapter 4*, includes the Joule, electrochemical reaction, and entropic heatings. In order to solve these equations, operation which manly has to do with the definition of the parameters in play in the equations presented above, a wide range of electrochemical models have arisen in the years: from the simple empirical-based models to fundamental physics-based ones, as previously discussed in the work. In ANSYS Fluent, the most important three in the literature have been implemented:

- NTGK model;
- ECM model;
- Newman P2D model.

In the particular case of this work, it has been chosen to focus on the ECM of a Li-Ion battery, and in particular on its 2RC-branch variant, where the battery’s electric behavior is mimicked by an electrical circuit. By default, Fluent adopts the six-parameter ECM model (R_S, R_1, R_2, …) with the values presented by Chen et all in their work [36]. Obviously, those values need to be replaced by the ones found in the specific case under analysis, obtained in the previous sections of this chapter, in the same way as it has also to be done for all the other cell-specific quantities.

Seeing then the ECM-related parameters, the voltage vs current relation of the battery is obtained in the computation by solving the following three electrical circuit’s equations:

$$V_{batt}(t) = V_{OC}(SoC) + V_1 + V_2 - R_S(SoC)\, I(t)$$

$$\frac{dV_1}{dt} = -\frac{V_1}{R_1(SoC)\,C_1(SoC)} - \frac{I(t)}{C_1(SoC)}$$

$$\frac{dV_2}{dt} = -\frac{V_2}{R_2(SoC)\,C_2(SoC)} - \frac{I(t)}{C_2(SoC)}$$

To these, the effect of the discharge/recharge of the cell is given thanks to the application of the Coulomb counting method with the following formula:

$$\frac{d(SoC)}{dt} = \frac{I(t)}{3600\,Q_{Ah}}$$

Here, apart from all the quantities that have already been presented, Q_{Ah} is the initial capacity of the cell expressed in Ah, a fixed value, differently from all the other parameters which turn out to be function of the SoC. Thus, coming back to the definition of the differential equations whose aim is to characterize both thermal and electrical fields, with the ECM approach the source terms are computed in the following way:

$$j = \frac{I}{Vol}$$

$$\dot{q} = \sigma_+\,\nabla^2\varphi_+ + \sigma_-\,\nabla^2\varphi_- + \frac{I}{Vol}\left(V_{OC} - (\varphi_+ - \varphi_-) - T\frac{dV_{batt}}{dT}\right)$$

Where with Vol the program takes into account the entire volume of the battery's active material, and, as it can be noted, only three parameter get passed from the ECM to Fluent: the current I and the two potentials V_{OC} and V_{batt}.

Hence, now that also the complete explanation of the theory under the Fluent ECM has been addressed, all the actions that are going to be taken will result clearer. Wanting to perform the correct operations within to the "MSMD Battery Model" window, in sequence, the user is required to:

1. Define the general model settings under the "Model Options" tab in order to entirely characterize the Li-Ion battery. This will include, among the others, the chosen type of model (ECM), the nominal capacity of the battery $(25.4\,Ah)$, and the C-Rate of CC discharges or, in case of pulsed tests, the current profile properly written in a $.txt$ file. Furthermore, there is also the possibility to change the upper as well as the lower voltage limits—the so called "cut-off" potentials.
2. Specify the type of parameters to be used for solving the model equations under the "Model Parameters" tab and enter the required values: here, with the choice of using the 5th order polynomial curves (for discharging tests only), the previously calculated six ECM polynomial parameters are going to be inserted within the appropriate boxes. Only remember that, among the different typologies of tests, the correct set of R_S's coefficients must be entered. At last, in this section, it is also required to specify both the initial capacity of the battery as well as the relative SoC level (always equal to 1) for the subsequent simulations.
3. Select the zones for the active material, the tabs, and the busbar components (i.e. the external electrical connections) under the "Conductive Zones" tab. Note only

that, since in this work is actually studied a single battery, no busbar components are required to be entered.

4. Define the contact surfaces of the cell with the BP's conductors and the external connectors themselves under the "Electric Contact" tabs. Once again, however, note that as it has been explained in the previous point only the contact surfaces will have to be selected, since no wiring is considered in the proposed design.

Dealing with the playlist presented above, hence, the following *table 17* will collect all the quantities, values, and selections that are required to be made in the "MSMD Battery Model" window.

TABLE 17 - MSMD Battery Model settings

MSMD Battery Model	Model Options	Model Parameters	Conductive Zones	Electric Contacts
Settings	• Approach: ECM • Capacity: 25.5 Ah • (1) C-Rate value or current profile from $.txt$ file • Max. Voltage: 3.5 V • (2) Min Voltage: 2.5 V	• Nominal capacity: 25.5 Ah • Initial SoC: 1 • Approach: 5th order polynomials (discharge only) • (3) Parameters: from *table 16*	• Active Zone: "$EMat\_Zone$" • Tab Components: "$NTab\_Zone$" and "$PTab\_Zone$"	• Negative Tab: "$NTab\_Zone$" • Positive Tab: "$PTab\_Zone$"

NOTES

(1) The C-Rate value needs to be changed for the different CC simulations between $\mathbf{0.5}$, $\mathbf{1}$, $\mathbf{2}$, and $\mathbf{3}$, changes that must also be done for the current profiles in the $\mathbf{.txt}$ format describing the pulsed discharges, obtained from the experimental data.
(2) The "Min Voltage" value may need to be changed for the different simulations: because of the way in which Fluent performs the different discharges, the cut-off potential will be lowered to $\mathbf{2\ V}$ for both the CC and pulsed tests performed at $\mathbf{2C}$ and $\mathbf{3C}$.
(3) The coefficients of the polynomial describing the $\boldsymbol{R_S}$ parameter need to be changed according to the C-Rate of the simulation for the CC discharges, while could be maintained in the case of pulsed discharges (see beginning of the chapter for explanation).

Now that the entire 3D component has been characterized as a Li-Ion battery, it is necessary to define and assign the appropriate materials to the different parts composing the system.

- **Assignment of materials**

In the specific Li-Ion battery model under analysis, one has to consider the presence and consequently assign the following materials:

- Aluminium for the rigid external case;
- Paper for both the upper and the lower paper separator;
- Copper for the positive tab as well as for the negative one;
- Air in environmental condition for the air gap, between the case and the inner active material;
- Active material for the inner volume of the cell.

The modelization of a material for the so-called "active" zone is nevertheless complex. According to the assumptions made so far, the MSMD battery model will indeed consider the portion of volume composed by cathodes, anodes, porous separators, and electrolyte, as a single body characterized by average physical properties. To find out these quantities, one could start by studying the composition of the active part, here simply schematized in the following *figure 67*.

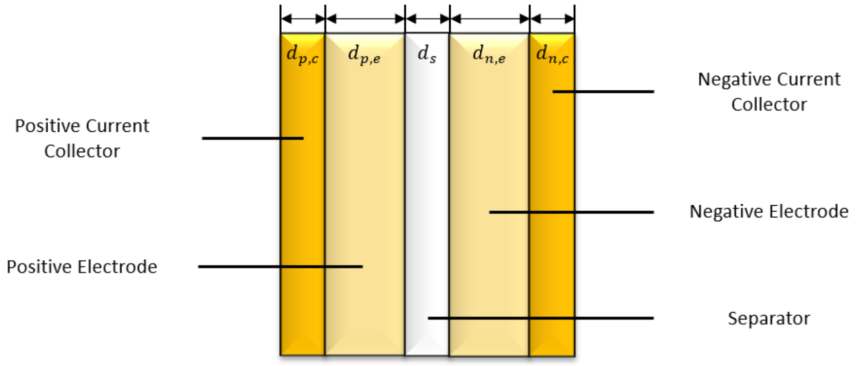

FIGURE 67 - Internal structure of the active material

Note that with "d" has been indicated the principal dimension of each part—i.e. its width.

Making, hence, once again, reference to the already cited work of Chen [36], the relevant physical properties of the different elements composing the Li-Ion LFP battery's active material could be easily found in the literature, and so get directly resumed in the *table 18* below. Take care because, as it has also been shown in the *figure 67*, both the positive and negative current collectors have been included in the analysis as part of the active material.

TABLE 18 - Active material structure's properties

Properties of the active material's elements	Positive Current Collectors	Positive Electrode	Separator	Negative Electrode	Negative Current Collector
Dimension, d $[\mu m]$	20	150	12	145	10
Density, ρ $[kg\ m^{-3}]$	2700	1500	1200	2500	8960
Specific heat, C_P $[J\ kg^{-1}\ K^{-1}]$	900	700	700	700	385
Thermal conductivity, k $[W\ m^{-1}\ K^{-1}]$	238	5	1	5	398
Electrical diffusivity, σ $[S\ m^{-1}]$	$3.8e * 10^7$	13.9	…	100	$6.33 * 10^7$

Wanting now to perform an analysis that will lead to the weighted average values of all the properties listed above, necessary in order to characterize the "new" active material's physical behaviour, one could use the following generic formula that will return the global physical property, here in the following simply called "P_{avg}". All the resulting values of interest will be shown then in the *table 19*.

$$P_{avg} = \frac{\frac{1}{2}\, p_{p,c}\, d_{p,c} + p_{p,e}\, d_{p,e} + p_s\, d_s + p_{n,e}\, d_{n,e} + \frac{1}{2}\, p_{n,c}\, d_{n,c}}{\frac{1}{2}\, d_{p,c} + d_{p,e} + d_s + d_{n,e} + \frac{1}{2}\, d_{n,c}}$$

Note that, in addition to P_{avg} which is the weighted average generical physical property, with p is considered the local one, specific to each element.

TABLE 19 - Global active material's properties

Active material	Weighted average properties
Density, ρ_{avg} $[kg\ m^{-3}]$	2092
Specific heat, $C_{P,avg}$ $[J\ kg^{-1}\ K^{-1}]$	678
Thermal conductivity, k_{avg} $[W\ m^{-1}\ K^{-1}]$	18.2
Electrical diffusivity, σ_p and σ_n $[S\ m^{-1}]$	$1.19 * 10^6$ and $9.83 * 10^5$

Take care that, concerning the electrical diffusivity of the active component, instead of a simple weighted average as done for the other properties, two different values have been defined: positive and negative diffusivity, indeed, were calculated here taking into account the exact proportions of the elements in play, according to the following two specific formulas:

$$\sigma_n = \frac{\frac{1}{2}\, d_{n,c}\, \sigma_{n,c} + d_{n,e}\sigma_{n,e}}{\frac{1}{2}\, d_{n,c} + d_{n,e}}$$

$$\sigma_p = \frac{\frac{1}{2}\, d_{p,c}\, \sigma_{p,c} + d_{p,e}\sigma_{p,e}}{\frac{1}{2}\, d_{p,c} + d_{p,e}}$$

At last, now that also all the theory under this part of the work has been faced up, the remaining task is to assign in Fluent the different materials to the correct zones. Opening the “Cell Zone Conditions” window and clicking on each named selections, it is then necessary to search for the materials within the Fluent library. There, air, aluminium, and copper could be easily found and consequently assigned, while the wood may be eventually used to substitute the paper of the separators. Concerning the previously discussed active material, on the other hand, this has to be created by entering the previously calculated user defined properties. Moreover, one last remaining adjustment needs to be done: the standard electrical conductivity of the copper will be simply replaced by the user-defined function provided as by the MSMD Battery Module.

- **Boundary conditions**

The environmental conditions that have been imposed in all the simulations tried to reflect as much as possible what has been recorded during the testing campaign.

First of all, it is necessary to determine and assign the behavior of the battery from a thermal point of view, also taking in consideration its conjunction with the surrounding environment: the right heat dissipation and the initial temperature values must be found and settled for each wall element created by the user. From a theoretical point of view, it is clear that the heat generated within a battery, as it has been treated in the *Chapter 4*, is mainly created due to Joule effect but it is not entirely retained in the case. This happens because of the properties of the materials constituting the various parts of the cell, all concurring in the well know thermal phenomena of conduction and convection. With the aim of considering this phenomena, the quantity which is of particular interest that needs to be assigned in Fluent is the convective heat transfer coefficient, namely "h", expressed in $Wm^{-2}K^{-1}$. Starting from a reference value of $5\ Wm^{-2}K^{-1}$, with an iterative method that considers the outcomes of the simulations and with the goal of wanting to be as much close as possible to the reality, the parameter was corrected until a match was obtained between simulation and tests at $35\ Wm^{-2}K^{-1}$. Then, for what concerns the environmental temperature, its detection was much easier thanks to the laboratory apparatus. In the following *table 20*, all the environmental temperatures settled for the different tests are collected.

TABLE 20 - Settled simulated discharges' ambient temperatures

Type of discharge	CC $0.5C$	CC $1C$	CC $2C$	CC $3C$	P $0.5C$	P $1C$	P $2C$	P $3C$
Ambient temperature $[K]$	299.5	299	300	298.5	301	299.5	297.5	296

- **Solution controls**

The last step which must necessarily be performed previously to the launch of the simulations in the Fluent environment deals with the adjustment of the simulations themselves.

Whenever one uses the MSMD battery model, two potential equations are solved in addition to other fluid-dynamic ones: in this case, the voltage equations at the two electrodes, named Phi^{+} and Phi^{-} by the program, are already activated within the "Equations" dialog box, together with the energetic and the flow ones. To speed up the entire computational process, the latter is going to be disabled since it is not necessary at all for the case treated in this work, where the environment is thought to be static and hence no flow of air is going to be taken into account. The control of the residuals of the computational process is then another fundamental aspect of the analysis. Fluent, indeed, divides the entire time-laps of the simulation in a certain number of time steps, in which for each of them it performs many iterations to bring the results in a certain safety-range of convergence. In other words, the program iterates the operations performed in each time step so that the outcomes are as close as possible to the reality. Here, however, a "large" number of iterations per time step is going to be settled without imposing any convergence criteria, since the residuals needs to be accurate enough before the program passes to another iteration cycle. In this way, it could be avoided the "problem" that arises whenever a certain residual goes under a settled threshold and hence Fluent passes to the next step without refining too much the results. Related to this latter aspect, it has been decided to use 20 iterations for each time step, which in turn globally covers $10\ s$ of the simulation. The choice of such values is not random: a $10\ s$ time step has been selected because of the resulting accuracy it carries out for the entire simulation process, being in particular short enough to let the program mimic in the right manner the dynamic phases of the discharges—of particular interest for what concerns the pulsed discharges—while the amount of 20 iterations per time step turns out with residuals' values ranging around the magnitude 10^{-6}. At last, the amount of time steps which have been selected, necessary to completely cover each discharge, are resumed in the following *table 21*.

TABLE 21 - Settled simulated discharges' amount of time steps

Type of discharge	**CC $0.5C$**	**CC $1C$**	**CC $2C$**	**CC $3C$**	**P $0.5C$**	**P $1C$**	**P $2C$**	**P $3C$**
Number of $10\ s$ time steps $[-]$	720	360	180	120	1260	1980	1800	1740

NOTES for the pulsed discharges:

- $\mathbf{0.5C}$: $\mathbf{10}$ pulses of $\mathbf{720\ s}$ each and $\mathbf{9}$ resting intervals of $\mathbf{600\ s}$ each.
- $\mathbf{1C}$: $\mathbf{10}$ pulses of $\mathbf{360\ s}$ each and $\mathbf{9}$ resting intervals of $\mathbf{1800\ s}$ each.
- $\mathbf{2C}$: $\mathbf{10}$ pulses of $\mathbf{180\ s}$ each and $\mathbf{9}$ resting intervals of $\mathbf{1800\ s}$ each.
- $\mathbf{3C}$: $\mathbf{10}$ pulses of $\mathbf{120\ s}$ each and $\mathbf{9}$ resting intervals of $\mathbf{1800\ s}$ each.

Hence, now that the general simulation's setup has been addressed, the program is enabled to start the FEM CFD analysis of the Li-Ion battery, and consequently provide graphs and numerical results available for the post-processing phase.

Multi-physics simulation – **Post processing**

It is now clear that in the ANSYS Fluent environment two different types of simulations are going to be performed, respectively trying to represent the CC discharges and the pulsed ones. For each of the two classes, then, four discharges respectively at $0.5C$, $1C$, $2C$, and $3C$ are actually simulated, for a total amount of eight different simulations. The important thing to remember is that, when acting in the same subset of discharges, from a certain C-Rate-defined one to another, many inputs must be changed within the program. In particular:

- The C-Rate, whose information in the case of this work gets actually provided thanks to a $.txt$ file carrying the current profile rather that by simply specifying it in the proper dialog box (it turns out being more accurate to follow the real detected quantities);
- The coefficients of the $5th$ order polynomial curve describing the behaviour of the serial resistance vs the state of charge of the cell, previously resumed in the *table 16*;
- The ambient temperature, whose values have been collected in the *table 20*;
- The amount of the $10\ s$ time steps, as reported by the *table 21*.

Hence, at this point, knowing also how to move between one simulation to the other one, as well as between the two different typologies of discharges, all the relevant plots, quantities, and results, are progressively going to be presented herein the following part of the section.

- **$0.5C$ constant current discharge simulation**

After having settled and launched the simulation as explained so far, once the computation is finished, the user can get the reports he wants directly on the screen. In the case of this work, it is important to ask Fluent the plot of:

- The residuals of the overall simulation (which is automatically performed);
- The maximum and the minimum facet temperatures detected for the "$Case\_Zone$" named selection;
- The superficial-weighted-average UDS (i.e. "user defined scalar") Phi^{+} computed at the positive tab (i.e. the phase potentials for the positive electrode).

Thanks to these graphs, indeed, one can first of all control the entire progress of the simulation by focusing on the expected relevant behaviours of the battery, necessary then to be compared with the outcomes of the testing campaign. For this purpose MATLAB has been used once again as the tool for the comparisons, whit the reports that can be once again obtained in Fluent, after their proper definition by using the "File…" command in the post processing environment. The quantities that are going to be "extracted" from the simulation remains those previously defined: indeed, the experimental computed temperature will be compared with the maximum and minimum simulated ones, while the resulting voltage profile at the tabs is going to be compared with the values of Phi^{+}.

Having run the simulation, it is possible to say that the plot of the residuals confirms the good accuracy of the analysis, being all the quantities of interest for the entire duration of this latter below the (absolute) value of 10^{-6}. In particular, the report will show the values taken by the two local potentials at both the positive and negative cathodes (i.e. the UDSs) and the energy equation.

Speaking then of the results of interest, the voltage profile, compared with the real experimentally detected one, is shown in the following *figure 68*.

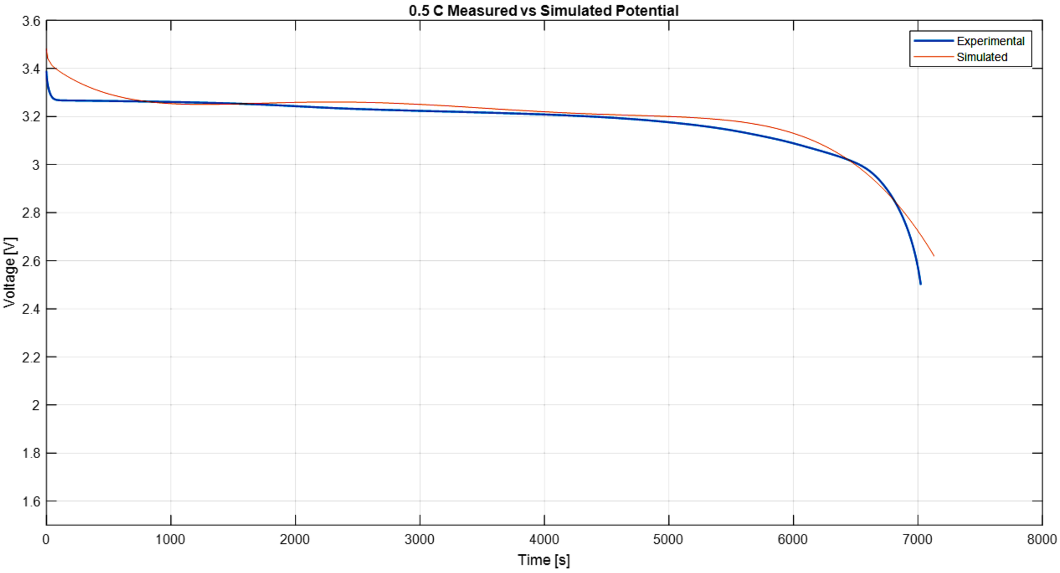

FIGURE 68 - $0.5C$ CC potential development

As it can be clearly seen, all the characterizing aspects that were originally found within the testing campaign show in the simulated voltage development their counterpart, from the initial and final falls of potential to the central “plateaux”, typical features of the Li-Ion batteries.

Dealing then with the temperature development represented in the following *figure 69*, the quite steady value of the quantity along the simulation is found for both the maximum and the minimum facet temperatures.

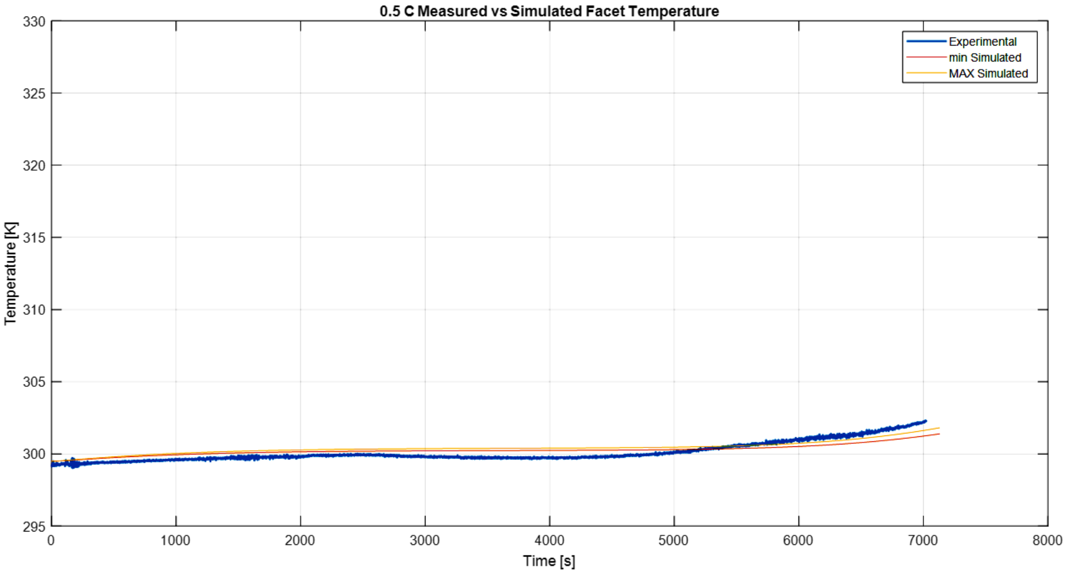

FIGURE 69 - 0.5C CC temperature development

Apart from the plots introduced above, the results of the analysis could be seen also from a graphical point of view thanks to the Fluent’s post processing abilities, where one can obtain very interesting pictures representing for instance the potential, temperature, and volumetric current density final distributions within the entire 3D component, element by element. The aim of these graphical representations is to provide, in addiction to the plots and to the numerical results, an user-friendly way with which the user may see what happens on the entire component. More in detail, once that the simulation is over, the user is allowed to deeply analyse the values of interest for the Li-Ion battery navigating inside the “Contour” section, feature of the program which allows to create the images represented in the next page.

By imposing for instance the reproduction by part of the program of the resulting temperature distribution at the final moment of the analysis, as shown in the following *figure 70*, it is possible to see where a $0.5C$ CC discharge may lead the battery from a thermal point of view. As it is clearly visible in the next page, the highest overall temperature is reached in the central portion of the active material, while the lower one is found to be present at the level of the external aluminum case, in corrispondence of the measuring point. Speaking then of the obtained values of interest, the two limit quantities introduced above are of, respectively, $304.19\ K$ and $301.39\ K$. As a consequence, it can be concluded that the temperature development of the cell leads to the aforementioned final value of $301.39\ K$ in the reference measuring point (i.e. the center of the external case’s biggest face), temperature which will be compared in the following sections of the work with its counterpart coming from the testing campaign. On the other hand, the maximum temperature which is detected at the level of the case turns out being in proximity of the tabs, where the current's circulation imposes a more sever temperature increase than in the measuring point, reaching a maximum value of $301.80\ K$.

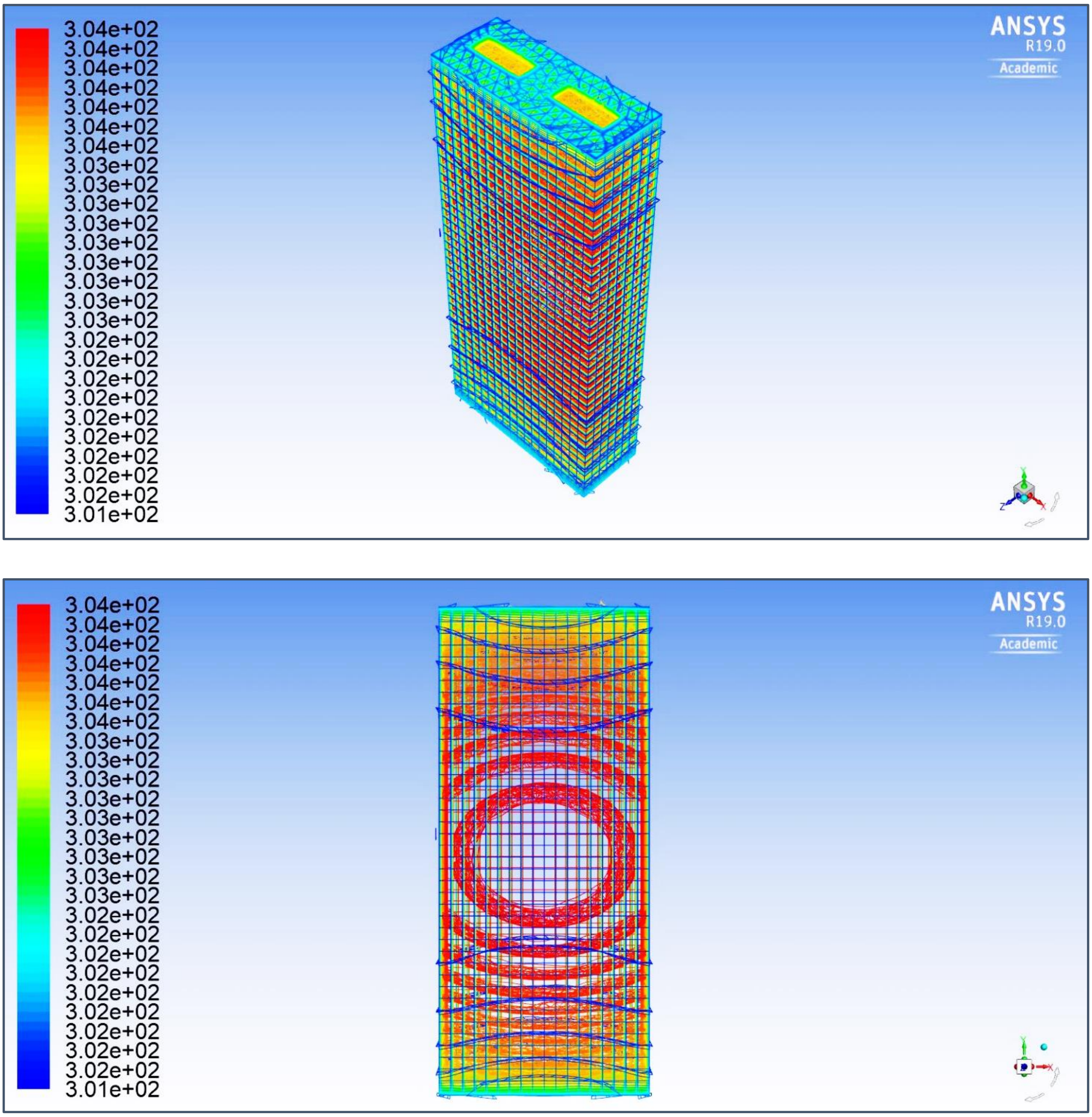

FIGURE 70 - $0.5C$ CC resulting temperature profile

Analysing then the final potential distribution within the battery, the *figure 71* is presented in the following page. It can be noted, for instance, from this latter how the internal three-dimensional finite element structure gets highlighted by the different contour bands. Here, in particular, the value of the final maximum computed voltage is found to be of $2.61\ V$. Take only in mind that all the outcomes obtained up to now are strongly coefficient-dependend, with reference to the $5th$ order polynomial curves: it is hence important to remind the fact that all the ECM's parameters have been obtained through a very long process from the data coming out from the testing campaign, and so an error could be present in the final quantities under study, however minimum.

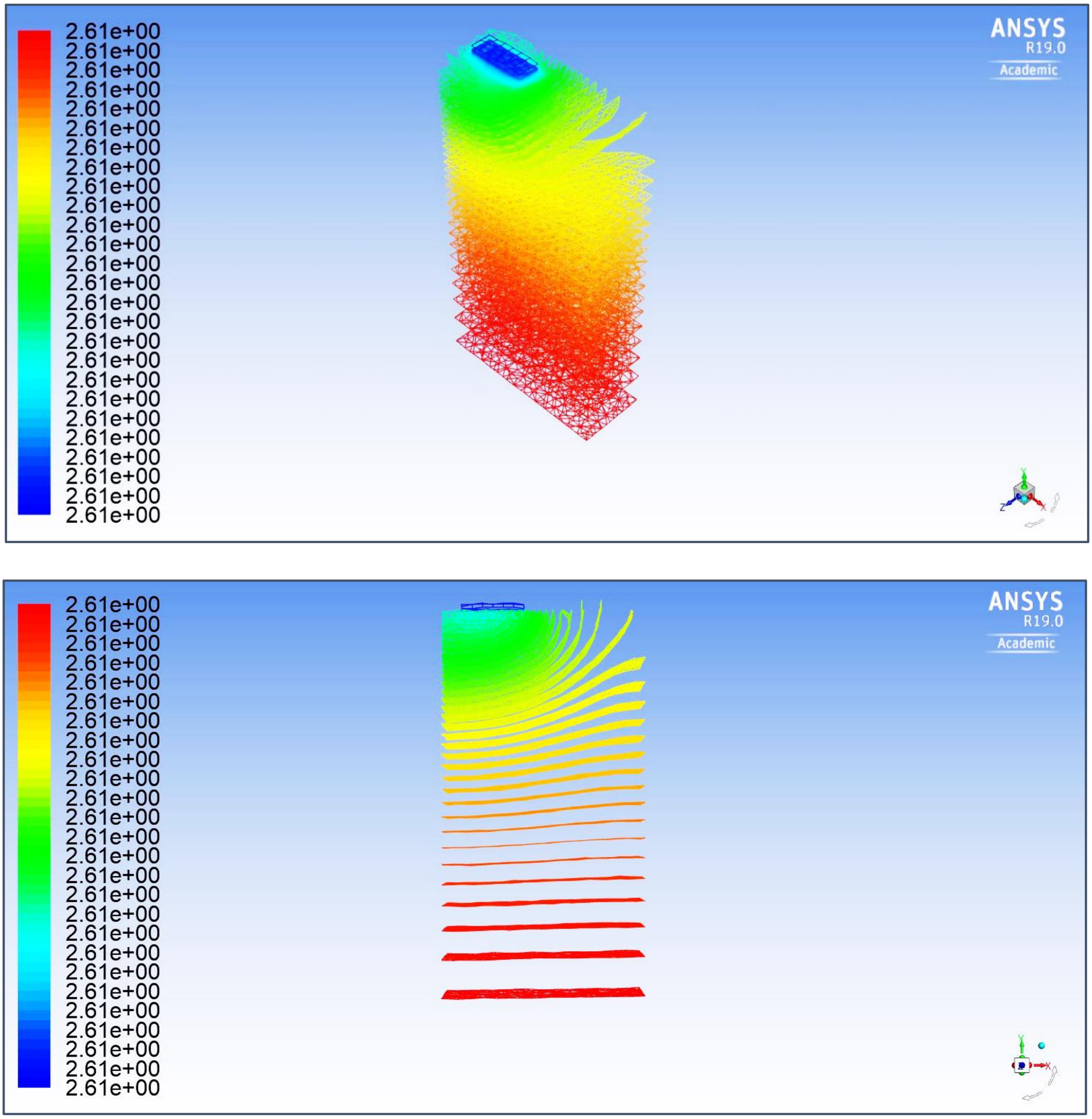

FIGURE 71 - $0.5C$ CC resulting potential profile

Finally, it could be also interesting to give a sight on the volumetric current density distribution, here represented in the next page within the *figure 72*. Note that in this case, rather than by using contour bands as done before, the small vectors defining both the direction and the magnitude of the quantity can be obtained by working in the "Vectors…" section within the post processing Fluent's environment. To obtain the following images, one has to search for the volumetric current density (i.e. j) contained in the user-defined memory's quantities. The resulting maximum final volumetric current density turns out being of $115844.6\,A\,m^{-2}$, close indeed to the regime value of $12.5\,A\,m^{-2}$ of a $0.5C$ discharge.

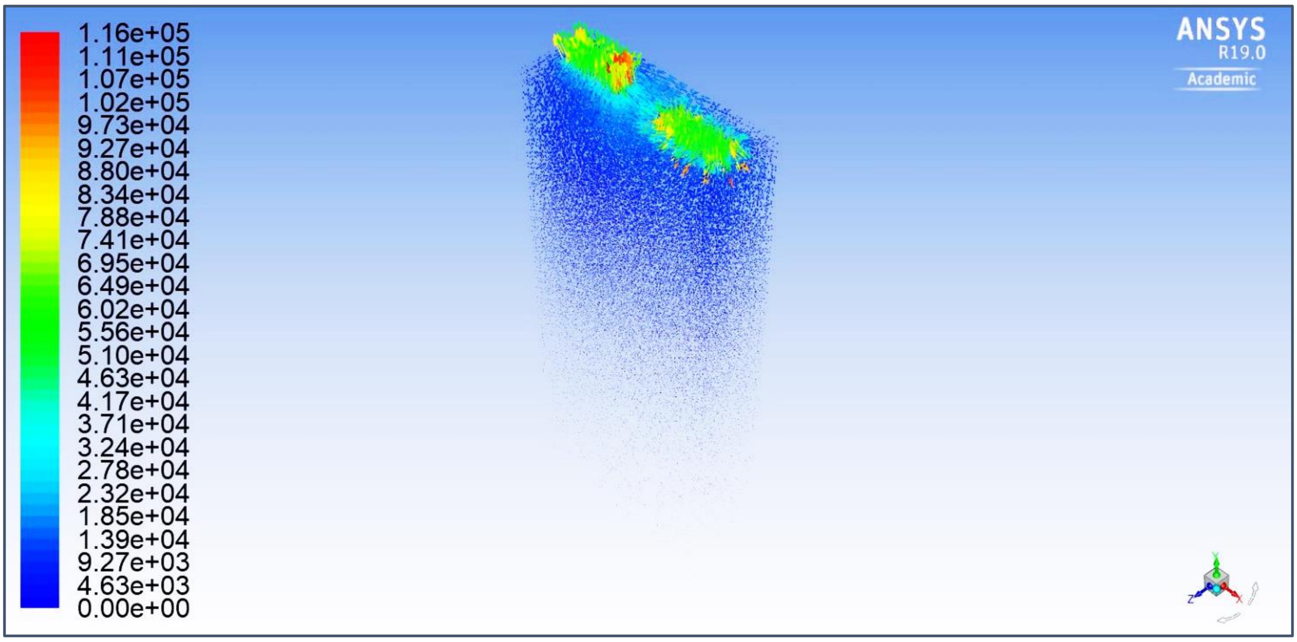

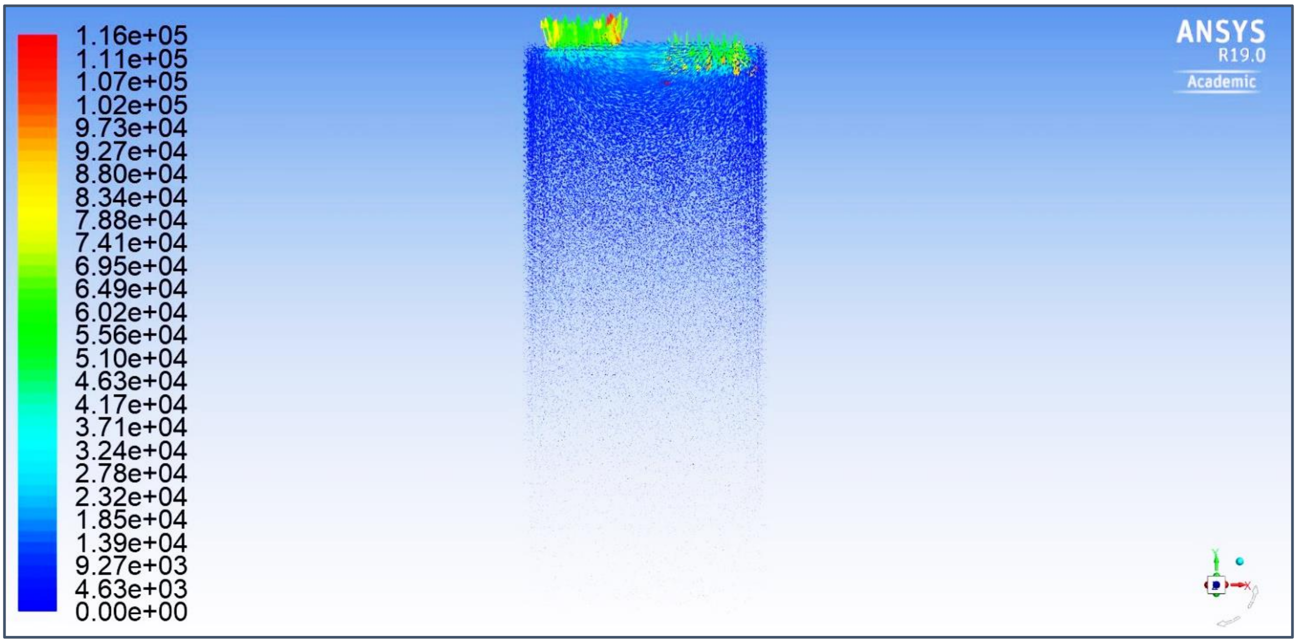

FIGURE 72 - $0.5C$ CC resulting current profile

Concluded this last part aimed at describing the results obtained with a $0.5C$ CC simulated discharges, it is possible to move faster for the other three similar tests (involving different C-Rates), since the grahical results turn out being exactly of the same shape of those seen up to now, and the numerical ones are going to be deeply analysed in the following section of the work, where a direct comparison with the simulated tests is going to be faced. Thus, from now on, only the plots representing the potential and thermal developments resulting from each simulation are going to be presented.

- **$1.0C$, $2.0C$, and $3.0C$ constant current discharge simulations**

Analysing the potential development along the simulation, the following *figure 73* collects the relevant set of plots.

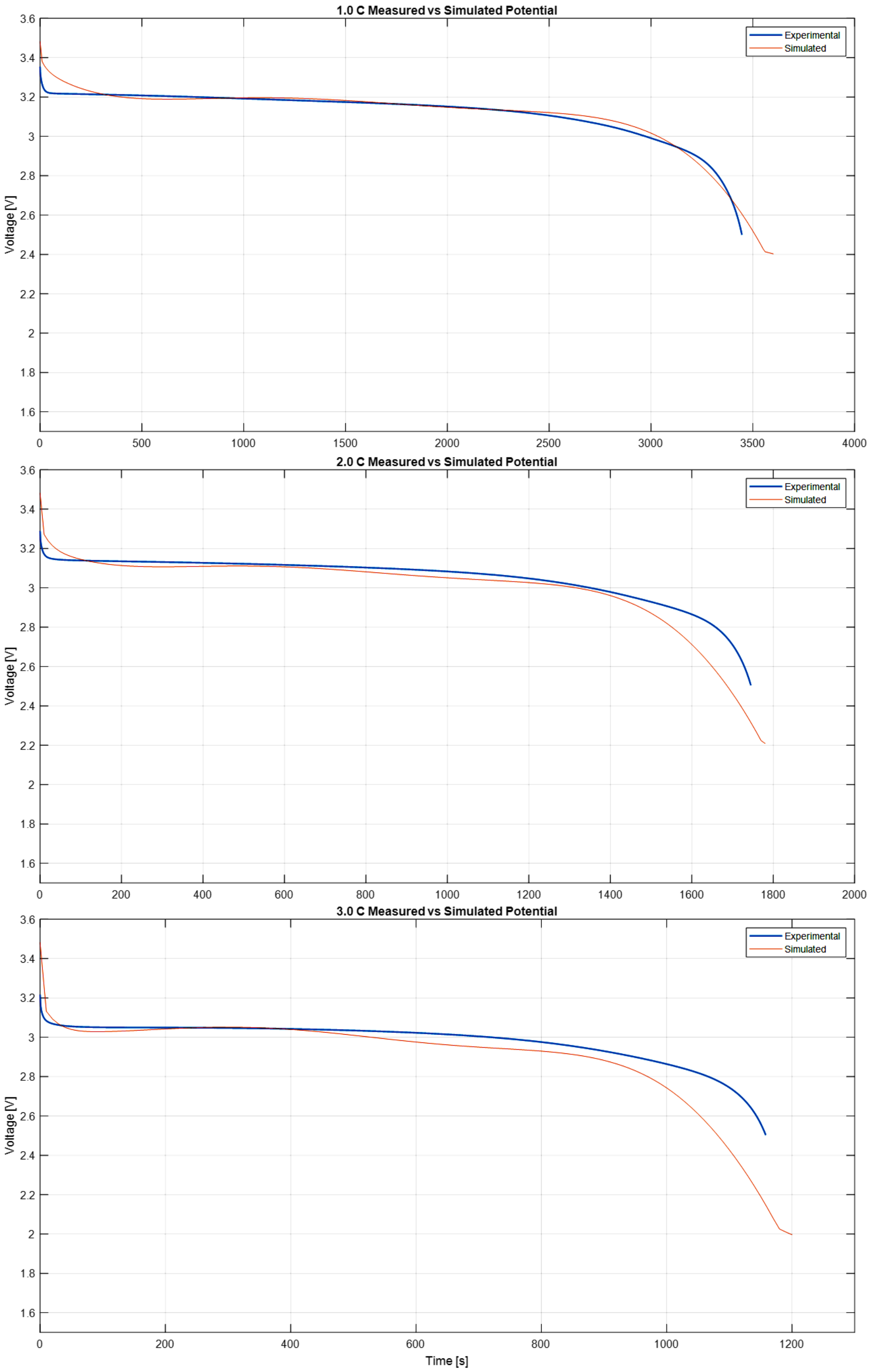

FIGURE 73 - Other CC discharges potential development

From the thermal development point of view, on the other hand, the important graphs are presented in the *figure 74*.

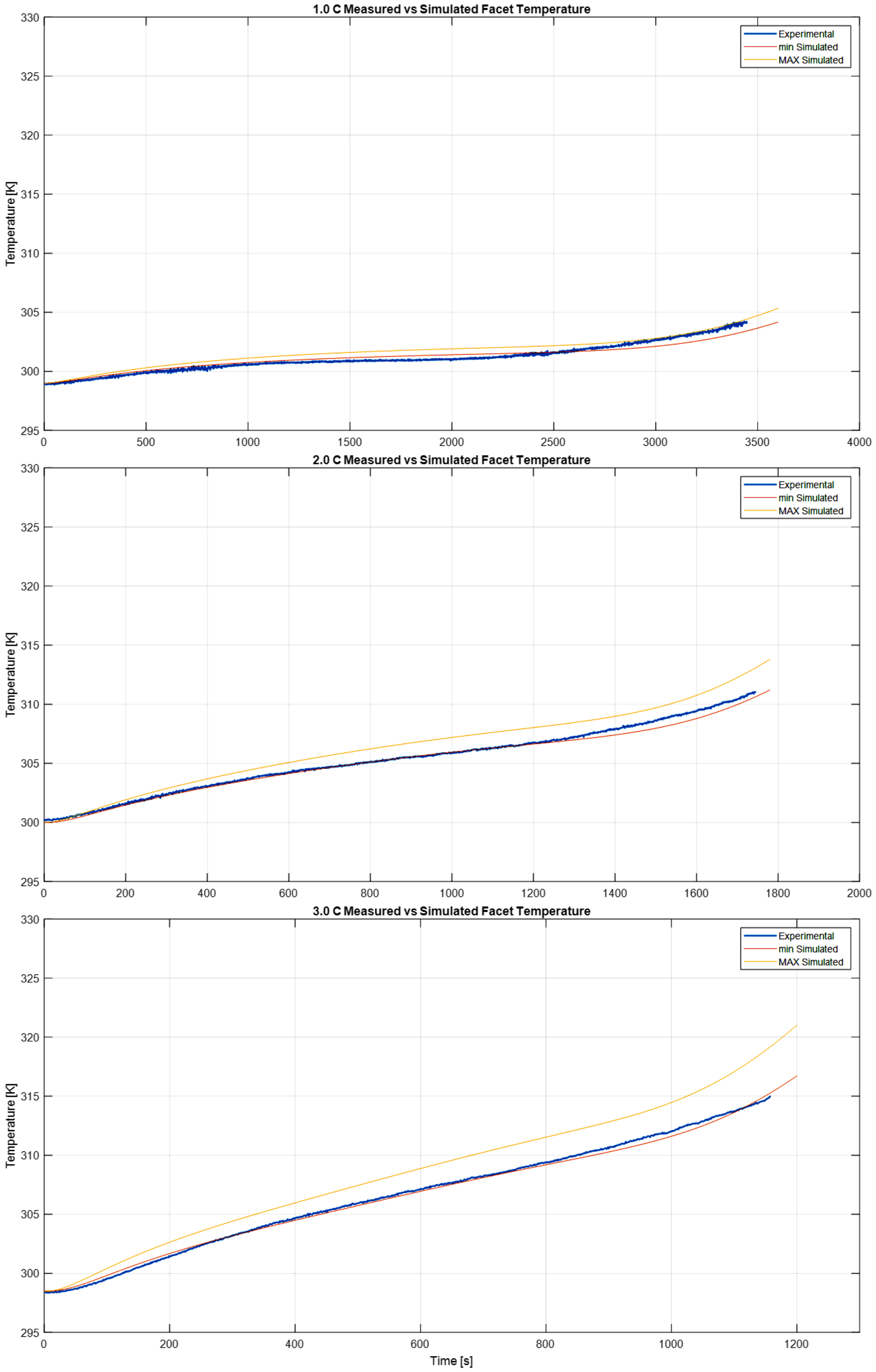

FIGURE 74 - Other CC discharges temperature development

Hence, concluded the presentation of the results coming from the CC simulated discharges, it could be now followed the same path presenting the outcomes coming from the simulating campaign applied to the so-called “pulsed discharges”. Once again, as it has been done before, a deeper explanation is going to be provided for what concerns the $0.5C$-based simulation (i.e. the first conducted), while for the other tests the relevant plots are simply going to be presented, with all the numerical results which are going to be detailly treated in the following section of the work.

- **$0.5C$ pulsed discharge simulation**

As already done before, in order to perform the right simulation, it is necessary to enter the correct R_S's polynomial coefficients in the appropriate dialog boxes, as well as the current profile which is given as input to the overall analysis. Studying the same type of cell, then, all the remaining polynomial coefficients are maintained due to their intrinsic battery-dependence nature. Subsequently, imposing the right number of time steps and the environmental temperature within the boundary conditions, the simulation is launched, and the results extracted and arranged within MATLAB in order to provide the following plots.

The resulting voltage development is presented in the following *figure 75*.

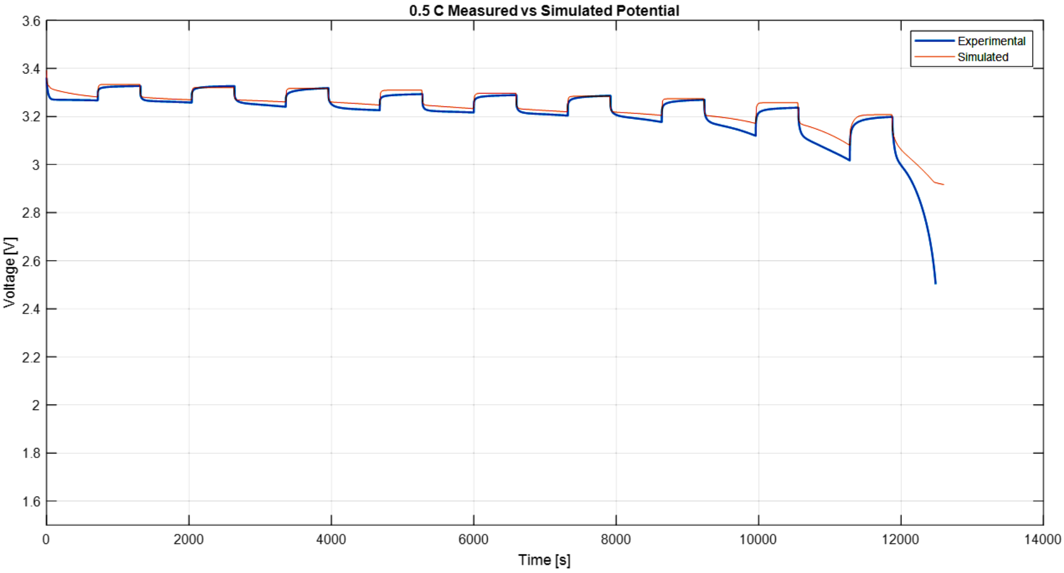

FIGURE 75 - $0.5C$ pulsed potential development

Once again, the thanks to the inputs that have been entered in the program, this latter is able to effectively mimic the real behaviour of the battery also under a pulsed discharge. Apart from the general trend of the curve, what really matters to be noted in this type of analysis is the simulation of the transitory phases which are described by the two RC-branches of the ECM. Thanks indeed to the accurate definition of the couples of parameters R_1 and C_1 as well as R_2 and C_2, the time constants (i.e. generally defined as $\tau_i = R_i\, C_i$) effectively reproduce the phases of the discharge in which the cell passes from being stressed to a resting condition, and vice versa.

Presenting then the overall thermal behaviour of the battery along the simulation, always considering as quantities of interest for the analysis both the minimum and the maximum facet temperatures (which are then going to be properly compared with the real measured one), the outcome is presented in the *figure 76*.

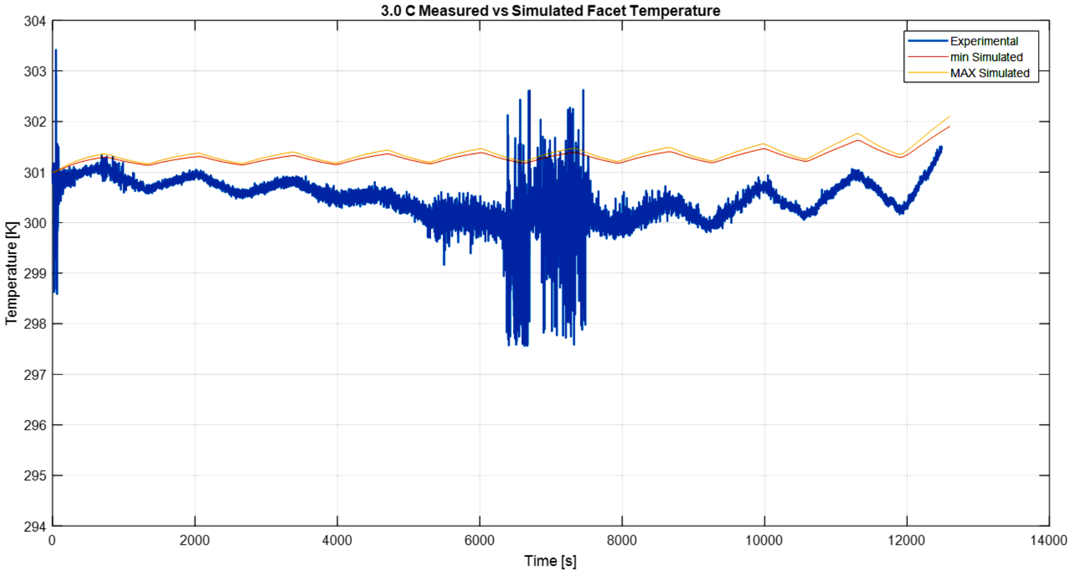

FIGURE 76 - $0.5C$ pulsed temperature development

Referring to this latter graph, there are some observations that need to be made. First of all, it is straightforward that the temperatures in play are smaller in these tests if compared with the CC discharges' ones, and hence the sensitivity of the instrumental apparatus could appreciated in a larger extent. As a consequence, two "errors" arose in the experimental activity, clearly visible from the plot.

- Some fluctuations appears between $6000\ s$ and $8000\ s$, probably given by some unexpected problems taking place at the level of the sensing element or of the climatic chamber.
- Furthermore, even more important, it has now to be considered that very long times characterize such tests, sometimes lasting several days, fact that makes it difficult to effectively maintain a stable environmental temperature. As a consequence, it could be seen that the real measurement's pattern is slightly deviated downwords in the central part of the test, maybe because of taking place during the colder night hours.

However, apart from the considerations reported above, once again, the simulation conducted in Fluent produces results that turn out to be very close to the real ones, at least in terms of "pulsating" behaviour and magnitudes. As it is going to be seen later on, then, for tests such as the $2C$ and $3C$ one, the stability of the enviromental temperature along the duration of the two experiments will help in recognize even more the fidelity that the simulated outcomes have with respect to the reality. At last, note that for what concerns the graphical results that could be obtained via the post processing environment of Fluent, they are not going to be reported in this work since exactly replicate the characteristics seen in th *figure 70*, *figure 71*, and *figure 72* (obviously presenting different numerical values).

Proceeding then in the same manner as done for the CC discharges, in the following part of the work are going to be presented the results concerning the other pulsed tests.

- **$1.0C$, $2.0C$, and $3.0C$ pulsed discharge simulations**

Starting from the measured potential developments, the plots are reported in the following *figure 77*.

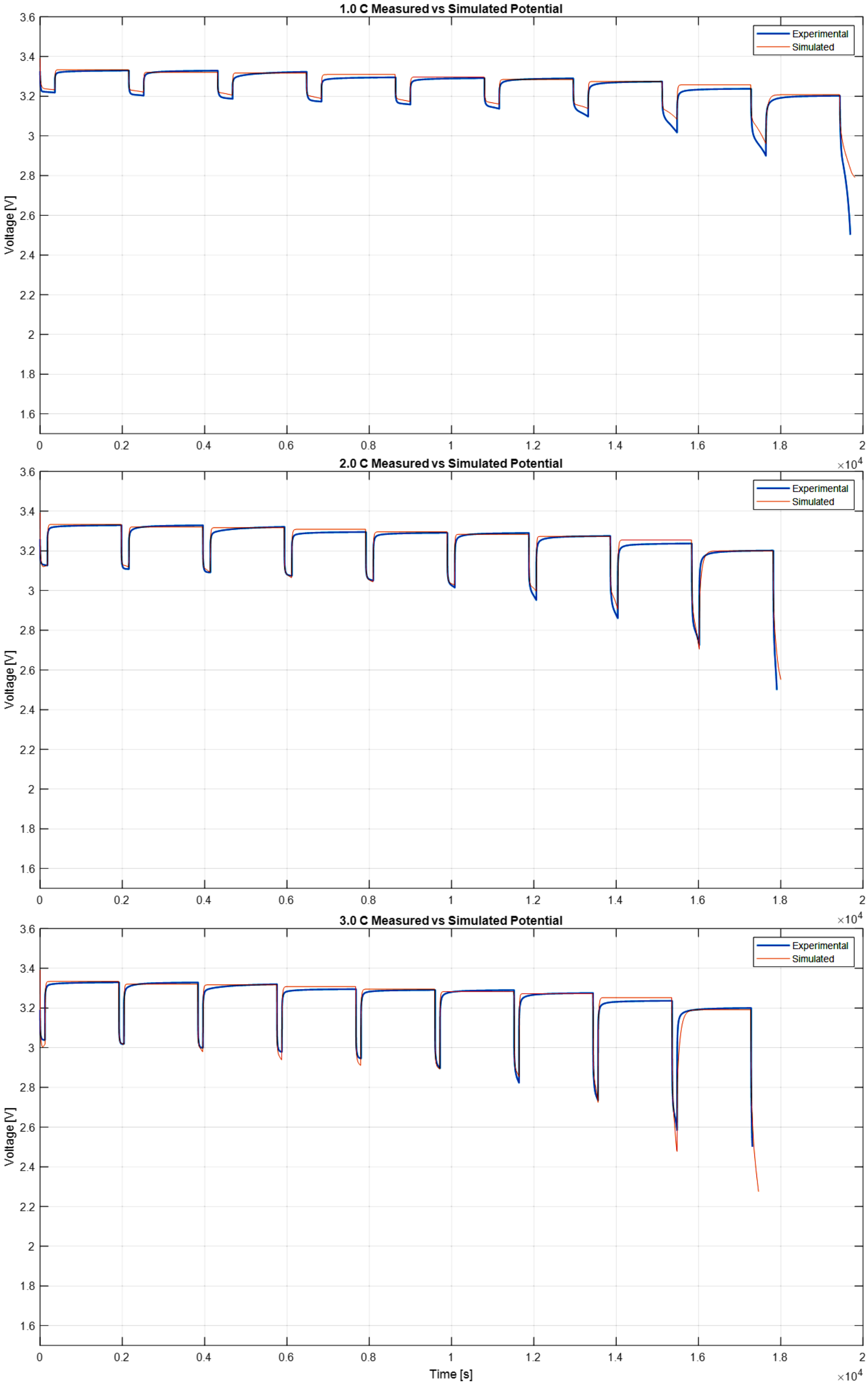

FIGURE 77 - Other pulsed discharges potential development

Accordingly, the resulting thermal behaviour of the cell within the different simulations is reported below.

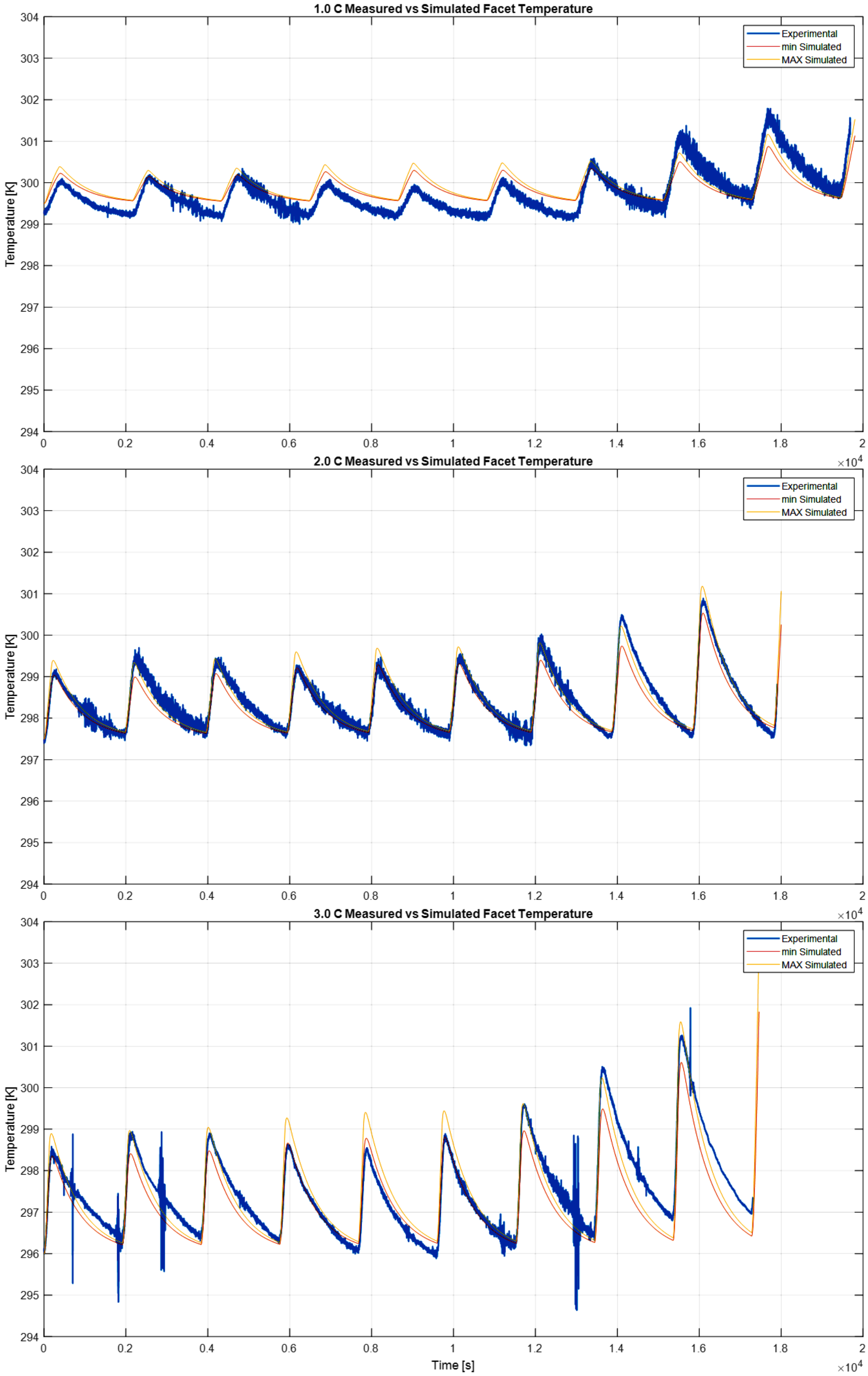
1.0 C Measured vs Simulated Facet Temperature

2.0 C Measured vs Simulated Facet Temperature

3.0 C Measured vs Simulated Facet Temperature

FIGURE 78 - Other pulsed discharges temperature development

Having finally concluded the presentation of the graphical results obtained thanks to the Fluent simulating capabilities, it is now necessary to work by properly analysing the numerical data in order to quantify the goodness of what has been achieved up to now with respect to its real counterpart.

Achievements

In this particular section belonging to the *Chapter 5*, as it has been said, the focus will be shifted on analysing the numerical data obtained by the previously conducted simulations, with the aim of quantifying the goodness of the simulating campaign itself. As it may be expected, the two different typologies of discharges that have been replicated in this work—i.e. the so-called “CC” and “pulsed” ones—needs to be treated differently, as briefly explained herein below.

- **CC discharges**

  Concerning these “steady-state” type of discharges, it is interesting to see where the simulation leads in terms of final results. Even if a sight on the curves’ trends must be given in order to assure the similarity between simulations and tests, what really characterizes these applications is the cumulative effect obtained by the constant current application, which as a result rises the temperature values sometimes arriving to dangerous levels.

- **Pulsed discharges**

  On the other hand, the analysis which is going to be performed dealing with the pulsed discharges will be treated more from a qualitative point of view, also because of the resulting power pulses’ applications which let the active material achieve temperatures in an acceptable safety range. Hence, what indeed is really important in this case, it to mimic as much as possible the curves coming from the experimental campaign, so that it could be eventually said that also the characterization of the dynamic behaviour of the cell has been successfully accomplished.

Thus, based on the comments that have been reported above, this section of the chapter is going to be divided in two parts: the first one simply reports the numerical results obtained from the simulations, while the final one shows the relative and absolute errors resulting from the former analysis. Hence, it could be said that, respectively, the former is more important for the characterization of the CC discharges while the latter mainly has to do with the pulsed one. One last thing to be kept in mind, finally, is that sometimes the simulation is found to have a slightly major duration than its real counterpart, mainly because the program, being based on the input current profile, lasts up to the completion of this latter even if in the reality the cell gets discharged a bit faster.

Achievements – **Numerical results**

Once that the simulation is over and the user moves in the post processing environment, it is possible to obtain the most important numerical results that characterizes the battery as it is found in the final time step. For what concerns the CC discharges, in particular, four quantities are of particular interest:

- The maximum body temperature, $T_{B,MAX}$, found in the central part of the active material's volume;
- The minimum body temperature, $T_{B,min}$, found in the central portion of the biggest face of the external aluminium case;
- The final maximum potential, simply called with P_{fin};
- The final maximum volumetric current density j.

Furthermore, two additional quantities could be added to the analysis by considering the report files which generate the plots seen in the former part of the work, hence the quantities which have been selected to be computed by the program:

- The maximum body facet temperature, $T_{f,MAX}$, found in the central part of the upper cover plate, exactly in between the two tabs;
- The minimum body facet temperature, $T_{f,min}$, which is actually equal to the previously mentioned $T_{B,min}$, i.e. the minimum body temperature.

Thus, in the table 22 below it is possible to collect all the magnitudes introduced above coming out from the CC discharges, found with the simulating process previously described.

TABLE 22 - CC simulations' results

Simulated CC discharges' outputs	$T_{B,MAX}$ $[K]$	$T_{B,min} = T_{f,min}$ $[K]$	P_{fin} $[V]$	j $[A\ m^{-2}]$	$T_{f,MAX}$ $[K]$
CC $0.5C$	304.1945	301.4395	2.6142	115844.6	301.8081
CC $1C$	311.7052	304.1744	2.404774	231543.4	305.3437
CC $2C$	328.8637	311.5561	2.196892	463441.3	313.8030
CC $3C$	344.7727	316.7262	2.001548	695421.7	321.0056

The first thing that comes up from the last table is the final temperature increase between the different tests, in accordance with the increase of the C-Rate. As one may conclude, the maximum body temperature resulting from a $0.5C$ CC discharge is surely not as harmful as the one obtained with a C-Rate of $3C$. More than $344\ K$ (i.e. more than $71\ °C$!) is surely a magnitude which is able to highlight the importance of an effectively working TMS, also because the value is reflected at the level of the case with a temperature locally higher than $316\ K$. Obviously, if nothing goes wrong during the functioning of a battery pack in an electric vehicle, these temperature levels are not sufficient to ignite fires or provoke the failure of the component, but for sure they lower the general performances of the ESS increasing its self-discharge rate, for instance, or generally reducing its health and consequently its life. Thus, as a conclusion for this analysis, the TMS turns out being a fundamental component in a battery pack: if the temperature at the level of the interface is kept low enough, then the forced conduction and convective phenomena may help also lowering the active material's one, improving all the behaviour that will otherwise be dangerous and unhealthy for the battery itself.

Apart from the thermal outcomes, then, another important quantity which has to be keep into account is the potential, whose behaviour have already been shown in the previously seen set of plots. As it was already expected by the experimental results, the level of the voltage profile along the entire simulation tends to decrease by increasing the C-Rate: this is something which is already well considered and simulated, but the particular drift between the compared curves on the last part of the simulation is going to be eventually discussed in the next chapter of the work.

Finally, the same type of table proposed in the last page could be as well reported describing the outcomes of the set of pulsed discharges, even if it turns out being less indicative for the characterization of these latter.

TABLE 23 - PD simulations' results

Simulated pulsed discharges' outputs	$T_{B,MAX}$ $[K]$	$T_{B,min} = T_{f,min}$ $[K]$	P_{fin} $[V]$	$T_{f,MAX}$ $[K]$
P $0.5C$	301.9046	303.2128	2.917768	302.1045
P $1C$	301.1282	303.7743	2.793022	301.5228
P $2C$	300.2518	305.7747	2.555515	301.0582
P $3C$	301.8292	313.7948	2.281032	303.5818

At a first sight it may seem that the results are wrong, because for instance the maximum facet temperature is found to be bigger for a “$0.5C$” pulsed discharge than it is for a “$3C$” one. However, as it has been seen, with such small temperatures in play the role of the environmental boundary conditions become prevalent, hence its necessary to integrate this latter set of data with the ambient temperatures collected in the *table 20*, which actually ends up defining the level at which the pulsating temperature trend refers to.

Achievements – **Computational errors**

Having seen the numerical results coming out from the simulating campaign, to finally complete and validate the whole procedure it is necessary to perform a comparative analysis, where for each type of discharge both the relative and the absolute thermal errors are computed. In particular, respectively:

- The relative thermal error ε_{rel}, computed at a certain time instant t, was calculated using the following formula:

$$\varepsilon_{rel} = \frac{T_{sim,t} - T_{real,t}}{T_{real,t}}$$

Where with T_{sim} is taken into account the simulated temperature value which is the natural counterpart of T_{real}, the real, experimentally detected temperature.

- The absolute thermal error ε_{abs}, on the other hand, has been calculated according to the following formula:

$$\varepsilon_{abs} = T_{sim,t} - T_{real,t}$$

In both the two calculations, nevertheless, it is important to remember that with the so-called "simulated temperature" it is intended the previously defined "facet temperature", which is actually the one which wants to replicate the real measured one. However, because of the fact that the minimum and maximum computed temperature at the level of the case are very close among them, it could be initially conducted an analysis which shows both of them used as the simulated counterpart to the experimental measured one. Thus, also recalling their name, T_{sim} will be considered to be possibly equal to $T_{f,min}$ and $T_{f,MAX}$, i.e. the two extreme cases. This consideration has been done because of the fact that the temperature measurement takes actually place in a point really close to the geometrical centre of the case's biggest face, and hence the measured value will be close, but to equal to, the minimum facet temperature (thus, from the point of view of the simulation, the measured counterpart will be between $T_{f,min}$ and $T_{f,MAX}$, i.e. the two extremes).

Once again, then, being different the results and in general the entire approaches between the two typologies of tests, it could be useful to present separately the outcomes of the comparative analysis. Note only that, before proceeding, all the following graphs are limited to the duration of the real experiments, which are in general shorter than their simulated counterparts, as it has already be seen.

- **Errors for the CC discharges**

The following *figure 79* reports the collection of the relative errors for the four CC simulated discharges.

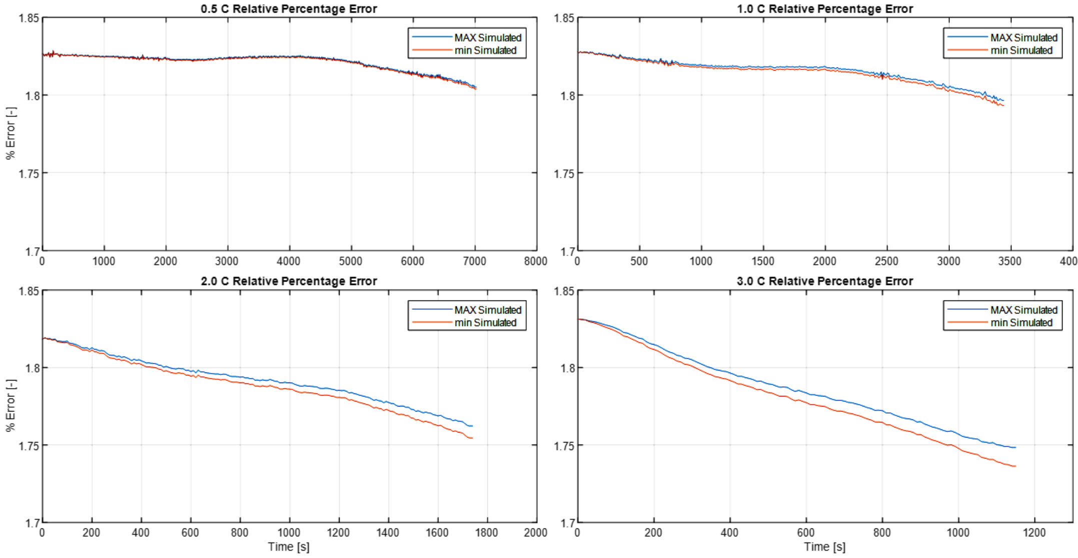

FIGURE 79 - CC relative errors

As it can be seen, a certain amount of error is always present along the entire simulation, even if this remains really small and tends to decrease along the simulations themselves. The particular behaviour could be simply explained by the fact that as the reference experimental temperature $T_{real,t}$ increases, the “relativization” becomes stronger. Obviously, being this latter value higher for a $3C$ discharge, the relative error turns out to be smaller than the ones found for smaller C-Rates. Nevertheless, it could be said that for all the analysed tests these values remain in the quite small and satisfactory range of $1.7 \div 1.85\ \%$.

A more interesting view on the results, on the other hand, could be presented considering the absolute errors reported in the following *figure 80*.

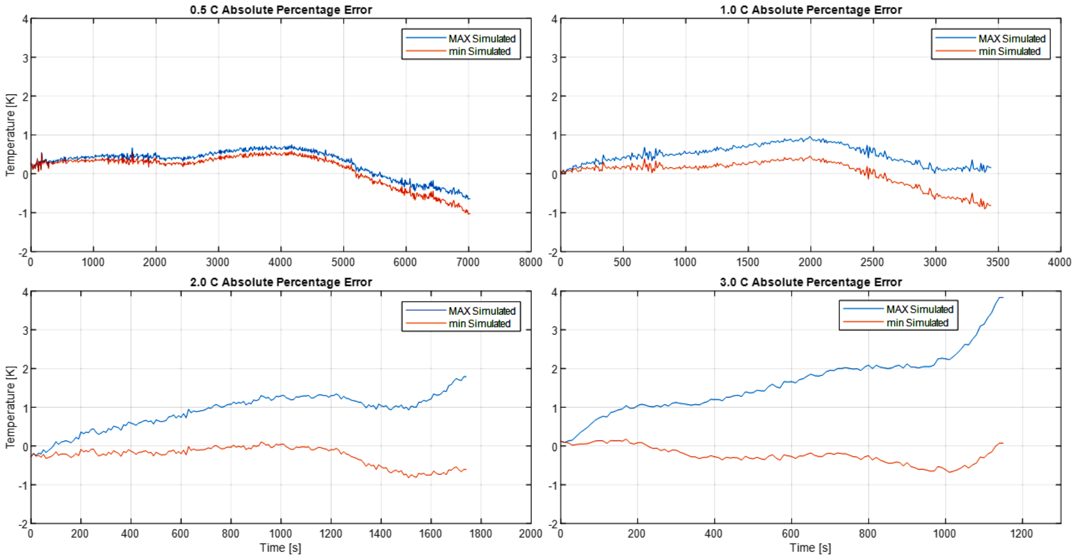

FIGURE 80 - CC relative errors

From this latter set of plots, it is straightforward that the computational error sums up from the beginning, when it is very close to zero, and arrives up to few degrees of difference from the experimental counterpart at the end of the simulation. However, being the absolute error in the range $-1 \div 4\ K$, it could be said once again that the simulation is very effective in mimicking the reality. Furthermore, it could be highlighted that all the red curves (i.e. the ones coming from the consideration of the simulated minimum facet temperatures) always remains in the surroundings or slightly below the $0\ K$ of error: considering that the real measuring point is almost in correspondence of the coldest one of the cell, this results to be another confirmation of the great achievements of the work. Accordingly, at this point, it could be confirmed that the real measured temperature could almost perfectly be replaced with the minimum facet one, i.e. $T_{f,min}$.

- **Errors for the pulsed discharges**

As it has been done dealing with the case of the CC discharges, the same type of comparative analysis is now applied to the pulsed tests. However, here in the following, the complexity of the graphs increases because of the higher amount of measured and simulated points, and hence, both the readings of the relative and absolute errors will need a more careful check.

With the *figure 81*, the behaviour of the relative error is presented in the next page.

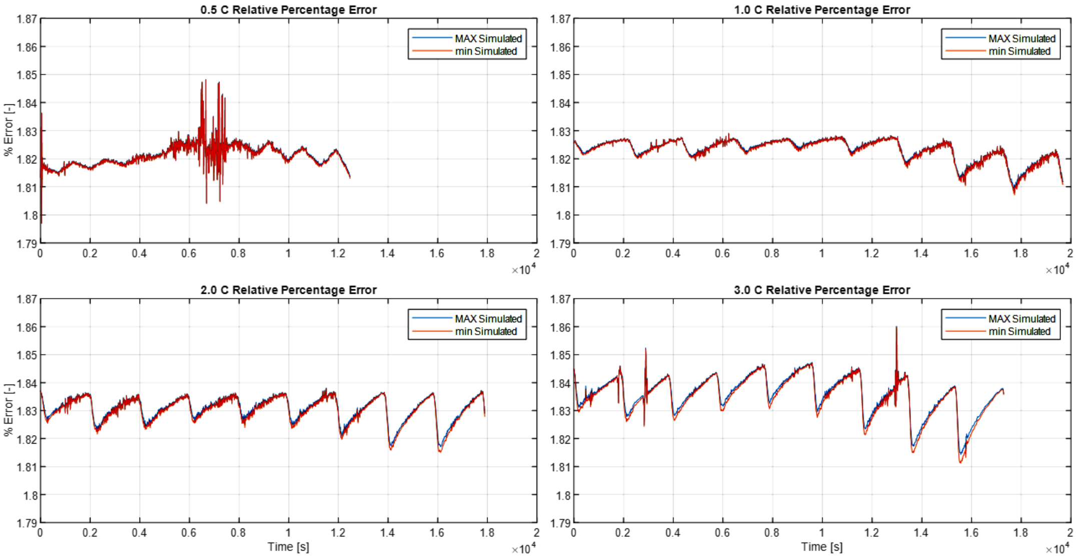

FIGURE 81 - Pulsed relative errors

As it can be seen from the set of images above, the two limit curves obtained by considering the maximum and the minimum facet temperatures are almost superimposed. This happens because of the small temperatures in play in the pulsed discharges: indeed, a small temperature development in the active material will only raise of a small extent this quantity at the level of the case. However, it could be in general recognized (especially in the plot regarding the "$3C$" discharge) that the blue curve (i.e. the one defined by the maximum facet temperature) is always above the red one: in other words, this points out a slightly major relative error when considered this latter quantity. Speaking then of the trends of the curves, it is important to highlight, once again, that whenever a power pulses is applied the temperature suddenly increases, fact that lowers the relative error because of the higher "relativizing" quantity.

Finally, the absolute thermal error is reported in the *figure 82*.

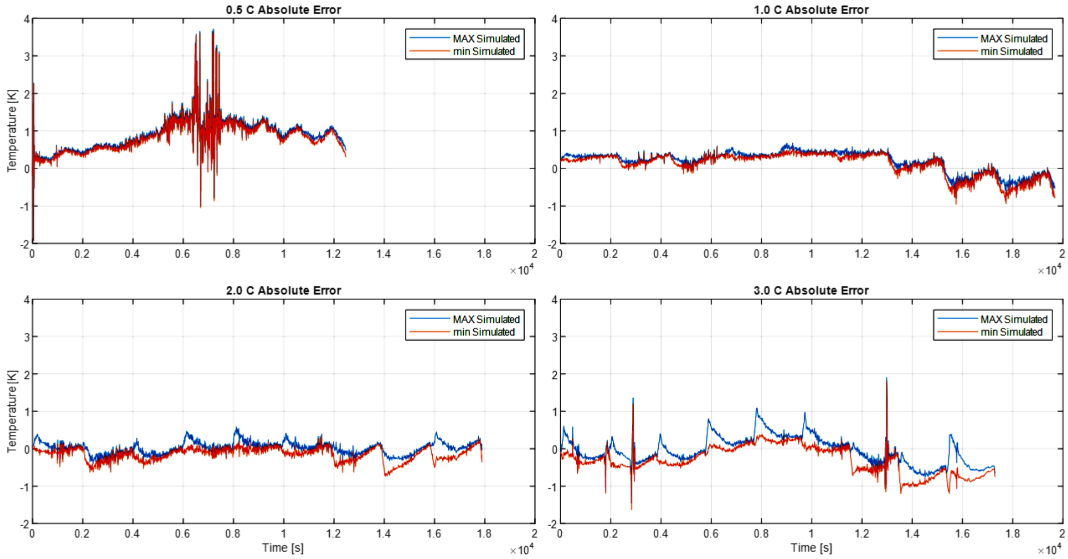

FIGURE 82 - Pulsed absolute errors

Many important conclusions can be made from the last set of graph. For instance, starting with the “$0.5C$” test, it is very important to be aware of the role played by the environmental temperature: having seen that this was not regular along the duration of the discharge, but rather decreased, the simulation turns out to overestimate the actual temperature values with respect to the real counterpart. However, the differences with the real measurements are so small Fluent managed to keep the absolute error still around $1\ K$. From all the other simulations, on the other hand, it could be seen that at small values of SoC (final instants of the discharge) the simulation underestimates the thermal results, producing “absolute errors” in the negative ranges. However, for intermediate values of SoC, the absolute error generally ranges around $0\ K$ of error, especially for what concerns the computation considering the minimum facet temperature. This last amazing result is able to prove once again the effectiveness of the simulations with respect to the validating experimental results, proposing an absolute error that in all the cases ranges between $-1 \div 1\ K$. Furthermore, it is once again straightforward the fact that the right simulated temperature of the cell to be selected for the comparative analysis is the minimum facet one, or, better, a value which is really close to this latter, fact that increases even of a grater extent the confidence of the entire simulative apparatus.

Concluding therefore this long chapter that deals with the simulated test campaign conducted with the ANSYS software, the numerical results that emerge from the practical analysis shows a very good accordance with the experimental data, with absolute errors lying in the range of $-1 \div 4\ K$ for the CC discharges and of $-1 \div 1\ K$ for the pulsed tests, even because of, obviously, it has to be reminded the fact that an higher temperature development takes place in the former than in the latter.

Chapter 6

Improving an ECM-based simulation

Adjustment of R_S

As the literature suggests, the parameters identifying the ECM of a Li-Ion battery are dependent on the cell itself and on its state of charge. V_{OC}, R_s, R_1, etc., are therefore all defined for a certain system, and take then different values depending on the energetic content of the battery, in addition to the previously seen effect of the chemical inner status of the active volume—i.e. if it is found to be "at rest" or "stressed". However, also the temperatures in play have an important role in the definition of such parameters that should be considered, so that hopefully these latters are allowed to vary accordingly. In other words, it will be really interesting to find a way to "overcome" the standard ECM only based on the parameter's dependency on the SoC, adding a further degree of freedom to the analysis considering the role played the temperature. Starting with the consideration that what happens in the reality is the best-reachable target of a computer-based simulation, engineers and researchers needs to focus their attentions in improving the solving algorithms so that what they finally obtain is something almost perfectly matching with what happens in the reality. With this purpose, in the present chapter, an innovative way to consider the temperature-dependence of an ECM is introduced. In particular, the development of the study in the following sections is mainly based at defining and characterizing the changes that should be considered in the definition of the ECM's serial resistance (R_S), which is the main source of error in the thermal analyses.

Because of the well-known Joule effect, it is straightforward that the higher is the ohmic value of a resistance, the higher is the heat generation of that component: if a resistance's magnitude is overestimated, summing up all the heat sources within a Li-Ion cell, the thermal outcomes turn out to present higher values than in the reality—which is actually what happened so far in the case of this work. To solve this problem, the key is to find a way to adjust the "overestimation" of R_S: since the standard ECM does not consider the R_S reduction as far as the temperature increases along the simulation, the thermal profile of the Li-Ion cell will surely be warmer than in the reality. Thus, as a starting point of the analysis, one has to focus on the real measurements already summarized in the *figure 59*, reporting the HPPC, CC, and pulsed discharges' resulting R_S's curves. The relative polynomials' parameters are one input data in Fluent, and once that they are correctly entered into the program through the appropriate windows, the simulation run smoothly because ANSYS acts in a certain manner as the SoC decreases within the model: the R_S it takes into account for the simulation is already defined for all the time steps of this. However, what is still missing in the solver is the definition of "what to do" with those values when the temperatures in play changes. Initially—and normally—the program simply does not mind of this because is not "instructed" in doing anything. Thus, the goal is to find a way to properly "instruct" the program in acting on the relative R_S values as soon as the temperature increases, so that the heat that would eventually be generated due to Joule effect by mean of the serial resistance gets adjusted, and consequently does the resulting thermal outputs.

For sake of clarity, in the following *figure 83* a simple scheme of the logic acting under this chapter is presented.

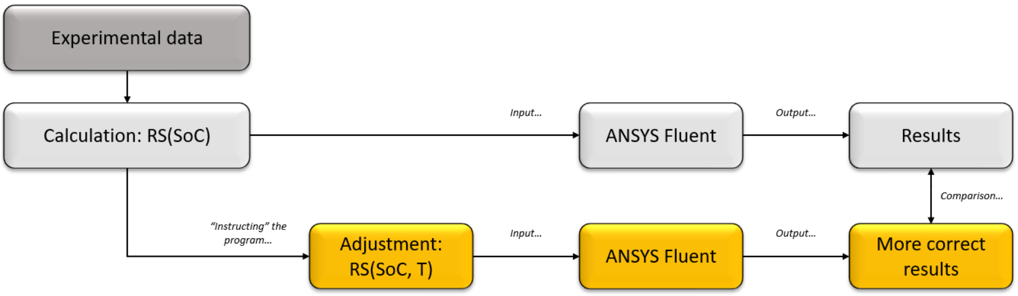

FIGURE 83 - R_S's modification logic

Two important steps need to be performed in the overall analysis before proceeding with the simulations in the ANSYS environment:

- Initially, it is necessary to find an effective way, according to the literature and to the previous works of the researchers, to include the temperature in the R_S's definition, so that the resulting polynomial curves are no longer only dependent on the SoC but also parametrized with respect to the temperature.
- Subsequently, since the program is still not able to process those kind of information, it will be needed to find a way to allow Fluent to work with such "2D" curves (the SoC and the T are now the two degree of freedom of the problem) instead of the simple "1D" ones.

Adjustment of R_S – Definition of the new curves

From a theoretical point of view, in this following section of the work, an innovative method able to include the temperature in the R_S's definition is going to be presented. Note only that, it could be said that no relative counterparts have been found in the literature.

The general idea at the basis of everything is to simply start from the relative $5th$ order polynomial curves describing the behaviour of the serial resistance parameter and to act on its $0th$ order coefficient, so that the shape of this latter is going to be maintained along the discharge but its quota (indeed, represented by the coefficient under analysis) changes as far as the temperature increases or decreases.

Using formulas, the standard definition of the R_S polynomial curve could be recalled herein below:

$$R_S(SoC) = p_0 + p_1 * SoC + p_2 * SoC^2 + \cdots + p_5 * SoC^5$$

Then, integrating the temperature dependence in the first coefficient, namely p_0, it yields the following:

$$R_S(SoC, T) = p_0'(T) + p_1 * SoC + p_2 * SoC^2 + \cdots + p_5 * SoC^5$$

What is now remaining to do is to define the way in which this latter temperature dependence is going to be imposed, here thanks to the definition of what in this work is going to be the so-called "rate" (R_{R_S}). Aimed at imposing a certain variation to the serial resistance, the rate's magnitude will be expressed in the form of Ω/K, and it will be multiplied for a given temperature difference with respect to a reference one. Thus, below, is reported the overall formulation of the "new" $0th$ order coefficient.

$$p_0' = p_0 + R_{R_S}(T - T_{ref})$$

Where as T_{ref} was thought to use the starting temperature of the test—i.e. the environmental one—so that the changes of R_S will be "relativized" to that precise reference point. Obviously, it is important to remember that there is not yet a precise value of R_{R_S} that could be found in the literature, also because of the different modelization of the active material as a single, uniform component. For this, several attempts are going to be provided in the analysis of this chapter, so that first of all the changes in the results are going to be appreciated, living however open the possibility for future research in the field aimed at defining a correct value of the rate, strictly dependent on the materials forming the active zone. Note only that negative values of rates are thought to be common and sensate attempts, so that whenever T is major than T_{ref} the corrected value of the serial resistance turns out to be minor than its "standard", original counterpart.

Adjustment of R_S – **Creation of user-defined libraries**

In order to instruct the software in acting as it is wanted, one could take advantage from some ANSYS Fluent's user guides tips. The reference that has been found in the web, for instance, and whose suggestions are herein the following reported, is the "ANSYS Fluent Battery Module Manual" [45]. The manual provides information about using the battery model available in the Fluent environment (the so-called "MSMD Battery Model" addon discussed in the previous chapter), together also with some theoretical discussion about the aforementioned system and a short description of how to use it to perform efficient CFD simulations. However, the relevant part of the manual which is of particular interest for the purpose of this chapter is the section discussing the creation, definition, and implementation of so-called "user-defined functions" (UDFs). Recalling the aim of this analysis, indeed, now it is necessary to find a way to incorporate the formulations reported in these last pages so that the program runs no longer a standard simulation, but rather an "user-imposed" one.

To achieve this latter objective, it is initially useful to introduce and explain the structure of the program itself, as installed within the computer, so that the entire process that brings to the modifications of the CFD computation is effectively and completely addressed. Beginning from the $ANSYS\ Inc$ folder and taking into account that in this case it has been installed the version 19.0 on a $64\ bit$ Windows-based architecture, one has to navigate throughout the following the path reported below in order to find the user-accessible source file where the modifications are going to be done:

$$\ldots \backslash ANSYS\ Inc \backslash v190 \backslash fluent \backslash fluent19.0.0 \backslash addons \backslash msmdbatt$$

Here, respectively:

- $ANSYS\ Inc$, as it has been said, is the global folder of the program which is created at the moment of the installation.
- $v190$ is the specific folder containing the actual installed ANSYS version.
- $fluent$, on the other hand, is the global folder of the "ANSYS Fluent" program—it is now clear that ANSYS WorkBench is based on the integration of different softwares, and Fluent is the one used to conduct the simulations.
- $fluent19.0.0$ is the specific folder containing the actual installed Fluent version.
- $addons$ is the folder where all the standard "addon" modules' files are contained—recalling that the so-called "addons" generate systems which are already implemented for the environment and ready for the use, as already introduced in the *Chapter 5* with the MSMD Battery Module.
- $msmdbatt$, finally, is the folder containing all the files at the basis of the specific addon used in this work, i.e. the "Multi System Multi Dynamics" Li-Ion battery model.

There, in the last, deeper-level folder, all the informatic "instruments" which allows the program to build and interpret the MSMD battery model are present. In the following *figure 84*, the structure and the content of the $msmdbatt$ folder is represented, being fundamental for the understanding of how the entire modification process subsequently is performed.

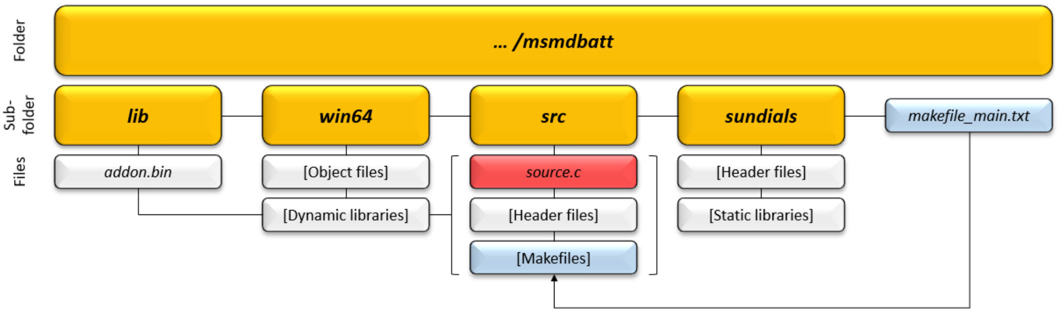

FIGURE 84 - Fluent's MSMD battery model files

As it can be seen from the image above, within the $msmdbatt$ folder many sub-folders and files are standardly created during the installation of ANSYS. In particular:

- lib contains the file named "$addon.bin$", whose aim is to store data and instructions in binary format, together with the directories where Fluent can find the static libraries over which the functioning of the entire program is based. This file is not editable, but everything is already set in the correct way for the future modifications.
- In $win64$ (folder that takes its name because of the architecture of the computer) it is possible to find some object files and dynamic libraries, elements which result from the correct compilation of the source code and the instructions contained within all the "makefiles".
- The src sub-folder turns out to be the most important one: it indeed contains the user-accessible editable source code, here named for simplicity "$source.c$", together with all the header files necessary for its complete compilation as well as two specific "makefiles".
- In $sundials$, then, other header files aimed at supporting the main source code are contained, together with the static libraries which allow the correct functioning of the

so-called “IDA”, i.e. the program’s solver. However, this particular folder is not of interest since it is not involved in the modification, and hence does not have to be edited.

- At last, the $msmdbatt$ folder also contains the reference upper-level “makefile”, here called $makefile\_main$ for simplicity, which is actually a short file in the $.txt$ format.

Knowing now the structure of the folder which is of interest for the modification of the CFD simulations, the process in its whole could be explained in the detail here in the following part of the work. However, it is first of all important to say that three informatic entities are the keys over which one has to act in order to successfully achieve the searched changes: the source code, the global “makefile”, and the static libraries. The first one, written in C language, contains the code that will be changed by adding a part so that the program then takes into account the role of the temperature in the definition of the ECM. The “makefile”, then, is a very important file which allows to create the on-demand modified libraries, which in turn will be the elements finally entered in Fluent thanks to the instructions contained in the $.bin$ file, subsequently interpreted by the program itself.

It is possible to closely analyse these elements.

- **Source code**

Within the source code, as it is going to be seen, there are several user-accessible functions which are intended to define the quantities of interest as well as the way in which Fluent performs the simulations. Among the others, one can find the definition of the copper’s conductivity, the entropic heat’s development rate, and many others. Furthermore, for each model which is available in the MSMD battery model’s addon there is a function contained in this source file which takes the entries of the user within the program and manage them, bringing to the final computation of the useful output quantities. At this level, in the particular analysis carried on, the modification is going to take place.

Making reference in particular to the used ECM of a Li-Ion battery, as it has been seen in the *Chapter 5*, at a certain point it is necessary to enter in Fluent the $5th$ order polynomial’s coefficients so that the program automatically builds up the curves in the parameter vs SoC plane for the future computations. Thus, regarding this particular model, the editable function of interest within the $source.c$ file is the following one:

$$Compute\_ECM\_VOC\_and\_CR$$

Nine arguments are automatically passed to the computing function by the code, here called within the file in the following manner (type of variable and variable itself):

$$real\ SoC, real\ T, int\ mode, real^*\ V_{OC}, real^*\ R_S, real^*\ R_1, real^*\ R_2, real^*\ C_1, real^*\ C_2$$

SoC, obviously, is the computed state of charge of the cell, while T is turns out being the volumetric-average temperature of the active material and $mode$, taking the values of either 0 or 1, defines if the battery is respectively charging or discharging along the simulation. For what concerns all the other ECM-related parameters, on the other hand, these are externally defined by another function (which is actually not editable) which uses the already known $5th$ order polynomials’ coefficients, whose values are taken by the program among those inserted in the appropriate boxes during the setup of the model. In other words, once that the coefficients are entered, the hidden-to-the-user accessible function organizes them in functions in the well-known form of parameter vs SoC. For sake of clarity, inside the code, the $5th$ order polynomials' coefficients are named as reported as shown below, concerning the R_S parameter only:

$$R_S\_coef\_poly[0], R_S\_coef\_poly[1], \dots, R_S\_coef\_poly[5]$$

To give then a complete view of the problem, the portion of the code under analysis within the $source.c$ file is shown here in the following.

```
#define USER_DEFINED_ECM_VOC_and_CR      0

void Compute_ECM_VOC_and_CR(real SoC, real T, int mode, real* VOC, real*
Rs, real* R1, real* R2, real* C1, real* C2)
{
    if (!USER_DEFINED_ECM_VOC_and_CR)
    {
        Compute_VOC_and_CR_standard(SoC, mode, VOC, Rs, R1, R2, C1, C2);
    }
    else
    {
        if (mode = 0)
        {
            /* ... FOR CHARGE, WITH USER_DEFINED_ECM_VOC_and_CR = 0 */
        }
        else
        {
            /* ... FOR DISCHARGE, WITH USER_DEFINED_ECM_VOC_and_CR = 1 */
        }
    }
}
```

To effectively integrate the modifications that are necessary for this work it is required to change the already provided "macro" of the code to 1: in this way, during the compilation of the script, the compiler runs directly in the user-editable area passing across the "standard" one. There, it has been decided to act maintaining the use of the same standard, not-editable function already used for the normal applications (i.e. the one named in the upper code as "$Compute\_VOC\_and\_CR\_standard$", highlighted in red), and subsequently overwrite the outputs of this latter by including the formulations reported at the beginning of the chapter. Like this, one ends up coding in the "$if\ (mode = 0)$" section within the "$else$".

Recalling then what it has been previously said when speaking about the theoretical approach that would eventually be used, it remains to be defined the serial resistance's "rate" together with the new global formulation of the R_S parameter that will overwrite the standard definition. Thus, putting things together, the final definitive portion of code which is going to be compiled is reported herein in the next page.

```
#define USER_DEFINED_ECM_VOC_and_CR      1

void Compute_ECM_VOC_and_CR(real SoC, real T, int mode, real* VOC, real*
Rs, real* R1, real* R2, real* C1, real* C2)
{
    if (!USER_DEFINED_ECM_VOC_and_CR)
    {
        Compute_VOC_and_CR_standard(SoC, mode, VOC, Rs, R1, R2, C1, C2);
    }
    else
    {
        if (mode = 0)
        {
            /* Nothing has been added in this section*/
        }
        else
        {
            real Rate = -0.0001;        /* EXAMPLE, in Ohm/K */
            real Tref = 300;            /* EXAMPLE, in K */
            if (T >= Tref)
            {
                RS_Coef_Poly[0] += Rate * (T-Tref);
            }
        }
    }
}
```

Note only that, at this point, the values that have been imposed for the "$Rate$" and the "T_{ref}" quantities have been randomly written, since they are dependent respectively on the cell and on the type of simulation performed, so that these are going to be properly addressed later on.

Concluded the modifications in the $source.c$ file, the way to achieve its correct compilation will be discussed in the subsequent part.

- **Main makefile**

In any directory that contains source files, such as the $msmdbatt$ folder, it is required to have a $.txt$ file technically called "makefile" whose role is mainly aimed at containing the instructions for compiling the code. For its correct execution, however, this needs to be called from an appropriate command prompt compatible with the operative system and the architecture of the computer. In the case of this work, as also reported in the *figure 84*, the makefile is already provided by the developers of ANSYS in order to allow modifications to the source code and acts in a tight integration with the two additional makefiles originally settled in the src folder. For what concerns the compiler and hence the command prompt necessary to "launch" the makefiles and interpret both the source code and the header files, on the other hand, the 2013 version of Windows Visual Studio has been installed and used (be aware of the fact that different versions of Visual Studio may not work because of the way they handle the so-called "environment variables" of the computer and due to other small technicisms)

Thus, to compile the modified source code, it is required first of all to open the Visual Studio's command prompt (the one called "$x64\ native\ tools$") and to navigate up to the $msmdbatt$ folder entering the following command:

$$cd\ \ C{:}\backslash \dots \backslash msmdbatt$$

Where "…" considers the right path to follow on the PC. Subsequently, always working within the command prompt and now in the aforementioned folder, the instruction to "activate" the functionality of the main makefile needs to be entered:

$$nmake\ /f\ makefile\_main.nt$$

Where $nmake\ /f$ is the given command that must be followed by the name of the $.txt$ file. As a consequence of this latter action, the compiler compiles the source code taking advantage from the features implemented in the already provided header files. In order, finally, object files and static as well as dynamic libraries get updated according to the new written code.

- **Dynamic libraries**

Obtained (or, better, updated) as explained in the previous points, the dynamic libraries are, putting it simply, the transduction of the code which is then going to be read by Fluent.

The last remaining step to be performed at this point is the loading of the updated libraries within the program, action which is technically called "hooking". This simple operation can be performed taking advantage of the user-friendly interface developed in Fluent. Considering to already have everything as we have left it in the last chapter, i.e. a certain simulation has been settled up and hence all the necessary quantities turn out being already correctly entered, it is required to go within the "User Defined" environment. Opening then the "Functions" section and subsequently on the "Manage" one, the "UDF Library Manager" window opens in order to allow the user to specify the path of the dynamic libraries used for the future computations. Normally, the following path is found:

$$\dots \backslash ANSYS\ Inc\backslash v190\backslash fluent\backslash fluent19.0.0\backslash addons\backslash msmdbatt$$

However, having modified what it's actually inside the folder, it is required to remove the address and load it again. Two messages finally appear within the console informing the user of the successful "hooking" of the used-defined libraries:

$$Opening\ "Library\ C{:}\backslash \dots\backslash\backslash msmdbatt"\ \dots$$

$$Library\ "C{:}\backslash \dots\backslash\backslash msmdbatt\backslash win64\backslash libudf\_mpi.dll"\ opened$$

Where, once again, "…" considers the complete path describing the specific address.

Hence, now that the entire process followed in order to correctly change, obtain, and hook the new user-defined libraries have been carefully described, it is possible to directly present the results obtained with this innovative approach which is able to considers the role of the temperature in the ECM's serial resistance.

Best achievements

Having addressed both the theoretical and the practical aspects which allow to understand and subsequently build up a new kind of simulating campaign, it is now possible to directly present the results that have been obtained with the use of the new user-defined libraries. Considering that all the simulations' setups are already defined and that it is not required to do anything more in the Fluent environment apart from the operations described in the last pages (hooking the libraries themselves), it is simply necessary to run once again the simulations and perform some post processing operations in order to compare the outcomes with the original "standard" ones. Before proceeding, however, the range of extension of the analysis has to be addressed since two main factors have yet to be defined.

- **The "Rates"**

  Different magnitudes of the so-called "rate" have been selected starting from an iterative analysis as thought to be relatively correct guesses. Indeed, with no references in the literature, it turns out to be initially difficult to end up with a definitive values. Nevertheless, the approach that has been used in this part of the work is aimed at modifying (or, better, at adjusting) the outcomes of the simulations so that both the temperatures' curves and potentials' ones along the discharge of the cell will mimic as much as possible the real experimental results, even more than done up to now. Thus, making reference to the portion of code previously reported, four attempts for the "$Rate$" parameter will be successively made taking the following values: -0.05, -0.1, -0.15, and $-0.20\ m\Omega\ K^{-1}$. In this way, as far as the temperature increases, the serial resistance of a specific test will decrease.

- **The reference temperatures**

  Apart from the rate parameter, the analysis is based on the temperature increment with respect a selected reference level, namely T_{ref} (as named in the code). Based on the theoretical assumptions that have been done, it could be a correct guess to assign the ambient temperature of each test to the T_{ref} parameter, since this latter is used as the reference initial temperature for each simulations. Obviously, it has to be reminded the fact that such value changes among the different tests, and hence needs to be properly and accurately changed during the simulating campaign.

Defined the parameter is play for the further analysis it is then necessary to decide where to focus the attention of this long characterizing work. Here in this chapter, only the cases where there is a great temperature increment are going to be presented, and in particular the "$2C$" and "$3C$" tests in both their format of constant current and pulsed discharges. This latter decision has been made because of the fact the in the "$0.5C$" and "$1C$" tests the temperatures always stay close to the reference ones, and hence the corrections will not be really appreciated. Furthermore, also from a graphical point of view, it is straightforward that there is already a good match between those simulations and the experimental results. On the other hand, whenever the temperature reaches high values many quantities need a correction, as also visible on the plots reported in *Chapter 5*. The potential, for instance, is far below its experimental counterpart because of an overestimation of the program of the R_S parameter, which will be eventually reduced thanks to introduction of the rate in the definition of R_S. Furthermore, adjusting the serial resistances will also results in a closer match between the measured simulated and experimental temperature because of a smaller heat generation: once again, a higher simulated temperature is surely given by the overestimated serial resistance which by means of the Joule effect heats up the entire active material, and consequently the whole cell.

At last, before seeing the obtained adjustments, it is necessary to remind the fact that passing from one modified simulation to another one requires to perform, between the setup of the simulation and its launch, three steps:

1. Entering the correct values of “$Rate$” and “T_{ref}” within the code (each time);
2. Compiling the code working on the Visual Studio command prompt (each time);
3. Hooking the updated libraries in the Fluent environment (each time).

Thus, concluding, it could be useful to present the following *figure 85* which shows the resume of the new set of simulations that are going to be performed in this part of the work.

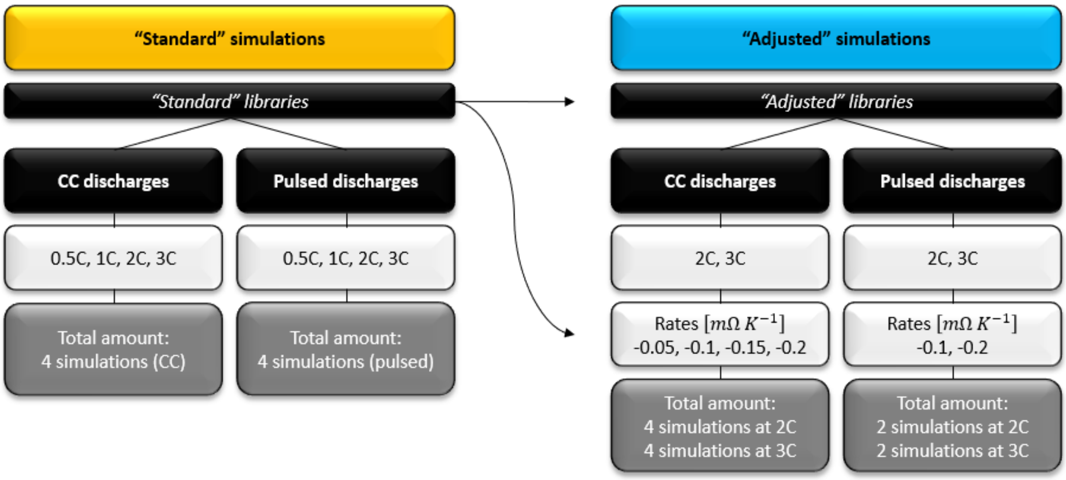

FIGURE 85 - Definition of standard and adjusted simulations

Note that, mainly for a matter of computational cost, only two values of “rates” have been tested in each of the two pulsed discharges under analysis instead of the four ones used in the CC tests.

Best achievements – **Adjusted results**

The obtained results are going to be presented following the same pattern previously used for the “standard” simulating campaign, thus stating from the plots representing the potential and temperature developments and ending up with the collection of the obtained numerical values. Concerning the graphs it is important to specify the notation that has been used: the curve labelled as “standard” represents the simulated quantity which could also be found in the *Chapter 5*, serving as a reference for the comparison with the adjusted values, while with “experimental” are indicated the real data coming from the experimental testing campaign. All the other curves, on the other hand, the so-called “modified” or “adjusted” ones, are going to be characterized by a precise colour whose association with a value of rate is specified in the legend of the plot. Hence, putting things together, six curves are going to be shown in each graph for what concerns the CC discharges and four (only two values of rates have been tested) in the pulsed ones.

- **CC discharges: standard, adjusted, and experimental outcomes**

The resulting collection of the potential developments is shown in the following *figure 86*.

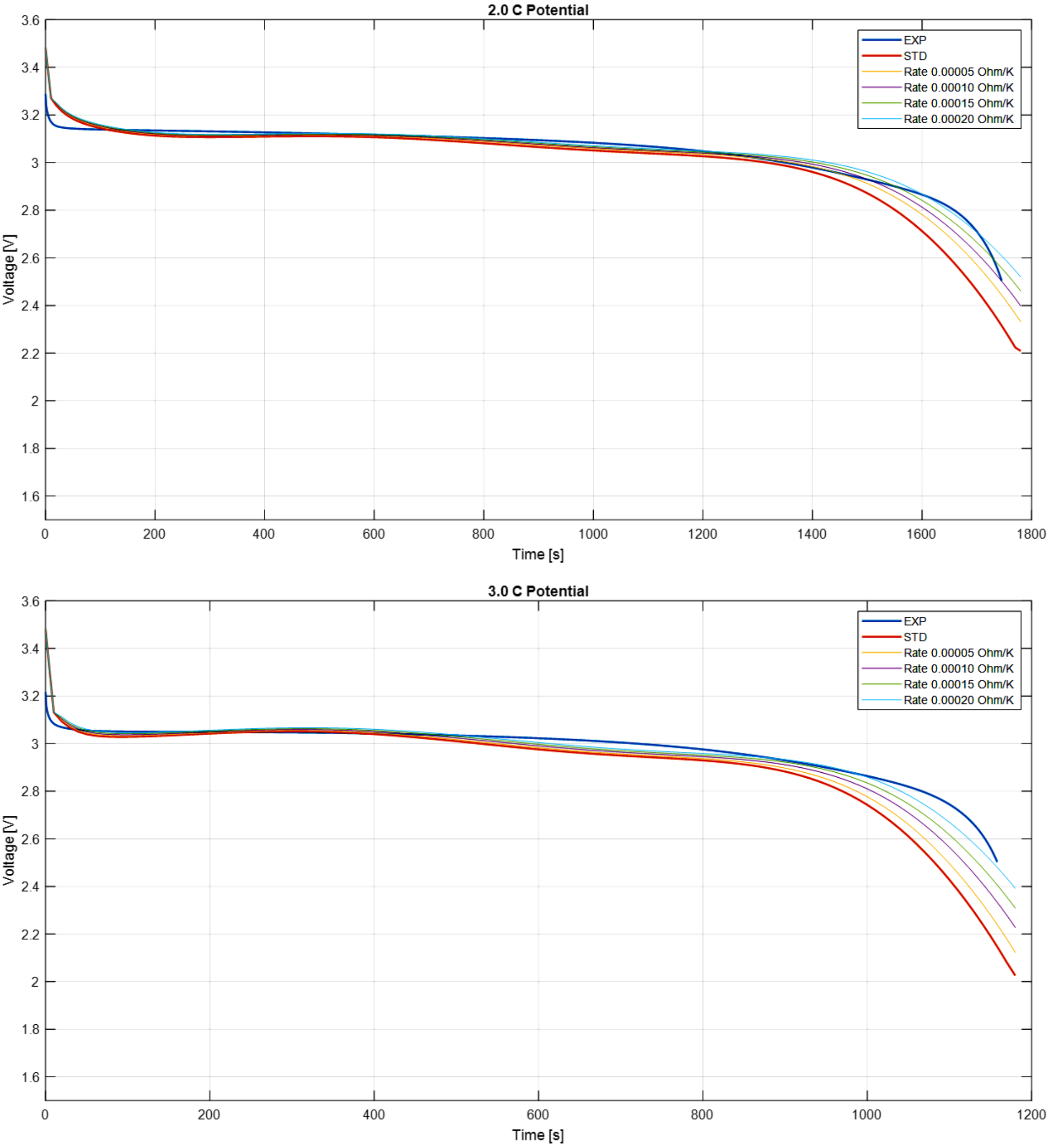

FIGURE 86 - $2C$ and $3C$ CC adjusted potential development

As it can be seen, the voltage value of the cell along each simulation already mimics in a good manner what happens in the reality, but with the inclusion of the corrective factors it does it even more, especially at low values of SoC (hence at the end of the discharge). This particular behaviour comes from the fact that the temperature of the active material is quite close to the reference one in the first moments of the analysis, but as far as this latter increases the correction gets more pronounced, reaching its maximum influence in the final instants where it is found a quite pronounced temperature increase. These explanations yields for both the tests ("$2C$" and "$3C$"), but it is straightforward that higher corrections are apported for higher C-Rates because of their major heating effects on the active material and consequently on the battery.

Speaking of the thermal outputs, on the other hand, having already selected the minimum facet temperature as the closest simulated quantity to the experimentally measured one, its corrected patterns along the discharges are presented in the *figure 87*.

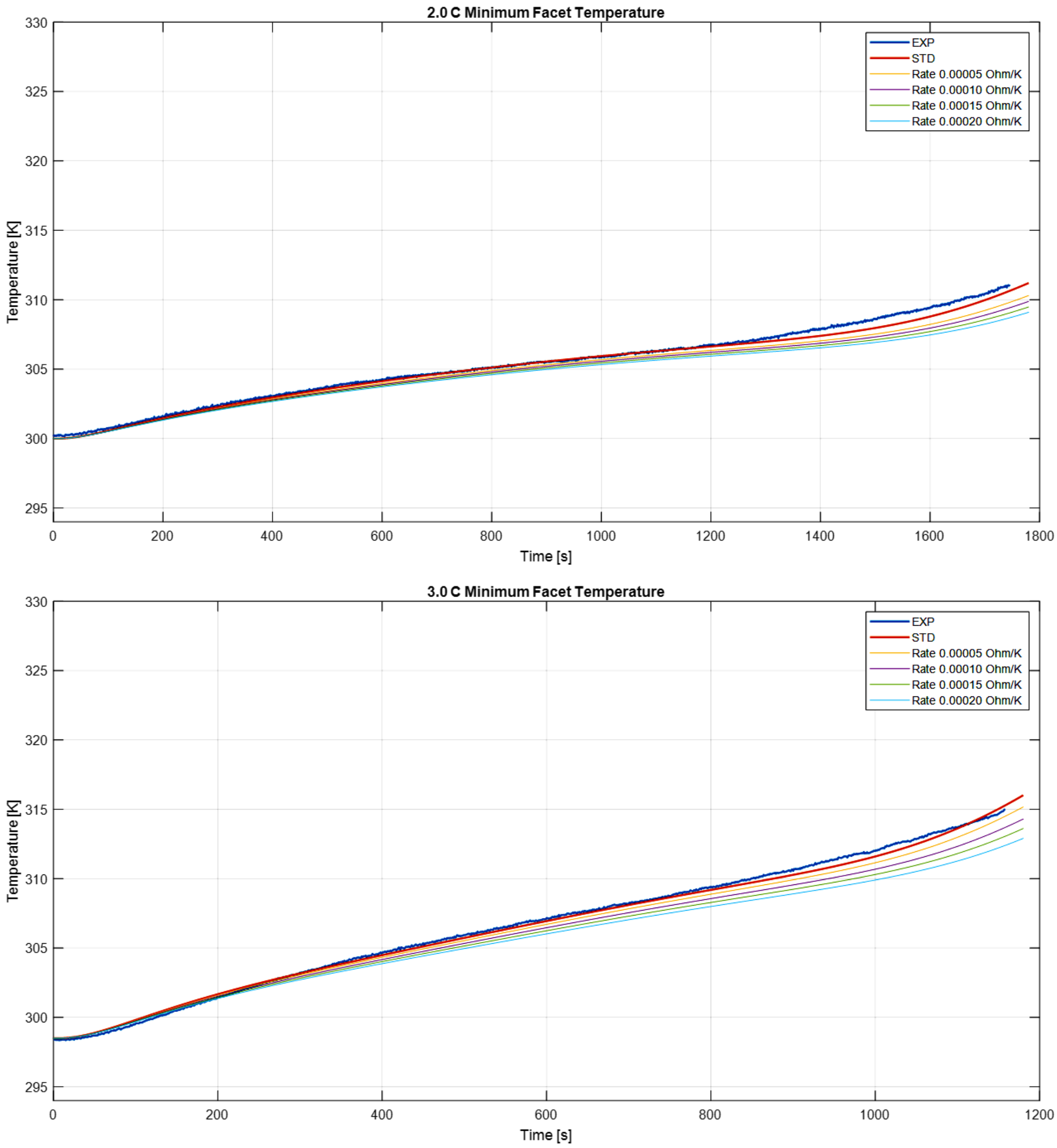

FIGURE 87 - $2C$ and $3C$ CC adjusted temperature development

In this case, the simulated minimum facet temperature which has been detected at the level of the case gets lowered of a certain extent. It has to be reminded the fact that this results comes from the combination of different factors: a lower temperature of the active material indeed reduces also the output at the surface of the battery, but there is not a one-to-one relationship because of the convective phenomena taking place in the air gap in between the two elements of the cell. However, because of the fact that now the potential curves are almost perfectly superimposed, a slightly major thermal error could be accepted being this latter indeed always small in magnitude, as it is going to be seen in the next section of the work.

Before presenting the obtained numerical results it could be also interesting to see the changes taking place at the serial resistance level. Starting from the curves represented in the *figure 59*, the inclusion of the different rates in their formulation ends up redefining them, as it could be seen in the following plots, lowering their development along the simulation.

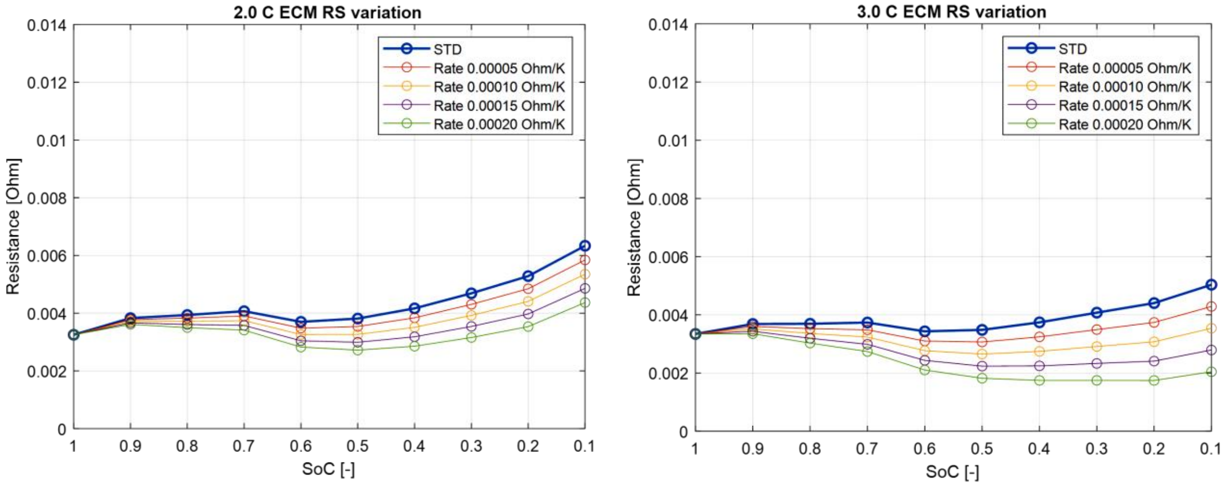

FIGURE 88 - $2C$ and $3C$ CC R_S variation

Concluding, an implementation of the *table 22* originally showing the CC simulation's numerical results could be presented in the *table 24*, considering the updates given by the adjustments apported in the analysis.

TABLE 24 - Adjusted CC numerical results

Adjusted CC outputs	$T_{B,MAX}\ [K]$	$T_{B,min} = T_{f,min}\ [K]$	$P_{fin}\ [V]$
Standard CC $2C$	$\mathbf{328.8637}$	$\mathbf{311.5561}$	$\mathbf{2.196892}$
$2C$ with $Rate$ $-0.05\ m\Omega\ K^{-1}$	326.4781	310.6169	2.263575
$2C$ with $Rate$ $-0.1\ m\Omega\ K^{-1}$	325.3443	310.1753	2.335653
$2C$ with $Rate$ $-0.15\ m\Omega\ K^{-1}$	324.2571	309.7531	2.403315
$2C$ with $Rate$ $-0.2\ m\Omega\ K^{-1}$	223.2169	309.35	2.466781
Standard CC $3C$	$\mathbf{344.7727}$	$\mathbf{316.7262}$	$\mathbf{2.001548}$
$3C$ with $Rate$ $-0.05\ m\Omega\ K^{-1}$	342.4514	315.8341	2.035068
$3C$ with $Rate$ $-0.1\ m\Omega\ K^{-1}$	339.994	314.906	2.126868
$3C$ with $Rate$ $-0.15\ m\Omega\ K^{-1}$	338.0653	314.1771	2.216624
$3C$ with $Rate$ $-0.2\ m\Omega\ K^{-1}$	336.0336	313.4141	2.308628

Once again, it has to be reminded that $T_{B,MAX}$ and $T_{B,min}$ are the maximum and minimum body temperatures (the latter is coincident with the minimum facet one), and P_{fin} is the final value reached by the potential development. From the numbers of the table in the last page it turns out that the minor heat generation induced by the presence of a smaller serial resistance ends up heating less all the elements of the cell: this decrement in the temperatures is major at the level of the active material, obviously, and less pronounced at the case's measuring point. On the other hand, the real gain obtained by applying this innovative approach is surely found in the simulated final voltage value, which gets closer and closer (by incresing in module the vale of the rate) to the cut-off potential used in the experimental tests of $2.5\ V$.

- **Pulsed discharges: standard, adjusted, and experimental outcomes**

Recalling that for this type of discharges only two levels of rates have been tested, the results are going to be rapidly presented as previously done, with the correction of the potential developments collected in the *figure 89*.

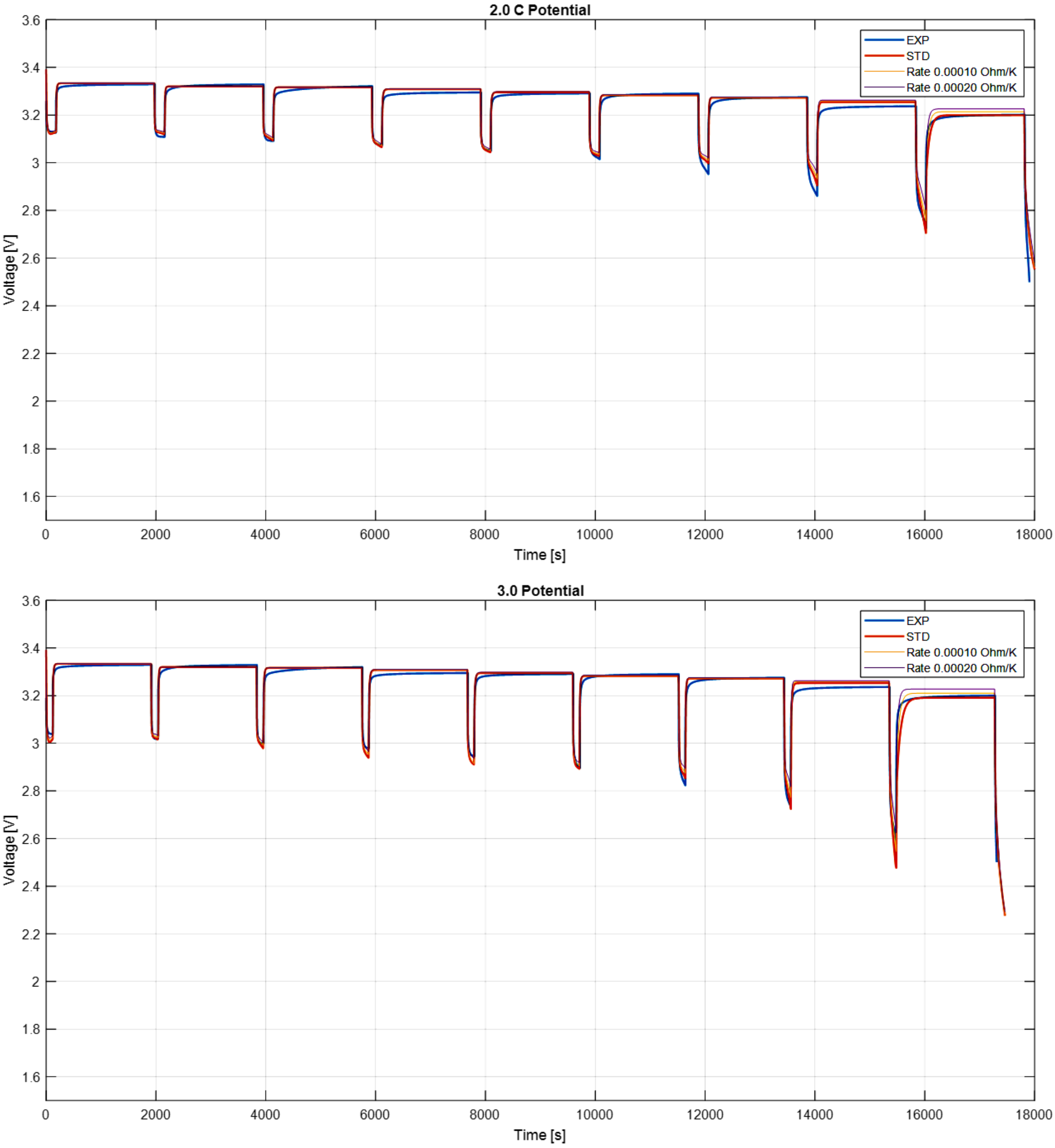

FIGURE 89 - $2C$ and $3C$ pulsed adjusted potential development

Subsequently, looking at the thermal outcomes, these are shown in the following *figure 90*.

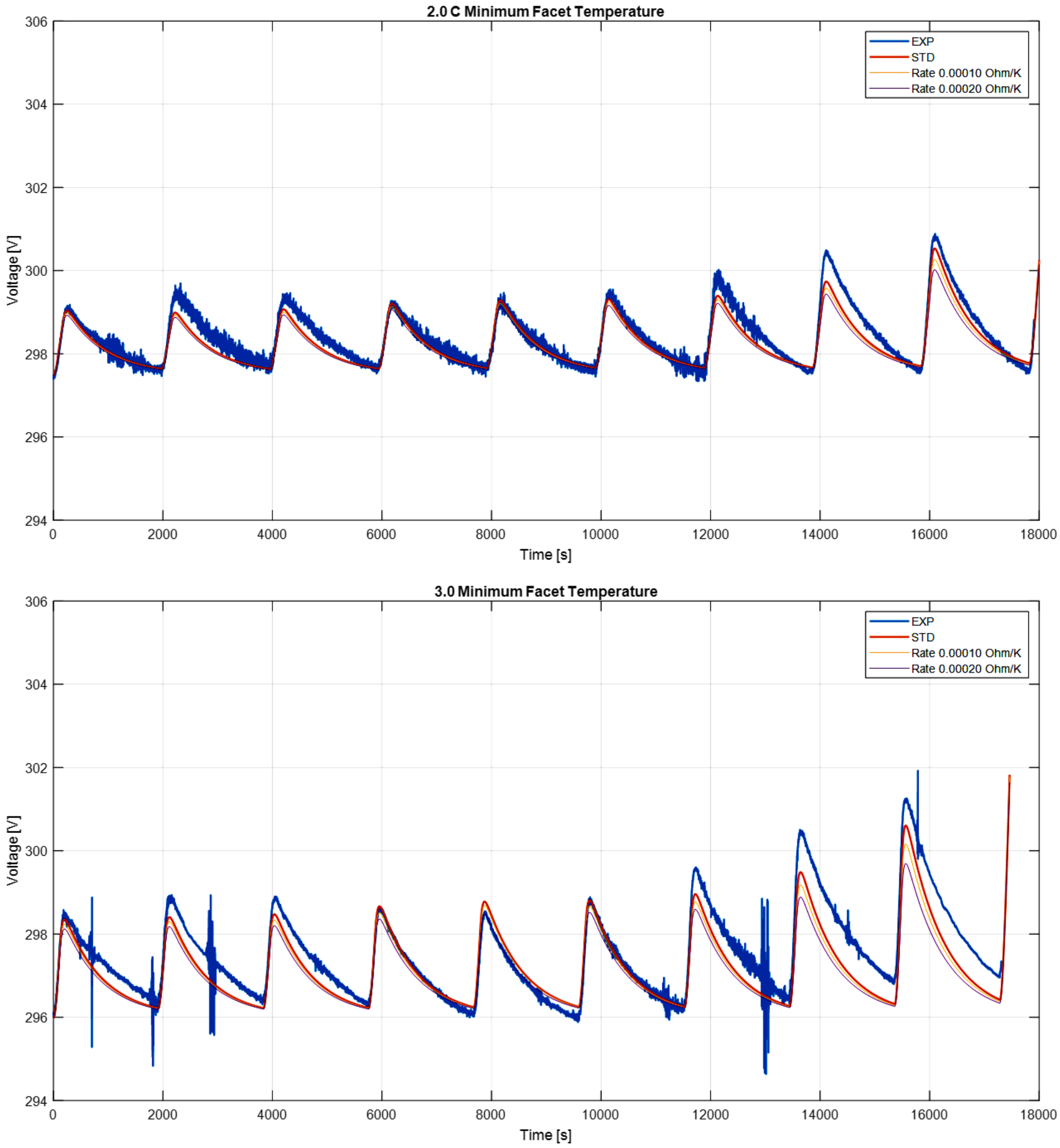

FIGURE 90 - $2C$ and $3C$ pulsed adjusted temperature development

Once again, the graphical results are straightforward: the correction of the pulsed discharges' serial resistance leads to an incredible match between the real experimental data and the simulated ones, especially from the electrical point of view: the latter phenomenon could be really appreciated in particular within the final part of the discharge where a bigger difference was initially found between the curves under analysis. Obviously, the adjustment of the overestimated resistance brings, as it has been previously seen, to a slight lowering of the curves simulated for what concerns the resulting thermal developments. However, it is very important to remember one last time that the minimum facet temperature does not completely corresponds to the real measured one, since the detection point is not exactly the central one of the case's biggest face. Thus, it can be concluded that being this measure a quite safe approximation of its real counterpart, also from a thermal point of view, the innovative approach aimed at correcting the standard simulations returns optimal results.

Speaking then of the adjusted serial resistance's curves, the following *figure 91* shows the change of the parameter given by the pulsating nature of the test, i.e. with subsequent increases rather than a decreases of temperature. Note that here, because of the particular pattern described by the pulsed discharges, the horizontal axis is expressed in time rather than with the SoC. This latter necessity arose from the fact that the decrease of the SoC in these types of tests, suddenly happens in a small instant of time with the reached value that is then maintained up to the following pulse. Thus, it has been decided to proceed with a parameter vs time plot because thought to be more correct for the representation (covering however the range in which the SoC varies between 1 and 0.1).

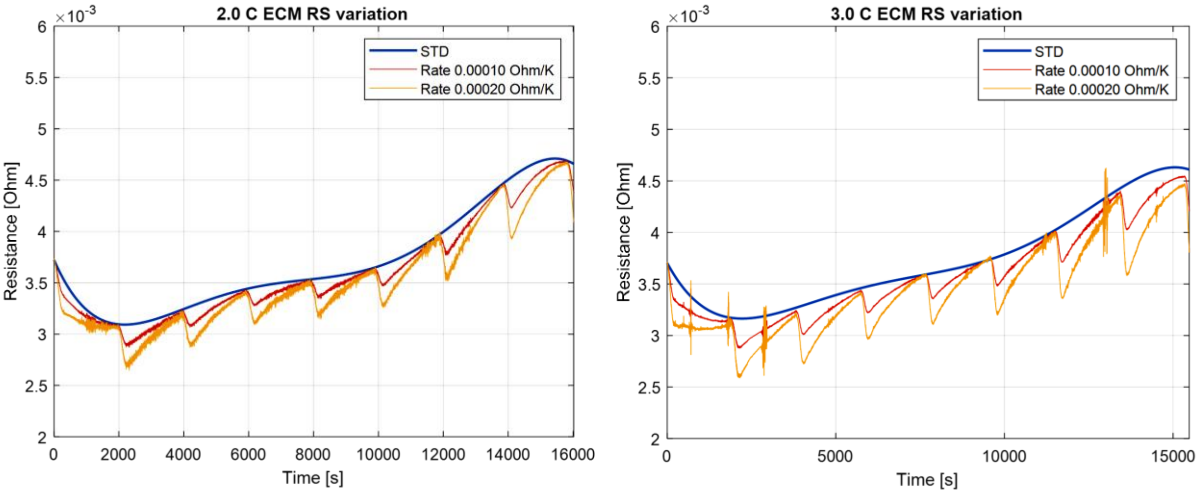

FIGURE 91 - $2C$ and $3C$ pulsed R_S variation

Some observations could be made looking at the two graphs above. Starting from the same standard curve (the fact that the blue line is the same in both the graphs has been explained in *Chapter 5*), each power pulses generates a temperature increment which suddenly decreases the R_S value, value which gets "recovered" towards its orgininal counterpart during the characteristic resting phases of such type of tests, with the consequent temperature decrement. This behaviour provides an interesting outcome: each time a power pulse is produced, the active material responds with a serial resistance which does not depend from the apported correction since time has passed in the previous resting phase and the temperature of the cell turns out being again initially equal to the evironmental one. In other words, the effect of the adjustments to the R_S parameters manifests only when the cell is active and a temperature increment takes place, and as a consequence gets anihiliated as far as the battery is at rest. What really produces a difference with the standard tests, concluding, is the modification of R_S during the pulses: the parameter is lowered because of the rising temperature, its initial overestimation is corrected and the generated heat decreased, and this happens each time a power pulse is applied to the cell which has not memory of what has happened previously—thanks to the precedent resting phases.

Finally, concluding this section of the work, the *table 25* is presented aimed at collecting the numerical results obtained within such analysis for the pulsed discharges.

TABLE 25 - Adjusted pulsed numerical results

Adjusted pulsed outputs	$T_{B,MAX}\ [K]$	$T_{B,min} = T_{f,min}\ [K]$	$P_{fin}\ [V]$
Standard puls. $2C$	**300.2518**	**305.7747**	**2.555515**
$2C$ with $Rate$ $-0.1\ m\Omega\ K^{-1}$	300.2304	305.6892	2.560983
$2C$ with $Rate$ $-0.2\ m\Omega\ K^{-1}$	300.146	305.4364	2.585788
Standard puls. $3C$	**301.8292**	**313.7948**	**2.281032**
$3C$ with $Rate$ $-0.1\ m\Omega\ K^{-1}$	301.7864	313.5742	2.285008
$3C$ with $Rate$ $-0.2\ m\Omega\ K^{-1}$	301.6369	313.061	2.297978

Note that all the conclusions that have been made for the constant current type of tests yields in the same way here in the following: generally, all the temperatures are found to slightly decrease while the potential value rises, arriving to cover the original, real voltage, found in the experimental tests.

Concluding the analysis conducted in this last chapter, the following results have been obtained thanks to the correction of the ECM R_S coefficient:

- As far as the temperature of the active material increases due to an applied power, the serial resistance decreases, and this decrement have been modellized to take place though the so-called “rate”.
- Decreasing the value of the serial reisistance, the amount of heat generated by the Joule effect gets lowered too, and consequently the cell warms up less.
- In paraller, the correction of the initially overestimated resistance (overestimated in particular in the last steps of the discharges, where the temperature had increased but the resistance kept the same value) brings to a closer match between simulated and experimental curves when analysing the potential de elopment.

The last thing remaining to do, finally, is the presentation of the thermal outcomes considering the computational error’s point of view.

Best achievements – **Adjusted computational errors**

Following again the pattern maintained within the *Chapter 5*, the thermal relative and absolute errors could be presented. Nevertheless it is worth to recall that, mainly thanks the goodness of the simulations as well as because of the high temperatures in play, the graphs reporting the absolute error turns out being more indicative of the outcomes, and as a consequence are the ones that are going to be presented in this section.

- **Errors for the CC discharges**

Concerning the constant current discharges, the following set of images collects the behaviour of the absolute error along the two simulations, conducted respectively with C-Rates equal to $2C$ and $3C$. Note that, as it has been done also in the original "standard" analysis, both the maximum and minimum facet temperatures have been considered, defining like this the upper and the lower limit for the error itself.

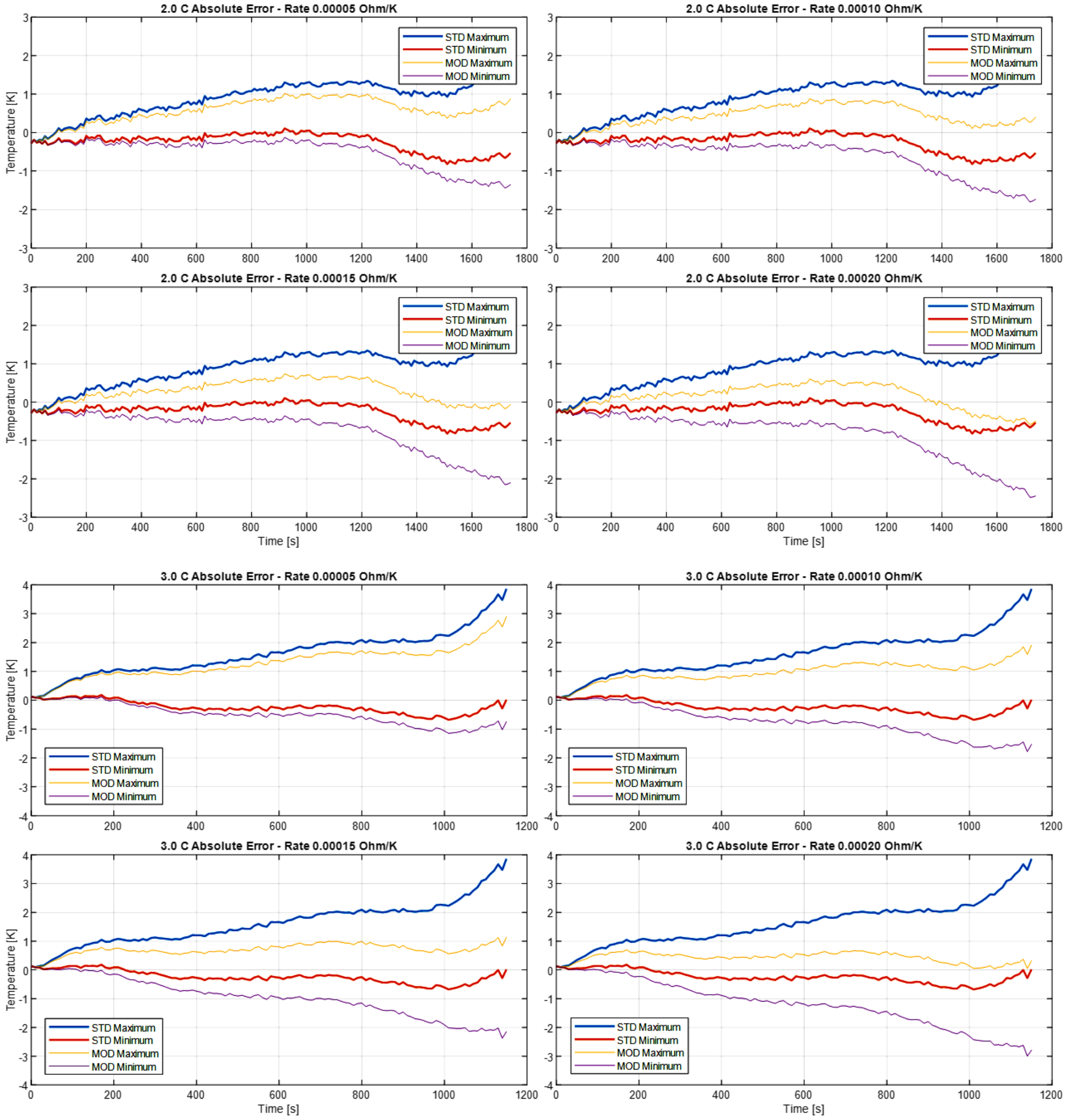

FIGURE 92 - $2C$ and $3C$ CC absolute error adjustment

In both the cases, the effects of now well known adjustments to the serial resistance is to lower the curve representing the absolute error development. The error characterizing the measuring point seems to be negative along the entire discharge, meaning that there is a certain kind of underestimation of the temperature, even if it has to reminded, again, that the actual real measurement's counterpart is slightly major than the simulated minimum facet temperature, and thus can be consequently thought to be around $0\ K$. The results, nevertheless, turn out maintaining a very good accuracy, with absolute errors in the range of $-2.5 \div 1\ K$ for a $2C$ CC discharge and $-3 \div 3\ K$ for a $3C$ one (considering the span covered by the use of all the rates).

- **Errors for the pulsed discharges**

As done for the CC discharges, the plots collecting the information about the absolute error development for the pulsed tests are shown in the following *figure 93*.

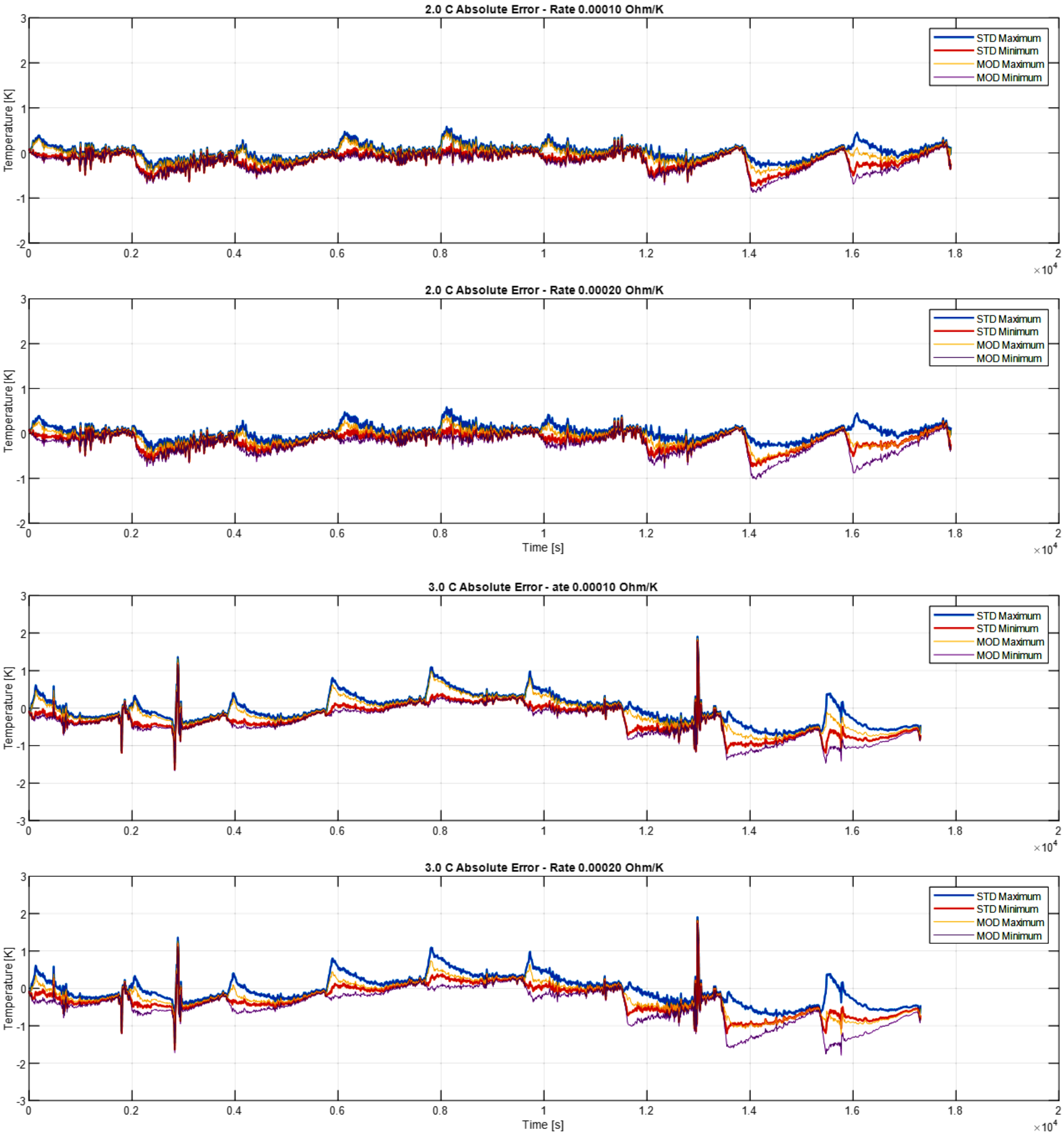

FIGURE 93 - $2C$ and $3C$ pulsed absolute error adjustment

The results obtained in the pulsed tests are even better than those achieved within the CC set of tests, with an absolute error that generally spans between $0 \div -1\ K$ in the $2C$ test and $0 \div -2\ K$ in the $3C$ one.

Thus, to conclude this last couple of sections belonging to the *Chapter 6*, it could be said one more time that with this new innovative approach the simulations manage to be closer to the reality from an electrical point of view (considering the potential curve, for instance), maintaining at the same time an almost negligible difference from the reference counterpart for what concerns the thermal behaviour: the changes turn out being actually improvements.

Design modifications

In the whole precedent part of the chapter it has been shown how to act in order to achieve better computational results by integrating together an “improved” theoretical background at the basis of a Li-Ion battery's ECM with some informatic functionalities of the solving software, namely ANSYS. However, another set of interesting results could be obtained by following a totally different approach aimed at changing the way the battery is thought from a design point of view.

More in detail, let's start considering that up to this point a thin layer of air has been placed between the active material and the lateral case of the cell, acting as an electrical insulator. In fact, if the battery was designed considering the direct contact between those two elements, a sudden short circuit would have taken place interrupting the development of the simulation—things that is avoided thanks to the insertion of the air gap. Therefore, even if in the reality the battery itself presents a direct contact of the electrically active component with the surrounding aluminium case, apart from very small clearances, the introduction of an intermediate layer was necessary to ensure the correct modelization of the device. The conductive nature of the fluid, however, affects of a large extent the thermal behaviour of the cell, and from here the idea of replacing it with a solid component to check the resulting differences that may emerge.

Two properties of the new solid layer must be taken from the previously used air gap:

- The material has to be a strong electrical insulator, therefore presenting a reasonable values of electrical conductivity which is standardly measured in Sm^{-1}, where S denotes the so-called "Siemens".
- The material has to be, of a certain extent, a thermal insulator. As it is well known, indeed, the exchange of heat through convection between two bodies is generally more difficult than that happening with convective phenomena: so, a reasonable value of thermal conductivity needs to be found out to finally compare the outcoming results between the two solutions.

To comply with the requirements listed above, a good guess is to substitute the air gap with a thin paper separator as done also at the interface of the active material and the cover plates. In this way, the presence of short circuits gets prevented while the heat transfer between the inner part of the cell and the external cover, although through a solid body rather than a fluid, does not take place within a highly conductive medium. Furthermore, also the possibility to use a material which is already defined in the Fluent libraries, i.e. the wood (as for the paper separators), is a great advantage because of its already defined physical properties, here collected in the *table 26*.

TABLE 26 - Wood's physical properties

Separating solid element	Density $[kg\ m^{-3}]$	Specific heat $[J\ Kg^{-1}\ K^{-1}]$	Thermal conductivity $[W\ m^{-1}\ K^{-1}]$	Electrical conductivity $[S\ m^{-1}]$
Wood (paper)	700	2310	0.173	10^7

Apporting such a change to the 3D CAD model of the battery will require to perform again few steps in the setup of the simulation, such as the generation of the mesh and the creation of a new named selection (which now will include the lateral, upper, and lower paper separators together). Apart from that, then, working in the Fluent environment, the process to follow is the same one described in the *Chapter 5*. Note also that no modifications are required to the ECM-related parameters, since the modelization of the active material does not change at all, and neither do its properties. Thus, in the following part of the chapter, the results obtained with the application of the set of the four CC discharges to this modified design are going to be presented, then putted in comparison with the ones formerly found—i.e. the “standard” achievements.

From an electrical point of view, the results are exactly the same obtained with the reference case study, i.e. the one considering the presence of an air gap. The following *figure 94* shows these achievements in the forms of the potential developments along the constant current simulations.

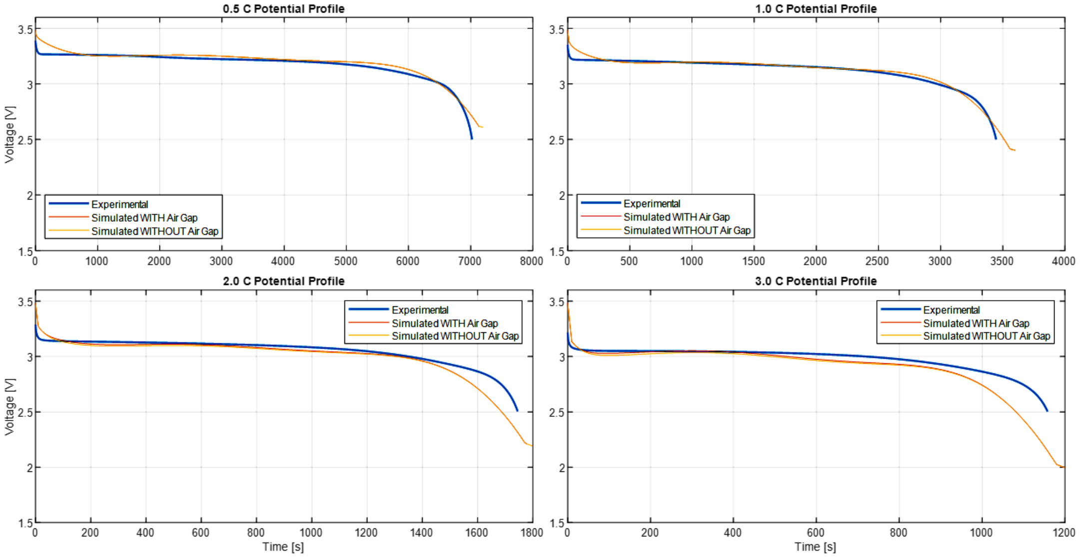

FIGURE 94 - CC potential developments comparison with and without air gap

As it can be noted, the red and the orange curves are perfectly superimposed and it cannot be detected any difference among the two of them, fact that could be simply explained by considered that the active material, and consequently all the ECM-related magnitudes, had not undergone to any change.

However, an information that could be eventually obtained by this set of plots regards the way in which Fluent processes the simulation. Indeed, in the subsequent part of this section it is going to be seen that there is a relevant difference in the generated thermal outputs between the two case studies, but the fact that no changes at all are found from an electrical point of view confirms that the program does not consider the temperature as a quantity having an active role in the definition of the ECM parameters. In other words, this last reading of the results suggests that no matter what the temperatures are because the ECM-related quantities are not affected at all by this magnitude.

Thus, it could be now presented what actually changes between the two implemented models: the thermal developments of the cell along the discharges. Once again, it is going to be considered the case in which the minimum facet temperature is the simulated reference to the real detected counterpart, or at least, better, the best guess. In the *figure 95* presented in the following page, hence, are collected all the thermal outcomes of the different tests with the relative experimental results.

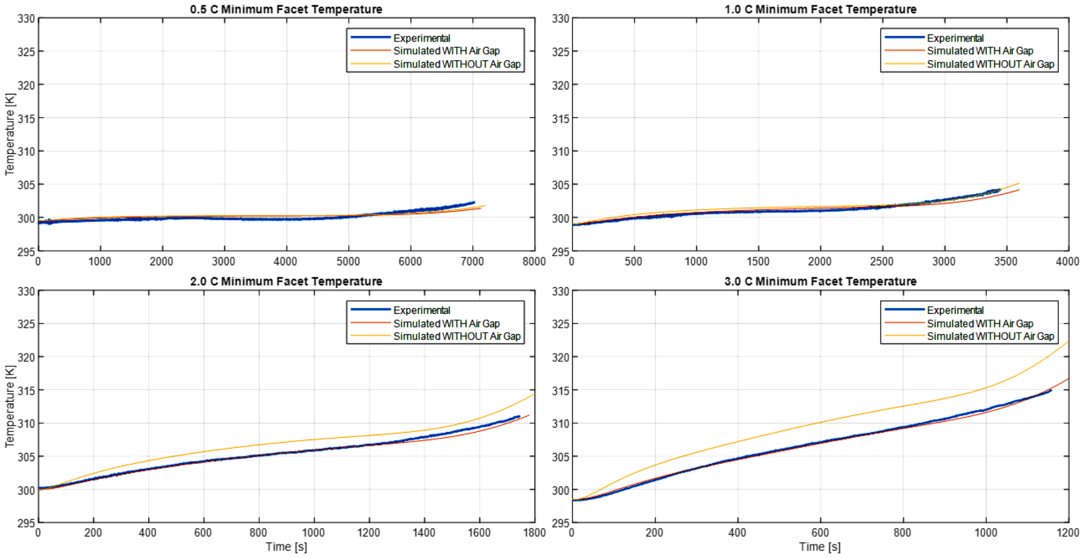

FIGURE 95 - CC thermal developments comparison with and without air gap

The results are straightforward: in all the cases shown above the yellow curves (which account for the design that considers the presence of the paper lateral separator rather than of an air gap) are higher than the red ones, fact that suggests an eased heat transfer between active material and aluminium case because of the thermodynamics of the conductive phenomena, heat transfer which in turns generates major temperatures in the point under analysis. Nevertheless, the discrepancy of the simulated results from the real data is clear: the program slightly overestimates the heat generation, but the difference could be once again recovered by applying the adjustments already presented in this chapter, lowering like this the simulated curve towards the experimental one.

Having seen the plots resulting from the collection of data, it could be then performed a graphical post processing analysis. The *figure 96*, for instance, shows the distribution of the temperature over the body reached after a CC discharge with a C-Rate of $3C$.

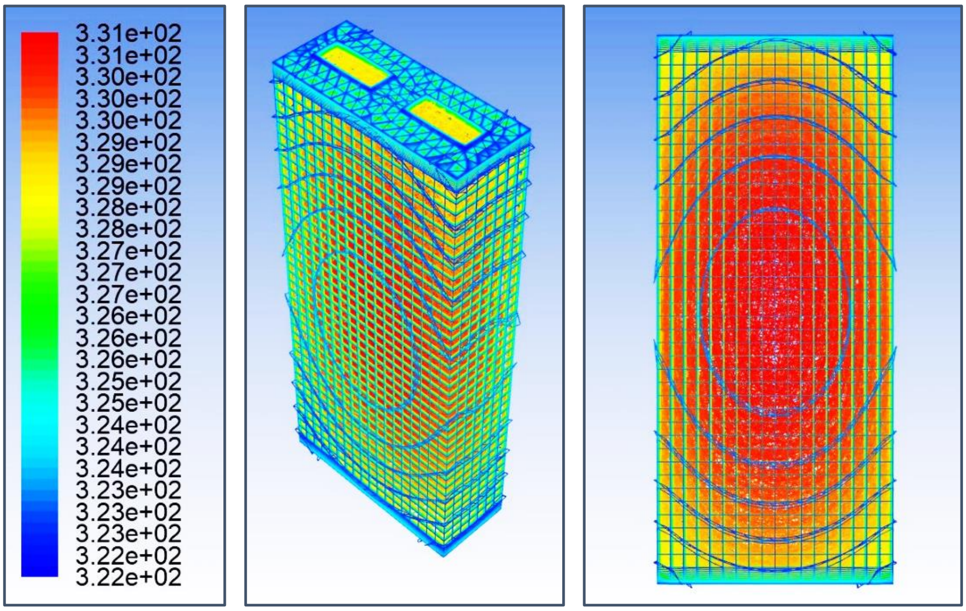

FIGURE 96 - $3C$ CC resulting temperature profile without air gap

As it can be noted from the image presented in the last page, the diffusion of the heat results to be more homogeneous than the one depicted for the CC discharges considering the presence of an air gap, providing as a consequence an homogeneous temperature profile in the overall body of the cell.

Finally, following the same pattern used up to now for presenting the results, the numerical simulated outcomes of this latter type analysis could be presented in comparison to the originally found ones.

TABLE 27 - CC new design numerical results

New design outputs	$T_{B,MAX}$ $[K]$	$T_{B,min} = T_{f,min}$ $[K]$	P_{fin} $[V]$
Standard CC $0.5C$	**304.1945**	**301.4395**	**2.6142**
With paper separator	302.548	301.7364	2.612128
Standard CC $1C$	**311.7052**	**304.1744**	**2.404774**
With paper separator	307.3109	305.0463	2.404855
Standard CC $2C$	**328.8637**	**311.5561**	**2.196892**
With paper separator	319.5952	314.1488	2.195923
Standard CC $3C$	**344.7727**	**316.7262**	**2.001548**
With paper separator	331.1111	321.9204	1.99996

It is now clear that in case a paper separator is used in place of an air gap, between the active material and the external case, the values reached by the potential keep being the same and that the minimum temperature of the cell—i.e. the minimum facet one—turns out being increased of a small extent. However, another really interesting result is given by the noticeable decrease of the maximum body temperature, at the centre of the active material. This latter outcome could be explained always by considering the physical nature of the paper separator which acts as a thermal insulator but turns out to ease the heat passage throughout it. As a consequence, the active material manages to “discharge” a larger amount of heat than done with an air gap, warming up less itself and increasing the temperature of the external aluminium case, now majorly “exposed” to the heat flux generated within the battery.

Final observations

Concluding the chapter, the following general observations could be made. The validation of the simulated behaviour of the cell by means of the experimental measurements conducted in the last section of the work has suggested the goodness of the simulative apparatus itself. Being the design of the component based on the presence of a small air gap rather than of a thin paper separator the accuracy of the results allows to say that an excellent match with the reality is actually reached. Improving then any of the two types of models with the informatic expedient presented early only helps in getting better such results, with an almost perfect behaviour of the cell from an electrical point of view and, on the other hand, a rather acceptable thermal one. However, having now clear the fact that the real measurement of the temperature is a value slightly major than the minimum facet one, it could be concluded that the principal type of analysis (i.e. the one with an air gap) produces the best results also from a thermal point of view, with the experimental curves regarding the temperature developments that are found to be slightly higher than the simulated ones, hence suggesting an overlap between the two measurement. Nevertheless, although with major relative and absolute errors, also the tested design considering wood instead of air produces impressively positive results. Thus, at the end of all and putting things together, it could be concluded that both the method can be considered as valid, as small variations one of the other that manage to produce a good match with what has been recorded to happen in the reality, but the presence of a small air gap is capable to mimic better the thermal phenomena that take place at the interface of the active material and of the aluminium case, elements that are actually in contact in the reality.

Chapter 7

Structural characterization

The swelling

Having completed the characterization of a Li-Ion battery both from a thermal and an electrical point of view within the last two chapters, this final part of the work is aimed at expanding the study about a cell adding to the previously obtained outcomes the ones coming from an innovative structural analysis, capable in describing the mechanical behaviour of the battery itself. In the past, indeed, the chemical and electrochemical ageing effects of Li-Ion batteries have got the major focus in the field of research: side reactions, solid electrolyte interphase (SEI) growth, and loss of lithium inventory have all been investigated in great detail. However, the influence of mechanical ageing has often been ignored and is only nowadays starting to attract attention. The mechanical design of a battery turns out being of major importance when creating applications willing to maximize the energy density and lifetime of the devices, as it happens in the automotive field. In this case, the most relevant concern is the volumetric variation of the body taking place during its functioning, of particular importance when an optimal integration of the cells within modules, packs, and systems is required. Consequently, geometrical variations and mechanical stresses changing with the state of charge of the device as well as with its state of health should be carefully considered in the early designing phases. In this context, an inappropriate design will lead to premature ageing of the components at all the levels, and, in the extreme cases, a mismatch of volume requirements and device integration can lead to catastrophic failure [46].

Going more in detail, the so-called “swelling”, i.e. the volume change of a battery, can have various causes.

- The principal one is given by the Li^+ migration, where the electrodes change in volume as a result of lithium intercalation and deintercalation in their crystal structures.
- Moreover, other phenomena have a certain impact on the structural behaviour of the cell: gas formation, occurring due to side reactions, lithium plating, and the growing presence of the products generated by the electrolyte’s decomposition.

Wanting to study this field, many measurement methods have been implemented and used to define the volumetric change: among the others, some takes advantage from thickness gauges, pressure sensors, digital image correlations and multi-scale investigations, showing at the end material-dependent variations in the size of the battery between a fully charged ESS and an “empty” one. Nevertheless, because of the quite big amount of topics that could be covered by the study, the following part of the work mainly concentrates in determining the effects given by the internal pressure variation in a prismatic Li-Ion battery. In particular, two different types of studies are going to be conducted:

1. The first one wants to replicate what happens during a single cycle of discharge and recharge, hence linking the behaviour of the cell with its SoC;

2. The second part, on the other hand, investigates what happens during the ageing of the device, considering hundreds and thousands of the previously mentioned cycles of charge and discharge.

Thus, previously to the presentation of the model implemented once again in the ANSYS environment, it could be useful to see more in detail the quantity of interest of the analysis together with the phenomena influencing it: the battery's internal pressure.

The swelling – **Internal pressure**

Although all the prismatic batteries are eventually equipped with a vent valve constructed so that it opens at a defined pressure level during abuse cases, the gas pressure inside a generic lithium-ion cell is a physical parameter which, as it has been said, has to be carefully considered during its design. In fact, as a consequence of the internal pressure, the superficial swelling of the battery's case is dangerous because of the protruding shape of the body it generates, with consequent concerns related to the strain and stress levels reached by the protecting element. However, the measurement of the gas pressure turns out being helpful in providing an additional source of information about the state of the battery, enabling like this advanced state estimation. Obviously, this would require the measurement of the fluid pressure during operation, difficult to achieve due to the sensors' positioning and costs of the hardware, but easily obtainable if one analyses the other magnitudes connected to the swelling: deformations of the case and stresses—since it could be thought that once one manages to define a pattern followed by a certain quantity during the discharge of a cell, this could be used to monitor the amount of energy still present within the device. Thus, putting things together, the aim of the section is to initially characterize the behaviour of the gas pressure during the battery's functioning, and subsequently connect it with other easily measured quantities thanks to the structural simulations conducted via ANSYS.

Starting from the general thermodynamic equation of an ideal gas, the pressure (p) inside a closed volume (V) depends on the amount of gas (n, i.e. the moles) enclosed in the volume itself and on the absolute temperature of the fluid (T) through the following general formula:

$$pV = nRT$$

Where R is the ideal gas constant. Note that the assumption of a fluid behaving as an ideal one usually turns out being a good approximation for the describing of the real gases.

Referring then in particular to the case of Li-Ion ESSs, it has been reported that the internal pressure level, namely p, is generally affected by the following phenomena:

- Reversible changes of electrode volume during intercalation and deintercalation of lithium ions within the specific lattice structures, resulting in a change of free volume V occupied by the gas inside the cell;
- Irreversible gas formation during ageing, increasing the amount of moles of the fluid within the limited volume.

It is important to remind that in the literature have been reported lots of experiments where the gas pressure inside a cell has been monitored during operation, but apart from the studies where the quantity has been explicitly measured, many others focused on the fundamental effects causing gassing inside lithium-ion batteries during formation and ageing. However, in the following part of the work the pressure measurements detected during the cycle ageing of a large-format lithium-ion cell for over a thousand equivalent full cycles are going to be presented and discussed, based in the results obtained in the work of Schmitt et all [47]. Based on the paper's outcomes, subsequently, it is possible to finally simulate thanks to the ANSYS capabilities the resulting values of absolute displacements, strains, and stresses, as a result of the internal gas pressure's levels. Also take in mind that a direct comparison of the simulated outcomes with the aforementioned results is possible since the dimensions of the battery under study are similar to the one already described in the *Chapter 5*.

Thus, after this introduction related to nature of the gas pressure within a Li-Ion cell—and previously to the direct presentation of the numerical results which are then going to be entered in the simulated mechanical model—it is necessary to spend a few words describing the huge testing campaign conducted by Schmitt et all on a large-format prismatic cell. This latter could be split in three main parts, here in the following summarized.

- **Initial characterization and cycling period**

  At the beginning of the experience, the battery was submitted to a particular initial characterizing test, not of interest for the purpose of this work and hence not technically explained. Subsequently, the device has been repeatedly cycled for 100 complete cycles of charge and discharge performed with a $1C$ current. Furthermore, after each current application, either charging or discharging the cell, there was a resting period of 10 minutes.

- **Electrochemical characterization**

  Completed the cycling period, the battery was submitted to an electrochemical characterization. The procedure at which the cell has undergoes consisted of repeated charging and discharging cycles with different values of C-Rates, followed by a low-current, quasi-stationary open-circuit voltage (OCV) measurement conducted with a $0.05C$ C-Rate. The quasi-stationary measurements were aimed at defining the values of capacity and taking the correlated pressure changes during charging and discharging of the battery, using the so-called "differential voltage analysis". Afterwards the cell was completely discharged, two final charging and a discharging pulses were applied. Also take in mind that the overall electrochemical characterization is both preceded and followed by a resting period of $6\ h$.

- **Galvanostatic intermittent titration technique with pressure sensing**

  Apart from the dynamic behaviour of the cell, also its condition at rest have been characterized thanks to the so called "galvanostatic intermittent titration technique" (GITT). Both the open-circuit voltage and gas pressure at rest were measured at different SoC levels using the GITT in order to analyse the influence of the SoC on gas pressure at equilibrium conditions, rather than with a "stressed" device. The experiment was carried out at $25\ °C$ with the cell that was firstly charged with a $1C$ current and subsequently kept under open-circuit conditions for $6\ h$. Only afterwards a $10\ s$ discharging pulse of a $1C$ current was applied, followed by one more minute of rest and by an approximate 5% of the overall initial capacity (referred to a fully charged battery) drawn away from the device by applying a constant current of $0.2C$. These steps were repeated until the terminal voltage reached $2.5\,V$, and the same procedure was subsequently applied in the charging direction.

The entire set of operations described above was replicated thirteen times, resulting in almost one year of duration and more than 1300 equivalent full cycles (EFC) of charge and discharge. As a support to better understand the experimental campaign, the following *figure 97* graphically shows the operations at which the cell was submitted.

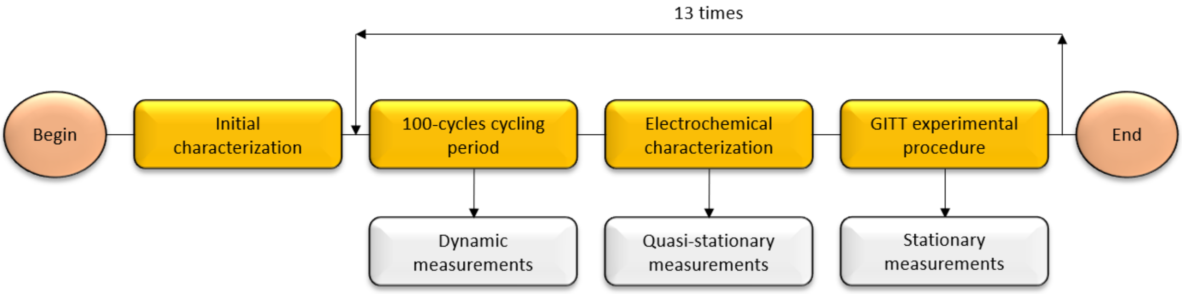

FIGURE 97 - Gas pressure measurement characterizing procedure

As a sensing element used to detect the gas pressure inside the cell case, the so-called "SP40" pressure sensor (produced by the German company "Infineon Technology AG") has been used. Here, a pressure-sensitive membrane lies beneath an opening in the sensor package and deforms upon variation of the level of gas pressure whose volume is in contact with the opening, enabling its measurement. The entire experimental setup of the cell is reported in the following *figure 98*, where one could also appreciate the presence of a sophisticated clamping system surrounding the prismatic body.

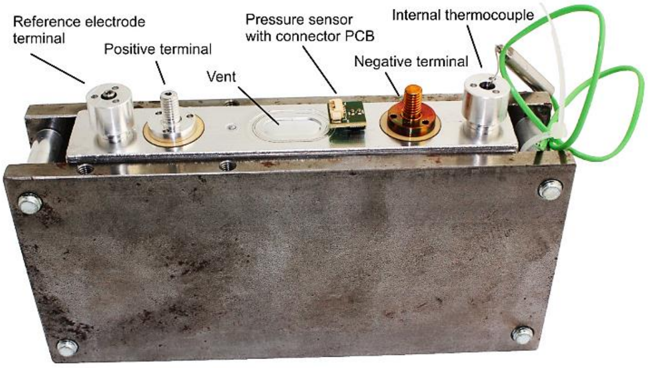

FIGURE 98 - Experimental setup (from the work of Schmitt et all)

At the end, putting together all the things that have been seen in this section, the complete experimental campaign is capable in providing three different types of results, as also summarized within the *figure 97*:

1. During the 100-cycles cycling period the cell has been dynamically tested, meaning that the resulting data acquired by the sensing apparatus reflect the "dynamic" behaviour of the cell during its functioning. Note that the true goal of this part of the testing campaign is to rapidly cycle the battery in order to highlight the irreversible

pressure increase taking place from the beginning to the end, rather than knowing what happen inside within specific cycle. Accordingly, the gas pressure level was recorded at the beginning and at the end of each charging and discharging single cycle.

2. The electrochemical characterization, on the other hand, always returns a p vs SoC information, acquiring these data via a quasi-stationary test. Here, differently from the previous point, the focus is truly on the single cycle itself rather than on a certain number of cycles as previously seen.
3. The GITT experimental procedure, finally, provides once again results in the form of p vs SoC with the pressure level that now, however, gets detected with a fully rested body in order to remove the effects of gas formation happening during operation.

To better understand the outcomes, the following *figure 99* collects part of the results obtained by the experience. From the left-hand-side plot to the bottom-right one, one can see the data relative to the aforementioned points 1, 2, and 3. Note only that in the latter plot, also the role played by the temperature has been investigated, but it is not of interest for the purpose of the analysis conducted in this work.

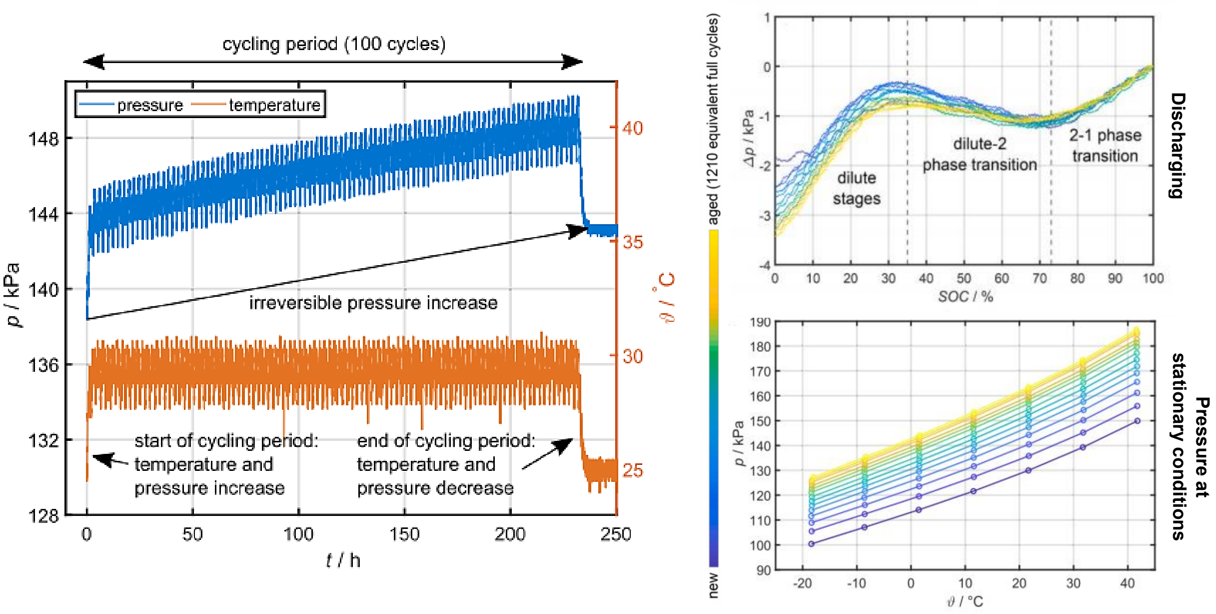

FIGURE 99 - Dynamic, quasi-stationary, and static measurements (by the work of Schmitt et all)

Few words should be spent on the set of graphs presented above.

- **Reversible pressure changes**

As it can be seen, the internal gas pressure measured at quasi-stationary conditions exhibits a non-linear dependence with respect to the SoC. In particular, there are three regions in the $0 \div 1$ SoC range with different correlation between pressure and SoC:

1. Within the upper SoC range, i.e. $> 70\%$, the internal pressure of the cell decreases along the discharge.
2. In the middle SoC region, on the other hand, the pressure could be considered to be almost constant.

3. In the lower SoC range, i.e. $< 35\%$, the pressure turns out, again, to strongly decrease along the discharge.

Considering that the reported behaviour is almost perfectly specular between discharge and charge of a cell, then, the theoretical background related to the Li-Ion ESSs helps in better understanding this aspects. As it has been seen, indeed, the gas pressure inside the case of a battery can be basically described by the ideal gas equation already provided in the precedent pages. Excluding the role played by the temperature in changing the quantity under analysis, thanks to the presence of a controlled climatic chamber, the major cause producing this particular pressure behaviour is the change in the free volume within the case. The so-called "free volume", indeed, depends on the expansion of both the anode and the cathode's lattice structures (especially in the work of Schmitt et all where the total volume inside the case stays constant during operations, as a consequence of the constrained deformation of the rigid case prevented by clamping system), and in particular on the combination of the relative volumetric changes. Considering indeed, for instance, a graphitic anode, its volumetric expansion during the reception of the Li^+ overcomes the cathodic volumetric shrinking in the high and low SoC ranges, producing this interesting pressure decrement during the discharge. In the middle level of charge, on the other hand, because of the creation of transitory phases forming at the level of the anodic lattice structure, the effects given by the volumetric changes are close to annihilate each other, providing an almost constant pressure level.

- **Irreversible pressure changes**

Besides the reversible changes in the gas pressure level, function of cell's state of charge, the general level of pressure irreversibly increases during the ageing of the device. The left-hand-side plot of the *figure* 99 represents, as an example, the pressure in within the first 100 cycles, clearly showing the progression of the pressure during the development of the cycling period. At the beginning of each period it could be noted that the pressure significantly increases by about $5\ kPa$ and subsequently follows a repeating pattern around a slightly increasing mean value. The former pressure increase is caused by the rising active material's temperature developed during cycling (major than the environmental one), while the nature of the pattern results from the superposition of the temperature changes during the different phases of cycling and the changes in the electrodes' volumes, as previously discussed. However, the most important feature to be discussed about the graph under analysis is the mean pressure value increase, resulting from the irreversible phenomena which generates a supplementary amount within the battery: gassing has been reported to be the main effect leading to an increase in pressure inside Li-Ion-based ESSs in the literature, even if the long-term increase could also be eventually the manifestation of an irreversible increase in electrode volumes. Nevertheless, the contribution of irreversible electrode swelling normally develops pressure increases in the order of a few kPa, negligible with respect to the tens found within the experimental activity.

Arrived at this point, knowing the phenomena taking place within a Li-Ion battery, pressure-wise, as well as most of the root causes generating them, it is necessary to collect and work on the data coming out from the experimental activity which will be subsequently entered in the user-built structural model in the ANSYS environment. Since the aim is to characterize both the behaviours of the cell from a single cycle and from and ageing point of view, two distinct datasets have to be created: the one describing the behaviour of a battery during its discharge and the one showing the ageing effects.

The swelling – **Relevant data**

The reversible pressure changes taking place during the discharges (i.e. function of the SoC) have been modelized starting from the data shown by the upper right-hand-sided graph presented in the *figure 99*. Considering a generic reference pressure level, the gas pressure loses $2.5\ kPa$ during a complete discharge and gains this gap back when charged. Note also that although small differences are present between a fresh and an aged cell, these have been considered as negligible within the following analysis. The generic curve describing the pressure decrement, then, could be replicated by initially considering the three different stages taking place during operation, from the discharging point of view:

1. Relative pressure decrement of $1\ kPa$ in the range of $SoC\ 1 \div 0.7$;
2. Relative pressure increment of $0.5\ kPa$ in the range $0.7 \div 0.35$ (meaning that small changes in the pressure are considered, hence not thought as constant);
3. Relative pressure decrement of $2\ kPa$ in the range $0.35 \div 0$.

Spreading uniformly the aforementioned decrements and increments along the entire duration of a discharge performed with a $1C$ current (i.e. $3600\ s$), it is possible to obtain a rough representation of the general curve in the plane p vs t. Note that, in this case, it has been used the time and not the SoC as the characteristic magnitude of the x axis because, as it is going to be seen, ANSYS will reasons in seconds rather that in % values. Subsequently, in order to smooth the entire representation and mimic as much as possible the real previously seen outcomes, a $5th$ order polynomial curve has been built by taking advantage of the "fitting" feature provided by MATLAB. Both the "rough" and the "real" curves are represented in the following *figure 100*.

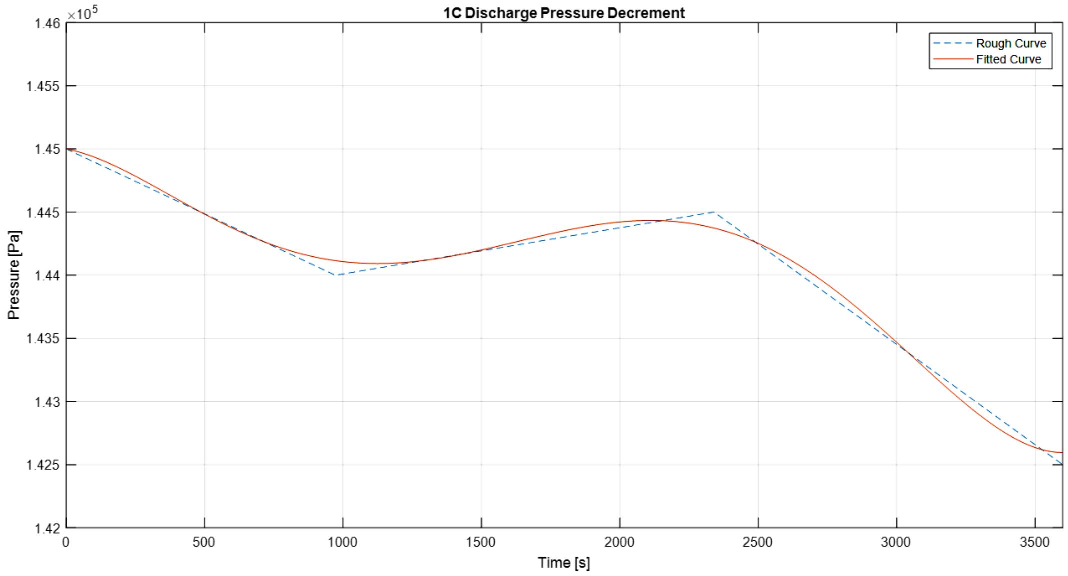

FIGURE 100 - Model of pressure decrement along a $1C$ discharge

The so-called “Fitted Curve” represented in the last page relies on the generic initial pressure level of $145\ kPa$, for now randomly selected. The following *table 28* wants to collect the resulting polynomials coefficients, useful to be known because of their utility on in the structural model’s definition, later.

TABLE 28 - Pressure polynomial curves coefficients

$i-th$ polynomial coefficient	p_0	p_1	p_2	p_3	p_4	p_5
Numerial value	TBD	-0.428	$-2.401E-3$	$2.896E-6$	$-1.088E-9$	$1.288E-13$

At last, it worths to remember that whenever there was the necessity to represent the pressure decrement taking place along a certain discharge, knowing that the general shape of the curve previously represented is maintained along the life of the device, it would be sufficient to change the $0th$ order polynomial’s coefficient so that a new "quota" will be going to be settled accordingly. This latter aspect is very interesting since it is able to effectively mimic the aforementioned phenomena also taking in consideration the irreversible pressure increases during the ageing of the battery: like this, for instance, it will be easy to pass from the representation of the $1st$ cycle of the overall cycling period to the $100th$ one. With this latter aim, the following *table 29* collects the gas pressure values at the beginning of three different discharges among the first 100-cycles cycling period, namely the $1st$, $50th$ (middle), and $100th$ ones (last).

TABLE 29 - $1st$ 100-cycles cycling period measurements at SoC 100%

$0th$ polynomial coefficient	$1st$ cycle over 100	$50th$ cycle over 100	$100th$ cycle over 100
Pressure $[kPa]$	144.3	148	149.5

Thus, with the rather simple set of data presented up to now, knowing both the behaviour of the pressure along a discharge and the initial gas pressure levels correspondent to the fully charged cell, the three cycles under analysis ($1st$, $50th$, and $100th$) are going to be simulated in the following chapter of the work in order to study the battery from a mechanical point of view, trying to end up with reliable values of the case’s real punctual displacements, deformations, and stresses, starting from knowing internal pressure solicitations.

Apart from this latter section aimed at obtaining the necessary quantities to subsequently study the “dynamic” behaviour of a Li-Ion battery, the work of Schmitt et all provides as well interesting results for the static analysis of the device, mainly focused in detecting the ageing effects caused by the irreversible swelling. In this case, one has to principally consider the bottom left-hand-sided graph reported in the *figure 99*: here, the gas pressure levels represented in the image have been recorded thanks to the GITT testing procedures, hence from a fully rested cell, at different temperatures and at a different amount of equivalent full cycles (EFC). Indeed, the complex and long experimental campaign involves the application of a large amount of cycles divided, as it has been explained, among general characterizations, 100-cycle cycling periods, and electrochemical characterizations. As the theory suggests, then, each full cycle of discharge and recharge applied to a battery submit this to a certain degree of ageing, lowering some of its performances. The purpose of the following part of the work is also to try to characterize this ageing, here accounted with the number of EFCs which the cell underwent. Hence, the two quantities that are now of interest could be obtained: the number of EFCs at which the static characterizations have been made and the relative gas pressure values presented by the device when this is completely "at rest" and fully charged. Note, at last, that the term "relative" refers to the number of EFCs and not to the pressure level, recalling the duality between absolute and relative measurements in the field. Finally, given that all the pressure measurements that are going to be presented are the ones referred to a $25\ °C$ imposed boundary condition (thanks to the controlled climatic chamber used in the experiments), the following *table 30* collects the data of interest for the future static analysis, i.e. the number EFCs and the respective static gas pressure levels.

TABLE 30 - Static measurements at $SoC\ 100\%$

# EFC	**12**	**113**	**207**	**300**	**393**	**485**	**578**
Pressure $[kPa]$ (at $25°C$)	134.5	140	144.5	148	151	153	156
# EFC	**669**	**763**	**854**	**944**	**1035**	**1124**	**1213**
Pressure $[kPa]$ (at $25°C$)	158.5	160.5	161.5	163	165	165.5	168

Thus, resuming and putting things together, it is possible to pass to the simulative part of the chapter with the following set of data:

- Internal pressure developments along "$1C$" CC discharges, with values referred to the first 100-cycles cycling period, for a "dynamic" structural analysis.
- Internal pressure static measurements conducted at rest with respect to a predefined set of EFCs for a "static" structural analysis.

Mechanical analysis

Knowing now the relevant data which will be used for the following structural analysis, this section of the chapter follows the same patter already seen when dealing with the thermal and electrical characterization of a Li-Ion battery. Thus, in sequence, it will be presented the mechanical model created in the ANSYS environment together with a brief explanation aimed at addressing its complete and correct setup. Subsequently, the simulated outcomes are going to be detailly discussed, with the final section which will be totally dedicated on the implications generated by the results, concerning in particular the observed presence of the so-called "fatigue". The only aspect which is important to address previously to the complete analysis regards the cell itself. In the experimental campaign of Schmitt et all, indeed, a large-format Li-Ion battery with a capacity of $34\ Ah$ has been tested, differently from the one previously studied in this work which presented a $25\ Ah$ capacity. However, the similarities of the two devices could allow a direct comparison: the dimensions of the bodies are similar, as well as the materials forming anode and cathode. Hence, the initial, strong assumption is that it is possible to take the data coming from a different but yet similar device and fit them in the specific one studied within this work. Therefore, it must be reminded that a validation is still necessary from the real counterpart of the simulated device in order to assure the goodness of the simulations themselves, but this entire study could eventually, and will, serve as a reliable basis for future developments within the field of research.

Mechanical analysis – **Model**

Starting from the reference 3D CAD model already presented within the *Chapter 5*, only a small change needs to be made: to reduce the previously used case thickness. Indeed, as one could remind, it has been previously used a $1\ mm$ thick body to replicate the aluminium-based chassis of the Li-Ion battery. However, accurate measurements revealed the dimension to be slightly minor, around $0.7 \div 0.8\ mm$, and even if this difference were not relevant in case of thermal and electrical measurements it would have had an impact for what concerns the mechanical behaviour of the body. Thus, adjusting the geometry of the body within the SpaceClaim environment and updating the information in ANSYS WorkBench, it is possible then to directly pass the CAD model in the Mechanical APDL environment. In the following, all the operations necessary in order to perform the correct setup of the Li-Ion battery are enlisted.

- **Mesh**

  Mechanical APDL will now serve as both meshing and simulation software for the structural analysis (it is no longer required to perform a CFD simulation, and hence Fluent does no longer suits for the purposes of the work). Initially, in order to lighten the computational burdens it is possible to "suppress" some elements of the geometry because not of interest for a mechanical analysis such as the one which is going to be performed. Wanting to consider all the external effects given by a certain internal gas pressure, hence, it is possible to only maintain the lateral case and the two cover plates. Note that also the air gap is no longer necessary in the model, since the load on the faces will be imposed as pressure-defined boundary conditions directly on the geometry. Then, after the suppression of all the elements apart the aforementioned ones, the discretization of the body could be performed exactly as reported in the *Chapter 5*: the FE (i.e. the so-called "primitives") will be quadratic tetrahedral bodies with a dimension of $4 * 10^{-3}\ m$.

- **Mechanical constraints**

  Before the definition of the solicitations, the mechanical constraints have to be selected. Working in the "Outline" environment, within the project tree, it is possible to insert and take advantage from the so-called "Fixed Support" feature provided by the program: apart from the nature of the constrain, the definition of a fixed support manages to maintain fixed the element which will be specified in its scope, whatever this is. Considering that a cell is vertically displaced in a battery pack array with respect to its main dimension, the lower cover could be thought to be constrained in its lower face as well as on its lateral ones defined by the $1\ mm$ thickness. The upper cover, on the other hand, is surely constrained by the presence of the tabs, and the eight faces in contact with these elements are going to be selected as well. Furthermore, also the four lateral faces are going to be included thinking that the overall motion of the cell would be in some way avoided by the presence of the spacers, plastic elements seen in the *Chapter 3*. Finally, dealing with the lateral case, this will be considered as joined with the two cover plates where the contact occurs, hence in its upper and lower faces. In total, seventeen faces have been selected and entered in the "Scope" section of the feature regarding the cover plates, while only two for what concerns the lateral case. Note, at last, that what brings to the definition of these reference planes is an assumption deriving from the particular positioning of the prismatic battery within a battery pack.

- **Boundary conditions**

As previously done with the "Fixed Support" feature, two boundary conditions need to be added to the model, here thanks to the inclusion of the "Pressure" feature within the project tree. The first boundary condition will replicate the external ambient pressure, which could be easily thought to be of $1\ atm$, i.e. $101.325\ kPa$. Navigating in the "Definition" section of the "Pressure" feature, it is simply required to enter the numerical value of the magnitude, define this as "Constant", and select all the external faces of the lateral case and of the covers in the "Scope" section, planes which are actually the ones submitted to this particular solicitation (twenty-two in total). The second boundary condition, always given in form of pressure, wants on the other hand to replicate the internal gas pressure of the device and needs to be applied to all the internal faces of the lateral case and of the covers (six in total). Depending on the type of analysis, two different types of internal boundary conditions must be addressed:

- For a dynamic-type simulation, the magnitude of the pressure is defined as "Function" and its value entered in the form of the $5th$ order polynomials previously introduced, whose coefficients needs to be multiplied by "$time$".
- In case of a static-type simulation, the introduction of the gas pressure absolute level is entered in the same way as previously done for the external ambient boundary condition.

Doing like this, the case and the cover will be subjected to a mechanical solicitation given by the pressure difference applied, respectively, inside and outside the elements. In case of a dynamic-type simulation, then, this pressure difference will be time-dependent, differently from the case in which the battery is statically studied, i.e. at rest.

- **Analysis setting**

To set up the simulations is going to be used the "Analysis Setting" feature standardly present within the project tree.

- In the cases in which a $1C$ CC discharge is going to be simulated, and consequently the dynamic behaviour of the cell is under study, it is simply necessary to define a single computational interval (i.e. set the "Number of Steps" to 1) with a “Step End Time” of $3600\ s$ and a “Time Step” length of $36\ s$, here thought to be sufficiently accurate.

- On the other hand, when dealing with an analysis which is not time dependent, such as for the simulations representing the cell at rest, the program only allows to work with the aforementioned quantities: as a consequence these will need to be settled again, with the “Step End Time” which is now at $1\ s$ and the “Time Step” length, accordingly, of $1\ s$.

At last, for all the simulations, it is finally necessary to define both the case and cover plates’ materials as “Standard Aluminium Alloy” (already provided by the ANSYS library and impose a body temperature of $25\ °C$, so that the properties of the materials get adjusted accordingly.

- **Reports**

Concluding, the last thing that remains to do is to define the computational reports, i.e. to indicate to the program what the user wants to compute and finally see at the end of the simulation. For both the typologies of tests, three different reports are going to be created, chosen among the ones provided by the program:

1. The “Deformation” report shows the punctual absolute displacement of the body;
2. The “Equivalent Elastic Strain” report shows the punctual equivalent elastic percentage deformation of the body;
3. The “Equivalent Stress” report shows the punctual equivalent effort of the body.

Take in mind that for all the three reports it is required to select the surfaces at which they refer to. Since this work is mainly aimed at analysing what happens at the level of the aluminium case, it is sufficient to select its external faces.

Thus, having addressed the setup for the dynamic-type of simulation as well as for the static-type one, it is possible to move on presenting the obtained results in the following section of the chapter.

Mechanical analysis – **Single-cycle vs ageing**

The results that are going to be presented will be subdivided in two macro sections. The first one will treat the outcomes generated by a $1C$ CC discharge taking place within the cycling period testing phase based on three different case studies: the $1st$, $50th$ and $100th$ cycles performed during the first 100-cycles testing procedure—i.e. suddenly after the initial characterizing set of tests. In this way, the relationship between the quantities obtained thanks to the reports and the SoC of the cell could be obtained. The second section, on the other hand, will be focused on the characterization of the ageing effects in Li-Ion batteries, where the results are a function of the number of EFC at which they refer to and consequently, through a computed capacity decrement, to the SoH of the device.

- **Single cycle analysis**

The input for this particular type of study are the polynomial curves describing the behaviour of the internal gas pressure along the discharges, whose six coefficients have been collected in *table 28* and *table 29* (specifically referred to the $0th$ order coefficient). Only remember that because of the way in which Mechanical APDL carries on the computation, the polynomials are described as a function of the time t. However by simply arranging the results in MATLAB it is possible to present the outcomes in the parameter vs SoC plane. Thus, the following *figure 101* shows the behaviour of the maximum absolute deformation, maximum percentage deformation (or strain), and maximum stress, all computed at the level of the lateral case.

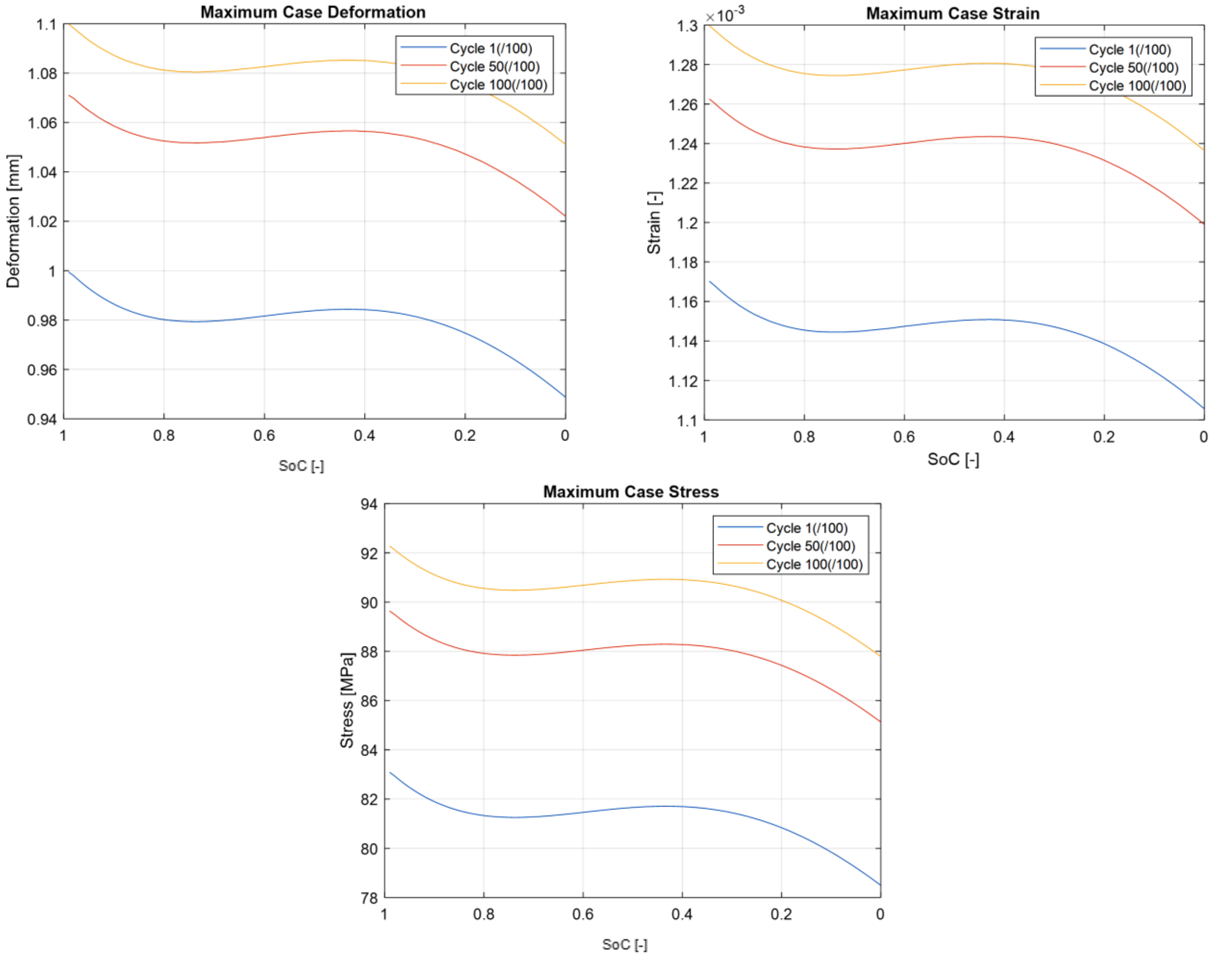

FIGURE 101 - Absolute deformation, strain, and stress dynamic behaviour

It is straightforward the fact that the analysed quantities follow the same pattern of the internal gas pressure, which is actually the source of solicitation for the element under study. However, many things may be highlighted from the set of plots above. First of all, being the battery always “overpressurized” with respect to the external environement, a certain absolute deformation is always found, meaning that the cell “occupies” more volume within a battery pack than initially tought during the design. Furthermore, being in the order of magnitude of $1\ mm$, these deformations are quite relevant: if one thinks that the final goal is to provide a densily packed set of batteries within a powertrain (together with TMS and BMS), if each of them is slightly deformed than in its original design, these differences may build up perhaps leading to dangerous contacts between the devices in some points. Moreover, as it can be noted, the pattern described by the deformations, as well as for all the other quantities, tend to grow as the cycling period proceeds, but however, to better address this latter aspect, the next analysis will provide a more complete set of data for what concerns the ageing of the device.

Apart from the deformations, another relevant quantity which provide interesting results is the maximum punctual stress simulated at the level of the cell. Always following the pattern of the gas pressure, the aluminimum case get solicitated by an alternating pressure if one thinks that a discharge is subsequently followed by a recharge which, as the experimental data suggest, replicatng the same curve represented in the upper left-hand side of the *figure 99*. The mean stress value turns out growing in time as the effect of the growing mean pressure as the battery gets cycled, with the alternating component that is generally maintained. To better address this fatigue-like phenomenon, however, the last section of the chapter will be completely aimed at verifying the resistance of the case during ageing. For now, nevertheless, it is enough to state that the aluminium alloys' yield streghts ranges between $250 \div 600\ MPa$ (depending on the alloying elements which are included within the material) and so it can be concluded that the chassis should withstand to such sollicitations. Take also in mind, at last, that the resulting values are strongly constraints-dependent, and the case studied in this work is assumed to be the worst scenario, hence providing a certain degree of confidence in the goodness of the outcomes.

From a graphical point of view, Mechanical APDL is able to provide clear representations to show the effects of the internal gas pressure on the body of the battery, and particularly relevant are the ones presenting the distribution of the absolute deformation (amplified to provide a better fist) on the device. Although it is possible to create animations covering the entire duration of the discharge, in the following *figure 102* it is shown, as an example, the initial instant of the so-called "$1st$ cycle" of the first 100-cycle cycling period, which founds its numerical counterpart in the relative plot previously shown in the *figure 101*.

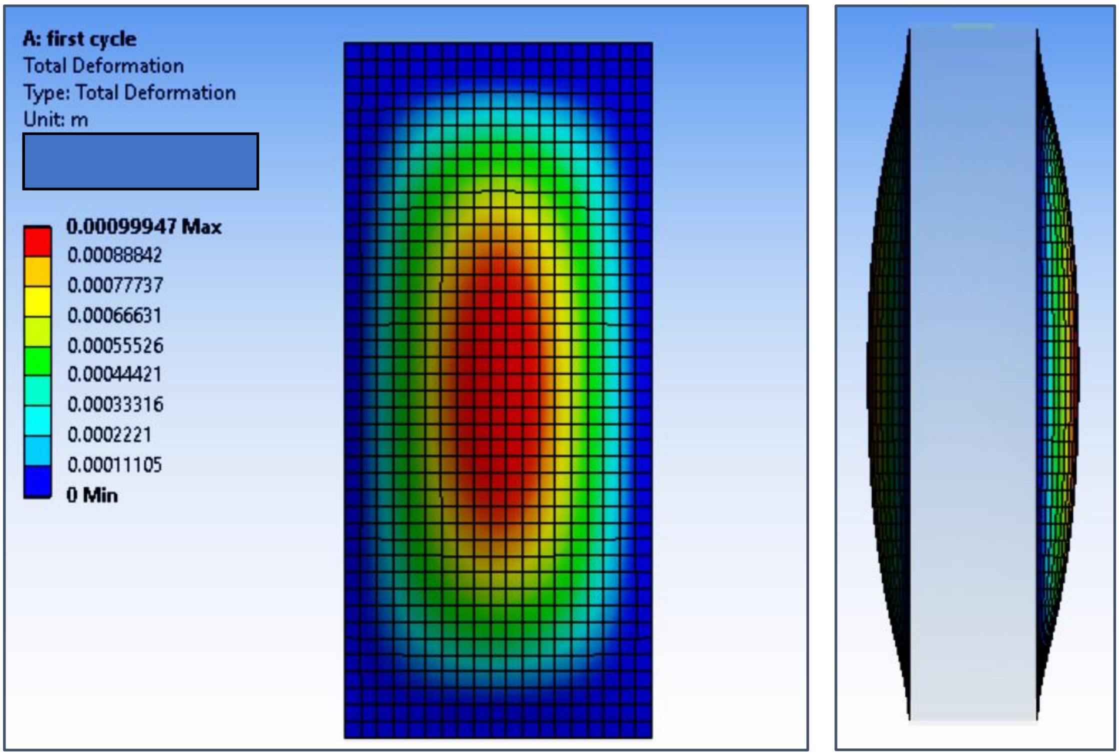

FIGURE 102 - Distribution of the $1st$ cycle initial absolute deformation (amplified deformation)

As it can be seen, the maximum asolute displacement (i.e. the quantity whose behaviour along the discharge is represented in the series of plot in the last page) takes place in the middle point of the major face of the aluminium case, which is obviously the portion of the body most prone to get deformed because settled far from the mechanical constraints. Furthermore, it could be generally said that the swelling happens in a symmetric manner with respect to the middle plane of the device, hence “isotropically”.

A totally different shape of distribution, on the other hand, is the one taken by the stress and consequently by the strain, recalling that the two quantities have a direct relationship. Thus, referring to the initial instant of the $1st$ $1C$ CC discharge as previously done, the following *figure 103* represents the distribution of efforts on the surface of the modelized Li-Ion battery.

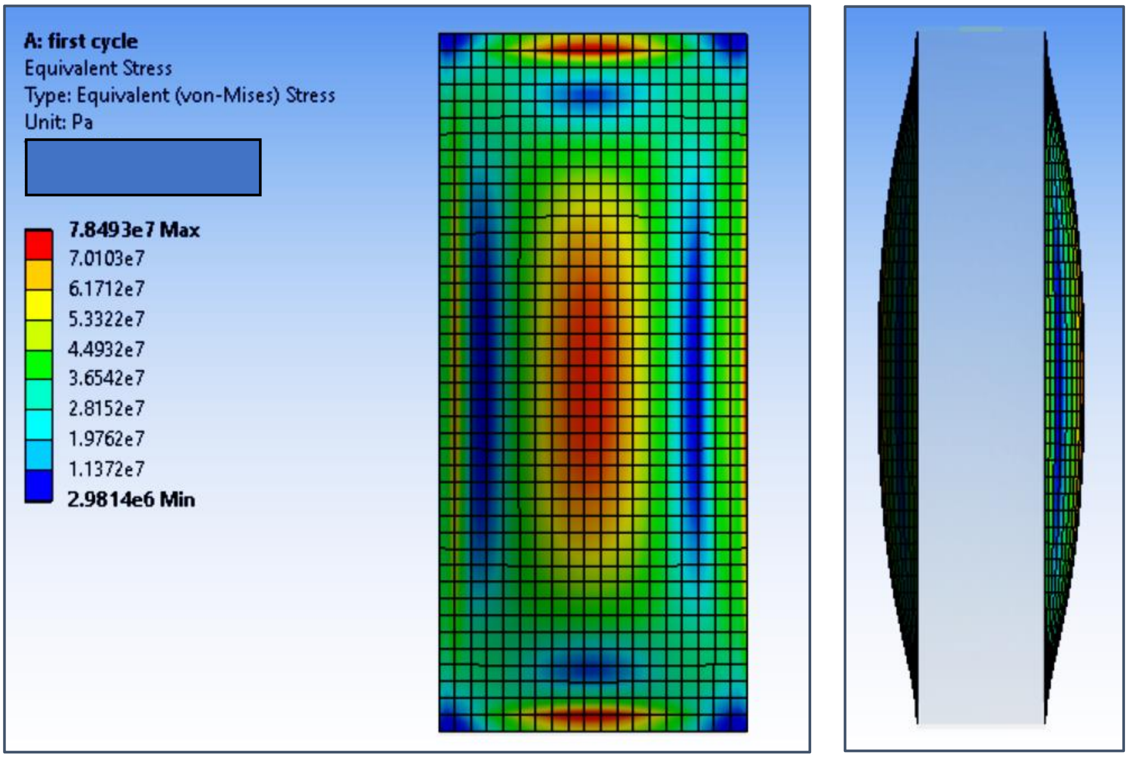

FIGURE 103 - Distribution of the 1st cycle initial stress (amplified deformation)

Once again, the highest magnitudes of the quantity under analysis are found in the centre of the major face. Nevertheless, it is clearly visible that many other spots presenting high stress levels are present over the surface, for instance close to the imposed mechanical constraints: these, indeed, manage in limiting the deformations in their proximity, action that therefore produces a rising in the local values of stresses. However, because of this strong dependence on the constraints (whose definitions are actually nothing more than assumptions made for this particular study), it has been chosen to focus the attention on the central part of the face rather than on secondary zones characterized by high efforts.

At the end of the section, putting things together, it could be interesting to summarize the most important numerical results obtained by the dynamic-type analysis, here within the following *table 31*, aimed both at giving a certain knowledge about the magnitudes in play as well as an initial sight on the ageing effects, deeply discussed in the next part of the work.

TABLE 31 - Reversible swelling simulated effects

Simulated discharge	Max. Abs. Deformation $[mm]$ (at $SoC = 1$)	Max. Abs. Deformation $[mm]$ (at $SoC = 0$)	Max. Stress $[MPa]$ (at $SoC = 1$)	Max. Stress $[MPa]$ (at $SoC = 0$)
$1st$ cycle over 100	0.99947	0.94871	83.087	78.493
$50th$ cycle over 100	1.071	1.022	89.636	85.126
$100st$ cycle over 100	1.0999	1.0511	92.278	87.785

- ## Ageing analysis

In the previous section of the work, the effects given by the presence of the reversible swelling have been modelized as a function of the state of charge of the battery, all computed at the centre of the major face of the case. What will be now of interest, on the other hand, as initially suggested by the theory and then confirmed by the experimental data (and subsequently by the simulations), is to study the change in the general level of the resulting quantities as a consequence of the increasing build-up of the so-called "irreversible swelling", phenomenon which, simply, generates an increase in the internal gas pressure as the electrochemical cell ages. Only remember that to account this ageing effect the number of EFCs has been previously introduced, even if the use of the SoH should result in a better understanding of the process and will be hence discussed more in detail later on. Apart from these considerations, let's start by showing the pattern described by the gas pressure along the life of the ESS under analysis, here reported in the following *figure 104*.

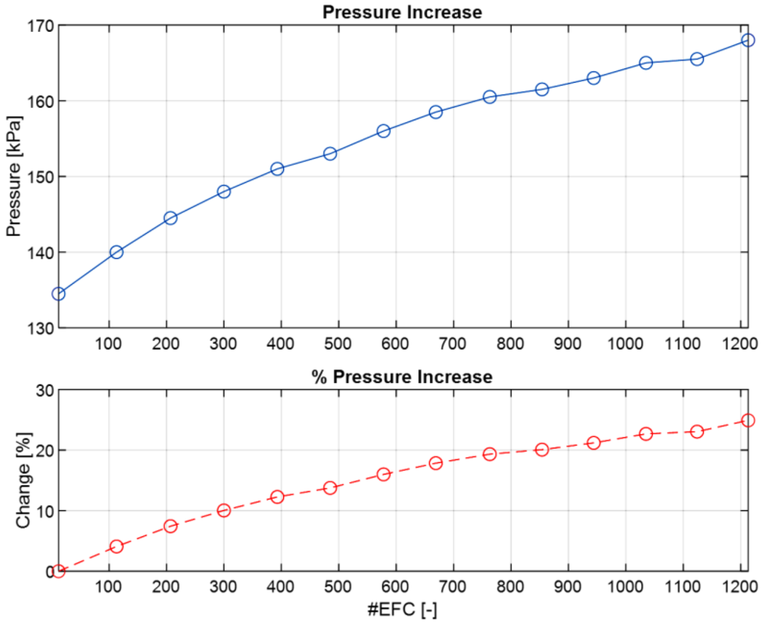

FIGURE 104 - Absolute and percentage pressure change during ageing

The plot in the last page collects the data regarding both the absolute and the relative gas pressure changes, so that especially working with the latter, eventually, one could then pass the results from the object under analysis to another cell, seeking for differences or similitudes—which is actually what may happen with a future testing campaign applied on the Li-Ion battery presented in this work. As it can be seen, the pressure clearly increases along the life of the device: its magnitude ends up reaching an overall growing of the 25%, passing from an initial value of around $130\ kPa$ up to $170\ kPa$. Starting hence from this latter set of inputs, whose exact numerical values have been collected in the *table 30* (in the form of gas pressure vs number of EFCs) and setting up the simulation as instructed in the precedent part of the chapter for a static-type analysis, the results regarding the absolute deformation of the case and the stress levels could be easily obtained. Once again, only take in mind that the outcomes which are going to be shown in the following part of the section are the most relevant ones in terms of magnitudes, since belonging to the centre of the major face of the aluminium chassis.

Beginning with analysing the simulated absolute deformations generated by such pressure levels, the build-up increase of this quantity with respect to the number of equivalent full cycles is shown in the following *figure 105*.

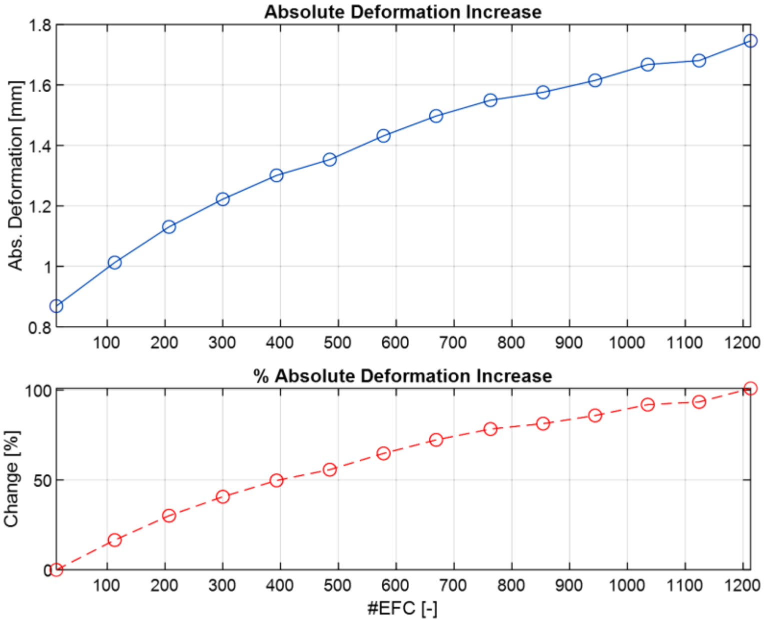

FIGURE 105 - Absolute and percentage dimensional change during ageing

Altought the pattern described by the dimensional changes during the ageing period exactly replicates the one previously described by the gas pressure level, it is very interesting to note the differences among the two "percentage" scales: the initial value of absolute deformation gets almost doubled after more that 1200 EFCs, with a rough 100% increase given by almost a 20% one from the pressure point of view. Thus, having that the cell's case of a fresh battery at rest is initially deformed slightly less than $0.9\ mm$, this latter arrives up to more that $1.7\ mm$ at the end of its life, meaning that the recurrent cycles at which the divice is submitted induce an irreversible deformation of its chassis. Again, as also previously stated, the dimension which is reached itself is not relevalt if compared to the overall size of the battery, but this has to be thought in a context where one seeks to maximize the energy density of the battery pack by integrating as much as possible the ESSs with the wirings, sensors, and tools for its efficient functioning. Thus, putting things together, the results depicted in the *figure 105* are both surprizing and alarming: they indeed suggests that the swelling is a real threat in systems intended to closely pack together many Li-Ion batteries, whose stability has now been highlithed to be highly dependent from the structural behaviour of the devices.

Accordigly, the maximum generated stresses by the gas pressure increase are collected in the following *figure 106*.

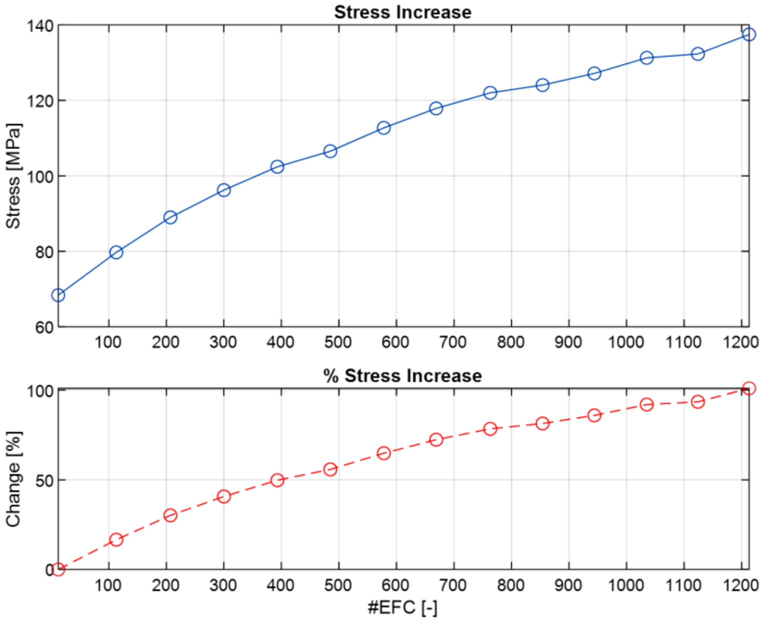

FIGURE 106 - Absolute and percentage stress change during ageing

Once again, it has to be reminded that there is a one-to-one correlation between absolute deformation and stresses, so that also in this case the percentage increase of apporximately the 100% of the quantity under analysis is maintained. Then, referring to the absolute values, even if the chassis of the battery seems to easily withstand the efforts (yield strength in the range of $250 \div 600\ MPa$), a more detailed analysis should be provided because of the effects induced by the fatigue generated by the subsequent application of charging and discharging cycles, study which will be detailly addressed in the last section of the work.

At last, having analysed the results from a graphical point of view, it could be also interesting to summarize the simulated numerical outcomes as also previously done introducing the following *table 32*. For each one of the studied quantities (absolute deformation and stress), in particular, it is going to be shown its value correspondent to a certain number of EFCs at which it refers to, together with the relative percentage increment with respect to the reference fresh battery.

TABLE 32 - Irreversible swelling simulated effects

Simulated ageing	Max. Abs. Deformation $[mm]$	Max. Abs. Deformation Increase $[-]$ (WRT EFC #12)	Max. Stress $[MPa]$	Max. Stress Increase $[-]$ (WRT EFC #12)
EFC #12	0.86871	0	68.383	0
EFC #113	1.0127	16.5752	79.724	16.5845
EFC #207	1.1306	30.1470	89.004	30.1552
EFC #300	1.2222	40.6914	96.221	40.7089
EFC #393	1.3008	49.7393	102.410	49.7594
EFC #485	1.3531	55.7597	106.530	55.7843
EFC #578	1.4317	64.8076	112.720	64.8363
EFC #669	1.4972	72.3475	117.870	72.3674
EFC #763	1.5495	78.3679	122	78.4069
EFC #854	1.5757	81.3839	124.060	81.4194
EFC #944	1.615	85.9078	127.150	85.9380
EFC #1035	1.6674	91.9398	131.270	91.9629
EFC #1124	1.6805	93.4478	132.310	93.4838
EFC #1213	1.7459	100.9762	137.460	101.0149

The last remaining thing to do, since in this section it has been analysed the ageing of a cell, is to connect together the results obtained so far with the state of health of the battery. Recalling its definition, the SoH is a percentage value which indicates the status of the device within its life span, considering the capacity decrement with respect to its fresh, new counterpart. The work of Schmitt et all, however, relies on an ESS which is only similar to the one studied in this work: it has indeed a reference capacity of $34\ Ah$ against the $25\ Ah$ assigned to the cell in analysis. Nevertheless, the two ESSs are similar both from a dimensional and from an electrochemical point of view. Therefor, to cope with this differences and similitudes, it is going to be applied an adimensional approach together with the strong assumption that what has been observed to happen within the $34\ Ah$ Li-Ion battery is likely to take place too in any similar device.

During the long experimental campaign, the cell's capacity has been carefully measured at each of the already mentioned EFCs with the application of a $0.05C$ CC discharge, within the electrochemical characterization conducted at environmental temperature. The battery clearly showed a decreasing value of capacity during its life, whose rate of decrease turns out being quite large for a fresh device, taking subsequently a low steady value and presenting hence an approximately linear fashion. Putting together the obtained numerical data and reorganizing them, the capacity's fade is shown in the following *figure 107*.

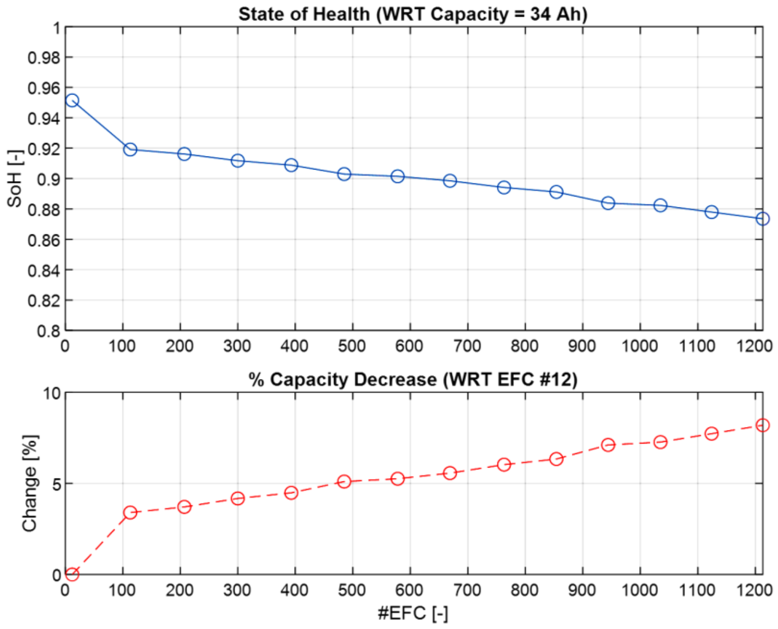

FIGURE 107 - SoH and capacity fade during ageing

Considering that the first point of the plots represents the relative quantity computed at the level of 12 EFCs, it is simple to see that there is that a sudden SoH decrement takes place within the very first use of the cell, particularity that keeps for the first part of its life up to around 100 complete EFCs. After this first decrement, the battery keeps losing some of its capacity but in a less remarkable amount throughout its entire life, usually falling below values of 0.9 for what concerns its state of health. Speaking with percentage quantities, then, referring to the capacity decrement, devices such these ones usually arrive to lose around the 10% of their capacity if no major damages to the their structure happen, such as for instance high current discharges (which involve a dangerous rise in temperature) or deep discharges. Hence, it could be said that the obtained outcomes reflect the scenario that is usually described within the broad literature.

Putting things together, the important thing that has been shown in this last section is correlation between the increase in gas pressure and the capacity loss in a Li-Ion battery, fact which enables the use of pressure measurements, coming from the sensing apparatus, for an accurate SoH determination. If one indeed thinks to equip the battery pack of an EV with such non-invasive membrane-based pressure sensors, their ability in detecting the gas pressure will result in the prediction of the health of the entire powertrain, battery-wise.

However, it should be finally said that further tests are necessary to fully exploit the capacities of this approach: a set of cells should be in fact integrated together in the complex environment which is a vehicle's battery pack, so that there would eventually be a better in-field evaluation in the ability of predicting the status of the ESSs in commercial applications. Then, if a correlation between the internal gas pressure level rise and the capacity decrease is specifically determined through aging experiments in the laboratory, in a similar way as presented in this work, a precise algorithm could be implemented in the battery management system. The algorithm measures the gas pressure whenever the battery pack is at rest and in thermal equilibrium, processes the influences on this latter given by temperature and by SoC, taken into account to apport the required corrections, and finally determines the remaining capacity of the battery from the corrected gas pressure value. Note that all the topics related with the definition of aforementioned requirements to build this innovative predictive device have been addressed in this work: gas pressure vs SoH, gas pressure vs SoC, and thermal behaviour.

Fatigue verification

The structural characterization of a Li-Ion battery has highlighted a particular fluctuating behaviour of the gas pressure level along an equivalent full cycle: there, respectively discharging and charging the device, the pressure lowers and rises as function of the SoC around a mean value which tends to increase in time. As a consequence, it has been thought to be interesting to finally conclude this section providing an approximative fatigue verification of the cell's chassis in its most stressed point.

The aluminium laminate which forms the case of the battery under analysis is a very common and cheap solution adopted for the manufacturing of thin elements, thanks in particular to its workability: the so-called “2024” alloy. The main mechanical properties of the material are enlisted in the following [48]:

- Tensile strength R_m of $483\ MPa$;
- Yield strength $R_{p,0.2}$ of $345\ MPa$;
- Modulus of elasticity $73.1\ GPa$.

For what concerns its fatigue-related quantities, on the other hand, one needs to initially identify the fatigue limit to infinite life (σ_{D-1}), i.e. such limit alternated stress for which the component, no matter the number of solicitations it is submitted to, could eventually last forever. As the theory suggests, there is not a well-defined fatigue limit to infinite life for non-ferrous alloys such as the aluminium ones, since these lack of the so-called “knee” in the Wohler characteristic diagram. However, the quantity could be simply deducted by using empirical formulas deriving from the experimental practices performed during decades of studies, and, as a good approximation for the case of this work, the fatigue limit to infinite life could be obtained as indicated by Zhang et all [49]:

$$\sigma_{D-1} \cong \frac{1}{3} R_m = 161\ MPa$$

Thus, having all the quantities of interest to perform such type of verification, this is going to be completely addressed in the present section by following the steps depicted below.

- **Wohler diagram**

The so-called "S-N" characteristic is represented in the diagram of Wohler: it is a statistic-based curve, which relates the alternating component of a fatigue cycle to the number of cycles a specimen undergoes before failure. Note that, because of this specimen-dependence, the resulting quantities are aimed at describing the behaviour of a material rather than the one of a physical component, but for the nature of our study, i.e. involving a very small alternating component, the former are assumed to be representative enough. With respect to the aluminium alloy here under analysis, the qualitative graph reported within the following *figure 108* will serve as a guide.

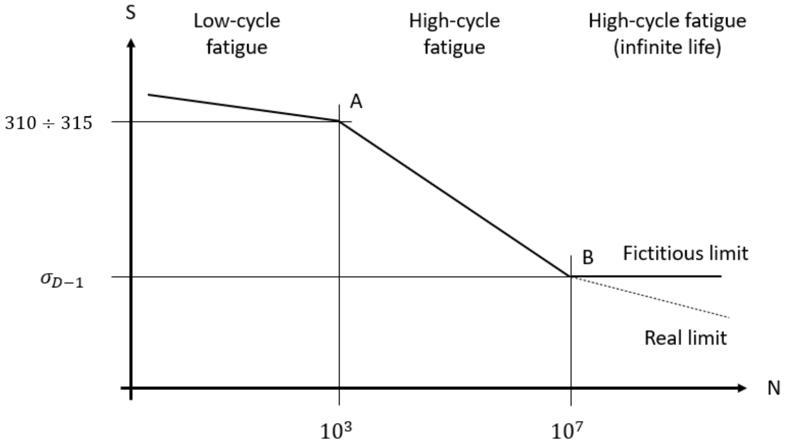

FIGURE 108 - Al-type Wohler diagram

The diagram is divided in three sections: low cycle fatigue for $N < 10^3$ cycles, high cycle fatige with limited life for N ranging between $10^3 \div 10^7$ cycles, and high cycle fatigue with "infinite" life for $N > 10^7$ cycles, with the latter value which is generally used in case of aluminium alloys and with the stress limit of $310 \div 315\ MPa$, for the low-cycle fatigue zone, that was obtained from the literature [50]. From the outcomes coming out in the previous part of the work, however, it has been decided that the case of the cell will be verified for a number of cycles equal to 1300. Thus, by knowing the two limits of the high-cycle fatigue region of the graph, i.e. A and B, the point of interest could be easily obtained by working on the following characteristic formula (recalling that the graph normally has a logarithmic x axis):

$$NS^k = b$$

Where k and b are two material-dependent coefficients.

Hence, let for now define the working condition with "$*$": by substituing the values of S and N with those defining the points A and B it is possible to find out the two characteristic coefficients, and by entering them in the formula depicted above, knowing already the value of N^*, i.e. 1300 cycles, S^* will be easily found out.

$$\begin{Bmatrix} N_A S_A^k = b \\ N_B S_B^k = b \end{Bmatrix} \rightarrow (k, b) \rightarrow N^* S^{*k} = b \rightarrow S^* = 305\ MPa$$

As it has been said, the value of S^* represents the limit alternating component of solicitation which the material could withstand for a certain number of cycles N^*

before failing, in this case considering a null mean value of stress. Thus, putting things together, this is actually the so-called “fatigue limit” to finite life, which is usually referred to as σ_{N-1}, with “-1” that is the value taken by the “solicitation factor” (R) in case the mean component of the stress is equal to zero.

- **Haigh diagram**

For a defined number of cycles the specimen has to withstand, the diagram of Haigh puts in relation the alternate component of the stress with its mean counterpart (σ_m), providing like this the limit values combination. Starting from the basic case in which σ_m is equal to 0, the limit alternate component is the one previously found in the Wohler diagram, i.e. σ_{N-1}. However, increasing the level of mean effort, the limit alternate component turns out decreasing, meaning that the material is able to withstand now only a smaller alternating effort. Following the standard rules for its construction, in the *figure 109* is represented a qualitative Haigh diagram complete of all the features that interest the case treated in this section.

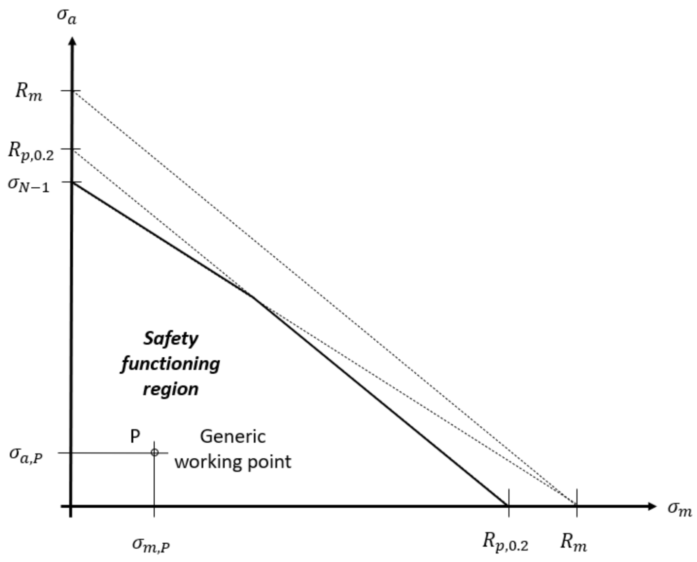

FIGURE 109 - Generic Haigh diagram

As it can be seen, a well-defined safety region in which the element could operate and lasts up to 1300 cycles is enclosed by the so-called “Goodman’s curve” and by the yield strength limit. Here, by specifying the alternated and mean components of the solicitation in play, the working point in the graph is settled resulting in the definition of some safety coefficients. The alternated component of the stress turned out being equal to $2.5\,MPa$, while for the mean component three different case studies have been selected, in order to highlight the effects given by the change of this latter: the σ_m value has been settled to 96.22, 117.87, and $137.46\,MPa$, reflecting the outcomes found respectively at 300, 669, and 1213 EFCs.

Thus, knowing now the magnitudes characterizing the three working points in analysis, dealing with the safety factors, it has to be reminded that a certain body could be verified in three ways:

1. With respect to its mean stress component when its value changes in time;
2. With respect to its alternated stress component when its value changes in time;

3. With respect to the both the stress components when their values change in time.

As it is now clear, the alternate component of the stress is maintained during the life of the Li-Ion battery, being it merely a function of the state of charge of the cell and consequently of the phenomena taking place within the discharges and recharges. On the other hand, the mean stress has been seen to increase in time because of some irreversible phenomena, and thus, accordingly, the first type of verification of those depicted above is the one which is going to be addressed.

Generally, the safety factor S_F referred to a generic working point P is function of a limit quantity, as indicated in the formula below:

$$S_{F,mean}|_P = \frac{\sigma_{m,lim}}{\sigma_m}|_P$$

With such a low alternated component of the stress, the limit mean value is defined by the yield strength limit curve. In other words, the sum of mean and alternated component should not overcome $R_{P,0.2}$. As a consequence:

$$\sigma_{m,lim}|_P = R_{P,0.2} - \sigma_a|_P = 342.5\ MPa$$

Thus, finally, the three safety factors could be computed as indicated above, providing the following set of results:

$$S_{F,mean}|_{\#300} = 3.59, \qquad S_{F,mean}|_{\#699} = 2.91, \qquad S_{F,mean}|_{\#1213} = 2.49$$

Within the following *figure 110*, a detailed view of the Haigh diagram now under study is shown, presenting the working points so far characterized.

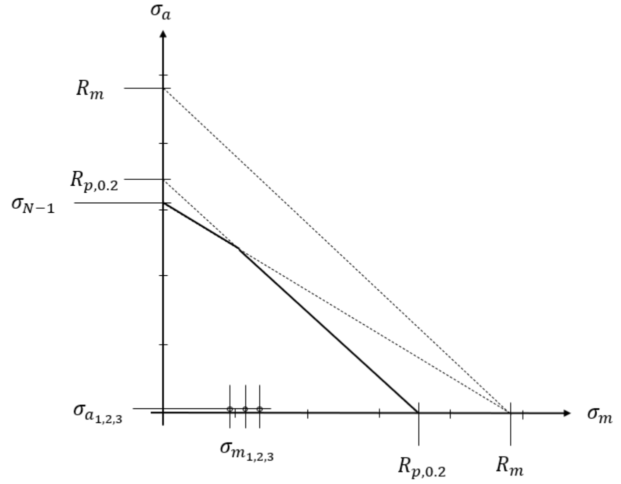

Figure 110 - Specific case study Haigh diagram

The outcomes of the fatigue verification are interesting under many point of view. Nevertheless, what really matters is that the safety coefficient which refers to the 1213 EFCs condition, being actually representative of the worst-possible condition, says that the battery’s case withstand well the efforts induced by the ageing swelling. However, it has to be said that this latter is a very rough and approximative analysis only aimed entering in the fatigue-induced problem. Broader studies will surely go deeper into the field, considering for instance the role played by notches, roughness, and bodies that perhaps turned out being initially slightly damaged, hence more “fragile” against a failure via fatigue.

Chapter 8

Conclusions

Having now reached the end of this long work, it would be useful and interesting to summarize all the results obtained along it, as well as to spend some thoughts on these achievements.

In the first part of the paper, much of the theoretical background concerning the topics of interest was treated. It started with the general scenario of electric mobility, then moved on to the more detailed fields of electrochemical cells and of the Li-Ion technology, concluding with a look at the use of these devices inside an EV. After that, the different types of tests to which the batteries are generally submitted in the research sector were extensively analysed, also considering the careful definition of the engineering parameters and of the different modelling techniques applied to the cells. Subsequently, the work moved to the presentation of the practical activity carried out by the research group in the recent months. More in detail, in sequence, the following topics were addressed:

- Presentation of the experimental testing campaign;
- Right definition of an ECM;
- Presentation of the electrical and thermal simulating campaign with consequent results;
- Presentation of improved electrical and thermal simulating campaign with consequent results;
- Definition of a rough structural analysis and presentation of the mechanical simulating campaign with consequent results.

However, although the details have already been extensively discussed during the course of the work, they lead to a number of serious conclusions.

The massive arrival of electric vehicles in the automobile market is revolutionizing the sector, and only in these years we are witnessing a real explosion in the spread of hybrid and electric vehicles. Although these now turn out to be "top-class" cars, mostly open to a niche market, the real turning point will be reached when the vehicles are truly made available to the average citizen: the consequent large-scale adoption may lead to long-term benefits regarding the reduction of harmful emissions and of pollution, and more generally to a more sustainable way of living.

The cost reduction for what concerns the technology can be achieved in various ways, but the engineering plays a very fundamental role in all of this. In this work, for instance, it has been seen the importance that a simulation capable of predicting the state of a cell in operation can have. If one thinks of achieving a "state of the art" also in the field of research and development, it is natural to think of considerable advantages. Among others, a device can be modelled from the earliest design stages avoiding complete component build/remodelling cycles, saving both time and money on costly tasks. Furthermore, particular applications can be studied on-demand avoiding the construction of a complex testing equipment, and still avoiding waste and long dead times for correct setup. In other words, putting things together, the so-called time-to-market of devices would certainly benefit from the improvements coming from the simulation field, and in general, thanks to many small savings scattered throughout the manufacturing chain, the new vehicle class electric could really become affordable and affordable for anyone.

References and sources

[1] E. Vergori, "Studio e simulazione di sistemi di accumulo per veicoli ibridi elettrici", MSc Thesis, Politecnico di Torino, 2016, Relator: Prof. A. Somà.

[2] C. C. Chan, Y. S. Wong, A. Bouscayrol, K. Chen, "Powering Sustainable Mobility: Roadmaps of Electric, Hybrid, and Fuel Cell Vehicles", Proceedings of the IEEE, Vol. 97, No. 4, April 2009

[3] C. C. Chan, "The State of the Art of Electric and Hybrid Vehicles", Proceedings of the IEEE, Vol.90, No. 2, 2002, Pages 247-75

[4] P. Cooke, "Gigafactory Logistics in Space and Time: Tesla's Fourth Gigafactory and Its Rivals", Sustainability, 2020

[5] K. S. Gallagher, E. Muehlegger, "Giving Green to Get Green: Incentives and Consumer Adoption of Hybrid Vehicle Technology", John F. Kennedy School of Government - Harvard University, 2008

[6] E. Karden, S. Ploumen, B. Fricke, T. Miller e K. Snyder, "Energy storage devices for future electric vehicles", Journal of Power Sources, Vol. 168, No. 1, December 2006, Pages 2-11

[7] https://www.edfenergy.com/for-home/energywise/how-do-electric-cars-work

[8] https://en.wikipedia.org/wiki/Drivetrain

[9] https://afdc.energy.gov/vehicles/how-do-all-electric-cars-work

[10] https://afdc.energy.gov/vehicles/how-do-plug-in-hybrid-electric-cars-work

[11] https://www.thetorquereport.com/volkswagen/vw-predicts-lithium-ion-battery-shortage-2025

[12] A. F. Burke, "Batteries and Ultracapacitors for Electric, Hybrid, and Fuel Cell Vehicles", Proceedings of the IEEE, Vol. 95, No. 4, April 2007

[13] https://insideevs.com/news/402992/tesla-model-y-size-weight

[14] https://www.tesla.com/blog/model-s-efficiency-and-range

[15] https://en.wikipedia.org/wiki/Electrochemical_cell

[16] G. Zubi, R. Dufo-Lopez, M. Carvalho, G. Pasaoglu, "The lithium-ion battery: State of the art and future perspectives", Journal of power sources - Renewable and Sustainable Energy Reviews, Vol. 89, March 2018, Pages 292-308

[17] https://en.wikipedia.org/wiki/Lithium-ion_battery

[18] https://www.wattalps.com/from-lithium-ion-cells-to-battery-system

[19] N. Nitta, F. Wu, J. T. Lee, G. Yushin, "Li-ion battery materials: present and future", Elsevier, Materials Today, Vol. 18, No. 5, June 2015

[20] Cordis STREP project (SuperLIB), "Cell Specification with Cell Data", lead for European Batteries OY, April 2012

[21] https://chargedevs.com/newswire/porous-powers-new-ceramic-battery-separator-aims-to-enhance-safety-cycle-life-and-performance-of-li-ion-batteries

[22] https://batteryuniversity.com/learn/article/types_of_battery_cells

[23] S. J. Gerssen-Gondelach, A. P. C. Faaij, "Performance of batteries for electric vehicles on short and longer term", Journal of Power Sources, Vol. 212, No. 1, April 2012, Pages 111-129

[24] https://neutrium.net/properties/specific-energy-and-energy-density-of-fuels

[25] https://forums.tesla.com/discussion/155960/tesla-model-3-battery-weight

[26] https://www.chemistryworld.com/news/fire-starting-battery-dendrites-go-with-the-flow/3008867.article

[27] https://mpoweruk.com/pack_construction

[28] https://www.electrive.com/2018/10/28/audi-and-umicore-develop-closed-loop-battery-recycling-concept

[29] S. Arora, W. Shen, A. Kapoor, "Review of mechanical design and strategic placement technique of a robust battery pack for electric vehicles", Journal of power sources - Renewable and Sustainable Energy Reviews, Vol. 60, March 2016, Pages 1319-1331

[30] S. Al Hallaj, H. Maleki, J. S. Hong, J. R. Selman, "Thermal modelling and design considerations of lithium-ion batteries", Journal of Power Sources, Vol. 83, January 1999, Pages 1-8

[30] Y. Barsukov, Q. Jinrong, "Battery Power Management for Portable Devices", Artech House, 2013.

[32] Y. Deng, C. Feng, J. E, H. Zhu, J. Chen, M. Wen, H. Yin, "Effects of different coolants and cooling strategies on the cooling performance of the power lithium ion battery system: a review", Applied Thermal Engineering, Vol. 142, June 2018, Pages 10-29

[33] L. Lu, X. Han, J. Li, J. Hua, M. Ouyang, "A review on the key issues for lithium-ion battery management in electric vehicles", Journal of Power Sources, Vol. 226, November 2012, Pages 272-288

[34] https://mpoweruk.com/soh

[35] W. He, M. Pecht, D. Flynn, F. Dinmohammadi, "A Physics-Based Electrochemical Model for LithiumIon Battery State-of-Charge Estimation Solved by an Optimised Projection-Based Method and Moving Window Filtering", Energies, Vol. 11, August 2018.

[36] L. Chen, R. Xu, W. Rao, H. Li, Y. P. Wang, T. Yang, H. B. Jiang, "Electrochemical Model Parameter Identification of Lithium-Ion Battery with Temperature and Current Dependence", International Journal of Electrochemical Science, Vol. 14, April 2019, Pages 4124–4143

[37] W. Sung, C. B. Shin, "Electrochemical model of a lithium-ion battery implemented into an automotive battery management system", Computers and Chemical Engineering, Vol. 76, February 2015, Pages 87-97

[38] J. Meng, G. Luo, M. Ricco, M. Swierczynski, D. I. Stroe, R. Teodorescu, "Overview of Lithium-Ion Battery Modeling Methods for State-of-Charge Estimation in Electrical Vehicles", Applied Science, Vol. 8, No. 5, April 2018, Pages from 659

[39] N. Damaya, C. Forgeza, M. P. Bichatb, G. Friedricha, "Thermal modeling of a large prismatic LiFePO4/graphite battery. Coupled thermal and heat generation models for characterization and simulation", Journal of Power Sources, Vol. 283, 2015, Pages 37-45

[40] K. E. Thomas, J. Newman, "Heats of mixing and of entropy in porous insertion electrodes", Journal of Power Sources, Vol. 119–121, 2003, Pages 844–849

[41] B. Scrosati, J. Garche, W. Tillmetz, "Advances in Battery Technologies for Electric Vehicles", Chapter 18, Advances in Battery Technologies for Electric Vehicles, Elsevier Science & Technology, 2015.

[42] ANSYS Inc., "Designing Next Generation Electric Powertrains Using CFD Simulation", White Paper

[43] R. Capuano, "Analisi numerica FEM termo-fluidodinamica di celle agli ioni di litio", MSc Thesis, Politecnico di Torino, 2019, Relator: Prof. A. Somà.

[44] https://it.wikipedia.org/wiki/metodo_degli_elementi_finiti

[45] ANSYS Inc., "ANSYS Fluent Battery Module Manual", Release 15.0, November 2013.

[46] L. K. Willenberg, P. Dechent, G. Fuchs, D. U. Sauer, E. Figgemeier, "High-Precision Monitoring of Volume Change of Commercial Lithium-Ion Batteries by Using Strain Gauges", Sustainability, Vol. 12, 2020.

[47] J. Schmitt, B. Kraft, J. P. Schmidt, B. Meir, K. Elian, D. Ensling, G. Keser, A. Jossen, "Measurement of gas pressure inside large-format prismatic lithium-ion cells during operation and cycle aging ", Journal of Power Sources, Vol. 478, 2020.

[48] https://www.gabrian.com/2024-aluminum-properties

[49] https://www.nature.com/articles/s41467-020-19071-7

[50] K. Al-Rubaie, "A general model for stress-life fatigue prediction", Materialwissenschaft Und Werkstofftechnik, Vol. 39, June 2008.